frontiers | Research Topics

# Characterization, effects, perception, and mitigation of air pollution in Asia for better air quality management

**Edited by**
Parth Sarathi Mahapatra, Dipesh Rupakheti and Juliana Jalaludin

**Published in**
Frontiers in Public Health
Frontiers in Earth Science
Frontiers in Ecology and Evolution

ISSN 1664-8714
ISBN 978-2-8325-4662-8
DOI 10.3389/978-2-8325-4662-8

## About Frontiers

Frontiers is more than just an open access publisher of scholarly articles: it is a pioneering approach to the world of academia, radically improving the way scholarly research is managed. The grand vision of Frontiers is a world where all people have an equal opportunity to seek, share and generate knowledge. Frontiers provides immediate and permanent online open access to all its publications, but this alone is not enough to realize our grand goals.

## Frontiers journal series

The Frontiers journal series is a multi-tier and interdisciplinary set of open-access, online journals, promising a paradigm shift from the current review, selection and dissemination processes in academic publishing. All Frontiers journals are driven by researchers for researchers; therefore, they constitute a service to the scholarly community. At the same time, the *Frontiers journal series* operates on a revolutionary invention, the tiered publishing system, initially addressing specific communities of scholars, and gradually climbing up to broader public understanding, thus serving the interests of the lay society, too.

## Dedication to quality

Each Frontiers article is a landmark of the highest quality, thanks to genuinely collaborative interactions between authors and review editors, who include some of the world's best academicians. Research must be certified by peers before entering a stream of knowledge that may eventually reach the public - and shape society; therefore, Frontiers only applies the most rigorous and unbiased reviews. Frontiers revolutionizes research publishing by freely delivering the most outstanding research, evaluated with no bias from both the academic and social point of view. By applying the most advanced information technologies, Frontiers is catapulting scholarly publishing into a new generation.

## What are Frontiers Research Topics?

Frontiers Research Topics are very popular trademarks of the *Frontiers journals series*: they are collections of at least ten articles, all centered on a particular subject. With their unique mix of varied contributions from Original Research to Review Articles, Frontiers Research Topics unify the most influential researchers, the latest key findings and historical advances in a hot research area.

Find out more on how to host your own Frontiers Research Topic or contribute to one as an author by contacting the Frontiers editorial office: frontiersin.org/about/contact

# Characterization, effects, perception, and mitigation of air pollution in Asia for better air quality management

**Topic editors**

Parth Sarathi Mahapatra – Deutsche Gesellschaft für Internationale Zusammenarbeit (GIZ) GmbH, India

Dipesh Rupakheti – Nanjing University of Information Science and Technology, China

Juliana Jalaludin – Universiti Putra Malaysia, Malaysia

**Citation**

Mahapatra, P. S., Rupakheti, D., Jalaludin, J., eds. (2024). *Characterization, effects, perception, and mitigation of air pollution in Asia for better air quality management*. Lausanne: Frontiers Media SA. doi: 10.3389/978-2-8325-4662-8

# Table of contents

frontiers | Frontiers in Earth Science

TYPE Editorial
PUBLISHED 13 March 2024
DOI 10.3389/feart.2024.1293817



OPEN ACCESS

EDITED AND REVIEWED BY
Ben Van Der Pluijm,
University of Michigan, United States

*CORRESPONDENCE
Dipesh Rupakheti,
drupakheti2@gmail.com,
dipesh.rupakheti@nuist.edu.cn

RECEIVED 13 September 2023
ACCEPTED 06 March 2024
PUBLISHED 13 March 2024

CITATION
Rupakheti D, Mahapatra PS and Jalaludin J (2024), Editorial: Characterization, effects, perception, and mitigation of air pollution in Asia for better air quality management. *Front. Earth Sci.* 12:1293817. doi: 10.3389/feart.2024.1293817



# Editorial: Characterization, effects, perception, and mitigation of air pollution in Asia for better air quality management

Dipesh Rupakheti[1,2]*, Parth Sarathi Mahapatra[3] and Juliana Jalaludin[4]

[1]Jiangsu Key Laboratory of Atmospheric Environment Monitoring and Pollution Control, Collaborative Innovation Center of Atmospheric Environment and Equipment Technology, Nanjing University of Information Science and Technology, Nanjing, China, [2]Institute of Fundamental Research and Studies, Kathmandu, Nepal, [3]Deutsche Gesellschaft für Internationale Zusammenarbeit (GIZ) GmbH, Delhi, India, [4]Department of Environmental and Occupational Health, Faculty of Medicine and Health Sciences, Universiti Putra Malaysia, UPM, Serdang, Selangor, Malaysia

KEYWORDS

**air quality, air quality management, air pollution, air pollution characteristics, Asia**

Editorial on the Research Topic
Characterization, effects, perception, and mitigation of air pollution in Asia for better air quality management

Air pollution affects billions of people globally and is a critical developmental challenge. Its presence is conspicuous and has a profound effect on people's lives and livelihoods in Asia (Maharjan et al., 2022), a major hotspot for air pollution. This has a large implications for both the continent and the global burden of diseases. Understanding the origins, causes, and ramifications of air pollution in this region is crucial for the present generation and the sustainable development of future generations. It is essential to recognize that majority of air pollution in Asia can be attributed to anthropogenic activities such as industrial emissions, domestic practices, construction and infrastructure development, transportation and others.

It is vital to address these anthropogenic factors to achieve on-ground air quality improvements across the continent. A comprehensive strategy incorporating scientific knowledge, thoughtful policymaking, readiness, and individual dimensions is required to mitigate the issue effectively. However, sometimes, policies alone cannot bring about the desired change without a basis of public awareness and individual responsibility. Therefore, to spread knowledge, increase awareness, and provide citizens the ability to make environmentally friendly decisions, governments, non-governmental organizations, and community leaders must work together. An excellent illustration of this is the introduction of "Mission LiFE" in India. Another crucial element in the fight against air pollution is preparedness. In addition to supporting long-term planning, creating resilient infrastructure, creating early warning systems, and putting emergency response plans into place help reduce the short-term effects of sudden spikes in air pollution levels. India implementing its Graded Response Action Plan (GRAP), Pakistan implementing its policy

to use only improved brick kilns to reduce pollution in winter, and Beijing issuing "red alert" closing schools, factories and construction sites and ordering half of all private cars off the road are some examples amongst many. Effective air quality management in Asia is contingent upon strategic planning and coordination at all levels—local, national, and international—due to the diversity of air pollution sources, sizable developing economies, the geography and landuse, population, and growth velocity, among other factors. Overcoming boundaries and ideologies is necessary for the joint effort to combat air pollution. One such initiative includes comprehending the complex air pollution problem in Pakistani and Indian Punjab (Shrestha et al., 2022). Implementing focused reduction methods and having a sophisticated grasp of risk assessment are necessary for mitigating the effects of air pollution.

Therefore, we endeavored to compile scientific data on several subjects pertaining to air quality in Asia for this Research Topic. This information would serve as the cornerstone for constructing reliable policy and future research and collaborations. A quick summary of articles published under this Research Topic is summarized here.

While COVID-19 did show the world what it needs to do for blue skies, several researches thereafter have consolidated these findings and supported mitigations efforts. In one of the research, Liu et al. investigated the impact of the COVID-19 lockdown on air quality in Lanzhou, a city in northwest China, using the time series decomposition method. The lockdown provided an opportunity to understand the changes in air pollution levels and to test the effectiveness of previous environmental protection measures. This study showed that temporary social closure measures (such as lockdown during COVID) have a limited effect on improving air quality in Lanzhou. In another study, Jethva et al. assessed the predictability of post-monsoon crop residue fires in Northwestern India which can support mitigation efforts in the South-Asian region. This study demonstrated a robust relationship between satellite measurements of vegetation index (a proxy for crop amounts, and post-harvest fires—a precursor of air pollution events), for predicting seasonal agricultural burning. Based on the spatial autocorrelation and geographically and temporally weighted regression model (GTWR), She et al. explored spatial-temporal characteristics and driving factors of PM2.5 through 252 prefecture-level cities in China. Results demonstrated that $PM_{2.5}$ concentrations showed a significant downward trend in North and Central China, and the reason might be the transition from a high environmental pollution-based industrial economy to a resource-clean high-tech economy since the implementation of the Air Pollution Prevention and Control Action Plan in 2013. Singh et al. investigated the seasonal concentrations of particulate and gaseous Polycyclic Hydrocarbons Carbon (PAHs) along with carcinogenic health risk assessment in the urban atmosphere of Delhi. The principal component and correlation were used to identify the sources of particulate and gaseous PAHs during different seasons. These studies could be used to focus mitigation efforts as laid under the National Clean Air Programme of India. Guo et al. measured the carbon emission efficiency of pig farming in 30 provinces of China by using the non-expected output SBM model and analyzed the spatial and temporal characteristics and the influencing factors by using the limited dependent variable model. Yuan et al. investigated the ambient air pollution and associated health risks and premature mortality in four functional (urban, suburban, industrial and rural) areas of Jining, China. The four functional areas exhibited the same seasonal variations and diurnal patterns in air pollutants, with the highest exposure excess risks (ERs) from ozone. Highest health-based air quality index (HAQI) in industrial area influences the HAQI in urban and suburban area through transport mechanism. Thus puts forward the requirements of mitigation efforts to be concentrated for different pollutants on a seasonal basis. Feng et al. explained the mechanism of national development zone policy affecting carbon emissions in China using the panel data of 285 cities in China from 2003 to 2020, and adopting the DID model to analyze its impact on carbon emissions through tests such as placebo test, dynamic test, endogeneity test, and parallel trend test. The findings show that the development zone policy indeed significantly reduces carbon emissions. From a large birth cohort (572,106 mother-infant pairs) in Chongqing, China, Zhou et al. explored the relationship between exposure to ambient air pollutants during pregnancy and the risk of very low birth weight (VLBW). The Generalized Additive Model were applied to estimate exposures for each participant during each trimester and the entire pregnancy period. Findings showed that the maternal exposure to high levels of PM2.5, PM10, NO2, and O3 might increase the risk of very low birth weight, especially for exposure on the first and second trimester. You et al. conducted this time series study to explore the association between ambient PM2.5 exposure and daily hospital admissions for circulatory system diseases (CSD) from 2016 to 2020 based on 201,799 hospitalized cases in Ganzhou, China by using generalized additive models (GAMs). Based on the panel data of 75 cities in the Yellow River Basin, China, Lu et al. constructed an evaluation index system and measured the environmental regulation efficiency using a super-EBM hybrid distance model. Regional differences and dynamic evolution characteristics of environmental regulation efficiency with the help of Dagum's Gini coefficient decomposition and kernel density estimation methods was also analyzed. These studies indicate the effects of air pollutants on health through different routes.

In conclusion, the issues of air quality stand out as a unique opportunity to put these concepts into practice, especially as integration and interdisciplinary studies are still popular subjects in many conversations. The complexity of air pollution in Asia, from its definition and impact to the way it is perceived and tackled, highlights the urgent need for a comprehensive and collaborative approach. The region can pave a path towards better air quality management by combining scientific knowledge, technical breakthroughs, sustainable urban design and infrastructres, policy frameworks, public awareness, behavioural change and preparedness measures. Through the adoption of well-designed and implementable solutions to combat air pollution, we can concurrently address broader global challenges. By working together, we can only hope to lessen the negative impacts of air pollution and ensure a healthier tomorrow, and a more sustainable future for the millions of people residing in Asia.

## Author contributions

DR: Writing–original draft. PM: Writing–review and editing. JJ: Writing–review and editing.

## Funding

The author(s) declare financial support was received for the research, authorship, and/or publication of this article. DR was supported by the Startup Foundation for Introducing Talent of NUIST (2022r024) and the Jiangsu Province "Double Innovation Doctor" Program (JSSCBS20220552).

## Acknowledgments

This Research Topic has been realized in collaboration with Dr. Pratima Singh, Research Scientist at the Centre for Study of Science, Technology and Policy (CSTEP), Bangalore, India. We wholeheartedly thank all the authors and reviewers who have participated in this Research Topic. The views and interpretations in this publication are those of the authors and are not necessarily attributable to their organisations.

## Conflict of interest

The authors declare that the research was conducted in the absence of any commercial or financial relationships that could be construed as a potential conflict of interest.

The author(s) declared that they were an editorial board member of Frontiers, at the time of submission. This had no impact on the peer review process and the final decision.

## Publisher's note



## References

Maharjan, A., Adhikari, S., Ahmad, R., Ahmad, U., Ali, Z., Bajracharya, S., et al. (2022). Air pollution exposure and its impacts on everyday life and livelihoods of vulnerable urban populations in South Asia. *Environ. Res. Commun.* 4 (7), 071002. doi:10.1088/2515-7620/ac77e0

Shrestha, M., Upadhyay, A., Bajracharya, S., Sharma, M., Maharjan, A., Gurung, K., et al. (2022). State of air pollution and potential mitigation mechanisms for the greater Punjab region. *Bull. Am. Meteorological Soc.* 103 (9), 2130. doi:10.1175/bams-d-22-0132.1

frontiers | Frontiers in Public Health

TYPE Original Research
PUBLISHED 17 November 2022
DOI 10.3389/fpubh.2022.1051116



OPEN ACCESS

EDITED BY
Dipesh Rupakheti,
Nanjing University of Information Science and Technology, China

REVIEWED BY
Shazia Rehman,
Pak-Austria Fachhochschule Institute of Applied Sciences and Technology, Pakistan
Qiangqiang Xu,
Northwest Institute of Eco-Environment and Resources (CAS), China
Dongyang Yang,
Henan University, China

*CORRESPONDENCE
Peng Wang
wangpengjlu@jxnu.edu.cn

SPECIALTY SECTION
This article was submitted to Environmental health and Exposome, a section of the journal Frontiers in Public Health

RECEIVED 22 September 2022
ACCEPTED 04 November 2022
PUBLISHED 17 November 2022

CITATION
She Y, Chen Q, Ye S, Wang P, Wu B and Zhang S (2022) Spatial-temporal heterogeneity and driving factors of $PM_{2.5}$ in China: A natural and socioeconomic perspective. *Front. Public Health* 10:1051116. doi: 10.3389/fpubh.2022.1051116



# Spatial-temporal heterogeneity and driving factors of $PM_{2.5}$ in China: A natural and socioeconomic perspective

Yuanyang She[1,2], Qingyan Chen[3], Shen Ye[1,2], Peng Wang[1,2]*, Bobo Wu[1,2] and Shaoyu Zhang[1,2]

[1]School of Geography and Environment, Jiangxi Normal University, Nanchang, China, [2]Key Laboratory of Poyang Lake Wetland and Watershed Research, Ministry of Education, Jiangxi Normal University, Nanchang, China, [3]Science and Technology College, Jiangxi Normal University, Jiujiang, China

**Background:** Fine particulate matter ($PM_{2.5}$), one of the major atmospheric pollutants, has a significant impact on human health. However, the determinant power of natural and socioeconomic factors on the spatial-temporal variation of $PM_{2.5}$ pollution is controversial in China.

**Methods:** In this study, we explored spatial-temporal characteristics and driving factors of $PM_{2.5}$ through 252 prefecture-level cities in China from 2015 to 2019, based on the spatial autocorrelation and geographically and temporally weighted regression model (GTWR).

**Results:** $PM_{2.5}$ concentrations showed a significant downward trend, with a decline rate of 3.58 $\mu g\ m^{-3}\ a^{-1}$, and a 26.49% decrease in 2019 compared to 2015, Eastern and Central China were the two regions with the highest $PM_{2.5}$ concentrations. The driving force of socioeconomic factors on $PM_{2.5}$ concentrations was slightly higher than that of natural factors. Population density had a positive significant driving effect on $PM_{2.5}$ concentrations, and precipitation was the negative main driving factor. The two main driving factors (population density and precipitation) showed that the driving capability in northern region was stronger than that in southern China. North China and Central China were the regions of largest decline, and the reason for the $PM_{2.5}$ decline might be the transition from a high environmental pollution-based industrial economy to a resource-clean high-tech economy since the implementation the Air Pollution Prevention and Control Action Plan in 2013.

**Conclusion:** We need to fully consider the coordinated development of population size and local environmental carrying capacity in terms of control of $PM_{2.5}$ concentrations in the future. This research is helpful for policy-makers to understand the distribution characteristics of $PM_{2.5}$ emission and put forward effective policy to alleviate haze pollution.

KEYWORDS

**$PM_{2.5}$, spatial-temporal heterogeneity, natural and socioeconomic factors, driving ability, GTWR**

# 1. Introduction

Rapid urbanization has resulted in serious air pollution, such as haze, dust and other terrible weather frequently, which bring a huge impact on people's lives, industrial and agricultural production (1–3). $PM_{2.5}$ (particulate matter with an aerodynamic diameter $\leq$2.5 μm), one of the major air pollutants, has been a popular research topic for academics in recent years (4–7). Many studies have shown that prenatal exposure of pregnant women to $PM_{2.5}$ increases the likelihood of respiratory infection and may even cause early-life respiratory tract diseases to newborns (8), and children exposed to polluted air for a long time may increase the possibility of hypertension, asthma, obesity and metabolic disorders (9). Recent researches have also shown that high concentrations of $PM_{2.5}$ are associated with high COVID-19 mortality (10). Thus, $PM_{2.5}$ pollution incidents have affected human and ecological health in the course of rapid socioeconomic development.

Numerous scholars have done extensive research on $PM_{2.5}$ in terms of components and sources, spatial variation and impact factors, and have proposed many corresponding control measures (11–16). Previous studies have shown that natural and socioeconomic factors have a significant impact on $PM_{2.5}$ (2, 17–19). For example, the increase in temperature is conducive to atmospheric flow, which enhances $PM_{2.5}$ dispersion, alike the higher summer temperature (lower heating energy consumption) are beneficial to the reduction of $PM_{2.5}$ concentrations (20). On the contrary, the higher temperatures promote the formation of secondary aerosols from gas precursors, thereby increasing $PM_{2.5}$ concentrations (21). The stronger air movement in areas with high levels of surface fine particles was likely to increase $PM_{2.5}$ concentrations, and air movement also has a diffusion and transport effect on $PM_{2.5}$ concentrations (22, 23), Precipitation and relative humidity played an important role in the deposition of $PM_{2.5}$, and increased relative humidity increases the water-soluble ion content of the air (24).

Meanwhile, some researches have shown that there was an inverted U-shaped relationship between $PM_{2.5}$ concentrations and the economic development in socioeconomic terms (25). Extensive economic development relying on energy and resource consumption will increase pollution sources and cause deterioration of air quality. Yet, the residents will pay attention to environmental conservation and health impacts from pollutants with improving standards of living (26). The Environmental Kuznets Curve (EKC) relationship was observed between per capita GDP and air contaminant (27, 28). Industrial structure is an important indicator of local social and economic development. It is generally believed that secondary industry generally refers to heavy industrial production, which is easy to cause greater environmental pollution. The tertiary industry mainly refers to business, finance, trust and service industries, which are generally considered to have low environmental pollution. The population density has a significant impact on $PM_{2.5}$ emissions across all sectors (3). For instance, the increase in population density led to increased consumption, increased travel and production activities, thereby increasing $PM_{2.5}$ emissions. However, the drivers of natural and social factors on $PM_{2.5}$ at different spatial and temporal scales are not well understood. Therefore, it is necessary to further clarify the effects of natural and social factors on $PM_{2.5}$ drivers at different scales.

China became the world's second-largest economy in 2010 after only 30 years of rapid economic evolution since the reform and opening up, and it has been one of the regions with the highest $PM_{2.5}$ concentrations in the world (13). There had been many studies on the temporal and spatial distribution characteristics and influencing factors of $PM_{2.5}$ in China (29–33). And yet, China is a country with a vast territory, a large population, complex landforms and climate, and unbalanced economic development. It poses major challenges for the research and governance of $PM_{2.5}$. Due to the differences in spatial-temporal scale and methods, the research results of dominant factors for spatial-temporal variation of $PM_{2.5}$ concentrations are different. Many studies indicated that $PM_{2.5}$ concentrations showed a spatial distribution characteristic of high overall in the north and low in the south. The pollution hotspots of $PM_{2.5}$ were mainly concentrated in eastern and central China, especially in the Beijing-Tianjin-Hebei region and its surrounding area. The Chinese government has taken a series of strategies to control air pollution such as the Air Pollution Prevention and Control Action Plan (Action Plan) from 2013. Since the implementation of the Action Plan, $PM_{2.5}$ concentrations have been effectively controlled and have shown a downward trend (34, 35). But there are few studies on the driving forces of the temporal and spatial variation of $PM_{2.5}$ in China since the implementation of the Action Plan using natural and socioeconomic factors.

Therefore, it is necessary to explore the driving of natural and socioeconomic factors on $PM_{2.5}$ concentrations in whole China. The present study focuses on the following questions by collecting the measured data of $PM_{2.5}$, natural and socioeconomic from 252 prefecture-level cities in China during 2015~2019: 1) The ability of natural and socioeconomic factors to drive the spatial distribution of $PM_{2.5}$ concentrations. 2) Whether natural or social factors dominate the main causes of $PM_{2.5}$ concentrations changes over time at different spatial scales. The result of this study may be useful to the government in the prevention and control of $PM_{2.5}$ concentrations in industrial restructuring and population development planning.

# 2. Materials and methods

## 2.1. Study area and data source

The data in this study was primarily divided into $PM_{2.5}$ data from 252 prefecture-level cities in China from 2015 to 2019, as well as related to urban natural and socioeconomic factors. $PM_{2.5}$ data were obtained from hourly $PM_{2.5}$ monitoring data by the China National Environmental Monitoring Centre (CNEMC, http://www.cnemc.cn/). Hourly $PM_{2.5}$ data were compiled into the daily average data of 252 cities according to the China Ambient Air Quality Standards (GB3095-2012), the China Ambient Air Quality Assessment Technical Regulations (HJ663-2013) and other relevant regulations. Cities with multiple monitoring stations had their data averaged and treated as daily urban average data. Based on previous studies and the physical geographic features of the country, 252 cities in the country were divided into seven major zones (Supplementary Figure S1 and Supplementary Table S1).

According to previous research (17, 20, 30, 36), eight main influencing factors were finally selected from the twelve factors preliminarily screened by the collinearity treatment. Natural factors include relative humidity (RH), temperature (TEMP), wind speed (WS) and precipitation (PCP), which were taken from the National Weather Science Data Centre (NWSDC). The annual-average values of RH, TEMP and WS were obtained on the average daily data. PCP was the total annual precipitation of the city. The secondary industry was selected as the driving factor of industrial structure on $PM_{2.5}$ in the majority of previous research. With the increase of the proportion of tertiary industry, its impact on $PM_{2.5}$ concentrations needs to be studied. Per capita GDP indicators generally represent the level of local economic development. So the socioeconomic factors included per capita GDP (GDPP), secondary industry share (SI), tertiary industry share (TI) and population density (PD) (year-end total population/total area of jurisdiction) from the China Urban Statistical Yearbook, with the missing data was interpolated by contemporaneous neighboring or around areas. The statistical description and overall spatial distribution of the eight selected driving factors from 2015 to 2019 are showed in Table 1 and Supplementary Figures S2, S3.

## 2.2. Study methods

### 2.2.1. Spatial autocorrelation analysis

Spatial autocorrelation analysis is a model to explore the similarity or correlation of spatial proximity observation results. Global spatial autocorrelation analysis focused on the correlation between observations in close proximity (37). Global Moran's $I$ is the most widely known and used statistic to test for the presence of spatial dependence in observations. The Moran's $I$ can be calculated using Eq:

$$I = \frac{\sum_{i-1}^{n}\sum_{j-1}^{n} w_{ij}(x_i - \bar{x})(x_j - \bar{x})}{\frac{1}{n}\sum_{i-1}^{n}(x_i - \bar{x})^2 * \sum_{i-1}^{n}\sum_{j-1}^{n} w_{ij}} \quad (1)$$

where $\bar{x} = \frac{1}{n}\sum_{i-1}^{n} x_i$, $n$ is the number of spatial units (in this study, $n$ =252); $x_j$ and $x_j$ are the observations of spatial units $i$ and $j$, respectively; $w_{ij}$ is an element of the spatial weight matrix $W$ which describes the spatial arrangement of all the spatial units in the sample, where $w_{ij}$ = 1 if spatial units i and j share a common border and $w_{ij}$ = 0 otherwise. Values of Global Moran's $I$ range from –1 to 1; a positive (or negative) correlation exists among the observations if 0 <$I$ <1(or -1 <$I$ <1), and the observations are distributed randomly (no correlation) in the space if $I$ is close to or equals 0.

The significance of Global Moran's $I$ is commonly measured by the standardized statistic $Z$ as shown in Eq:

$$Z(I) = \frac{I - E(I)}{\sqrt{Var(I)}} \quad (2)$$

where $E(I)$and $Var(I)$ are the expected value and variance of Moran's $I$, respectively; the methods used to calculate them are listed in the Supplementary materials.

The specific location and distribution pattern of local spatial clustering were further determined by a local spatial autocorrelation. The local Moran's $I$ was represented by local indicators of spatial association (LISA), which were calculated as follows:

$$LISA = \frac{(x_i - \bar{x})}{\sqrt{S^2}} \sum_{j} w_{ij}(x_i - \bar{x}) \quad (3)$$

$$S^2 = \frac{1}{n}\sum_{i=1}^{n}(x_i - \bar{x}) \quad (4)$$

A local spatial autocorrelation analysis can detect four cluster types with statistical significance: high-high clusters (high-incidence areas enclosed by high incidence areas); high-low clusters (high incidence areas enclosed by low-incidence areas); low-high clusters (low-incidence areas enclosed by high-incidence areas); and low-low clusters (low-incidence areas enclosed by low-incidence areas). The results were visualized in ArcGIS 10.6 software.

### 2.2.2. Geographically and temporally weighted regression model

The geographically and temporally weighted regression (GTWR) model (38) can effectively deal with Spatial-temporal non-stationarity by introducing a temporal dimension based on spatial heterogeneity. This model can simulate $PM_{2.5}$ concentrations at a higher spatial resolution and accuracy across

TABLE 1 Description of the data used in this study.

| Indicators | Data source | Symbol | Unit | Mean | SD | Minimum | Maximum |
|---|---|---|---|---|---|---|---|
| Relative humidity | Resource and | RH | % | 68.74 | 10.74 | 29.81 | 99.61 |
| Temperature | Environmental | TEMP | °C | 14.43 | 5.31 | −0.20 | 25.44 |
| Wind speed | Science data | WS | m/s | 2.21 | 0.67 | 0.74 | 6.44 |
| Precipitation | Center | PCP | mm | 1034.85 | 602.39 | 21.45 | 4102.50 |
| Per capita GDP | | GDPP | CNY | 69110.59 | 36309.00 | 15356.00 | 217313.00 |
| Secondary industry share | China City | SI | % | 42.41 | 10.08 | 10.68 | 72.90 |
| Tertiary Industry share | Statistical | TI | % | 48.12 | 9.67 | 26.12 | 83.52 |
| Population density | Yearbook | PD | person/$km^2$ | 408.73 | 347.95 | 1.66 | 2836.22 |

China than some previous models (39). The basic formula is as follows (40):

$$Y_i = \beta_0(\mu_i, \nu_i, t_i) + \sum \beta_k(\mu_i, \nu_i, t_i)X_i t + \varepsilon_i \quad (5)$$

where $(\mu_i, \nu_i, t_i)$ is the spatial-temporal coordinate of the $i$th sample; $\mu_i, \nu_i, t_i$ are the longitude, latitude and time of the ith sample point, respectively; $\beta_0(\mu_i, \nu_i, t_i)$ denotes the regression constant at the $i$th sample point, i.e., the constant term in the model; $X_{it}$ is the value of the $k$th independent variable at the $i$th point; $\varepsilon_i$ is the residual; $\beta_k(\mu_i, \nu_i, t_i)$ is the kth regression parameter for the $i$th sample point, which is estimated as follows:

$$\hat{\beta}(\mu_i, \nu_i, t_i) = [X^t W(\mu_i, \nu_i, t_i)X]^{-1} X^T W(\mu_i, \nu_i, t_i)Y \quad (6)$$

where $\hat{\beta}(\mu_i, \nu_i, t_i)$ is the estimated value of $\beta_k(\mu_i, \nu_i, t_i)$; $X$ is the matrix of independent variables; $X_t$ is the transpose of the matrix; $Y$ is the matrix of composition in the sample; $W(\mu_i, \nu_i, t_i)$ is the spatial-temporal weight matrix. $W$ is chosen as the Gaussian distance function, the spatial-temporal weight matrix is obtained using the bi-square spatial weight function, and the spatial-temporal distance between sample $i$ and sample $j$ is:

$$d_{ij} = \sqrt{\delta[(U_i - \mu_j)^2 + (v_i - \mu_j)^2 + \mu(t_i - t_j)^2]} \quad (7)$$

where the choice of bandwidth affects the establishment of spatial-temporal weights, this paper adopts the Akaike Information Criterion (AICc) law for adaptive bandwidth.

### 2.2.3. Stability estimation of coefficients

To analyze the spatiotemporal heterogeneity of each variable, we applied the Kernel function to check the stability of the correlation coefficients, and use the coefficient distribution to observe the spatiotemporal characteristics (41). The density function of the variable $x$ is as follows:

$$f(x) = \frac{1}{Nh} \sum_{i-1}^{n} k\left(\frac{x_i - \bar{x}}{h}\right) \quad (8)$$

where $x_i$ is the coefficients subordinated to independent and identical distributions. $n, h, \bar{x}$ represent the number of $x$, bandwidth and mean value, respectively. The Epanechnikov function was adopted as the kernel function for estimation in this work.

## 3. Results and analysis

### 3.1. Spatial-temporal characteristics of $PM_{2.5}$ concentrations

The Central, East, Northwest and North China were the regions with high mean $PM_{2.5}$ concentrations, which were 54.03 ± 13.86, 44.71 ± 14.52, 40.38 ± 12.55, and 37.34 ± 18.53 μg $m^{-3}$, respectively, (Figures 1, 2). The mean concentrations of $PM_{2.5}$ in southwest China was lowest (26.50 ± 13.41 μg $m^{-3}$), followed by South China (33.98 ± 5.95 μg $m^{-3}$). The area-weighted mean concentrations of $PM_{2.5}$ in China from 2015 to 2019 were 44.24 ± 17.68, 40.24 ± 15.76, 37.54 ± 14.66, 33.19 ± 12.60, 32.52 ± 13.77 μg $m^{-3}$, respectively, and it was 37.55 ± 15.62 μg $m^{-3}$ in 5 years. The mean concentrations

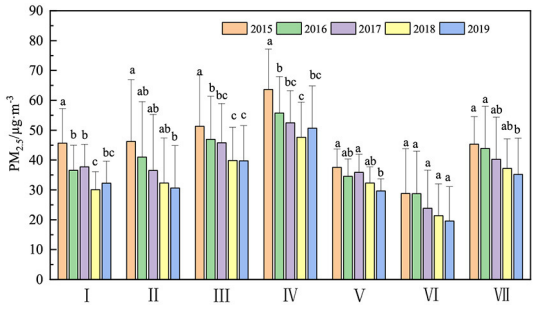


FIGURE 1
Variation characteristics of $PM_{2.5}$ in different regions from 2015 to 2019 (I) Northeast China, (II) North China, (III) East China, (IV) Central China, (V) South China, (VI) Southwest China, and (VII) Northwest China (Letters denote the result of One-way ANOVA).

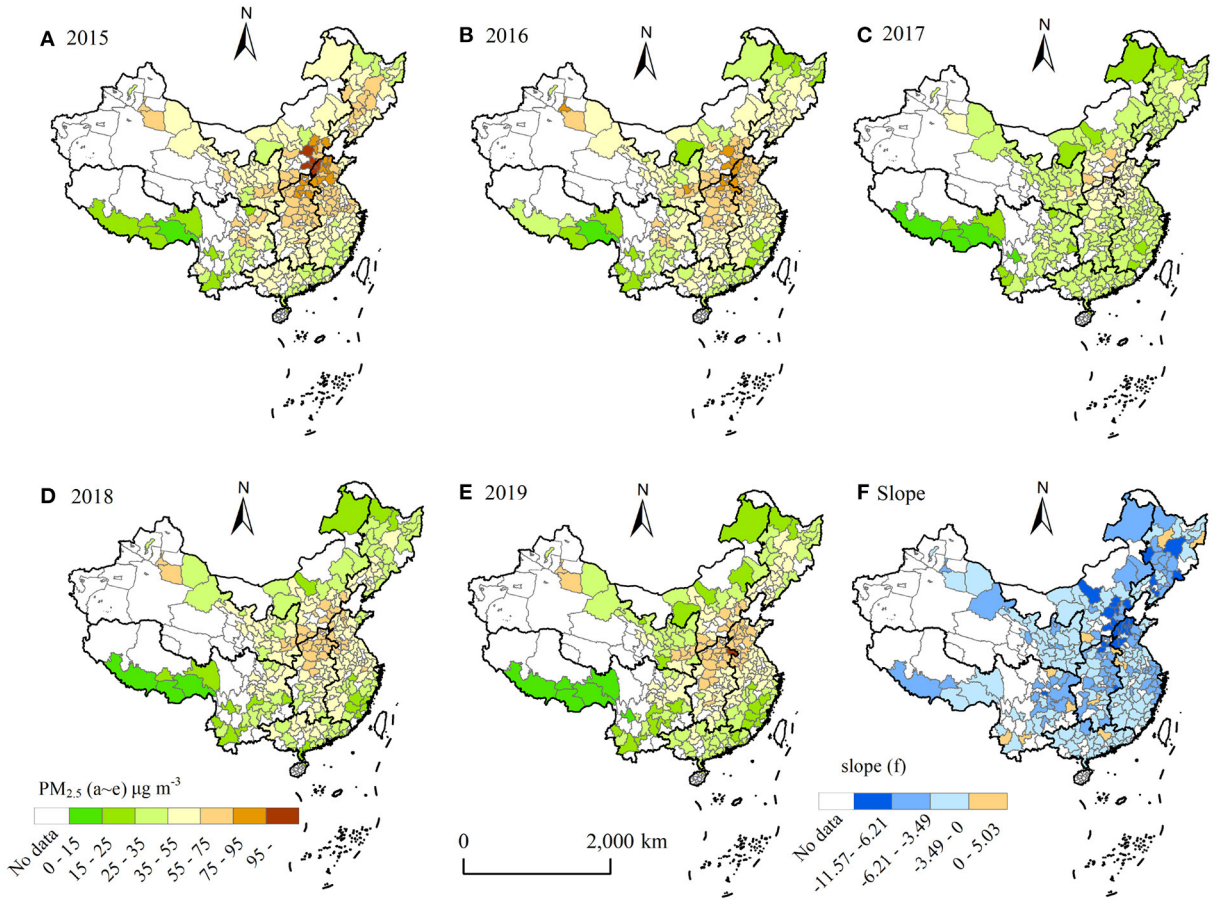


FIGURE 2
Spatial variation characteristics of $PM_{2.5}$ concentrations during 2015-2019 [**(A–E)** denote the spatial distribution of $PM_{2.5}$ concentrations in 2015, 2016, 2017, 2018, and 2019, respectively, and **(F)** denotes the slope of $PM_{2.5}$ concentrations from 2015 to 2019, slope (5-year linear trend slope)].

of $PM_{2.5}$ exceeded the annual $PM_{2.5}$ grade II standard (35 μg $m^{-3}$) (GB3095 2012) in 2015, 2016 and 2017, which exceeded 26.4 % in 2015, and 5.2%, 7.1% below annual $PM_{2.5}$ grade II standard in 2018,2019, respectively. The downward trend of $PM_{2.5}$ concentrations was 3.58 μg $m^{-3}$ from 2015 to 2019, with a percentage decrease of 26.49% in 2019 compared to 2015. $PM_{2.5}$ concentrations of 240 cities showed a decreasing trend among the 252 cities, with the proportion of decreasing cities reaching 95.24%, of which 42 cities had a decrease rate of more than 5 μg $m^{-3}$ $a^{-1}$, accounting for 16.67% of the total number of decreasing cities (Figures 1, 2). Although whole regions presented a downward trend from 2015 to 2019, $PM_{2.5}$ concentrations exhibited an obvious spatial heterogeneity in the different regions. The largest decline occurred in North China (–3.99 μg $m^{-3}$ $a^{-1}$), followed by central China (–3.41 μg $m^{-3}$ $a^{-1}$). The region with the smallest decline was North China (-1.80 μg $m^{-3}$ $a^{-1}$). In this study, the slope of change was divided into four classes according to the natural breakpoint method [strong negative (-11.5∼ -6.21 μg $m^{-3}$ $a^{-1}$), mid negative (-6.21∼ -3.49 μg $m^{-3}$ $a^{-1}$), weak negative (–3.49 μg $m^{-3}$ $a^{-1}$) and weak positive (0∼5.03 μg $m^{-3}$ $a^{-1}$)]. It can be found that the strong negative area was mainly located in the Beijing-Tianjin-Hebei region and parts of the northeast, the mid negative region was mainly located in Central China and Cheng-Yu Region, East China, Northeast China and the majority of the other areas were weak negative growth regions. The weak positive area was scattered throughout the country without obvious aggregation areas (Figure 2F).

To further detect local agglomeration of $PM_{2.5}$ concentrations, we adopted a local Moran's *I* test (Table 2). From 2015 to 2019, the average value of the global Moran's *I* was 0.57($p$ <0.01), indicating that $PM_{2.5}$ concentrations showed a club convergence trend. In addition, we also calculated local Moran's *I*, the results of which revealed a detailed local pattern of spatial clustering with changes in $PM_{2.5}$ concentrations. The Moran's *I* value showed a trend of decreasing and then increasing, with the lowest value in 2017 and the highest values in 2018

TABLE 2 Global spatial autocorrelation test.

| Year | Moran'I | Z | *P* |
|---|---|---|---|
| 2015 | 0.57 | 26.55 | 0.001 |
| 2016 | 0.56 | 26.17 | 0.001 |
| 2017 | 0.52 | 22.83 | 0.001 |
| 2018 | 0.59 | 27.26 | 0.001 |
| 2019 | 0.59 | 26.35 | 0.001 |

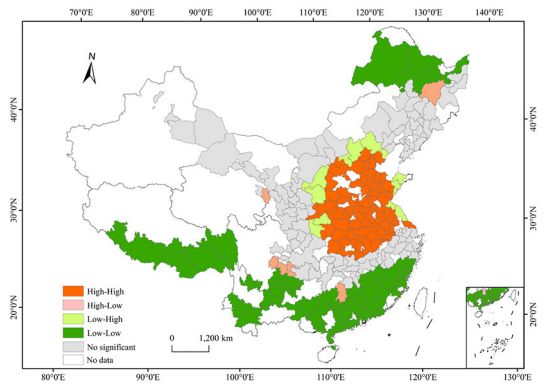


FIGURE 3
Average of spatial clustering for $PM_{2.5}$ concentrations from 2015 to 2019.

and 2019, which indicated that an overall trend toward aggregation.

It was discovered that high-high clusters regions were primarily distributed in China's East-central region, including Beijing, Tianjin, Hebei, Shaanxi, Shanxi, Henan, Hubei, Anhui, and Shandong provinces through local spatial autocorrelation analysis. In contrast, low-low clusters were mainly located in the south and southwest provinces of China, including Tibet, Sichuan, Yunan, Guangxi, Hainan, Guangdong, and Fujian. In addition, low and low aggregation areas also appeared in northeastern Inner Mongolia and northwestern Heilongjiang. The high-low agglomeration area and the low-high agglomeration area were small in scope and are distributed near the high-high and low-low agglomeration areas (Figure 3).

## 3.2. Driving forces of variation of $PM_{2.5}$ concentrations

This study selected the GTWR model to analyze the driving forces of temporal and spatial variation of $PM_{2.5}$ concentrations. In order to avoid the deviation of the estimation results caused by the interaction between the indicators, eight driving factors were determined by collinearity test. The results showed that the variance inflation index of each factor was less than 10, and the condition index was also less than 30, indicating that the factor selected in this study does not have a collinear relationship (Table 3). At the same time, in order to avoid the influence of data on the magnitude, $PM_{2.5}$ concentrations and eight driving factors were standardized before modeling. Then the temporal and spatial non-stationary relationships were modeled using the plug-in for ArcGIS 10.6 (with automatic optimal bandwidth settings) in GTWR produced by Huang et al. (38). The AICc value of the GTWR model was -2736.53. The determination coefficient ($R^2$) and adjustment determination coefficient ($R^2_{adj}$) of the GTWR model were 0.78. To evaluate the validity of GTWR results, ordinary least squares regression (OLS) was chosen to compare with geographically weighted regression (GWR), which describes the relationship between variables by building a global model, while GWR expresses the spatial non-stationarity of the relationship between variables through a local model with spatial dependence of parameters. The results showed that AICc values of the GTWR model were lower than those of the OLS and GWR models, and the $R^2$ was significantly higher, indicating that GTWR results were better than those of the OLS and GWR models (Table 4). The GTWR model coefficients can reflect the direction and intensity of $PM_{2.5}$ driving capability. The positive value indicates the positive driving effect of explanatory variables on $PM_{2.5}$ concentrations, and higher values indicate higher drive capacity, while negative coefficients indicate the opposite.

## 3.3. Stability analyzes of coefficients

From the Kernel distribution of coefficients of different variables (Figure 4), we can see that the coefficients of RH, TEMP, WS and PCP in natural factors were concentrated at approximately −0.01, 0.2, −0.1, and −0.7, respectively. This result indicates that the increase in WS and PCP had a opposite effect on $PM_{2.5}$ concentrations in most cities, while the increase in TEMP had the promotion effect. Among the four socioeconomic factors we analyzed, the largest density of coefficients of PD was distributed at 0.5 (almost no negative values), which illustrates that with the increase in PD, $PM_{2.5}$ concentrations in most cities were promoted. Simultaneously, the coefficients of SI was distributed at 0.2, indicating that the increase in SI will increase $PM_{2.5}$ concentrations of most cities. In contrast, the coefficients of GDPP was left-distributed, and the peaks emerged at approximately −0.16, indicating that the increase of GDPP is beneficial to reduce the urban $PM_{2.5}$ index in most cities during our study period.

TABLE 3 Co-linearity test and coefficients statistic description of variables.

| Factors | Co-linearity test | | | GTWR coefficients statistic description | | | | |
|---|---|---|---|---|---|---|---|---|
| | Standardization coefficient | Tolerances | VIF | Median | Mean | SD | Minimum | Maximum |
| Intercept | - | - | - | 0.38 | 0.42 | 0.23 | −0.22 | 1.43 |
| RH | −0.04 | 0.60 | 1.68 | −0.02 | 0.08 | 0.10 | −0.44 | 0.29 |
| TEMP | −0.01 | 0.31 | 3.22 | 0.00 | 0.26 | 0.31 | −0.69 | 0.81 |
| WS | −0.10 | 0.80 | 1.26 | −0.11 | 0.13 | 0.12 | −0.44 | 0.27 |
| PCP | −0.30 | 0.41 | 2.44 | −0.42 | 0.43 | 0.34 | -3.13 | 0.22 |
| GDPP | −0.19 | 0.66 | 1.51 | −0.09 | 0.11 | 0.11 | −0.29 | 0.49 |
| SI | 0.34 | 0.34 | 2.94 | 0.19 | 0.22 | 0.21 | -1.47 | 0.62 |
| TI | 0.14 | 0.36 | 2.77 | 0.01 | 0.11 | 0.16 | −0.91 | 0.47 |
| PD | 0.39 | 0.66 | 1.52 | 0.44 | 0.55 | 0.74 | 0.00 | 8.65 |

The mean value is the average of the absolute values of the coefficients.

TABLE 4 Result of accuracy evaluation of different model.

| Model | AICc | $R^2$ | $R^2_{adj}$ |
|---|---|---|---|
| OLS | −1606.03 | 0.34 | – |
| GWR | −2501.28 | 0.71 | 0.70 |
| GTWR | −2736.53 | 0.78 | 0.78 |

## 3.4. Spatial distribution characteristics of the factor driving force

The GTWR model demonstrated that the force of the driving factor presented different driving distribution characteristics in China (Figure 5). The coefficients of natural factors on $PM_{2.5}$ concentrations were bidirectional at the national scale. RH, WS and PCP showed predominantly negative correlations. Through the analysis of the absolute value of the coefficient, influence intensity of natural factors on the regional $PM_{2.5}$ concentrations was as follows: PCP (0.43) >TEMP (0.26) >WS (0.13) >RH (0.08). The RH coefficient was between −0.13 and 0.17. The proportion of cities with negative driving factors accounts for about 66.67% of all cities. The core region with the strongest negative impact of RH was the northeast, northwest and north China, while central China, southwest and southern China were dominated by weak positive regression coefficients. The TEMP coefficient showed positive and negative equivalence (−0.56 ∼ 0.66), and positive correlation regions (48.41%) were mainly distributed in North China, Northeast China and Northwest China. The WS coefficient was mainly negative, accounting for 86.11%, and it was mainly located in the eastern, northeastern and southwestern, and the positive effect was mainly in the northwest region. The PCP coefficient of most cities (95.24%) was negative, and the high negative value area was mainly distributed in northwest and north China.

In socioeconomic factors, except that PD was positively correlated with the $PM_{2.5}$ concentrations in each region, other factors presented a two-way impact on $PM_{2.5}$ concentrations. The order of the absolute values of the driving factors for $PM_{2.5}$ was PD (0.55) >SI (0.22) >GDPP (0.11) >TI (0.11). The coefficient of GDPP has a positive effect on $PM_{2.5}$ concentrations in Southwest and Northwest China (21.03%), while North, Northeast and East China showed a negative driving relationship. The SI coefficient was mainly positive (94.05% of the total number of cities), which was negatively correlated only in the underdeveloped western region, while positively correlated in the central and eastern regions. The TI coefficient range from −0.63 to 0.26. Positively driven cities (67.46% of the total) were mainly distributed in North, Northeast and East China, but the number of cities is significantly lower than that of SI (94.05%). In particular, PD coefficient was positive throughout the region and vary considerably (0.04 to 6.93).There was an increasing trend from southeast to northwest. The lowest region was located in Guangdong and Fujian, the highest region was distributed Tibet, Inner Mongolia, Gansu and Xinjiang (Figure 5).

## 3.5. Temporal characteristics of driving factors

The result of the GTWR model demonstrated that the capability of driving factor was different in time scale (Figure 6). The coefficient value of the eight driving factors was between −0.50 and 0.71 in the whole region. PD (0.55) was highest average positive driving factor, followed by SI. The highest negative driving factor was PCP (−0.42), followed by WS, and the absolute values of the average coefficient of the other factors were all less than 0.05. From the analysis of the time trend, PD has the obvious downward trend (*slope* = 0.07), WS has the significantly

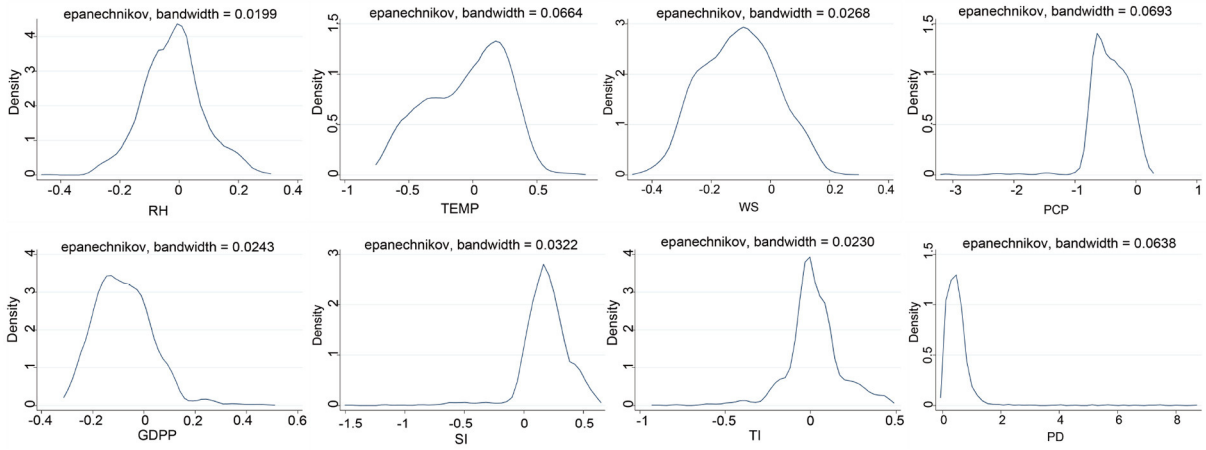


FIGURE 4
Kernel density distribution of each variable coefficient.

upward trend (*slope* = 0.06), and the trends in other factors were not significant ($|slope| \leq 0.04$).

From 2015 to 2019, the coefficient ranges of driving factors in Northeast and North China were −0.77 ∼ 0.75 and −0.76 ∼ 0.91, respectively (Figure 6). Positive driving factors of highest average value were PD (0.60, 0.67) in these two regions, followed by SI (0.22, 0.29) and TEMP (0.21, 0.32). The highest negative factor was PCP (−0.42, −0.76) in these two regions. Negative driving factors included WS (−0.15), GDPP (−0.14) and RH (−0.08) in Northeast China and included GDPP (−0.18) and RH (−0.07) in North China, the slope of other factors tend to be stable. From the analysis of the time change trend, the coefficient of PD and SI has obvious downward trend in Northeast China (*slope* = −0.04), PCP and WS has an upward trend (*slope* = 0.13, 0.06), and the annual trend of RH, TEMP, GDPP and SI were no obvious ($|slope| \leq 0.02$). In North China, PD and SI had obvious downward trend (both *slope* = −0.04), PCP and WS had an upward trend (*slope* = 0.13, 0.06), the annual trend of RH, TEMP, GDPP, SI were no obvious ($|slope| \leq 0.02$).

The coefficient ranges of driving factors in East, Central and South China were −0.60 ∼ 0.44, −0.59 ∼ 0.53 and −0.63 ∼ 0.19 from 2015 to 2019 (Figure 6). The driving factor of the highest positive coefficient was PD (0.31, 0.37, 0.10) in the three regions, followed by SI. PCP (−0.51, −0.47) was the driving factor with the highest negative coefficient in East and Central China. The driving factor of the highest negative coefficient was TEMP (−0.46) in South China. The coefficients of SI and PD decreased significantly from 2015 to 2019 (*slope* = −0.04, −0.03) in East China. The coefficients of PD in Central and South China had a relatively obvious downward trend (*slope* = −0.06, −0.03). The coefficients of WS and TEMP had an obvious upward trend in East, Central and South China. The change trends of the other driving factors were no obvious ($|slope| \leq 0.03$).

The coefficient ranges of driving factors were −0.32 ∼ 0.94 and −0.77∼1.70 in the southwest and northwest regions from 2015 to 2019 (Figures 6G,H and Supplementary Figure S2). The driving factors of highest average positive coefficient were both PD (0.66, 1.4) in these regions, followed by GDPP (0.06) and TEMP (0.14,) respectively. The driving factor of the highest negative was PCP (−0.15,−0.60) in both the southwest and northwest, while other driving factors were no obvious ($|slope| \leq 0.08$). The coefficient of PD decreased significantly in the southwest and northwest from 2015 to 2019 (*slope* = −0.12, −0.14). The coefficients of TEMP and WS in the southwest region had an upward trend (*slope* = 0.07). The trends of the other driving factors were insignificant ($|slope| \leq 0.04$).

The distribution characteristics of nuclear density of each coefficient are given in Figure 7. The change of left-biased peak distribution of RH was not obvious from 2015 to 2017, and it was concentrated in positive values in 2018, whereafter the largest density of coefficients of RH was distributed at −0.4 in 2019. The temperature coefficient shown a bimodal distribution, with a main peak of about 0.3, which indicates that the rising temperature will increase the concentration of $PM_{2.5}$ in most cities. The coefficient of PCP was left-distributed during 2015∼2019, but the peak has shifted significantly to the right in 2019, indicating that the negative driving ability was weakening. The coefficient of WS showed a multi-peak distribution from 2015 to 2019, except that the peak distribution was negative in 2018. Among the four socioeconomic factors, the GDPP coefficient showed a multi-peak distribution from 2015 to 2019. The main peak was promotion effect in 2015, and then turned negative. The coefficient of SI and TI showed a multi-peak distribution from 2015 to 2019, compared with the TI, the coefficient of SI showed a right distribution, and the coefficient of TI showed a double distribution, which was close to zero,

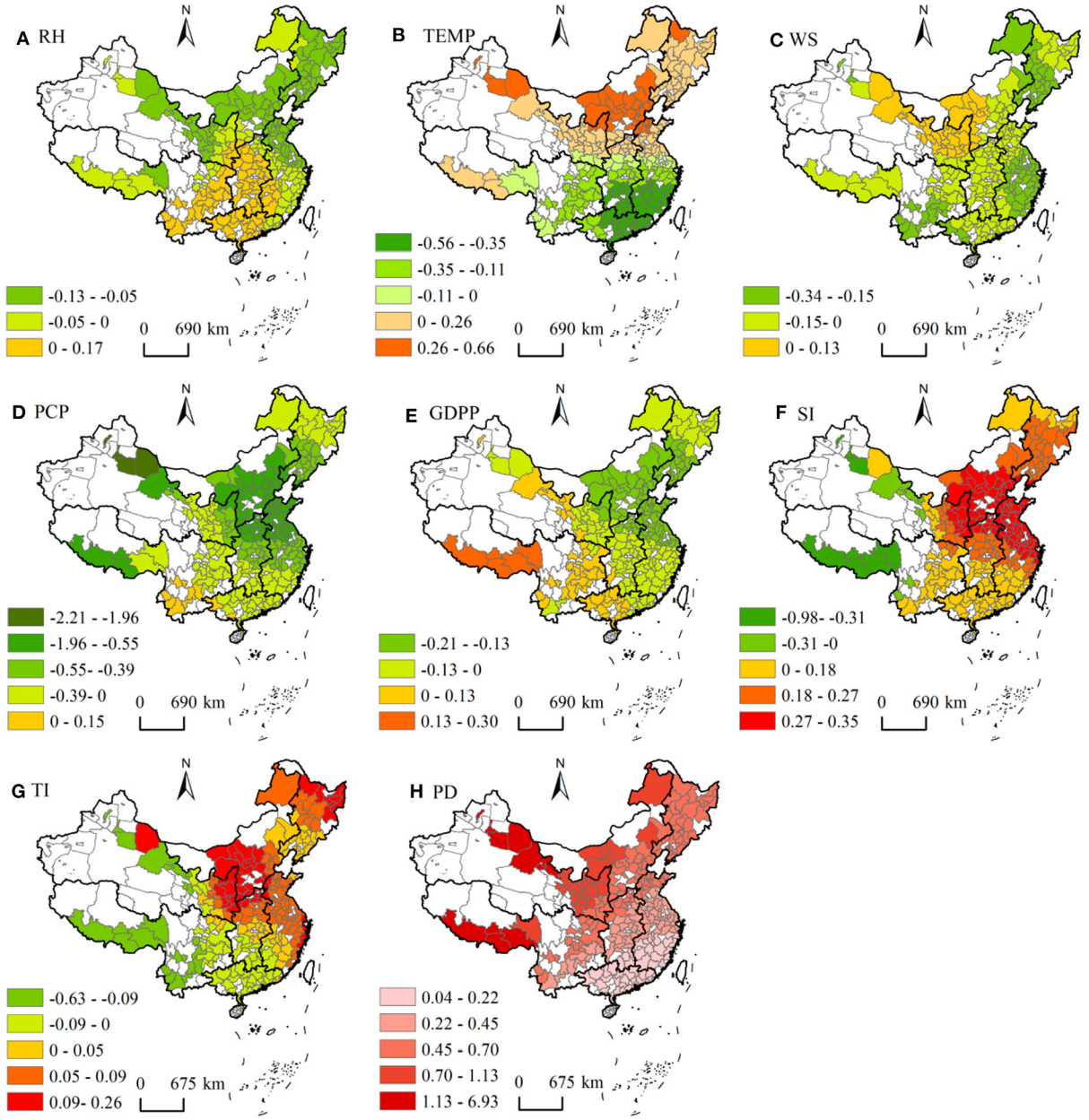


FIGURE 5
Spatial distribution of coefficients for each driving factor **(A)** Relative humidity, **(B)** Temperature, **(C)** Wind speed, **(D)** Precipitation, **(E)** per capita GDP, **(F)** Secondary industry share, **(G)** Tertiary Industry share, and **(H)** Population density; The white area represents no data.

indicating that the contribution of TI to $PM_{2.5}$ is smaller than that of SI. The coefficients of PD had almost no negative values during 2015∼2019, and had a multi-peak distribution.

Generally, among the natural factors selected in this study, except that temperature had obvious positive and negative driving effects on $PM_{2.5}$ concentrations, the driving effects of PCP, WS and RH were mainly negative. In socioeconomic factors, GDPP and $PM_{2.5}$ concentrations was two-way driving, PD, SI and TI had significant positive driving effects on $PM_{2.5}$. The order of driving capability was PD >PCP >TEMP >SI >WS >TI >GDPP >RH. The coefficient of PD decreased most obvious in the whole study period (*slope*=−0.07), and the coefficients of SI and GDPP were decreased slightly, yet the coefficients of WS and TEMP showed an upward trend (0.06, 0.04; Supplementary Table S3). Using the global multiple regression model, a similar conclusion was reached, namely PD

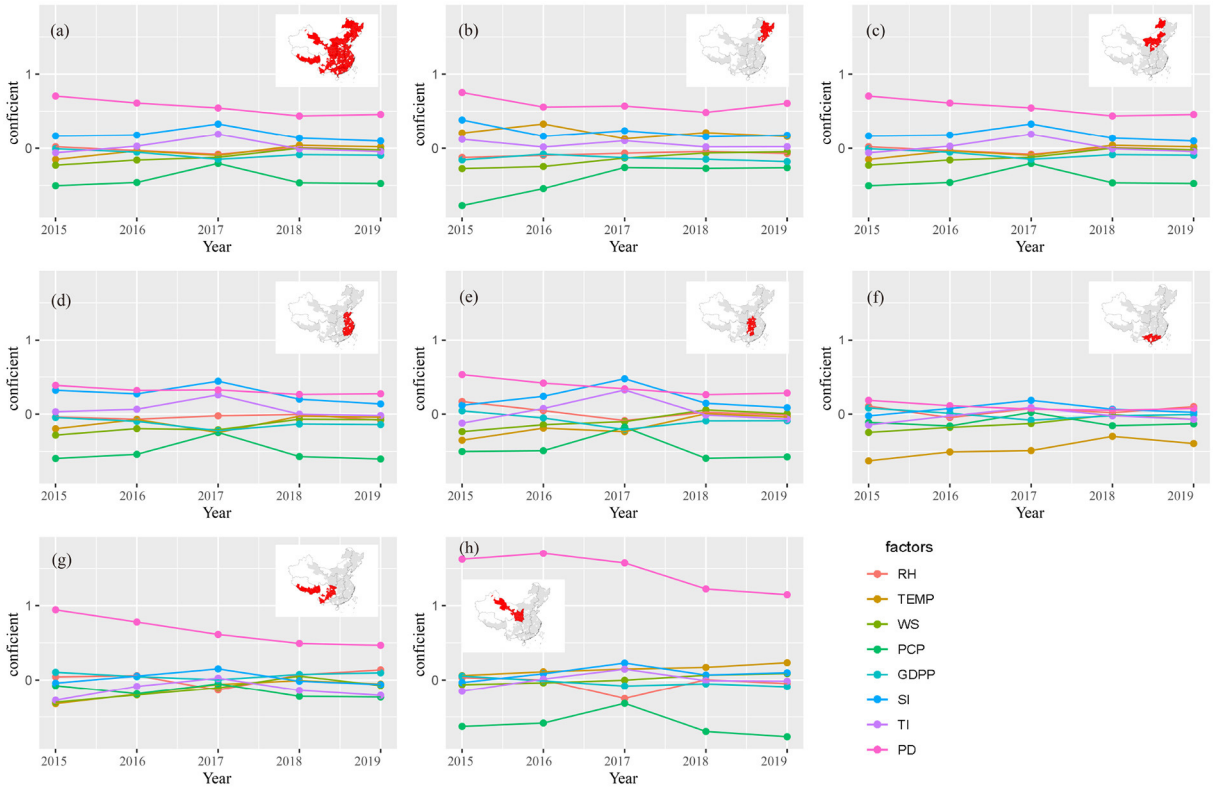


FIGURE 6
Trends in driving capability of each factor in different spaces from 2015 to 2019 **(a)** Whole region, **(b)** Northeast China, **(c)** North China, **(d)** East China, **(e)** Central China, **(f)** South China, **(g)** Southwest China, and **(h)** Northwest China.

(positive) and PCP (negative) were the first two drivers of $PM_{2.5}$ concentrations ($p < 0.001$; Supplementary Table S4).

## 4. Discussion

This research presented that the $PM_{2.5}$ concentrations in different areas decreased with varying degrees, with an average decrease of 3.58 $\mu g\ m^{-3}\ a^{-1}$. The series actions of energy-saving, emission-reduction and clean air proposed by the government in recent years have received some achievement. Central and East China with the higher mean $PM_{2.5}$ concentrations have higher population densities, developed industries, intensive human activities and particulate matter emissions. The $PM_{2.5}$ concentrations in North and central China hugely dropped may because that the developed industrial, agriculture and intensive human activities was controlled by the above actions.

Many previous studies have concluded that the severely polluted areas in China by $PM_{2.5}$ were located in Beijing, Tianjin and Hebei and the surrounding areas (35, 42, 43). Some studies have also shown that Xinjiang has high concentrations of $PM_{2.5}$ in China (44–47). North China was not the region with the highest $PM_{2.5}$ concentrations in this study because it included Inner Mongolia and other areas with relatively low $PM_{2.5}$ concentrations. The difference of these results may be due to the spatial scale. In addition, the lack of data in parts of Xinjiang also has some impact on the overall results of the country.

We demonstrated that the capacity of driving factors was PD >PCP >TEMP >SI >WS >TI >GDPP >RH. PD was the positive main driving factor, indicating that the increase of population density will lead to the rise of $PM_{2.5}$ concentrations. The higher population density is frequently accompanied by high emissions from household activities (e.g., cooking, heating and smoking) and local transportation (48, 49). Besides, the traffic congestion caused by population agglomeration is unfavorable for the complete combustion of motor fuel (50). In addition, the region with higher population density is often accompanied by dense buildings, which is not conducive to the diffusion of $PM_{2.5}$. The rational layout and design of urban buildings could promote the dispersion of pollutants and improve air quality (51), but the diffusion capacity of $PM_{2.5}$ is rarely specified in urban building design. Exposure risk of toxic pollutants in

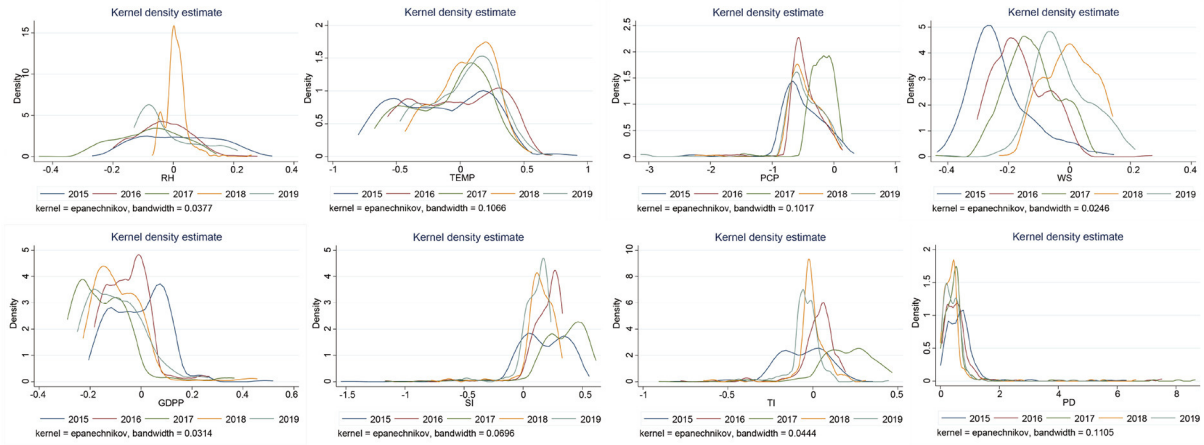


FIGURE 7
Kernel density distribution of each variable coefficient in different year.

densely populated areas is higher than that in sparsely populated areas (46). Therefore,we should pay attention to the effect of population density on $PM_{2.5}$ concentrations.

PCP and RH were the negative main driving factors in this study, possibly because that they can enhance airborne $PM_{2.5}$ condensation and deposition, thus reducing $PM_{2.5}$ concentrations (52). SI had a positive driving effect on $PM_{2.5}$ in most areas. It is well known that SI is dominated by heavy industries such as machinery, chemicals, and energy, and that it is the primary source of pollutants in the atmosphere. We found that the driving coefficient of the TI (0.11) was obvious small than that of the SI (0.22), which indicated that the TI also had a positive driving effect on $PM_{2.5}$, but its driving capacity was equivalent to half of that of the SI. The nonlinear relationship occurred between GDPP and $PM_{2.5}$ concentrations, such as $PM_{2.5}$ concentrations in developed eastern regions was being controlled by advances in science and technology, as well as the optimization of industrial structure. Similar research conclusion has previously been discovered (26). Therefore, to ensure economic development while controlling pollution, the government should formulate waste emission standards, strengthen supervision and law enforcement, gradually optimize the industry, transition from SI to TI, implement strict emission standards, and compel polluting industrial enterprises to improve production capacity. Furthermore, regional industrial development should take into account the carrying capacity of the local natural environment, particularly fragile areas like the northwest.

The driving capability of PD was descending in space from northwest to southeast, which was reverse with the spatial distribution of population density. This might be because the ecological environment in Northwest China was more fragile, the environmental carrying capacity was lower, the available land was limited, and the industrial and agricultural activities were more concentrated. This study discovered that precipitation driving capability was significantly stronger in the north than that in the south, probably because the abundant rainfall in the south and the $PM_{2.5}$ condensed has reached the threshold. Therefore, the precipitation appears to be more important for $PM_{2.5}$ deposition in the north of China compared to the south China, due to the little rainfall, the dry climate, and the lower vegetation cover. Similar findings have been found in previous studies, which are subject to the law of diminishing marginal effect (53, 54). The result in this study is generally consistent with the that of previous studies (55).

In this study, the region of positive driving of temperature was mainly distributed in the north China and the Qinghai-Tibet Plateau with the lower annual-average temperature. The possible reason was that the annual-average temperature in these regions was relatively lower, and the increase in temperature on the flow of the atmosphere was not enough to make $PM_{2.5}$ diffusion, instead, promoting the flow of dry surface particulate matter. On the contrary, even though the temperature was high in the southern region, the diffusion ability was enhanced, but the small surface dust is conducive to lower the $PM_{2.5}$ concentrations. The driving capability of WS was stronger in the north than that in the south (Figure 4), it may be caused by flat terrain in the north which provides better diffusion conditions for atmospheric pollutants, and the increase in wind speed is more conducive to the diffusion of $PM_{2.5}$, thereby improving regional air pollution (56). It is worth noting that WS has a stronger positive driving effect on $PM_{2.5}$ concentrations in central and western Inner Mongolia, Xinjiang, Shaanxi, Gansu, and northeastern Sichuan. Due to these regions located on the Loess Plateau or the edge of the desert, the soil is relatively loose. When the wind speed reaches a certain level, it will also

roll up loose dust on the ground, resulting in an increase in the concentrations of $PM_{2.5}$ in the downwind area (22). The relationship of GDPP and $PM_{2.5}$ concentrations were negative correlation in the central and eastern regions of China, especially in the Bohai Bay economic zone. While there was a weak positive correlation in the central and western regions, indicating that pollution may decrease as per capita GDP increases (57).

The two regions with the largest decrease in $PM_{2.5}$ concentrations were North and Central China (*slope* = -3.99 $\mu g\ m^{-3}\ a^{-1}$, *slope* = -3.41 $\mu g\ m^{-3}\ a^{-1}$) (Figures 1, 2). Central China was the region with the highest mean $PM_{2.5}$ concentrations in this study, and many studies have shown that Beijing-Tianjin-Hebei in North China has always been a high-value area of $PM_{2.5}$ in China (53, 54). The two regions are located in mid-eastern region of China and are more developed in industry and agriculture. There are slight differences (relative humidity stabilized, temperature increased slightly, and precipitation and wind speed slightly decreased) in trends of four natural factors in North China. The trend of GDPP was increased, the trends of SI and PD decreased significantly, and the trend of TI was no significant. The main negative driving factors (PCP, RH, WS) and positive driving factors (PD, SI) showed a trend of decreasing in two regions, which indicated that the decline reason of $PM_{2.5}$ concentrations might be due to the capability weakening of the positive driving factors (PD, SI). However, trends of TEMP and WS in Central China were opposite (weakly increased in North China and weakly reduced in Central China) that in North China, and the other factors were the similar (Supplementary Figure S4), but the driving directions of TEMP and WS were different in these regions, indicating that the causes of $PM_{2.5}$ concentrations decrease in Central and North China were similarly. This result further shows that in the case of constant or even adverse natural factors, a series of emission reduction measures introduced by the state after 2013, such as increasing green area, limiting vehicles, industrial emission purification, coal gasification in heating facilities, and industrial transformation, can alleviate or even cover up the impact of population density increase on the increase of $PM_{2.5}$ concentrations.

Overall, this study found that the annual-average values of the main negative driving factors (PCP and RH) showed a downward trend (-42.78mm·$a^{-1}$, –0.39%· $a^{-1}$), and the trends of WS and TEMP did not change significantly (0.01m·$s^{-1}$· $a^{-1}$) (Supplementary Figure S4), indicating that natural factors were not particularly favorable for driving the decrease of $PM_{2.5}$ concentrations. Among the socioeconomic factors, except Northeast China, the trend of PD in other regions was rise, the trend of SI was decline significantly (-1.21%· $a^{-1}$), while the trend of TI was increase (0.78%· $a^{-1}$) (Supplementary Table S2). However, the positive main driving factor (PD) showed an upward trend, but the driving force of PD showed a significantly downward trend. The shift trend of industrial structure was from the secondary industry to the tertiary industry (the driving capacity of the secondary industry was higher that of the tertiary industry). It further demonstrated that the main reason for the decrease of $PM_{2.5}$ concentrations may be the weakening of the driving ability of positive driving factor (PD) and the transfer from secondary industry to tertiary industry.

## 5. Conclusions

We comprehensively analyzed the spatial-temporal characteristic of $PM_{2.5}$ and investigated the factors influencing $PM_{2.5}$ concentrations by natural and socioeconomic factors in China. The results showed that 1) The mean $PM_{2.5}$ concentrations was 37.55 ± 15.62 $\mu g\ m^{-3}$ during 2015-2019, the decreasing trend of $PM_{2.5}$ concentrations was 3.58 $\mu g\ m^{-3}\ a^{-1}$, a decrease of 26.49% in 2019 compared to 2015, The regions with higher concentrations were mainly distributed in North China and South China, which were also the regions with the greatest decline in 5 years. 2) The capability of driving factors was PD >PCP >TEMP >SI >WS >TI >GDPP >RH, and the driving capability of socioeconomic factors on $PM_{2.5}$ was slightly higher than that of natural factors. The strongest positive and negative driving factors were population density and precipitation, respectively. 3) North China and Central China were the two regions with the largest decreases in $PM_{2.5}$ in the country from 2015 to 2019. The decrease in $PM_{2.5}$ concentrations is primarily due to the implementation of a series of energy-saving and emission-reduction control measures after the Action Plan, such as clean air action and the adjustment of industrial structures by secondary and tertiary industries, which effectively offsets the impact of rising population density on $PM_{2.5}$ concentrations.

The analysis above revealed that we should reduce $PM_{2.5}$ concentration by improving socio-economic factors rather than waiting for natural factors to change. The industrial structure should be actively regulated and gradually changed from secondary to tertiary industry under the condition of ensuring stable economic growth, which is an important measure to ensure the socioeconomic effect while reducing $PM_{2.5}$ concentrations. In the future, we must formulate a reasonable population policy so that population growth can be adapted to regional development, especially ecologically sensitive areas. In addition to we must consider environmental carrying capacity in urban planning and construction, balance population distribution, and other factors. Government departments should continue to develop and implement energy conservation and emission reduction measures in China, particularly densely populated areas, achieving win-win between economic development and environmental management.

## Data availability statement

The original contributions presented in the study are included in the article/Supplementary material, further inquiries can be directed to the corresponding author.

## Author contributions

YS: conceptualization, methodology, writing—original draft, and writing—review and editing. QC: methodology, formal analysis, and writing—review and editing. SY: data curation, methodology, writing—original draft, and writing—review and editing. PW: methodology, investigation, writing—review and editing, and supervision. BW: investigation and writing—review and editing. SZ: writing—review and editing. All authors contributed to the article and approved the submitted version.

## Funding

This work was supported by the National Natural Science Foundation of China (42167013).

## Conflict of interest

The authors declare that the research was conducted in the absence of any commercial or financial relationships that could be construed as a potential conflict of interest.

## Publisher's note

All claims expressed in this article are solely those of the authors and do not necessarily represent those of their affiliated organizations, or those of the publisher, the editors and the reviewers. Any product that may be evaluated in this article, or claim that may be made by its manufacturer, is not guaranteed or endorsed by the publisher.

## Supplementary material

The Supplementary Material for this article can be found online at: https://www.frontiersin.org/articles/10.3389/fpubh.2022.1051116/full#supplementary-material

## References

1. Canh NP, Hao W, Wongchoti U. The impact of economic and financial activities on air quality: a Chinese city perspective. *Environ Sci Pollut Res*. (2021) 28:8662–80. doi: 10.1007/s11356–020-11227-8

2. Fang Z, Wu PY, Lin YN, Chang TH, Chiu Yh. Air pollution's impact on the economic, social, medical, and industrial injury environments in China. *Healthcare*. (2021) 9:261. doi: 10.3390/healthcare9030261

3. Guo Q, Wang Y, Zhang Y, Yi M, Zhang T. Environmental migration effects of air pollution: micro-level evidence from China. *Environ Pollut*. (2022) 292:118263. doi: 10.1016/j.envpol.2021.118263

4. Malley CS, Lefèvre EN. Measurement-based assessment of the regional contribution and drivers of reduction in annual and daily fine particulate matter impact metrics in Paris, France (2009-2018). *Atmos Environ*. (2019) 211:38–54. doi: 10.1016/j.atmosenv.2019.04.061

5. Fu Z, Li R. The contributions of socioeconomic indicators to global $PM_{2.5}$ based on the hybrid method of spatial econometric model and geographical and temporal weighted regression. *Sci Total Environ*. (2020) 703:135481. doi: 10.1016/j.scitotenv.2019.135481

6. Ho CC, Chen LJ, Hwang JS. Estimating ground-level $PM_{2.5}$ levels in Taiwan using data from air quality monitoring stations and high coverage of microsensors. *Environ Pollut*. (2020) 264:114810. doi: 10.1016/j.envpol.2020.114810

7. Song Y, Xu T. The threshold and spatial effects of $PM_{2.5}$ pollution on resident health: evidence from China. *Front Public Health*. (2022) 10:908042. doi: 10.3389/fpubh.2022.908042

8. Jedrychowski WA, Perera FP, Spengler JD, Mroz E, Stigter L, Flak E, et al. Intrauterine exposure to fine particulate matter as a risk factor for increased susceptibility to acute broncho-pulmonary infections in early childhood. *Int J Hyg Environ Health*. (2013) 216:395–401. doi: 10.1016/j.ijheh.2012.12.014

9. Kim JB, Prunicki M, Haddad F, Dant C, Sampath V, Patel R, et al. Cumulative lifetime burden of cardiovascular disease from early exposure to air pollution. *J Am Heart Assoc*. (2020) 9:e014944. doi: 10.1161/JAHA.119.014944

10. Coker ES, Cavalli L, Fabrizi E, Guastella G, Lippo E, Parisi ML, et al. The effects of air pollution on COVID-19 related mortality in northern Italy. *Environ Resour Econ*. (2020) 76:611–34. doi: 10.1007/s10640–020–00486-1

11. Yang L, Hong S, He C, Huang J, Ye Z, Cai B, et al. Spatio-temporal heterogeneity of the relationships between $PM_{2.5}$ and its determinants: a case study of Chinese cities in winter of 2020. *Front Public Health*. (2022) 10:810098. doi: 10.3389/fpubh.2022.810098

12. Van Donkelaar A, Martin RV, Li C, Burnett RT. Regional estimates of chemical composition of fine particulate matter using a combined geoscience-statistical method with information from satellites, models, and monitors. *Environ Sci Technol*. (2019) 53:2595–611. doi: 10.1021/acs.est.8b06392

13. Lim CH, Ryu J, Choi Y, Jeon SW, Lee WK. Understanding global $PM_{2.5}$ concentrations and their drivers in recent decades (1998-2016). *Environ Int*. (2020) 144:106011. doi: 10.1016/j.envint.2020.106011

14. Shanmuga Priyan R, Peter AE, Menon JS, George M, Shiva Nagendra S, Khare M. Vertical distribution of PM10 and $PM_{2.5}$ emission sources and chemical composition during winter period in Delhi city. *Air Quality Atmosphere Health*. (2022). 15:255–271. doi: 10.1007/s11869–021–01092-w

15. Pak U, Ma J, Ryu U, Ryom K, Juhyok U, Pak K, et al. Deep learning-based $PM_{2.5}$ prediction considering the spatiotemporal correlations: a case study of Beijing, China. *Sci Total Environ*. (2020) 699:133561. doi: 10.1016/j.scitotenv.2019.07.367

16. Yu GH, Park S. Chemical characterization and source apportionment of $PM_{2.5}$ at an urban site in Gwangju, Korea. *Atmospheric Pollut Res*. (2021) 12:101092. doi: 10.1016/j.apr.2021.101092

17. Gui K, Che H, Wang Y, Wang H, Zhang L, Zhao H, et al. Satellite-derived $PM_{2.5}$ concentration trends over Eastern China from 1998 to 2016: relationships to emissions and meteorological parameters. *Environ Pollut*. (2019) 247:1125–33. doi: 10.1016/j.envpol.2019.01.056

18. Han X, Li H, Liu Q, Liu F, Arif A. Analysis of influential factors on air quality from global and local perspectives in China. *Environ Pollut*. (2019) 248:965–79. doi: 10.1016/j.envpol.2019.02.096

19. Timmermans R, Kranenburg R, Manders A, Hendriks C, Segers A, Dammers E, et al. Source apportionment of $PM_{2.5}$ across China using LOTOS-EUROS. *Atmosph Environ*. (2017) 164:370–86. doi: 10.1016/j.atmosenv.2017.06.003

20. Wang S, Liu X, Yang X, Zou B, Wang J. Spatial variations of $PM_{2.5}$ in Chinese cities for the joint impacts of human activities and natural conditions: a global and local regression perspective. *J Cleaner Product*. (2018) 203:143–52. doi: 10.1016/j.jclepro.2018.08.249

21. Zhang R, Wang G, Guo S, Zamora ML, Ying Q, Lin Y, et al. Formation of urban fine particulate matter. *Chem Rev*. (2015) 115:3803–55. doi: 10.1021/acs.chemrev.5b00067

22. Yang X, Wang S, Zhang W, Zhan D, Li J. The impact of anthropogenic emissions and meteorological conditions on the spatial variation of ambient $SO_2$ concentrations: a panel study of 113 Chinese cities. *Sci Total Environ*. (2017) 584:318–28. doi: 10.1016/j.scitotenv.2016.12.145

23. Kim E, Kim BU, Kim HC, Kim S. Direct and cross impacts of upwind emission control on downwind $PM_{2.5}$ under various NH3 conditions in Northeast Asia. *Environ Pollut*. (2021) 268:115794. doi: 10.1016/j.envpol.2020.115794

24. Nguyen TH, Nagashima T, Doan QV. Air quality modeling study on the controlling factors of fine particulate matter ($PM_{2.5}$) in Hanoi: a case study in December 2010. *Atmosphere*. (2020) 11:733. doi: 10.3390/atmos11070733

25. Zhao L, Zhang X, Zhao F. The impact of high-speed rail on air quality in counties: econometric study with data from southern Beijing-Tianjin-Hebei, China. *J Clean Prod*. (2021) 278:123604. doi: 10.1016/j.jclepro.2020.123604

26. Apergis N, Ozturk I. Testing environmental Kuznets curve hypothesis in Asian countries. *Ecol Indic*. (2015) 52:16–22. doi: 10.1016/j.ecolind.2014.11.026

27. Buehn A, Farzanegan MR. Hold your breath: a new index of air pollution. *Energy Econ*. (2013) 37:104–13. doi: 10.1016/j.eneco.2013.01.011

28. Sica E, Sušnik S. Geographical dimension and environmental Kuznets curve: the case of some less investigated air pollutants. *Appl Econ Lett*. (2014) 21:1010–6. doi: 10.1080/13504851.2014.904485

29. Li G, Fang C, He S. The influence of environmental efficiency on $PM_{2.5}$ pollution: evidence from 283 Chinese prefecture-level cities. *Sci Total Environ*. (2020) 748:141549. doi: 10.1016/j.scitotenv.2020.141549

30. Wang Y, Liu C, Wang Q, Qin Q, Ren H, Cao J. Impacts of natural and socioeconomic factors on $PM_{2.5}$ from 2014 to 2017. *J Environ Manag*. (2021) 284:112071. doi: 10.1016/j.jenvman.2021.112071

31. Zhao S, Yin D, Yu Y, Kang S, Qin D, Dong L. $PM_{2.5}$ and O3 pollution during 2015-2019 over 367 Chinese cities: Spatiotemporal variations, meteorological and topographical impacts. *Environ Pollut*. (2020) 264:114694. doi: 10.1016/j.envpol.2020.114694

32. Zhao Y, Wang L, Huang T, Tao S, Liu J, Gao H, et al. Unsupervised $PM_{2.5}$ anomalies in China induced by the COVID-19 epidemic. *Sci Total Environ*. (2021) 795:148807. doi: 10.1016/j.scitotenv.2021.148807

33. Zhou X, Strezov V, Jiang Y, Kan T, Evans T. Temporal and spatial variations of air pollution across China from 2015 to 2018. *J Environ Sci*. (2022) 112:161–9. doi: 10.1016/j.jes.2021.04.025

34. Wang Y, Gao W, Wang S, Song T, Gong Z, Ji D, et al. Contrasting trends of $PM_{2.5}$ and surface-ozone concentrations in China from 2013 to 2017. *Natl Sci Rev*. (2020) 7:1331–9. doi: 10.1093/nsr/nwaa032

35. Shi G, Liu J, Zhong X. Spatial and temporal variations of $PM_{2.5}$ concentrations in Chinese cities during 2015-2019. *Int J Environ Health Res*. (2021) 32:2695–707. doi: 10.1080/09603123.2021.1987394

36. Jia C, Huang W. What causes differences in $PM_{2.5}$ concentration in China? structures are more important. *Econ Finan Lett*. (2022) 9:28–39. doi: 10.18488/29.v9i1.2936

37. Anselin L. *Spatial Econometrics: Methods and Models. vol. 4*. Springer Science & Business Media (1988).

38. Huang B, Wu B, Barry M. Geographically and temporally weighted regression for modeling spatio-temporal variation in house prices. *Int J Geograph Inf Sci*. (2010) 24:383–401. doi: 10.1080/13658810802672469

39. Guo B, Wang X, Pei L, Su Y, Zhang D, Wang Y. Identifying the spatiotemporal dynamic of $PM_{2.5}$ concentrations at multiple scales using geographically and temporally weighted regression model across China during 2015-2018. *Sci Total Environ*. (2021) 751:141765. doi: 10.1016/j.scitotenv.2020.141765

40. Rey SJ. Spatial empirics for economic growth and convergence. *Geogr Anal*. (2001) 33:195–214. doi: 10.1111/j.1538-4632.2001.tb00444.x

41. Shi T, Zhang W, Zhou Q, Wang K. Industrial structure, urban governance and haze pollution: spatiotemporal evidence from China. *Sci Total Environ*. (2020) 742:139228. doi: 10.1016/j.scitotenv.2020.139228

42. An Z, Huang RJ, Zhang R, Tie X, Li G, Cao J, et al. Severe haze in northern China: a synergy of anthropogenic emissions and atmospheric processes. *Proc Natl Acad Sci USA*. (2019) 116:8657–66. doi: 10.1073/pnas.1900125116

43. Jiang Z, Jolleys MD, Fu TM, Palmer PI, Ma Y, Tian H, et al. Spatiotemporal and probability variations of surface $PM_{2.5}$ over China between 2013 and 2019 and the associated changes in health risks: an integrative observation and model analysis. *Sci Total Environ*. (2020) 723:137896. doi: 10.1016/j.scitotenv.2020.137896

44. Lu D, Xu J, Yang D, Zhao J. Spatio-temporal variation and influence factors of $PM_{2.5}$ concentrations in China from 1998 to 2014. *Atmosph Pollut Res*. (2017) 8:1151–9. doi: 10.1016/j.apr.2017.05.005

45. Yang D, Wang X, Xu J, Xu C, Lu D, Ye C, et al. Quantifying the influence of natural and socioeconomic factors and their interactive impact on $PM_{2.5}$ pollution in China. *Environ Pollut*. (2018) 241:475–83. doi: 10.1016/j.envpol.2018.05.043

46. Chen J, Zhou C, Wang S, Hu J. Identifying the socioeconomic determinants of population exposure to particulate matter ($PM_{2.5}$) in China using geographically weighted regression modeling. *Environ Pollut*. (2018) 241:494–503. doi: 10.1016/j.envpol.2018.05.083

47. Guo P, Umarova AB, Luan Y. The spatiotemporal characteristics of the air pollutants in China from 2015 to 2019. *PLoS ONE*. (2020) 15:e0227469. doi: 10.1371/journal.pone.0227469

48. Li YJ, Sun Y, Zhang Q, Li X, Li M, Zhou Z, et al. Real-time chemical characterization of atmospheric particulate matter in China: a review. *Atmos Environ*. (2017) 158:270–304. doi: 10.1016/j.atmosenv.2017.02.027

49. Wang Y, Yuan Y, Wang Q, Liu C, Zhi Q, Cao J. Changes in air quality related to the control of coronavirus in China: Implications for traffic and industrial emissions. *Sci Total Environ*. (2020) 731:139133. doi: 10.1016/j.scitotenv.2020.139133

50. Wang S, Zhou C, Wang Z, Feng K, Hubacek K. The characteristics and drivers of fine particulate matter ($PM_{2.5}$) distribution in China. *J Cleaner Product*. (2017) 142:1800–9. doi: 10.1016/j.jclepro.2016.11.104

51. Zhang Y, Gu Z. Air quality by urban design. *Nat Geosci*. (2013) 6:506–506. doi: 10.1038/ngeo1869

52. Blanco-Becerra LC, Gáfaro-Rojas AI, Rojas-Roa NY. Influence of precipitation scavenging on the $PM_{2.5}$/PM10 ratio at the Kennedy locality of Bogotá, Colombia. *Revista Facultad de Ingeniería Universidad de Antioquia*. (2015) 76:58–65. doi: 10.17533/udea.redin.n76a07

53. Li R, Wang Z, Cui L, Fu H, Zhang L, Kong L, et al. Air pollution characteristics in China during 2015-2016: spatiotemporal variations and key meteorological factors. *Sci Total Environ*. (2019) 648:902–15. doi: 10.1016/j.scitotenv.2018.08.181

54. Liu Q, Wu R, Zhang W, Li W, Wang S. The varying driving forces of $PM_{2.5}$ concentrations in Chinese cities: insights from a geographically and temporally weighted regression model. *Environ Int*. (2020) 145:106168. doi: 10.1016/j.envint.2020.106168

55. Wang J, Wang S, Li S. Examining the spatially varying effects of factors on $PM_{2.5}$ concentrations in Chinese cities using geographically weighted regression modeling. *Environ Pollut*. (2019) 248:792–803. doi: 10.1016/j.envpol.2019.02.081

56. Wang Y, Chen J, Wang Q, Qin Q, Ye J, Han Y, et al. Increased secondary aerosol contribution and possible processing on polluted winter days in China. *Environ Int*. (2019) 127:78–84. doi: 10.1016/j.envint.2019.03.021

57. Zhou C, Chen J, Wang S. Examining the effects of socioeconomic development on fine particulate matter ($PM_{2.5}$) in China's cities using spatial regression and the geographical detector technique. *Sci Total Enviro*. (2018) 619:436–45. doi: 10.1016/j.scitotenv.2017.11.124

frontiers | Frontiers in Earth Science

TYPE Brief Research Report
PUBLISHED 20 December 2022
DOI 10.3389/feart.2022.1047278



OPEN ACCESS

EDITED BY
Parth Sarathi Mahapatra,
Deutsche Gesellschaft für Internationale Zusammenarbeit (GIZ) GmbH, India

REVIEWED BY
Asish Saha,
University of Burdwan, India
Vignesh Prabhu,
Center for Study of Science, Technology and Policy—CSTEP, India

*CORRESPONDENCE
Hiren Jethva,
hiren.t.jethva@nasa.gov

SPECIALTY SECTION
This article was submitted to Geoscience and Society, a section of the journal Frontiers in Earth Science

RECEIVED 17 September 2022
ACCEPTED 08 December 2022
PUBLISHED 20 December 2022

CITATION
Jethva H (2022), Assessing predictability of post-monsoon crop residue fires in Northwestern India.
*Front. Earth Sci.* 10:1047278.
doi: 10.3389/feart.2022.1047278



# Assessing predictability of post-monsoon crop residue fires in Northwestern India

Hiren Jethva[1,2]*

[1]Morgan State University, Goddard Earth Sciences Technology and Research (GESTAR) II, Baltimore, MD, United States, [2]NASA Goddard Space Flight Center, Greenbelt, MD, United States

Over the past five decades, the Green Revolution in India has been a great success resulting in significantly increased crop yields and food grain productivity. Northwestern India, also known as the country's breadbasket, alone produces two-thirds of the wheat and rice grains under the crop rotation system. Our previous study has shown that the post-monsoon rice crop production in the Punjab state of India has increased by 25%. The crop yields produce proportionate amounts of residue, a large part of which is subjected to burn in the open fields due to the near-absence of a wide-scale, affordable, and environmentally sustainable removal mechanism. A significant increase in crop productivity coincides with a 60% increase in post-harvest crop residue burning during 2002–2016. The study also demonstrated a robust relationship between satellite measurements of vegetation index—a proxy for crop amounts, and post-harvest fires—a precursor of air pollution events, for predicting seasonal agricultural burning. In this report, the efficacy of the proposed prediction model is assessed by comparing the forecasted seasonal fire activity against the actual detection of active fires for the post-monsoon burning seasons of 2017–2021. A simple linear regression model allows efficient prediction of seasonal fire activity within an error of up to 10%. In addition to forecasting seasonal fire activity, the linear regression model offers a practical tool to track and evaluate the effectiveness of the residue management system intended to reduce fire activities and resulting air pollution.

KEYWORDS

**crop residue fires, NDVI, post-monsoon, Northwestern India, prediction, assessment, MODIS**

## 1 Introduction

The movement of the Green Revolution in India, initiated in the 1960s, has brought great success in terms of significantly increased crop yield and productivity, particularly in staple food grains such as wheat, rice, and other crop varieties. This has been achieved through technology adaptation, high-yielding seed varieties, mechanized agricultural machinery, pesticides, fertilizers, expanded acreage, and a dual cropping system (Parayil, 1992; Pingali, 2012). Especially in the heartland of the Green Revolution, the northern states of Punjab and Haryana have seen a multifold increase in the yield and production of

wheat and rice under the crop rotation system in the last several decades (Duxbury, 2001). For instance, the compiled data of crop production by the Punjab University shows an eleven-fold increase in rice crop productivity in Punjab, i.e., ~1 million tons in 1965 to ~11 million tons in 2007. Furthermore, Jethva et al. (2019), using the crop production data compiled by the Ministry of Agriculture and Farmers Welfare, Govt. of India, has shown that rice crop production has increased from ~9 million tons in 2002 to ~13 million tons in 2016, i.e., a net increase in the productivity by 25%.

Prior to the mid-1980s, seasonal crop harvesting in northwestern (NW) India had traditionally been carried out manually. Since then, the practice of manual harvesting has been gradually replaced by the advent of automatic combine harvesters (Singh and Kaskaoutis, 2014). Although mechanized harvesting has reduced labor, machinery leaves a significant part of the crop stem rooted in the ground. Increasing labor cost of manual harvest, the lack of affordable crop residue removal mechanisms that farmers can bear financially, and a shorter time window for preparing the land for the next seasonal crop, are prime reasons behind farmers resorting to burning the residue in open fields (Badarinath et al., 2006).

Several studies published in recent years, using satellite and ground observations, have adequately highlighted the impact of post-monsoon rice straw burning on extreme levels of air pollution affecting one of the most densely populated regions of the world, i.e., Indo-Gangetic Plain (IGP) (Kaskaoutis et al., 2014; Cusworth et al., 2018; Jethva et al., 2018). Using a 15-year-long record (2002–2016) of NASA's A-train satellite observations of thermal anomalies (fires) and aerosols (MODIS, OMI, CALIOP), Jethva et al. (2018) have shown an increasing trend in post-monsoon agricultural fires (~617 per year) and aerosol loading (0.031 and 0.04 per year in aerosol optical depth and UV aerosol index) in November. Furthermore, an intentional delay in the rice growing season from May to June enforced by the Punjab Preservation of Subsoil Water Act 2009 has led to a delay in crop harvesting, followed by the peak residue burning window by about 2 weeks (Jethva et al., 2019; Liu et al., 2021).

In a follow-up study by Jethva et al. (2019), a strong positive trend in fires was attributed to the increased rice crop production by 25%, supported by a net increase in vegetation index (NDVI) by 21%. Concurrently, the post-harvest agricultural fire activity rose by a net ~60%, leading to a nearly 43% increase in aerosol loading over the IGP region. In addition, the ground-level particulate matter ($PM_{2.5}$) downwind over New Delhi also showed a concurrent upward trend of 60%. An increase in crop yields implies the generation of proportionate amounts of residue. The relative ratio, also quantified as residue to crop production ratio (RCR), varies considerably depending on crop type, harvesting practice, and environmental factors (Kumar et al., 2015). Previous studies have estimated RCR values in the range of 1.5–2.25 for rice crops in northern India (Gupta et al., 2004; Badarinath et al., 2006). In other words, the amount of agricultural waste generated post-harvest is estimated to be 1.5 to 2.25 times the actual quantities of the crop. Due to the lack of affordable and effective removal mechanisms, farmers resort to burning crop residue in open fields to clear and prepare the land for the following seasonal crop.

Increasing agricultural fire activities implies greater availability of crop residue to burn, and the generation of agricultural waste is proportional to the crop production amounts reflected in NDVI measurements. Following this hypothesis, Jethva et al. (2019) showed a reasonably well-correlated ($R^2$ = 0.70) long-term relationship between NDVI and seasonally accumulated fire counts over NW India. While earlier studies have examined different aspects of the crop burning issue in NW India, the prediction of the totality of seasonal fire activities wasn't explored until the work of Jethva et al. (2019). The NDVI-fires relationship opened up the possibility of predicting seasonal fire activities in advance by looking at the regional mean NDVI values prior to the onset of the burning season.

In this brief report, the predictability of crop residue fires in NW India, based on the work of Jethva et al. (2019), is assessed for the post-monsoon crop burning seasons of 2017–2021. The accuracy of the predicted seasonal fire activity is evaluated by comparing it to near real-time remote sensing data of thermal anomalies from the Aqua/MODIS sensor. The method section briefly describes the satellite datasets and further refinements applied to the fire counts vs. NDVI relationship. The results section presents the assessment analysis of predicted seasonal fire activity against actual near real-time observations of fire occurrences for the years 2017–2021. Finally, concluding remarks on the findings and future applications are presented in the discussion section.

## 2 Methods

The methodology adopted in Jethva et al. (2019) used the monthly NDVI dataset (product name MYD13C2) and seasonally accumulated fire counts derived from Aqua/MODIS (product name MYD14) for the pre-burning and burning periods, respectively, over NW India. The selection of the geographical boundaries of the study region over NW Indian subcontinent (Longitudes: 74°–77°E, Latitudes: 29°–32°N) was based on the long-term average of active fire detection from MODIS sensor on board Aqua satellite encompassing prominent areas of residue burning in Punjab and Haryana states of India. A further revision of the derived relationship revealed that the use of the 16-day NDVI product (product name MYD13C1) correlates even better with the total fire counts detected during the post-monsoon season (see Figure 1). The 16-day NDVI dataset provides an improved correlation coefficient and standard fitting error of 0.74 and 1,482, respectively, compared to 0.70 and 1,583 obtained using the monthly NDVI dataset. Because of the improved correlation

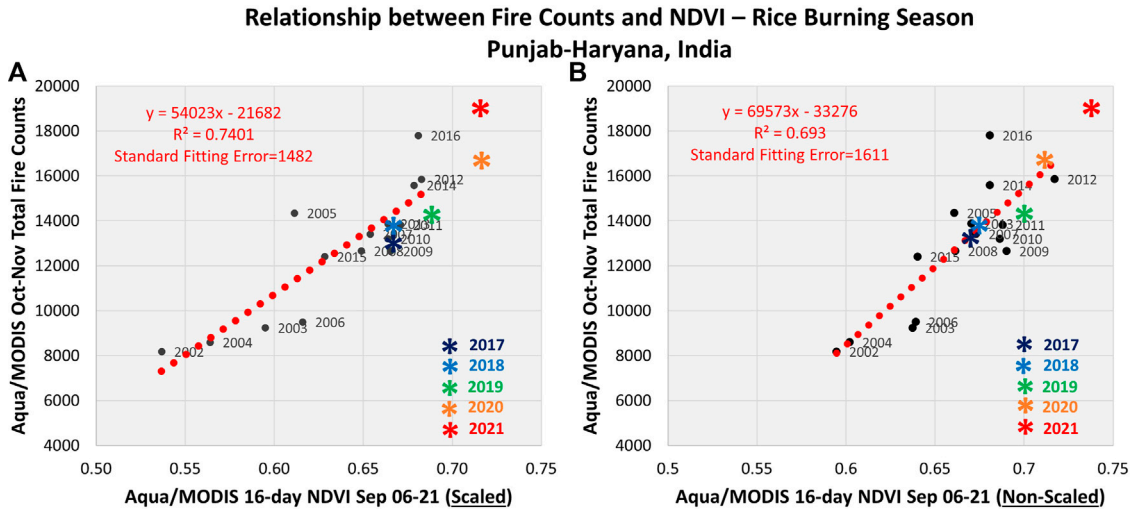


FIGURE 1
Multi-year (2002–2016) relationships between the pre-burning season NDVI and the total number of fire counts during post-monsoon crop burning monthsderived following scaled **(A)** and non-scaled **(B)** methods. See the section Method for the description. Both datasets are derived from Aqua/MODIS sensor over NW India. Black-filled circles show values for individual years, whereas the red dotted line represents a linear regression, the statistical measures of which are given on the top-left of each plot. Color-coded asterisk symbols are values observed for the years 2017–2021 not used in the regression.

and lower fitting error, the 16-day NDVI is correlated with fire counts to assess the accuracy of the proposed linear regression model. The MYD13C1 dataset consists of cloud-free spatial composites of 16-day 1-km MYD13A2 data and is available as a Level 3 product projected on a 0.05 degree (5,600 m) geographic climate model grid (Didan, K., 2015). The dataset was obtained from LP DAAC online data holdings at the URL https://e4ftl01.cr.usgs.gov/MOLA/.

The monthly, area-averaged NDVI dataset used in Jethva et al. (2019) was scaled by a factor that accounts for interannual variations in the spatial extent of NDVI measurements over the crop area. The factor was calculated by normalizing the total number of NDVI measurements for each year with respect to the maximum number of pixels detected during a particular year over the period 2002–2016. In this study, both scaled and non-scaled (simple area averaged without scaling) 16-day NDVI datasets are used to compare their relative performance in predicting seasonal fire counts.

The MODIS Thermal Anomaly/Fire product provides the geolocation of active fire spots and fire radiative power over land at a spatial resolution of 1 $km^2$ × 1 $km^2$. Active fire detection is physically based on the strong emission of mid-infrared radiation from fires used as a signal in a contextual algorithm (Giglio et al., 2003, 2016). The Aqua/MODIS Thermal Anomalies/Fire 5-Min L2 Swath 1-km data MYD14 (Collection 006, Giglio and Justice, 2015), both post-processed (2002–2016) and near-real time (2017–2021), was obtained from the NASA Fire Information for Resource Management System (FIRMS) (https://earthdata.nasa.gov/earth-observation-data/near-real-time/firms). Fire detection pixels flagged with a confidence value of 30%–80% and 80%–100% that correspond to the "nominal" and "high" classes, respectively, were considered in this study.

# 3 Results

## 3.1 Rice residue burning season

Figure 1 displays the multiyear (2002–2016) linear regression relationship between the post-monsoon seasonally accumulated total fire counts (y-axis) observed during the 2-month long burning season (October and November) and 16-day NDVI (x-axis) over the same region for the pre-burning period in September. The black dots represent values for individual years, whereas the red dotted line is a derived linear regression. The results shown here are derived using the scaled (left) and non-scaled (right) NDVI datasets, as described in the method section. The colored asterisk symbols represent observations, not used in the linear regression, in both parameters for the post-monsoon season of 2017 through 2021. Overall, both relationships are found to adequately predict the severity of the residue fire season. However, the differences between the predicted and actual total fire counts remain, which are quantified as % difference and tabulated in Table 1.

Though the scaled version of the relationship delivers better correlation and lower fitting error relative to the non-scaled

**TABLE 1** Values of Aqua/MODIS NDVI for the pre-burning period (September), predicted and actual fire counts for the post-harvest burning season (October and November), and difference (%, predicted-actual) between the latter two for NW India for the years 2017–2021.

| Year | NDVI scaled/non-scaled | Predicted fire counts scaled/non-scaled | Actual fire counts | Difference (%) scaled/non-scaled |
|---|---|---|---|---|
| 2017 | 0.6652/0.6683 | 14,256/13,220 | 13,081 | 8.98/**1.06** |
| 2018 | 0.6612/0.6727 | 14,035/13,526 | 13,825 | **1.52**/−2.16 |
| 2019 | 0.6851/0.6991 | 15,239/15,362 | 14,070 | **8.94**/9.19 |
| 2020 | 0.7091/0.7131 | 16,626/16,336 | 16,751 | **−0.74**/−2.47 |
| 2021 | 0.7066/0.7393 | 16,492/18,159 | 19,188 | −14.05/**−5.36** |

The values derived from both scaled and non-scaled NDVI methods are reported. The % difference numbers printed in bold represent relatively lower error in the prediction between the two methods.

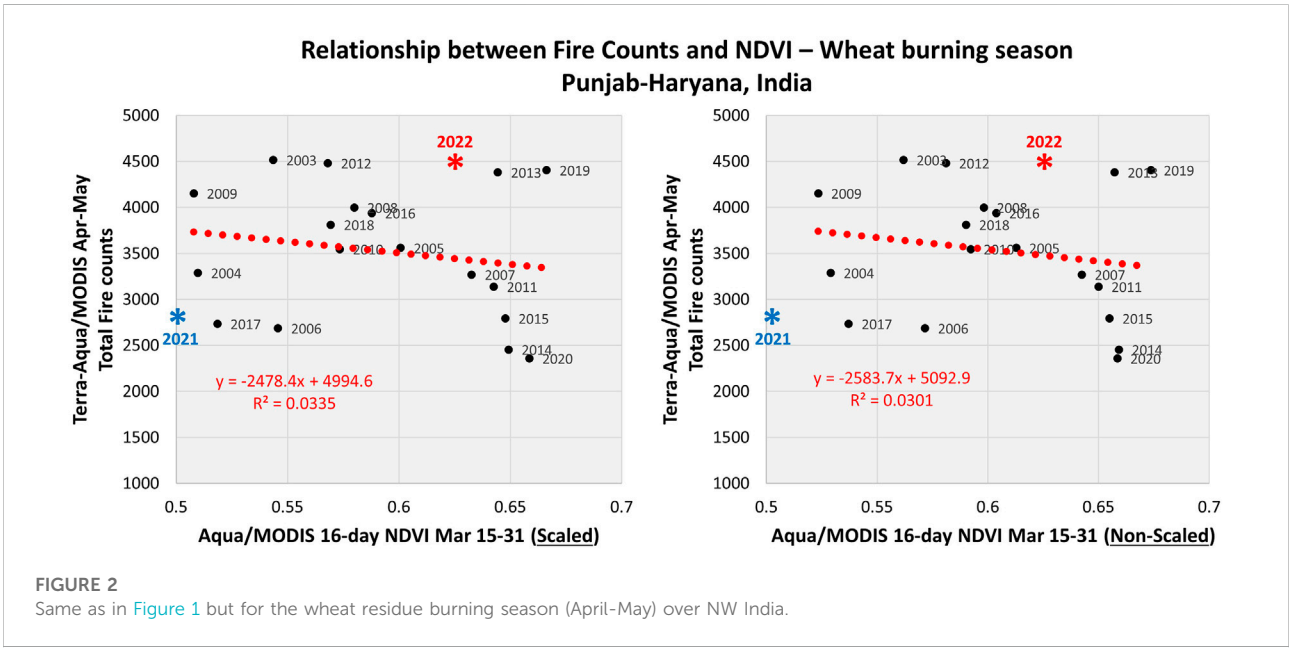


FIGURE 2
Same as in Figure 1 but for the wheat residue burning season (April-May) over NW India.

version, the % error yield with the latter is found to be lower for the years 2017 and 2021. Both methods render similar accuracy in predicting seasonal fires for the years 2018 and 2019. While it is hard to pinpoint the exact reason behind larger errors encountered in the prediction during specific years, the observed spread in the fires-NDVI relationship, thus associated error in the prediction, could be attributed to several factors, including inherent uncertainties in the detection of active fires and derivation of NDVI, cloud cover affecting sampling of both fires and NDVI, unaccounted fire activities occurring before and/or after Aqua overpass time, a saturation of NDVI in dense vegetation canopies, and variabilities in RCR and percentage of total crop residue burned.

Overall, when averaged over the years 2017–2021, the mean error (absolute error) produced by the scaled and non-scaled methods is calculated to be 0.93% (7%) and 0.052% (4%). Regardless of how the NDVI dataset was used, both methods deliver reasonably a good estimate of seasonally accumulated fire counts with an error of up to 10% for 2017–2021.

## 3.2 Wheat residue burning season

Contrary to the rice residue burning during post-monsoon (October-November), the total fire activities during the springtime wheat residue burning season in April-May are noted to be about four to six times lesser (Jethva et al., 2018). Significantly lower residue burning post wheat harvest may be attributed to the usage of residue as fodder and fuel in power generation. An extension of the fire counts vs. NDVI relationship to the wheat crop burning season (2002–2020), shown in Figure 2, reveals no systematic behavior between the two parameters. The linear regression relationships, both scaled

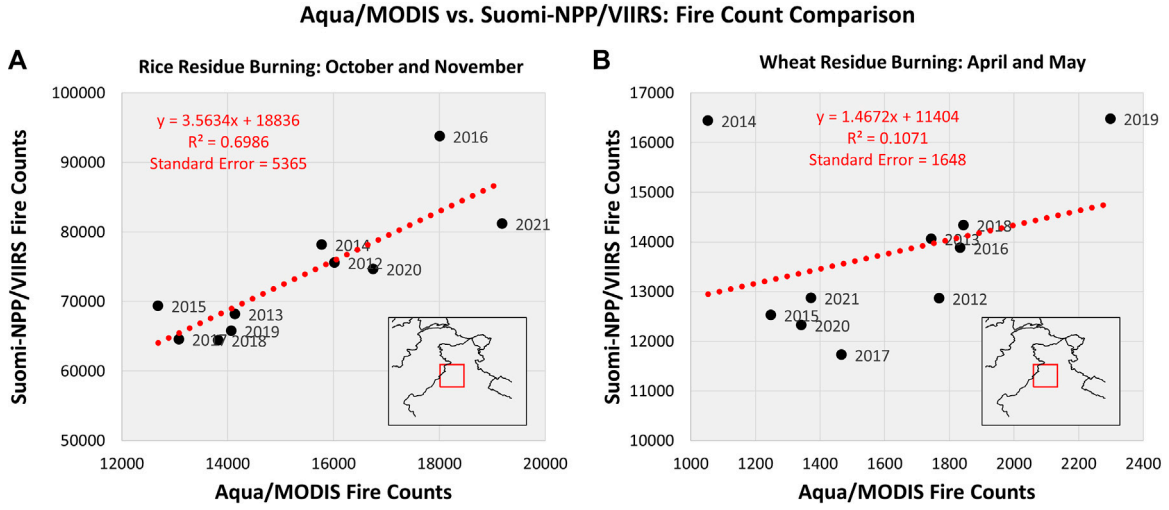


FIGURE 3
Relationship comparing post-monsoon **(A)** and springtime **(B)** total fire detection from Aqua/MODIS and Suomi-NPP/VIIRS sensors over NW India(red box inside an inset map). Thermal anomaly data with confidence levels >30% for MODIS and 'nominal' and 'high' classes for VIIRS are included. Black filled circles show values for individual years (2012-2021), whereas the red dotted line represents a linear regression the statistical measures of which are given at the top left.

and non-scaled, yield poor correlation ($R^2$ = 0.03) with a large spread in data for the individual years around linear fit and a slight negative slope. Since the main focus of the present report is to assess the predictability of fire activities during post-monsoon, a detailed analysis of the wheat crop burning is left out in this report. It demands a separate study involving year-to-year dynamics of crop yield and production, burning practices, and residue usage for other purposes (fodder, power generation, etc.).

## 3.3 Scaling fire detection from MODIS to VIIRS

Since 2012, the VIIRS sensor onboard the Suomi-NPP satellite has provided continuity in the global remote sensing of atmospheric and land parameters, including thermal anomalies. VIIRS detects active fire locations at 375-m resolution—a significant improvement in spatial resolution over MODIS, which provides fire detection at 1-km resolution. Owing to higher spatial resolution, VIIRS is expected to detect smaller-scale fires, which MODIS might miss due to its relatively coarser resolution. The linear regression model developed by Jethva et al. (2019) is based on MODIS observations of NDVI and fire counts. Therefore, it is strictly valid for predicting seasonal fire activity as it would detect by MODIS at a 1-km nominal resolution.

Such a prediction model has not been developed using observations from VIIRS. To extend the seasonal fire prediction to VIIRS, a relationship, as shown in Figure 3, comparing the total fire activity from both sensors over the crop residue burning region of NW India is warranted. The VIIRS thermal anomaly data was accessed from the NASA FIRMS platform. The seasonal fire counts detected during the rice (left) and wheat (right) burning seasons from both sensors over the overlapping period 2012–2021 (black filled circles) are used to derive a linear regression (red dotted line). It shows that VIIRS detects about 3.56 (1.47) times more fire incidences with a positive offset of 18,836 (11,404) than those observed from MODIS for the rice (wheat) residue burning season. The spread of observations around the linear fit can be attributed to how two instruments see the active fires, algorithmic differences, spatial resolution, and temporal changes in fire occurrences between the overpass time (typically within 30 min). Such an empirical relationship comparing fire statistics from two sensors can be helpful in converting MODIS-based fire prediction to that from the VIIRS sensor.

# 4 Discussion

The linear regression model correlating post-monsoon seasonal fire activities and vegetation index NDVI over NW India proposed by Jethva et al. (2019), with refinements applied in this article, offers a practical tool to predict, track, and monitor the severity of the agricultural fire season in advance about one to 2 weeks prior to the onset of a 2-month long burning season. An assessment of the predictability of such an empirical model carried out in this report using the satellite data for the years 2017–2021 shows adequate accuracy of the proposed method, in

which the predicted total fire counts are found to be within 10% of the satellite-observed, near real-time data.

The concerns and general awareness about the seasonal crop residue burning and its detrimental impact on air quality and health in the region have grown in recent years, particularly after the anomalous, elevated levels of residue burning and resulting extreme bad air pollution episodes of post-monsoon 2016. With the growing attention and concern year by year, it is expected that an effective, economical, and farmer-friendly crop residue management policy will be implemented in the region to control and curb seasonal burning activities. Under such a favorable scenario, the proposed empirical prediction model discussed in this report will be further helpful in tracking and monitoring the effectiveness of the residue management policy. For instance, reduced burning activities as a result of the strict implementation of such policies would deviate (underestimation) from the expected seasonal crop fire statistics under the "as usual" scenario derived from the proposed linear model. The difference between the two, beyond the inherent uncertainties in the proposed method, can be interpreted as a net reduction in fire activities.

Beginning the post-monsoon season of 2017, the prediction of the total fire activities over NW India was announced and made available to the authorities, academic and government institutions in India, and the public in general on social media (such as Twitter) prior to the onset of seasonal burning. The Earth Observatory—an outreach platform and a part of the EOS Project Science Office at NASA Goddard Space Flight Center has referred to and highlighted the seasonal forecast values in their story/image of the day articles published around the peak time of the residue burning (first 2 weeks of November) almost every year. One such article for the year 2020 can be accessed at the URL https://earthobservatory.nasa.gov/images/147547/a-busy-season-for-crop-fires-in-northwestern-india.

The early forecast assumes importance in gauging the severity of the fire activities, thereby serving as a guideline for planning and preparedness for better management of extreme air pollution episodes. Furthermore, the prediction of the totality of seasonal fires can be useful to gauge the overall spatiotemporal variations in PM2.5 and aerosol loading over the source as well as in the downwind region by assimilating its spatial and temporal distribution over a two-month long season (based on the patterns observed during previous years) into the regional modelsfor making the short-term to even seasonal forecast. The work presented in the report meets at the intersection of land and atmosphere disciplines of Earth Science. While increasing crop production of the staple grain food of wheat and rice secures the nation's food demand, agricultural practices and crop residue management require urgent attention, particularly in NW India, which is a major contributor to the agricultural output of the country. Until an effective, economical, and farmer-friendly crop residue management is in place, it is expected that farmers, in the wake of no other alternatives, will continue to follow the traditional burning of crop residues in open fields for clearing agricultural land.

The extreme episodes of air pollution resulting from the open field burning of residue in NW India not just affect the source region but encompasses the length and breadth of the populous IGP, as evident from ground instrumentation and satellite maps of aerosol retrievals. The $PM_{2.5}$ concentration measured at ground stations in the region during the peak period of residue burning (i.e., the last week of October and the first 2 weeks of November) often exceeds the 24-h averaged safe guideline value set by WHO (the standards adopted by the Central Pollution Control Board of India) by a factor of 10–30 (8–15), leading to a situation of a public health emergency. Such hazardous level of air pollution is further enhanced by the wintertime meteorology (i.e., colder temperatures, temperature inversion, and shallower boundary layer) coupled with the possible semi-direct effect of smoke aerosols (Mhawish et al., 2022), resulting in the trapping of particulate matter near-surface.

Increasing crop fires and proportionately deteriorating air quality over IGP is a pressing concern. The work presented here stands as scientific evidence urging the policymakers in India to implement an effective, economical, and farmer-friendly crop residue management system towards eliminating the burning practice, which otherwise may continue to be responsible for the seasonal, hazardous air pollution in the region, affecting the health of millions.

## Data availability statement

The MODIS NDVI dataset used in this study can be obtained from the NASA EOSDIS Land Processes Distributed Active Archive Center (LP DAAC) at https://www.earthdata.nasa.gov/eosdis/daacs/lpdaac. The thermal anomaly/fire spots data for MODIS and VIIRS sensors were obtained from the NASA Fire Information for Resource Management System (FIRMS) at https://firms.modaps.eosdis.nasa.gov/. The crop production data mentioned in the paper were accessed from the Crop Production Statistics Information System (http://aps.dac.gov.in/APY/Index.htm) designed and developed by the Agriculture Informatics Division, National Informatics Centre, Ministry of Communication and IT, Government of India. The results derived in this research report can be obtained from the author on request.

## Author contributions

HJ formulated the concept, carried out all analyses presented in this research report, and wrote the

manuscript. The sole author of the manuscript (HJ) conducted the research work independently out of his own research interest and as a follow-up study of the previous two research papers led by him in the same subject matter.

## Acknowledgments

We acknowledge the NASA EOSDIS Land Processes Distributed Active Archive Center (LP DAAC) data portal for the online availability of the 16-day Aqua/MODIS NDVI product (MYD13C1) used in this study. The thermal anomaly/active fire data for MODIS and VIIRS sensors were obtained from the NASA Fire Information for Resource Management System (FIRMS).

## Conflict of interest

The author declares that the research was conducted in the absence of any commercial or financial relationships that could be construed as a potential conflict of interest.

## Publisher's note



## References

Badarinath, K. V. S., Kiran Chand, T. R., and Krishna Prasad, V. (2006). Agriculture crop residue burning in the indo-gangetic plains: A study using irs-P6 AWiFS satellite data. *Curr. Sci.* 91 (8), 1085–1089.

Cusworth, D. H., Mickley, L. J., Sulprizio, M. P., Liu, T., Marlier, M. E., DeFries, R. S., et al. (2018). Quantifying the influence of agricultural fires in northwest India on urban air pollution in Delhi, India. *Environ. Res. Lett.* 13 (4), 044018. doi:10.1088/1748-9326/aab303

Didan, K. (2015). *MYD13C1 MODIS/Aqua vegetation indices 16-day L3 global 0.05Deg CMG V006 [data set]*. South Dakota, United States: NASA EOSDIS Land Processes DAAC.

Duxbury, J. M. (2001). Long-term yield trends in the rice-wheat cropping system. *J. Crop Prod.* 3 (2), 27–52. doi:10.1300/J144v03n02_02

Giglio, L., Descloitres, J., Justice, C. O., and Kaufman, Y. (2003). An enhanced contextual fire detection algorithm for MODIS. *Rem. Sens. Environ.* 87, 273–282. doi:10.1016/S0034-4257(03)00184-6

Giglio, L., and Justice, C. (2015). *MYD14 MODIS/Aqua thermal anomalies/fire 5-min L2 Swath 1km V006 [data set]*. South Dakota, United States: NASA EOSDIS Land Processes DAAC.

Giglio, L., Schroeder, W., and Justice, C. O. (2016). The collection 6 MODIS active fire detection algorithm and fire products. *Rem. Sens. Environ.* 78, 31–41. doi:10.1016/j.rse.2016.02.054

Gupta, P. K., Sahai, S., Singh, N., Dixit, C. K., Singh, D. P., Sharma, C., et al. (2004). Residue burning in rice–wheat cropping system: Causes and implications. *Curr. Sci.* 87 (12), 1713–1717.

Jethva, H., Chand, D., Torres, O., Gupta, P., Lyapustin, A., and Patadia, F. (2018). Agricultural burning and air quality over northern India: A synergistic analysis using NASA's A-train satellite data and ground measurements. *Aerosol Air Qual. Res.* 18, 1756–1773. doi:10.4209/aaqr.2017.12.0583

Jethva, H., Torres, O., Field, R. D., Lyapustin, A., Gautam, R., and Kayetha, V. (2019). Connecting crop productivity, residue fires, and air quality over northern India. *Sci. Rep.* 9, 16594. doi:10.1038/s41598-019-52799-x

Kaskaoutis, D. G., Kumar, S., Sharma, D., Singh, R. P., Kharol, S. K., Sharma, M., et al. (2014). Effects of crop residue burning on aerosol properties, plume characteristics, and long-range transport over northern India. *J. Geophys. Res. Atmos.* 119, 5424–5444. doi:10.1002/2013JD021357

Kumar, P., Kumar, S., and Joshi, L. (2015). *Socioeconomic and environmental implications of agricultural residue burning, A case study of Punjab India*. Springer Briefs in Environmental Science. doi:10.1007/978-81-322-2014-5_2

Liu, T., Mickley, L. J., Gautam, R., Singh, M. K., DeFries, R. S., and Marlier, M. E. (2021). Detection of delay in post-monsoon agricultural burning across Punjab, India: Potential drivers and consequences for air quality. *Environ. Res. Lett.* 16, 014014. doi:10.1088/1748-9326/abcc28

Mhawish, A., Sarangi, C., Babu, P., Kumar, M., Bilal, M., and Qiu, Z. (2022). Observational evidence of elevated smoke layers during crop residue burning season over Delhi: Potential implications on associated heterogeneous PM2.5 enhancements. *Rem. Sens. Environ.* 280, 113167. doi:10.1016/j.rse.2022.113167

Parayil, G. (1992). The Green Revolution in India: A Case Study of Technological Change. *Technol. Cult.* 33 (4), 737–756. doi:10.2307/3106588

Pingali, P. (2012). Green Revolution: Impacts, limits, and the path ahead. *Proc. Natl. Acad. Sci.* 109 (31), 12302–12308. doi:10.1073/pnas.0912953109

Singh, R. P., and Kaskaoutis, D. G. (2014). Crop residue burning: A threat to south asian air quality. *Eos Trans. AGU* 95 (37), 333–334. doi:10.1002/2014eo370001

frontiers | Frontiers in Earth Science

TYPE Original Research
PUBLISHED 09 January 2023
DOI 10.3389/feart.2022.1011536



OPEN ACCESS

EDITED BY
Dipesh Rupakheti,
Nanjing University of Information Science and Technology, China

REVIEWED BY
Worradorn Phairuang,
Kanazawa University, Japan
Shani Tiwari,
Council of Scientific and Industrial Research, India

*CORRESPONDENCE
Ye Yu,
yyu@lzb.ac.cn
Dunsheng Xia,
dsxia@lzu.edu.cn

SPECIALTY SECTION
This article was submitted to Atmospheric Science, a section of the journal Frontiers in Earth Science

RECEIVED 04 August 2022
ACCEPTED 14 September 2022
PUBLISHED 09 January 2023

CITATION
Liu H, Yu Y, Ma X, Liu X, Dong L and Xia D (2023), Monitoring the impact of the COVID-19 lockdown on air quality in Lanzhou: Implications for future control strategies.
*Front. Earth Sci.* 10:1011536.
doi: 10.3389/feart.2022.1011536



# Monitoring the impact of the COVID-19 lockdown on air quality in Lanzhou: Implications for future control strategies

Hui Liu[1], Ye Yu[2,3]*, Xiaoyi Ma[1], Xinying Liu[1], Longxiang Dong[2,3] and Dunsheng Xia[1]*

[1]Key Laboratory of Western China's Environmental Systems (Ministry of Education), College of Earth and Environmental Sciences, Lanzhou University, Lanzhou, Gansu, China, [2]Key Laboratory of Land Surface Process and Climate Change in Clod and Arid Regions, Northwest Institute of Eco-Environment and Resources (NIEER), Chinese Academy of Sciences (CAS), Lanzhou, Gansu, China, [3]Pingliang Land Surface Process and Severe Weather Research Station, Chinese Academy of Sciences (CAS), Pingliang, Gansu, China

China implemented a one-month lockdown after the 2020 Spring Festival to prevent the spread of COVID-19. The closure measures provide a rare opportunity to understand the resulting changes in air pollution levels and to test the effectiveness of previous environmental protection measures. We used the time series decomposition method to quantify the air pollution in Lanzhou during the closure period. The results showed that during the epidemic lockdown period, although the concentration of $SO_2$ in Lanzhou decreased substantially, there was a significant increase in the concentration of $O_3$ (by 19.14%), followed by a gradual return to the normal level. Most of the changes during the COVID-19 lockdown were within the range of fluctuations over the past five years. The trend of decreasing $SO_2$ and CO in 2020 was less than that during 2015–2019, and the continuous decline of the $PM_{10}$ concentration exceeded expectations. $NO_2$, $PM_{2.5}$ and $O_3$ maintained the trend of the previous five years. Our results show that temporary social closure measures have a limited effect on improving air quality in Lanzhou, and they emphasize the importance of reducing the $O_3$ concentration in the future.

KEYWORDS

**lockdown, Lanzhou, $O_3$, particulate matter, COVID-19**

## 1 Introduction

The outbreak of the Corona Virus Disease 2019 (COVID-19) pandemic in 2020 has had major impacts on economic activity and human health. To control the spread of COVID-19, China implemented lockdown policies and urban traffic and industrial production were strictly limited. Lanzhou, the capital city of Gansu Province, announced the Level I response (shut down commercial activities, restrict travel, and require people to stay at home) to major public health emergencies on 25th January, two days after the confirmation of two pneumonia cases with new coronavirus infections in

the city. Control measures such as self-isolation at home, store closures, and traffic control were implemented. After 27 days of these strict control measures, more than 90% of areas in Gansu Province were designated as being of low-risk of infection, and the emergency response level for COVID-19 prevention and control in Gansu Province was reduced to Level III on 21st February.

This short-term lockdown severely restricted the movement of people and economic activities (He et al., 2020), the economy was adversely affected, and industrial energy consumption decreased; especially, there was significant reduction in traffic volume. Reduced pollution levels during the COVID-19 lockdown have been reported in different countries and regions worldwide (Chen et al., 2020; Donzelli et al., 2020; Li et al., 2020; Singh et al., 2020). However, several studies have pointed out that air quality improvements are notably more limited than some earlier reports or observational data suggest (Pei et al., 2020; Shi et al., 2021; Wang et al., 2021). For example, Wang et al. (2020) reported that the concentrations of $NO_2$ and particulate matter in Beijing during the period of strictest travel restrictions (Level I control measures) were significantly lower than before the closure of the city, while Brimblecombe & Lai (2021) found no obvious decrease in pollutant concentrations in Beijing during the lockdown, compared to the same period in 2019. Similar differences between the effects of lockdown on pollutant concentrations among different studies for the same area were reported for the United Kingdom (Munir et al., 2021). These findings suggest that evaluating the impact of the COVID-19 lockdown on air quality is more complicated than initially reported. Due to differences in research methods, slightly different results were obtained for the extent of the COVID-19 impact in the same region. Compared with the sequential method (comparing the lockdown period with the period before lockdown), the parallel method is more suitable for this type of intervention analysis (Munir et al., 2021).

With the implementation of the Air Pollution Prevention and Control Measures since 2012, the air quality in urban Lanzhou has improved significantly and the phenomenon of "Lanzhou Blue" is frequent (Zhao et al., 2018). Nevertheless, the local government is faced with major challenges in further improving the air quality. In this context, the strict control measures implemented during the COVID-19 epidemic provide the opportunity to observe the relationship between human activities and environmental quality, which may help formulate future air pollution control strategies for Lanzhou.

In this study we compared measured pollution data during the interval of 1st January–30th September 2020 with those for the previous five years (2015–2019) in Lanzhou. Based on the changes in the trends of six pollutants ($PM_{2.5}$, $PM_{10}$, $SO_2$, $NO_2$, $O_3$, and CO) from 2015 to 2019, the air pollution level that would have occurred in 2020 without an epidemic was reconstructed. The impact of the COVID-19 lockdown on the air quality in the city is discussed using the difference between the reconstructed and observed pollutant concentrations. Our results may help formulate forward-looking intervention policies for improving the air quality in the city.

## 2 Materials and methods

To quantify the impact of the COVID-19 lockdown intervention on the air quality in Lanzhou, we divided the study interval, from 1st January 2020 to 30th September 2020, into four periods. P1 (1st–24th January 2020) is pre-lockdown, P2 (25th January–20th February 2020) is the Level I response period, with strict controls on traffic and prohibition on gathering. P3 (21st February–10th May 2020) is the Level III response period with public places opening in an orderly manner, and schools and living services resuming, P4 (11st May–30th September 2020) is the relaxation period.

### 2.1 Study area

Lanzhou, the capital city of Gansu province, is located in the semi-arid area of Northwest China (102°35′-104°34′E, 35°34′-37°07′N), in a long and narrow valley. The average altitude of the valley floor is ~1,500 m. Lanzhou has a temperate continental climate, with an annual average air temperature of 11.5°C, relative humidity of 26.8%, wind speed of 1.49 m/s, and an average annual precipitation of 327 mm (which is concentrated in the summer months) (Ma et al., 2020). Lanzhou is located on the sandstorm transport path originating from the Taklimakan Desert, the Badain Jaran Desert, and the Hexi Corridor, the dust intrusions from upstream regions in spring time make Lanzhou one of the most severely air-polluted cities in China. Lanzhou is also an important industrial city in Northwest China (Yan et al., 2021), major industries in the urban area are petrochemical refinery and manufacturing (Wang et al., 2009).

### 2.2 Air quality data

Hourly concentrations of particulate matter ($PM_{2.5}$, $PM_{10}$), nitrogen dioxide ($NO_2$), sulfur dioxide ($SO_2$), carbon monoxide (CO) and 8 h moving average ozone ($O_3$–8h) at four air quality monitoring stations in Lanzhou City from 2015 to 2020 were obtained from the China National Environmental Monitoring Network (http://www.cnemc.cn). Three of the monitoring stations are in the urban area and one is in a suburban of Lanzhou. The averages of the four sites is used to represent the overall pollution situation in Lanzhou. The following quality control measures were applied to the monitoring data. When the hourly concentration of $PM_{2.5}$ exceeded the concentration of $PM_{10}$ at the same hour, both the $PM_{2.5}$ and $PM_{10}$ for that hour

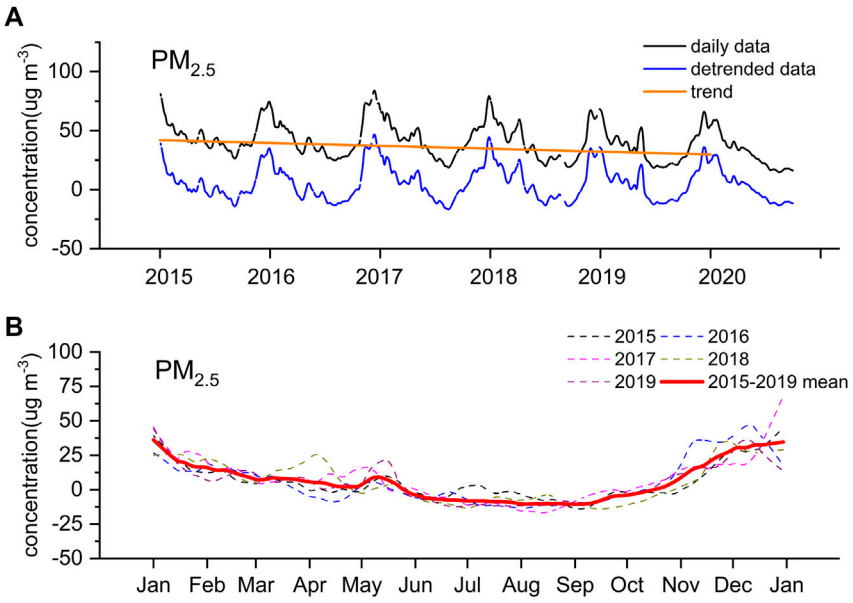


FIGURE 1
**(A)** Time series of daily $PM_{2.5}$ concentration averaged across all sites in Lanzhou (black) and the trend (orange) calculated using the data for 2015–2019. **(B)** Seasonal cycle of $PM_{2.5}$ after removing the inter-annual trend. The data are smoothed using a LOWESS filter (30 days).

were discarded; if more than three consecutive hours had the same value, the records were discarded; all zero values and outliers (values exceeding the measurement range of the instrument) were removed (Liu et al., 2016; Wu and Zhang, 2018). After the application of these criteria, if there were more than four missing data in a day, the daily average for that day was recorded as missing.

## 2.3 Time series decomposition

The level of air pollutants in Lanzhou has shown a clear downward trend in recent years (Tan et al., 2009; Yin et al., 2020), and therefore the data needed to be detrended before the effect of the COVID-19 lockdown could be evaluated by comparing the concentrations of each pollutant in previous years with that in 2020. Besides the trend of the inter-annual change, seasonal variations and the Spring Festival effect were also considered.

The non-parametric Mann-Kendall trend test (http://www.mathworks.com/matlabcentral/fileexchange/authors/23983) (Burkey, 2006) was used to obtain the trend of the interannual change for the six pollutants during 2015–2019, and the Theil-Sen method (Theil, 1992; Sen, 1968) was used to determine the magnitude (Sen's slope) of the trend. All the slopes were calculated in MATLAB using the daily averaged pollutant concentrations.

The Theil-Sen method has been widely used in long-term trend analysis (Neeti and Eastman, 2011; Munir et al., 2013). It is a non-parametric technique for robustly fitting a line to data while minimizing the influence of outliers. Sen's slope (Q) is determined by finding the median of all slopes between pairs of data points in a time series (i.e., time series of the daily averaged pollutant concentrations from 2015 to 2019):

$$Q = median\left(\frac{x_i - x_j}{i - j}\right) \quad 1 < j < i < n$$

Where $x_i$ and $x_j$ are daily average concentrations of $PM_{2.5}$, $PM_{10}$, $NO_2$, $SO_2$, CO, or the daily 8-h maximum $O_3$ ($O_3$_8 h) for day i and j, and n is the number of days in the five years. A positive Q value represents an increasing trend, while a negative Q value represents a decreasing trend.

The daily $PM_{2.5}$ concentrations from 2015 to 2019 were used to calculate the inter-annual trend (orange line in Figure 1A). The seasonal variation was calculated after removing the interannual trend from the daily averaged data (Figure 1B). An average seasonal variation for 2015–2019 was obtained (red line in Figure 1B) and further removed from the detrended data to obtain the residual (similar Figures for other pollutants are presented in the Supplementary Information, see Supplementary Figure S1). The graphical fitting process was performed on the data shown in Figure 1 using locally weighted scatterplot smoothing (LOWESS) (Cleveland et al.,

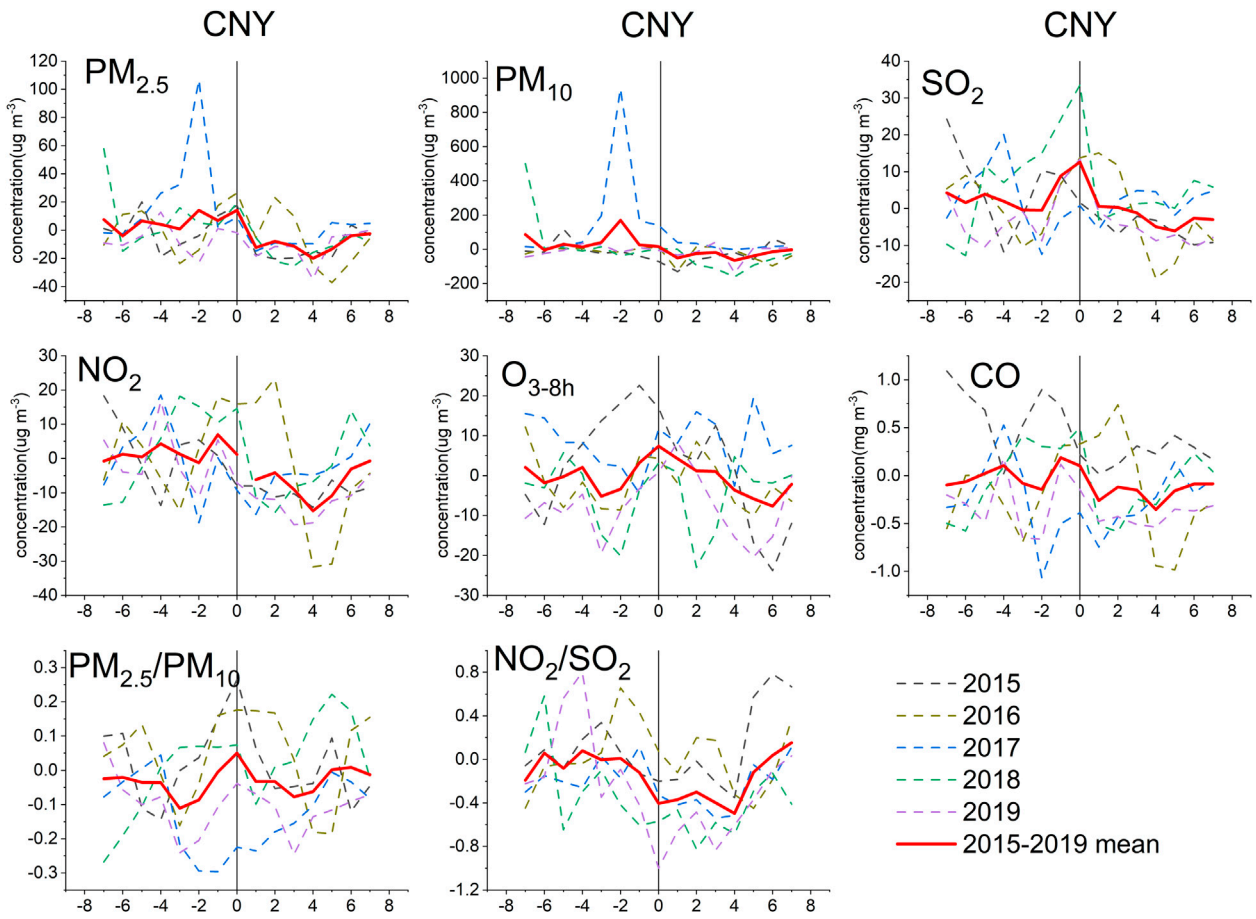


FIGURE 2
Average 2015–2019 detrended and deseasonalized concentrations of six pollutants, $PM_{2.5}/PM_{10}$ and $NO_2/SO_2$ during the Chinese New Year (CNY). The Spring Festival data for each year are stripped of trend and seasonal cycle.

2017). LOWESS smoothing was conducted in Origin 2021 software. The 5-year daily data were processed using the LOWESS data smoothing algorithm with a 30-day window. After removing the inter-annual trend (blue line in Figure 1A), the pollutant concentrations in different years were found to be more comparable, which facilitated the analysis of the impact of COVID-19.

Lanzhou announced its lockdown on 25$^{th}$ January 2020, which is also the first day of the Chinese New Year (CNY) and the most important festival in China. Therefore, the holiday effect would potentially cause errors in assessing the impact of the COVID-19 lockdown. Obvious differences in air pollutant concentrations during CNY and non-CNY have been confirmed by many studies (Tan et al., 2009; Shi et al., 2014; Zhao et al., 2014), and thus proper treatment of the CNY effect is important when comparing pollutant concentrations across years (Silver et al., 2020). The date of the CNY is determined according to the Lunar calendar in China, and the official Chinese New Year Festival lasts for seven days. Here, we consider the 7 days prior to and the 7 days after (total of 15 days) the CNY as the period affected by the Chinese Spring Festival. The 15-day time series after detrending and deseasonalizing were averaged for each pollutant to obtain the CNY signal (red line in Figure 2).

The above processing was applied to each pollutant at each site, using the daily averaged data series during 2015–2019. As a result, the time series for each pollutant were divided into four components: inter-annual trends, season variations, fixed events (i.e., the CNY effect), and noise or residuals. The patterns of the first three components were used to reconstruct the daily concentrations of each pollutant at each site in 2020. The residuals for each pollutant were used to assess the deviation of each pollutant concentration due to the COVID-19 lockdown from their expected value in the absence of COVID-19. In 2020, the most likely source impacting these residual concentrations was the COVID-19 lockdown, although meteorological contributions cannot be excluded.

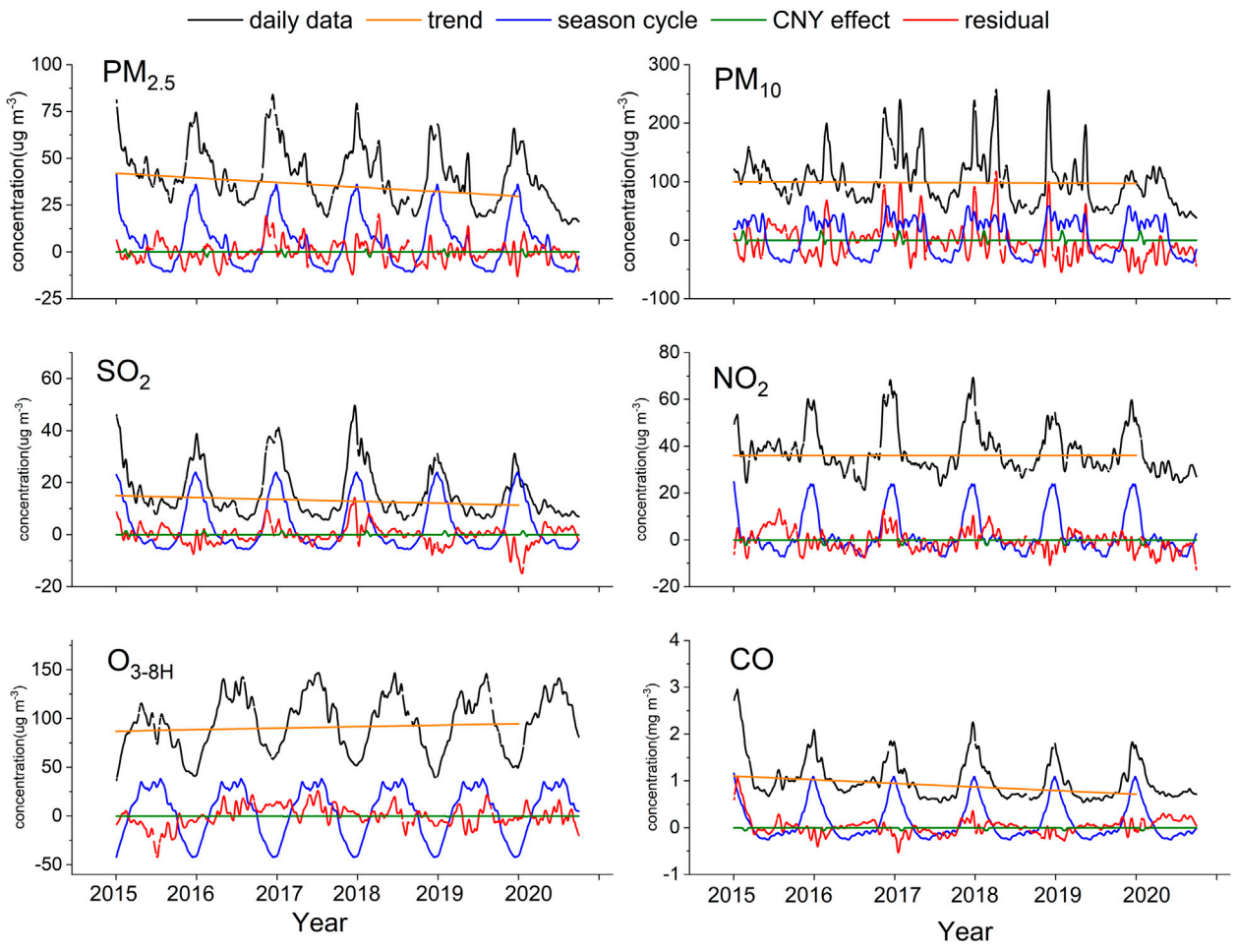


FIGURE 3
Daily time series for six pollutants (black), decomposed into the trend (orange), seasonal cycle (blue), Chinese New Year (CNY) effect (green) and residual (red) components. The data are smoothed using a LOWESS filter.

# 3 Results

## 3.1 Temporal variations of the pollutants

As shown in Figure 3, during the period of 2015–2019, $PM_{2.5}$, $PM_{10}$, $SO_2$ and CO in Lanzhou all show a decreasing trend, while $O_3$ shows a significant increasing trend. There is no obvious trend in $NO_2$. The inter-annual trends of all pollutants are all significant at $p$ <0.05. $PM_{2.5}$ and CO have the strongest negative trend, with a median trend of −6.81% $year^{-1}$ or −2.44 $\mu g\ m^{-3}\ year^{-1}$ and −8.43% $year^{-1}$ or −0.08 $mg\ m^{-3}\ year^{-1}$, respectively. $PM_{10}$ and $SO_2$ have a negative trend of −0.55% $year^{-1}$ or −0.55 $\mu g\ m^{-3}\ year^{-1}$ and −5.54% $year^{-1}$ or −0.73 $\mu g\ m^{-3}\ year^{-1}$, respectively, while $O_3$ has a positive trend of 1.69% $year^{-1}$ or 1.53 $\mu g\ m^{-3}\ year^{-1}$. $NO_2$ increased slightly with a median trend of 0.05% $year^{-1}$ or 0.02 $\mu g\ m^{-3}\ year^{-1}$. These values are comparable to those in Silver et al. (2018), who found that the annual average $PM_{2.5}$ concentration of 1,689 monitoring sites in China decreased by 3.4 $\mu g\ m^{-3}\ year^{-1}$ or 7.2% $year^{-1}$ between 2015 and 2017, and that there was no median trend in annual mean $NO_2$ concentration (0.0 $\mu g\ m^{-3}\ year^{-1}$ or 0.1% $year^{-1}$). The increase in $O_3$ concentration and decrease in $PM_{2.5}$ and $SO_2$ were also observed in other regions in China in recent years (Fan et al., 2020; Kuerban et al., 2020). The decreasing trend indicates the effectiveness of the Air Pollution Prevention and Control Measures implemented since 2012 in reducing high loading $PM_{2.5}$ and $SO_2$ therein. For ozone, several studies have reported that decreases in $PM_{2.5}$ could increase ozone through decrease in aerosol sink of hydroperoxy ($HO_2$) radicals and increase of photolysis rates (Li et al., 2019). For example, a recent study by Zhao et al. (2021) in Lanzhou noticed an increase of mean ambient temperature and net radiation at noon during 2017–2019 compared with 2015–2016, and attributed it partly to large $PM_{2.5}$ reductions. Both the increase of mean ambient temperature and net radiation could increase the production of ozone. The role played by

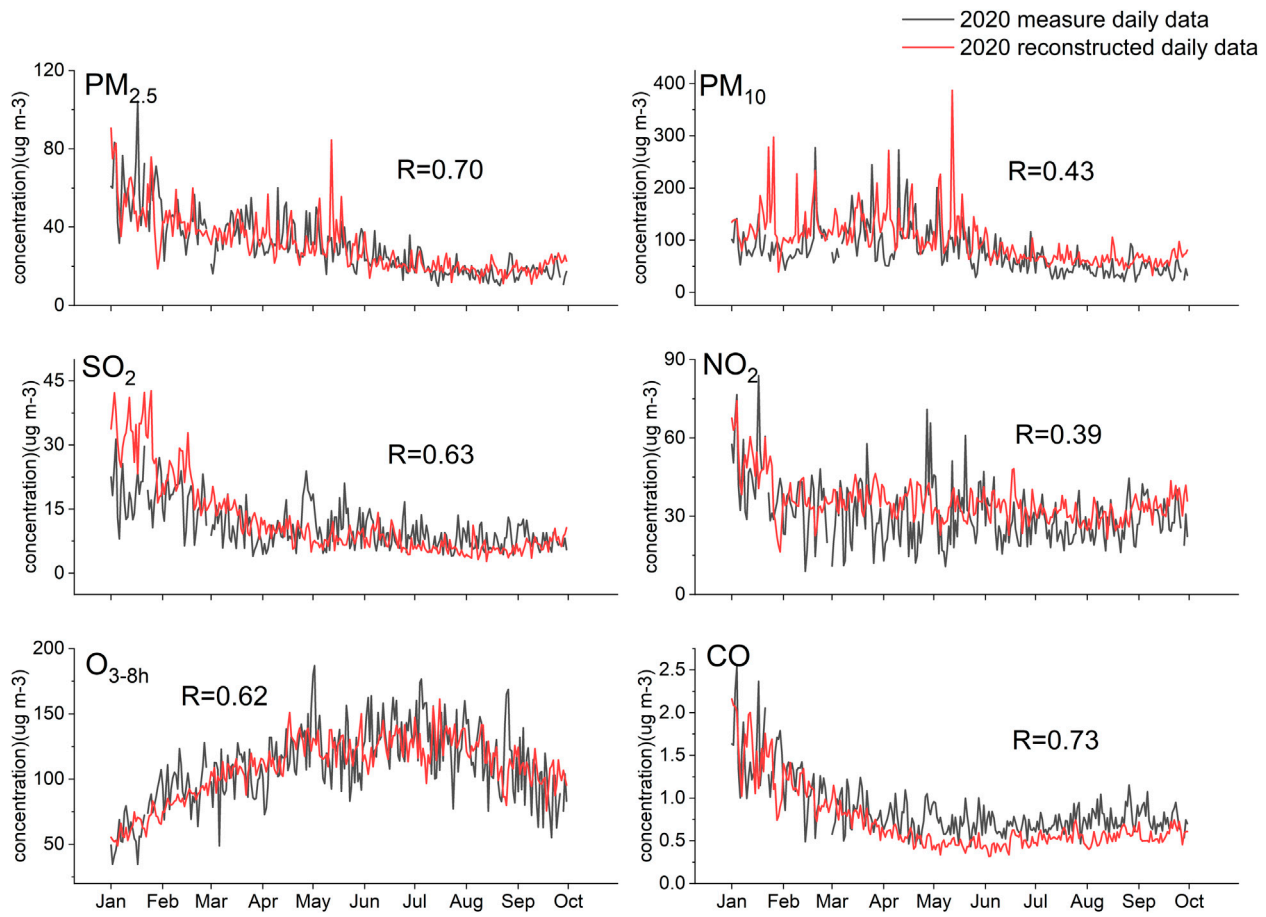


FIGURE 4
Comparison of the observed pollutant concentrations in 2020 with those reconstructed using the three components of the inter-annual trends, seasonal variations and CNY events, based on the data for 2015–2019.

meteorological conditions and its interaction with aerosols in ozone trends in the study area need further investigation.

Although there are fluctuations in some months, the $PM_{2.5}$, $PM_{10}$, $SO_2$, $NO_2$ and CO concentrations during 2015–2019 generally showed high values in winter and spring, and low values in summer and autumn, which is a combination effect of both strong emissions of pollutants and relatively stable atmospheric condition in winter (Ma et al., 2019). The variation of the $O_3$ concentration, with a peak in summer, is different from the other pollutants, which is mainly due to the enhanced photochemical reactions with abundant sunlight and high temperature in summer (Li et al., 2014; Li et al., 2019). However, there are still debates on whether anthropogenic pollution or stratospheric intrusion plays a more dominant role (Liu et al., 2019; Li et al., 2020).

Figure 3 demonstrates the effect of the Spring Festival on the concentration of pollutants, which show a generally increasing trend during the 7 days interval prior to CNY and a decreasing trend during the 7 days after CNY. $PM_{2.5}$ peaked on two days before CNY (-2) and CNY day (0). $PM_{2.5}/PM_{10}$ was small during CNY (-2), largely caused by the floating dust event occurred during 25–26 January 2017 (Sand-dust Weather Almanac, 2017). A peak in $PM_{2.5}/PM_{10}$ occurred on the CNY day, when $SO_2$ and $O_3$_8 h also peaked, which may be related to emissions from fireworks. The concentrations of the six pollutants were lower than usual during the 7 days after the CNY; $PM_{2.5}$ and $NO_2$ decreased by 10.19 μg $m^{-3}$ and 7.05 μg $m^{-3}$ respectively. $O_3$ concentrations decreased by 0.59 μg $m^{-3}$ on average during the 7-day holiday, and a significant fall 3 days before the CNY was observed before the upward trend, which was contrary to the change in $PM_{10}$.

## 3.2 Residuals analysis

The time-series decomposed components (i.e., the trend, seasonal cycle and effect of the CNY based on the 2015–2019 time series) were used to reconstruct the time series of

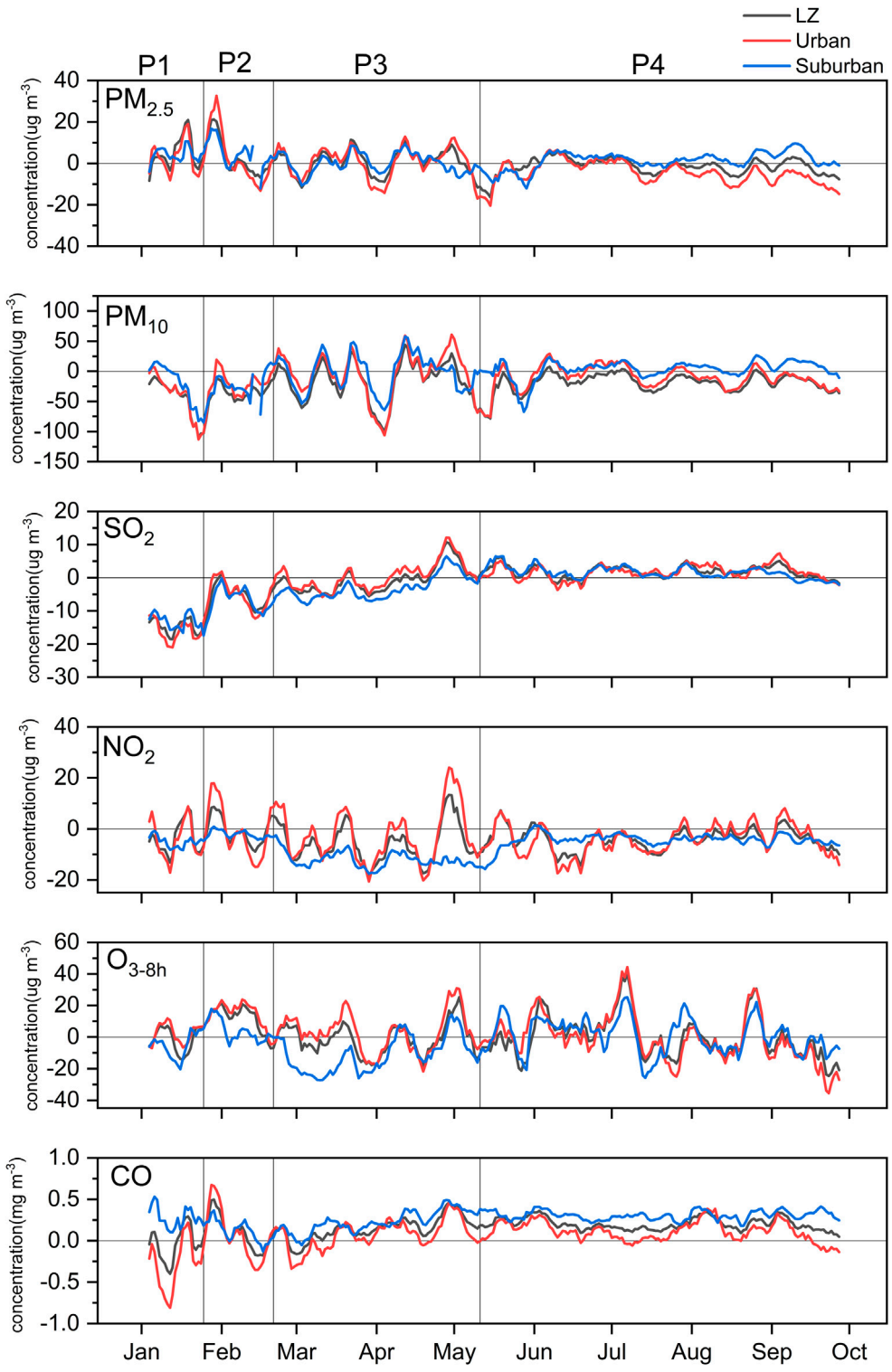


FIGURE 5
Changes in 7-day moving average residuals of six pollutants for all, urban and rural sites in 2020. P1, pre-lockdown; P2, Level I response period; P3, Level III response period; P4, relaxation period.

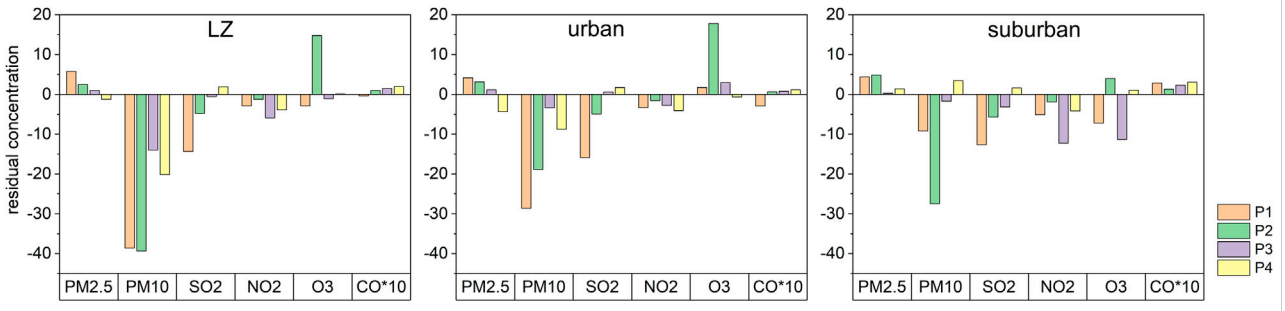


FIGURE 6
Comparison of the 7-day moving average residuals of the six pollutants at different stages of the epidemic. Note: CO is multiplied by ten for clarity.

the daily concentrations of each pollutant in 2020 (red lines in Figure 4). As shown in Figure 4, the reconstructed time series are in overall good agreement with the observations. The highest correlation coefficient (0.73) is for CO, while that for $NO_2$ is the smallest (0.43). This indicates that the changes in the CO concentration were relatively stable, while $NO_2$ was more variable.

Figure 5 shows the 7-day moving average residuals (observation minus reconstructed values) of the six pollutant concentrations in 2020, at different stages of the COVID-19 epidemic. The residuals of the six pollutants fluctuate around zero. The variation of the residuals are very well correlated at the urban and suburban sites, except for $NO_2$ and $O_{3-8h}$ during P1, with the residuals at urban sites being more positive and generally larger than that at the suburban sites. Reference to the average residuals for the different periods (Supplementary Table S1) shows that the pollutant concentrations in Lanzhou did not decrease as sharply as might have been expected during P2.

During P2 the $PM_{2.5}$ concentration in Lanzhou increased by 2.48 μg $m^{-3}$, an increase of 15.86% compared to the reconstructed value, and a decrease of 3.26 μg $m^{-3}$ compared to pre-lockdown (Supplementary Table S1). In Figure 6, we compare the residuals of different pollutants during the four phases. $PM_{2.5}$, $SO_2$ and CO show monotonic changes during the four periods, which indicates that COVID-19 had a limited effect on the concentrations of the three pollutants. The residuals of $PM_{2.5}$ decreased monotonically and that of CO increased monotonically during the study period, which may be related to the large seasonal decrease in the background concentration or a reduction of the inter-annual trend. Although $SO_2$ showed a monotonic increase during the four stages of the study period, the concentration of $SO_2$ was lower than the reconstructed value, except during P4.

$PM_{10}$ decreased during the COVID-19 lockdown, falling by 23.40% if only the P2 stage, with the strictest controls, is considered. $PM_{10}$ decreased by 1.81 μg $m^{-3}$ compared to pre-lockdown (Supplementary Table S1). The variation of $PM_{10}$ differed between urban and suburban areas during the study period. The $PM_{10}$ at urban sites during P2 increased by 9.79 μg $m^{-3}$, an increase of 14.86%, compared with pre-lockdown. $PM_{10}$ in the suburban site decreased by 13.56% compared to pre-lockdown. During the period when the COVID-19 lockdown was relaxed (P4) and the restrictions were lifted, the concentration of $PM_{10}$ at the suburban site rebounded to the reconstructed value, although it did not reach the expected values.

$NO_2$ was low during the Level III response period (P3) (-5.91 μg $m^{-3}$, -14.65%), while a slight decrease occurred during the strict lockdown period (P2). The decline during P3 was mainly at the suburban site. The $NO_2$ in the suburban of Lanzhou decreased by 53.91% compared to the expected values. $NO_2$ decreased more during P3 than during P2, which may be due to the overlap of the CNY and the epidemic during this period. We removed the New Year effect to determine the impact of the epidemic, but during CNY, people gather in families to celebrate the holiday, which is to some extent the same behavior as the response to the home isolation measures undertaken to control the epidemic. As a result, the impact of the epidemic may have been reduced by removing the effect of CNY. Ignoring the CNY holiday, it can be inferred that the $NO_2$ concentration 14 days after CNY decreased by 0.48% compared to the 14 days before CNY, and by 8.63% compared to the reconstructed values during the same period. During the P3 stage, the difference between urban and suburban areas indicates that the suburban areas were more affected by the control measures implemented during the COVID-19 lockdown than urban areas. In general, for Lanzhou, the COVID-19 lockdown had a relatively small impact on $NO_2$ concentrations.

Among the pollutants studied, $O_3$ was the most obviously affected by the COVID-19 lockdown, and the difference in residuals between the urban and the suburban areas during the lockdown period was also the largest. During the strict lockdown (P2), the $O_3$ concentration in Lanzhou increased by 19.14% compared to the reconstructed value. Both urban and suburban sites showed an increase during the P2 stage, with the urban areas increasing more, with an increase of 24.60%. This rise in $O_3$ during the lockdown period has been widely reported in China and even globally (Silver et al., 2020; Grange et al., 2021). In particular, during the Level III response (P3), the $O_3$ concentration in Lanzhou

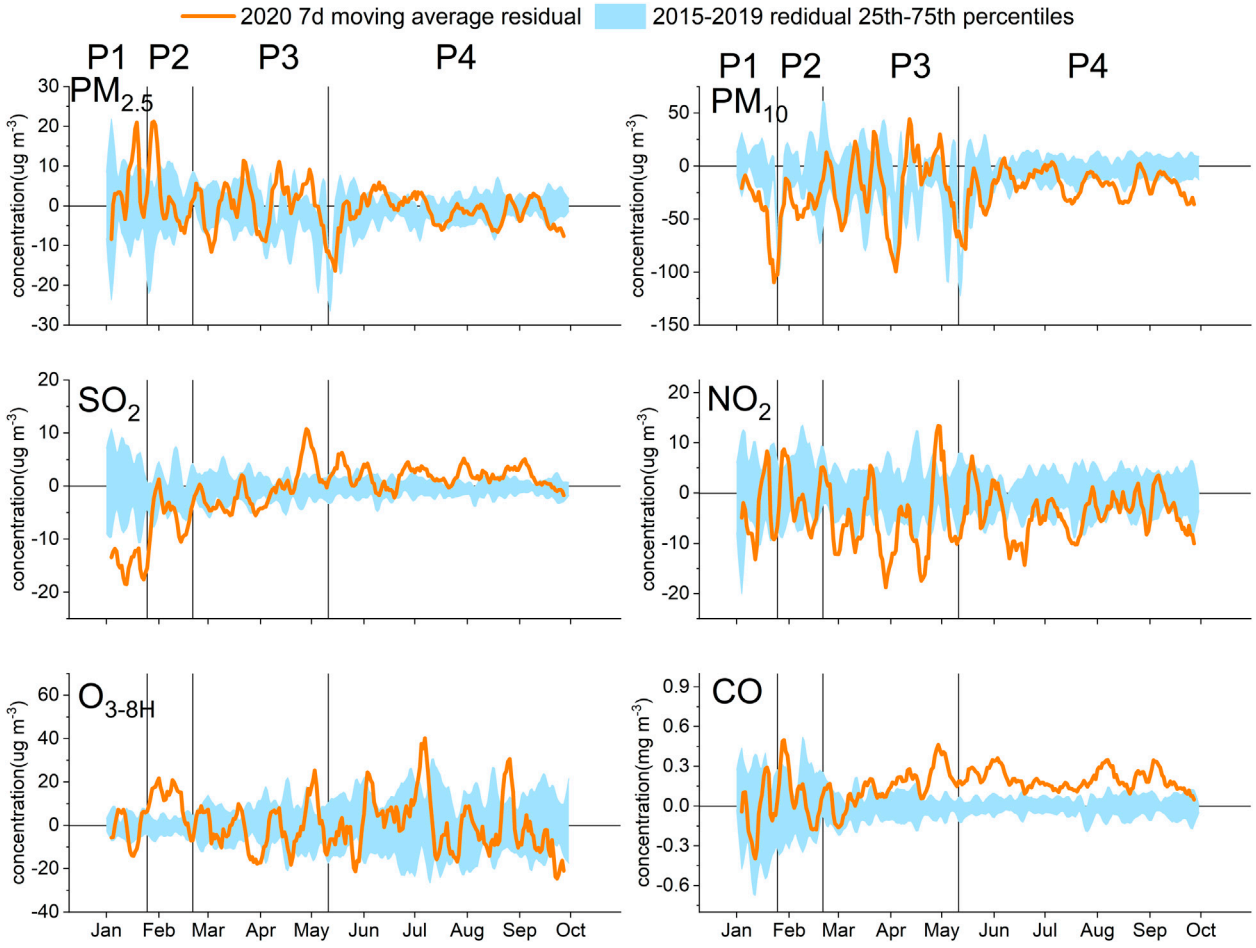


FIGURE 7
Comparison of the residual concentrations of pollutants in 2020 with those for same period in 2015–2019. The 25th and 75th percentiles of averaged detrended concentrations for 2015–2019 (blue shading) are shown.

decreased by 19.80% compared to the strict control phrase (P2). Both urban and suburban sites showed a decrease during P3. The $O_3$ concentration in suburban areas decreased by -11.31 μg $m^{-3}$ (-7.97%) compared with the reconstructed value during P3, and it decreased by 13.07% compared to P2. The $O_3$ concentration in urban areas increased by 2.97 μg $m^{-3}$ (3.54%) compared to the reconstructed value in P3, but it decreased by 21.06% compared to P2. The analysis of $O_3$ is complicated by the spatio-temporal heterogeneity of its production and the nonlinear chemical response to $NO_X$ and VOC emissions (Jin and Halloway, 2015). Due to the influence of atmospheric chemistry, changes in the $NO_2$ concentration do not reflect the same relative change in $NO_X$ emissions (Keller et al., 2021). Previous studies have reported that the elevated $O_3$ during lockdowns was mainly attributed to the enhanced atmospheric oxidation capacity in northern China (Le et al., 2020), the North China emission reduction during lockdown (Zhu et al., 2021). Chemistry of secondary aerosols and ozone as well as the meteorological conditions may have contributed positively to the anomalous enhancement in $O_3$ during the lockdown in Lanzhou, which merit further investigation.

## 3.3 Comparison of residuals between 2020 and 2015–2019

Figure 7 compares the 7-day moving average residuals during the study period with those of the same period of the previous five years. In addition to changes related to the inter-annual trend, the seasonal cycle and the CNY effect, there are complex interactions between atmospheric chemistry and meteorology. To assess the impact of the restriction measures after the COVID-19 outbreak, we consider the change in residuals during the same period of 2015–2019 as the normal range of fluctuation of the pollutants. A Student t test at the 0.1 significance level revealed a large negative $SO_2$ anomaly and

positive $O_3$ anomaly during the lockdown (P2), with a large positive CO anomaly and a negative $PM_{10}$ anomaly during the relaxation period, compared to the anomalies during the previous five years. A large positive $SO_2$ anomaly (significant at the 0.25 level) and a negative $NO_2$ anomaly (significant at the 0.25 level) were also observed during P4. This indicates that there was a reduction in the trend of decreasing CO and $SO_2$ in 2020 compared with that during 2015–2019, while $PM_{10}$ continued to decrease beyond expectations. This indicates the effectiveness of air pollution control measures, and it also shows that air quality management is a long-term process. The $PM_{2.5}$, $NO_2$ and $O_3$ residuals maintained the same rate of change as during the previous five years. The increase in $O_3$ in urban areas during the strict lockdown period and the decrease in $NO_2$ in suburban areas during the Level III response were significantly beyond expectations (Supplementary Figure S2).

The impact of the COVID-19 lockdown measures on air quality was not as great as we expected. A similar conclusion was reached in other studies, although different methods were used. The results of Wang et al. (2021) showed that the lockdown temporarily improved the air quality in China, but the rate of reduction of $SO_2$, $NO_2$, and CO was very small. Pei et al. (2020) believed that the air quality in the urban areas of China did not improve overall during the lockdown. Under the restrictions imposed to reduce COVID-19 infections, there were several improvements in air quality, but they were not as effective as we expected. To further improve the air quality in Lanzhou City, detailed source-response studies are needed.

## 4 Conclusion

Time-series decomposition was used to quantify the changes in air quality in Lanzhou City during the COVID-19 epidemic. During the epidemic prevention and control period in Lanzhou, only $PM_{10}$ decreased (by 23.40%) compared with the expected values over the same period, with a 1.80 μg $m^{-3}$ decrease compared with that before the lockdown. The $NO_2$ concentration 14 days after CNY fell by 0.48% compared with that 14 days before, and by 8.63% compared with the reconstructed value for the same period. The $O_3$ response depends on the season, time scale, and environment. During the period of the COVID-19 lockdown, the $O_3$ concentration in Lanzhou increased by 19.14% compared to the reconstructed value during P2, and it then decreased by 19.80% during the Level III response (P3). Compared with the past five years, the changes during the COVID-19 epidemic were generally within the normal range of fluctuations. The $PM_{10}$ concentration in Lanzhou continued to decrease, but there was a reduction in the rate of decrease in $SO_2$ and CO, while $PM_{2.5}$, $NO_2$ and $O_3$ maintained the same trend as during the previous five years. It is important to determine the cause of the widespread increase in $O_3$ in future studies. In short, we believe that the COVID-19 lockdown did indeed reduce the levels of several air pollutants in Lanzhou, but the temporary social lockdown measures were insufficient to further improve the atmospheric environment. Atmospheric pollutants require comprehensive and coordinated mitigation measures, which highlights the importance of reducing the concentration of $O_3$ in the future.

## Data availability statement

Publicly available datasets were analyzed in this study. This data can be found here: the China National Environmental Monitoring Network (http://www.cnemc.cn).

## Author contributions

HL: Conceptualization, Methodology, Writing-original draft. YY: Conceptualization, Data curation, Methodology, Writing-review and editing, Supervision. DX: Writing-review and editing, Supervision. XM: Methodology. XL: Methodology. LD: Methodology.

## Funding

This work was supported by the Gansu Science and Technology Plan (18JR2RA005).

## Acknowledgments

Thanks to Jan Bloemendal from the University of Liverpool for suggestions and proofreading the article.

## Conflict of interest

The authors declare that the research was conducted in the absence of any commercial or financial relationships that could be construed as a potential conflict of interest.

## Publisher's note



## Supplementary material

The Supplementary Material for this article can be found online at: https://www.frontiersin.org/articles/10.3389/feart.2022.1011536/full#supplementary-material.

# References

Brimblecombe, P., and Lai, Y. (2021). Diurnal and weekly patterns of primary pollutants in Beijing under COVID-19 restrictions. *Faraday Discuss.* 226, 138–148. doi:10.1039/D0FD00082E

Burkey, J. (2006). *A non-parametric monotonic trend test computing Mann-Kendall Tau, Tau-b, and Sen's slope written in Mathworks-MATLAB implemented using matrix rotations.* Seattle, Washington. USA: King County, Department of Natural Resources and Parks, Science and Technical Services Section. Available at: http://www.mathworks.com/matlabcentral/fileexchange/authors/23983 (accessed March 13, 2021).

Chen, L., Chien, L. C., Li, Y., and Lin, G. (2020). Nonuniform impacts of COVID-19 lockdown on air quality over the United States. *Sci. Total Environ.* 745, 141105. doi:10.1016/j.scitotenv.2020.1411055

Cleveland, W. S., Grosse, E., and Shyu, W. M. (2017). *Local regression models. Statistical models in S.* England,UK: Routledge, 309–376.

Donzelli, G., Cioni, L., Cancellieri, M., Llopis Morales, A., and Morales Suárez-Varela, M. M. (2020). The effect of the Covid-19 lockdown on air quality in three Italian medium-sized cities. *Atmosphere* 11 (10), 1118. doi:10.3390/atmos11101118

Fan, H., Zhao, C., and Yang, Y. (2020). A comprehensive analysis of the spatio-temporal variation of urban air pollution in China during 2014–2018. *Atmos. Environ. X.* 220, 117066. doi:10.1016/j.atmosenv.2019.117066

Grange, S. K., Lee, J. D., Drysdale, W. S., Lewis, A. C., Hueglin, C., Emmenegger, L., et al. (2021). COVID-19 lockdowns highlight a risk of increasing ozone pollution in European urban areas. *Atmos. Chem. Phys.* 21 (5), 4169–4185. doi:10.5194/acp-2020-1171

He, G., Pan, Y., and Tanaka, T. (2020). The short-term impacts of COVID-19 lockdown on urban air pollution in China. *Nat. Sustain.* 3 (12), 1005–1011. doi:10.1038/s41893-020-0581-y

Jin, X., and Holloway, T. (2015). Spatial and temporal variability of ozone sensitivity over China observed from the Ozone Monitoring Instrument. *J. Geophys. Res. Atmos.* 120 (14), 7229–7246. doi:10.1002/2015JD023250

Keller, C. A., Evans, M. J., Knowland, K. E., Hasenkopf, C. A., Modekurty, S., Lucchesi, R. A., et al. (2021). Global impact of COVID-19 restrictions on the surface concentrations of nitrogen dioxide and ozone. *Atmos. Chem. Phys.* 21 (5), 3555–3592. doi:10.5194/acp-21-3555-2021

Kuerban, M., Waili, Y., Fan, F., Liu, Y., Qin, W., Dore, A. J., et al. (2020). Spatio-temporal patterns of air pollution in China from 2015 to 2018 and implications for health risks. *Environ. Pollut.* 258, 113659. doi:10.1016/j.envpol.2019.113659

Le, T., Wang, Y., Liu, L., Yang, J., Yung, Y. L., Li, G., et al. (2020). Unexpected air pollution with marked emission reductions during the COVID-19 outbreak in China. *Science* 369 (6504), 702–706. doi:10.1126/science.abb7431

Li, K., Jacob, D. J., Liao, H., Shen, L., Zhang, Q., and Bates, K. H. (2019). Anthropogenic drivers of 2013–2017 trends in summer surface ozone in China. *Proc. Natl. Acad. Sci. U. S. A.* 116 (2), 422–427. doi:10.1073/pnas.1812168116

Li, L., Li, Q., Huang, L., Wang, Q., Zhu, A., Xu, J., et al. (2020). Air quality changes during the COVID-19 lockdown over the Yangtze River Delta Region: An insight into the impact of human activity pattern changes on air pollution variation. *Sci. Total Environ.* 732, 139282. doi:10.1016/j.scitotenv.2020.139282

Li, X., Liu, J., Mauzerall, D. L., Emmons, L. K., Walters, S., Horowitz, L. W., et al. (2014). Effects of trans-Eurasian transport of air pollutants on surface ozone concentrations over Western China. *J. Geophys. Res. Atmos.* 119 (21), 12, 338–412, 354. doi:10.1002/2014JD021936

Liu, J., Li, W., and Li, J. (2016). Quality screening for air quality monitoring data in China. *Environ. Pollut.* 216, 720–723. doi:10.1016/j.envpol.2016.06.037

Liu, N., Lin, W., Ma, J., Xu, W., and Xu, X. (2019). Seasonal variation in surface ozone and its regional characteristics at global atmosphere watch stations in China. *J. Environ. Sci.* 77, 291–302. doi:10.1016/j.jes.2018.08.009

Ma, X., Jia, H., Sha, T., An, J., and Tian, R. (2019). Spatial and seasonal characteristics of particulate matter and gaseous pollution in China: Implications for control policy. *Environ. Pollut.* 248, 421–428. doi:10.1016/j.envpol.2019.02.038

Ma, Y., Ma, B., Jiao, H., Zhang, Y., Xin, J., and Yu, Z. (2020). An analysis of the effects of weather and air pollution on tropospheric ozone using a generalized additive model in Western China: Lanzhou, Gansu. *Atmos. Environ.* 224, 117342. doi:10.1016/j.atmosenv.2020.117342

Munir, S., Habeebullah, T. M., Seroji, A. R., Gabr, S. S., Mohammed, A. M., and Morsy, E. A. (2013). Quantifying temporal trends of atmospheric pollutants in Makkah (1997–2012). *Atmos. Environ. X.* 77, 647–655. doi:10.1016/j.atmosenv.2013.05.075

Munir, S., Luo, Z., and Dixon, T. (2021). Comparing different approaches for assessing the impact of COVID-19 lockdown on urban air quality in Reading, UK. *Atmos. Res.* 261, 105730. doi:10.1016/j.atmosres.2021.105730

Neeti, N., and Eastman, J. R. (2011). A contextual mann-kendall approach for the assessment of trend significance in image time series. *Trans. GIS* 15 (5), 599–611. doi:10.1111/j.1467-9671.2011.01280.x

Pei, Z., Han, G., Ma, X., Su, H., and Gong, W. (2020). Response of major air pollutants to COVID-19 lockdowns in China. *Sci. Total Environ.* 743, 140879. doi:10.1016/j.scitotenv.2020.140879

Sen, P. K. (1968). Estimates of the regression coefficient based on Kendall's tau. *J. Am. Stat. Assoc.* 63 (324), 1379–1389. doi:10.1080/01621459.1968.10480934

Shi, G. L., Liu, G. R., Tian, Y. Z., Zhou, X. Y., Peng, X., and Feng, Y. C. (2014). Chemical characteristic and toxicity assessment of particle associated PAHs for the short-term anthropogenic activity event: During the Chinese new year's festival in 2013. *Sci. Total Environ.* 482, 8–14. doi:10.1016/j.scitotenv.2014.02.107

Shi, Z., Song, C., Liu, B., Lu, G., Xu, J., Van Vu, T., et al. (2021). Abrupt but smaller than expected changes in surface air quality attributable to COVID-19 lockdowns. *Sci. Adv.* 7 (3), eabd6696. doi:10.1126/sciadv.abd6696

Silver, B., He, X., Arnold, S. R., and Spracklen, D. V. (2020). The impact of COVID-19 control measures on air quality in China. *Environ. Res. Lett.* 15 (8), 084021. doi:10.1088/1748-9326/aba3a2

Silver, B., Reddington, C. L., Arnold, S. R., and Spracklen, D. V. (2018). Substantial changes in air pollution across China during 2015–2017. *Environ. Res. Lett.* 13 (11), 114012. doi:10.1088/1748-9326/aae718

Singh, V., Singh, S., Biswal, A., Kesarkar, A. P., Mor, S., and Ravindra, K. (2020). Diurnal and temporal changes in air pollution during COVID-19 strict lockdown over different regions of India. *Environ. Pollut.* 266, 115368. doi:10.1016/j.envpol.2020.115368

Tan, P. H., Chou, C., Liang, J. Y., Chou, C. C. K., and Shiu, C. J. (2009). Air pollution "holiday effect" resulting from the Chinese New Year. *Atmos. Environ. X.* 43 (13), 2114–2124. doi:10.1016/j.atmosenv.2009.01.037

Theil, H. (1992). "A rank-invariant method of linear and polynomial regression analysis," in *Henri Theil's contributions to economics and econometrics* (Berlin, Germany: Springer), 345–381.

Wang, M., Liu, F., and Zheng, M. (2021). Air quality improvement from COVID-19 lockdown: Evidence from China. *Air Qual. Atmos. Health* 14 (4), 591–604. doi:10.1007/s11869-020-00963-y

Wang, S., Feng, X., Zeng, X., Ma, Y., and Shang, K. (2009). A study on variations of concentrations of particulate matter with different sizes in Lanzhou, China. *Atmos. Environ.* 43 (17), 2823–2828. doi:10.1016/j.atmosenv.2009.02.021

Wang, Y., Wen, Y., Wang, Y., Zhang, S., Zhang, K. M., Zheng, H., et al. (2020). Four-month changes in air quality during and after the COVID-19 lockdown in six megacities in China. *Environ. Sci. Technol. Lett.* 7 (11), 802–808. doi:10.1021/acs.estlett.0c00605

Wu, L., and Zhang, J. (2018). Assessing population movement impacts on urban heat island of beijing during the Chinese new year holiday: Effects of meteorological conditions. *Theor. Appl. Climatol.* 131 (3), 1203–1210. doi:10.1007/s00704-017-2043-7

Yan, C., Wang, L., and Zhang, Q. (2021). Study on coupled relationship between urban air quality and land use in Lanzhou, China. *Sustainability* 13 (14), 7724. doi:10.3390/su13147724

Yin, Z., Huang, X., He, L., Cao, S., and Zhang, J. J. (2020). Trends in ambient air pollution levels and PM2. 5 chemical compositions in four Chinese cities from 1995 to 2017. *J. Thorac. Dis.* 12 (10), 6396–6410. doi:10.21037/jtd-19-crh-aq-004

Zhao, S. P., Yu, Y., and Qin, D. H. (2018). From highly polluted inland city of China to "Lanzhou Blue": The air-pollution characteristics. *Sci. Cold Arid. Reg.* 10 (1), 12–26. doi:10.3724/SP.J.1226.2018.00012

Zhao, S. P., Yu, Y., Yin, D. Y., and Qin, D. H. (2021). Contrasting response of ultrafine particle number and PM2:5 mass concentrations to Clean Air Action in China. *Geophys. Res. Lett.* 48, e2021GL093886. doi:10.1029/2021GL093886

Zhao, S., Yu, Y., Yin, D., Liu, N., and He, J. (2014). Ambient particulate pollution during Chinese Spring festival in urban Lanzhou, northwestern China. *Atmos. Pollut. Res.* 5 (2), 335–343. doi:10.5094/APR.2014.039

Zhu, S., Poetzscher, J., Shen, J., Wang, S., Wang, P., and Zhang, H. (2021). Comprehensive insights into $O_3$ changes during the COVID-19 from $O_3$ formation regime and atmospheric oxidation capacity. *Geophys. Res. Lett.* 48 (10), e2021GL093668. doi:10.1029/2021GL093668

frontiers | Frontiers in Public Health

TYPE Original Research
PUBLISHED 10 January 2023
DOI 10.3389/fpubh.2022.1070663



OPEN ACCESS

EDITED BY
Dipesh Rupakheti,
Nanjing University of Information Science and Technology, China

REVIEWED BY
Ravindra Khaiwal,
Post Graduate Institute of Medical Education and Research (PGIMER), India
Deep Chakraborty,
Sri Ramachandra Institute of Higher Education and Research, India
Saifi Izhar,
Indian Institute of Technology Dhanbad, India

*CORRESPONDENCE
Bhupendra Pratap Singh
✉ bpsingh0783@gmail.com

SPECIALTY SECTION
This article was submitted to Environmental health and Exposome, a section of the journal Frontiers in Public Health

RECEIVED 15 October 2022
ACCEPTED 14 December 2022
PUBLISHED 10 January 2023

CITATION
Singh BP, Zughaibi TA, Alharthy SA, Al-Asmari AI and Rahman S (2023) Statistical analysis, source apportionment, and toxicity of particulate- and gaseous-phase PAHs in the urban atmosphere. *Front. Public Health* 10:1070663. doi: 10.3389/fpubh.2022.1070663



# Statistical analysis, source apportionment, and toxicity of particulate- and gaseous-phase PAHs in the urban atmosphere

Bhupendra Pratap Singh[1,2]*, Torki A. Zughaibi[3,4], Saif A. Alharthy[3,4], Ahmed I. Al-Asmari[4,5] and Shakilur Rahman[6]

[1]Department of Environmental Studies, Deshbadhu College, University of Delhi, New Delhi, India, [2]Delhi School of Climate Change and Sustainability, Institute of Eminence, University of Delhi, New Delhi, India, [3]Department of Medical Laboratory Sciences, Faculty of Applied Medical Sciences, King Abdulaziz University, Jeddah, Saudi Arabia, [4]Toxicology and Forensic Science Unit, King Fahd Medical Research Center, King Abdulaziz University, Jeddah, Saudi Arabia, [5]Laboratory Department, Ministry of Health, King Aziz Hospital, Jeddah, Saudi Arabia, [6]Department of Medical Elementology and Toxicology, School of Chemical and Life Sciences, New Delhi, India

**Introduction:** The concentrations of particulate and gaseous Polycyclic Hydrocarbons Carbon (PAHs) were determined in the urban atmosphere of Delhi in different seasons (winter, summer, and monsoon).

**Methodology:** The samples were collected using instrument air metric (particulate phase) and charcoal tube (gaseous phase) and analyzed through Gas chromatography. The principal component and correlation were used to identify the sources of particulate and gaseous PAHs during different seasons.

**Results and discussion:** The mean concentration of the sum of total PAHs (TPAHs) for particulate and gaseous phases at all the sites were found to be higher in the winter season (165.14 ± 50.44 ng/m$^3$ and 65.73 ± 16.84 ng/m$^3$) than in the summer season (134.08 ± 35.0 ng/m$^3$ and 43.43 ± 9.59 ng/m$^3$), whereas in the monsoon season the concentration was least (68.15 ± 18.25 ng/m$^3$ and 37.63 1 13.62 ng/m$^3$). The principal component analysis (PCA) results revealed that seasonal variations of PAHs accounted for over 86.9%, 84.5%, and 94.5% for the summer, monsoon, and winter seasons, respectively. The strong and positive correlation coefficients were observed between B(ghi)P and DahA (0.922), B(a)P and IcdP (0.857), and B(a)P and DahA (0.821), which indicated the common source emissions of PAHs. In addition to this, the correlation between Nap and Flu, Flu and Flt, B(a)P, and IcdP showed moderate to high correlation ranging from 0.68 to 0.75 for the particulate phase PAHs. The carcinogenic health risk values for gaseous and particulate phase PAHs at all sites were calculated to be 4.53 × 10$^{-6}$, 2.36 × 10-5 for children, and 1.22 × 10$^{-5}$, 6.35 × 10$^{-5}$ for adults, respectively. The carcinogenic health risk for current results was found to be relatively higher than the prescribed standard of the Central Pollution Control Board, India (1.0 × 10$^{-6}$).

KEYWORDS

**PAHs, PCA, correlation, seasonal variation, carcinogenic health risk**

# Introduction

In the last few decades, urban air pollution has become a serious environmental problem, especially in developing countries, including India (1–4). Widespread industrialization, rapid urban planning, and a large increase in the number of vehicles with a high population density have been responsible for a deterioration in the ambient air quality (5–8). Among air pollutants, polycyclic aromatic hydrocarbons (PAHs) are among the most important due to their impact on both health and climate (9–11).

Polycyclic aromatic hydrocarbons are a group or class of hydrocarbons with multiple aromatic rings fused in various configurations that appear to have a universal presence in the environment and are the first atmospheric pollutants whose carcinogenic and mutagenic nature has been assessed (12, 13). Several studies reported that incomplete combustion of fossil fuels contributed to approximately 60% of the global emission of PAHs (14–16). The emission of PAHs to the atmosphere comes from both natural and anthropogenic sources. The emission of PAHs from natural sources is combustion from forest fires and volcanic eruptions (17, 18), whereas anthropogenic sources are due to incomplete combustion of fossil fuels (coal, wood oil, diesel, and petrol) at high temperatures (12, 19–22). Several studies reported that high concentrations of PAH were also found in petroleum products, coal tar, crude oil, creosote, and roofing tar (23–25). The partitioning of PAHs into a particular gaseous phase is determined by the molecular weight of the compounds as well as the meteorological parameters (26).

The principal sources of PAHs are the incomplete combustion of fuels and other organic substances, which contribute in the range of 70–90% (27). Many studies have pointed out that the levels, human exposure, and composition may vary by geographical area (12, 28). PAHs are the products of incomplete combustion and domestic activities, which contribute to ∼ 60% of global emissions of PAHs into the environment (29). Naturally, PAHs can be eliminated by hydrolysis, biodegradation, and photolysis so that the concentration of PAHs in the environment is always maintained in dynamic equilibrium (27).

Currently, the widespread distribution of PAHs in the atmosphere is of great concern to scientists, which has led to their critical study for proper monitoring of concentration and release into the environment (30). Bioaccumulation of PAHs is highly influenced by the particle phases in the atmosphere and their partitioning between the gaseous phases (13, 31, 32), and the most dominant forms of PAHs that exist in the environment are the particulate and gaseous phases (33). The most common PAHs associated with particulates were pyrene, phenanthrene, acenaphthylene, and fluoranthene, which were associated with diesel and gasoline exhaust particles. PAHs with a low ring structure exist only in the gaseous form (33–35), while PAHs with a high ring structure are mainly associated with the particulate form, which adsorbs on the surface of particles in large amounts (36).

Several studies reported that PAHs are considered to be carcinogenic and mutagenic agents (32, 37), even in India with a high concentration of PAHs with potential exposure risks (38–40). Moreover, long-term exposure to PAHs may cause damage to our human cell lines, cardiopulmonary mortality, and pulmonary tissue damage (14, 29, 41). In addition, a variation in the health risks caused by PAHs has been seen among different age groups and different genders. Several studies showed that the risks of cancer caused by PAHs are ∼ 4.83 times higher in adults than those in children through the inhalation pathway due to their longer exposure time and the larger body weight (42). In addition, several literature studies associated PAHs with various diseases, including cardiovascular diseases, bone marrow diseases, immune system suppression, liver diseases, reproductive diseases, and cancer (18, 43, 44).

Based on the aforementioned assessment of PAH levels, especially in the gaseous phase in the urban ambient atmosphere, fuel consumption from transport (driven by petrol and diesel) is attributed as a predominant source of PAHs (10). Few studies in the literature have assessed particulate-phase PAHs, resulting from the gaseous phase, and their correlation is limited in the scientific literature. Therefore, this current study aimed to evaluate the different levels of particulate- and gaseous-phase PAHs in the urban city of Delhi, with the following objectives: (a) to compare particulate- and gaseous-phase PAHs in different seasons, (b) to determine the source apportionment of PAHs using different statistical analyses, and (c) to estimate the health risk assessment of particulate- and gaseous-phase PAHs with exposure to different age groups.

# Methods and materials

## Sampling area

In this study, five topographical sites in Delhi were identified for the study of PAH concentration in ambient air. These sites included JNU, Mukherjee Nagar, Rohini, Anand Vihar, and CP. The basis of this selection included land use and its pattern of coverage, the number of automobiles, the presence of electricity, and safety. The details of sampling coordination and meteorological parameters are presented in Supplementary Tables 1, 2. In total, 96 samples were collected from each monitoring station for particulate and gaseous emissions.

## Monitoring of particulate-phase and gaseous-phase PAHs

For the particulate-phase PAHs, an air sampler (Airmetrics Minivol) was used for sampling. This device was operated with a reusable battery, a 24-h backup, and a low consumption rate. It maintains a 5 L/min flow rate to ensure steady performance throughout the sampling period of the impactors, which are fitted at 1.5 m above the second floor of household apartments at every chosen location. The air sampler collected $PM_{2.5}$ on a 47-mm polytetrafluoroethylene (PTFE) filter sheet (45).

The gaseous phase of PAHs was collected on an absorbent tube (ORBO$^{TM}$) with a polyurethane foam (PUF) plug and glass cassettes with XAD-2 resin. Most scholars claim that this resin shows greater efficiency in the separation of naphthalene (46). The fluidity rate of the samples was taken using a rotameter (accuracy ±1%). Then, the samples were covered with a silver foil, stored in a very clean screw-capped vial using a Teflon cap liner, and then placed in refrigerated containers (4°C temperature) for further transport.

Ambient air samples through both XAD-2 and the filter were kept at room temperature to warm them. The resin from the XAD-2 tubes was placed in 4-ml screw-top vials. The front and back sections of the XAD-2 resin were placed in different vials and labeled front and back with a marker. The PTFE filter was first used to cut the samples into small pieces, and they were also placed in separate 4-ml screw-top vials. In each vial, 2 ml of methyl chloride was added and shaken for 2 min. Laboratory and field blanks were also extracted in the same way. From each vial containing XAD resin or filter, 1 ml of the extract was transferred to an autosampler vial for further analysis by gas chromatography/mass spectrometry (GC/MS). The analysis was carried out on a Bruker 450GC (gas chromatograph) equipped with a DB-5 capillary column (30 m × 0.25 mm × 0.25 μm film thickness). According to the procedures listed by the National Institute for Occupational Safety Health (NIOSH) Method 5515, the analysis of PAHs in air samples was performed (47). The details for the extraction and chemical analysis method are presented in Supplementary Table 1.

## Method validation

Several studies suggested the calculation and validation methods for PAH concentration, which include various parameters such as linearity, recovery, precision, limits of detection (LOD), and limits of qualification (LOQ). In this study, linearity was estimated through spiked calibration levels, ranging between 10 and 500 ng/l. To estimate the recovery accuracy, three spiked blank samples were prepared at different concentration levels of 25, 50, and 200 ng/l. LOD and LOQ were calculated according to the sample PAH concentration at a signal-to-noise ratio of 3–10. The amount of PAHs in particulate- and gaseous-phase samples was estimated by interpolating the peak areas of each PAH to the internal standard peak area in the sample (Supplementary Figures 1, 2).

## Principal component analysis

Principal component analysis (PCA) is one of the important tools that changes a set of observations of possibly linked variables into a set of values that are not linked. In this study, PCA was performed at five different monitoring stations in Delhi to determine the relationship between PAHs and to identify the causes of ambient air pollution. The PCA process was used to identify the source contribution based on the variability of the measured element in a large number of samples. PCA results indicate which factors can explain the main part of the data variance (24). PCs are the eigenvectors of a covariance matrix or a correlation matrix, and each PC extracts a maximal share of the total variance. A PC with an eigenvalue greater or equal to 1 is considered statistically significant (48). In this study, factor loading, the percentage variance, and the cumulative percentage are explained by each factor and each component for the data obtained. In addition, the following sources of PAHs have been incorporated from various literature sources that use the PCA method to increase the accuracy of emission source identification (24, 48, 49).

## Health risk calculation

In this study, B(a)P is considered as a reference to calculate the toxicity equivalent factor (TEF) of all PAHs. The toxicity equivalent concentration (TEQ) of PAH equation broadening performed for health risk assessment can be calculated as described below (33, 35, 50):

$$TEQs = \sum C_i \times TEF_i \quad (1)$$

Here,

$C_i$ = level of PAHs.

$TEF_i$ is the amount of toxic equivalence of samples.

Health assessments were carried out in previously published studies (10, 33).

The incremental lifetime cancer risk (ILCR) was estimated as the risk of exposure to chemicals suspected to have carcinogenic effects based on the USEPA standard models (51–53). ILCR was calculated based on the corresponding lifetime average daily dose (LADD) of PAHs by considering two different age groups: children (age 6 years) and adults (age 52 years). LADD indicates the amount of PAH intake per kilogram of body weight per day. LADD and ILCR were estimated in Equations 2 and 3, respectively.

$$LADD\,(mg\,kg^{-1}day^{-1}) = (Cs \times IR \times CF \times EF \times ED) / (BW \times AT)Cancer\ risk\ (ILCR) \quad (2)$$

$$Cancer\ risk\ =\ LADD \times CSF\ (Slope\ Factor) \quad (3)$$

where Cs is the total of converted amount of PAHs based on toxic equivalents of BaP (ng $m^{-3}$) using the toxic equivalency factor (TEF) value. IR is the air inhalation rate ($m^3$ $day^{-1}$) (53), CF is the unit conversion factor ($1 \times 10^{-6}$ mg $kg^{-1}$), EF is the exposure frequency (day $year^{-1}$), and ED is the exposure duration (day $years^{-1}$) (54). ED is the value for children (6 years) and adults (52 years). BW represents body weight (kg) (53). AT represents the carcinogen averaging time (days) (55), and CSF represents the inhalation cancer slope factor (3.85 mg $kg^{-1}$ $day^{-1}$).

## Statistical analyses

Statistical analyses, such as factorial analysis and correlation, were performed using Statistical Package for the Social Sciences (SPSS) version 26.0 (SPSS, Inc., Chicago, IL, USA). Factorial analysis and correlation were performed to identify the correlated variables in different seasons for both particulate- and gaseous-phase PAHs in the ambient atmosphere.

## Results and discussion

### Seasonal variation in particulate- and gaseous-phase PAHs

In this study, 14 out of the 16 PAHs were identified as having a higher molecular weight associated with the particulate phase, while low molecular weight PAHs (acenaphthylene and acenaphthene) were not detectable in particulate-phase PAHs. Similarly, 8 out of the 16 PAHs were identified as having a low molecular weight associated with the gaseous phase, while high molecular weight PAHs [Chr, B(a)A, B(k)F, B(b)F, B(a)P, IcdP, DahA, and B(ghi)P] were not detectable in gaseous-phase PAHs.

The amount of total PAHs (TPAHs; particulate and gaseous phases) in all areas was higher in the winter season (165.14 ± 50.44 and 65.73 ± 16.84 ng/$m^3$) than in the summer season (134.08 ± 35.0 and 43.43 ± 9.59 ng/$m^3$), whereas in the monsoon season, the concentration was lower (68.15 ± 18.25 and 37.63 ± 13.62 ng/$m^3$), as similar results were obtained in Delhi (India) by Singh et al. (56). A study conducted in eastern India reported a much higher average annual PAH concentration, ranging from 797.9 ± 39.1 to 1,015.1 ± 42.7 ng/$m^3$ compared to the present study (57). Gaseous-phase PAHs showed less significant variation during the different seasons due to more local sources of origin, whereas particulate-phase PAHs might be local but could translocate away from the emission site. Some barometric factors also played a significant role in controlling the concentration of PAHs in all areas; at the same time, area-specific emission sources might have influenced their concentration in the surrounding atmosphere (10, 58, 59). Several studies reported a much lower TPAH concentration compared to the present study, such as 70.4 ng/$m^3$ in Italy (60), 39.5 ng/$m^3$ in La Plata, Argentina (59), and 20.9–65.4 ng/$m^3$ in Spain (61).

The availability of more PAHs in the sample over Anand Vihar during the winter was due to the lower amount of photochemical destruction, the restricted mixing layer, and the continuous production of the temperature inversion layer. During the hot season and monsoon, a higher amount of photochemical destruction and mixture layers in the atmosphere might result in a lower PAH concentration in the samples, and also humidity and precipitation might play an important role during the monsoon period (10).

In the winter season, particulate-phase TPAHs were found to be higher as compared to gaseous-phase PAHs in the winter season. It ranged from 91.99 ± 6.51 (JNU) to 210.94 ± 14.30 ng/$m^3$ (Anand Vihar) for particulate-phase PAHs but from 41.40 ± 1.19 (JNU) to 82.37 ± 8.0 ng/$m^3$ (Mukherjee Nagar) for gaseous-phase TPAHs in the winter season. In the summer season, the amount of particulate-phase TPAHs was reported to be higher as compared to gaseous-phase PAHs. It ranged from 74.64 ± 5.03 (JNU) to 163.61 ± 9.17 ng/$m^3$ (Mukherjee Nager) for particulate-phase PAHs but from 30.53 ± 1.90 (Anand Vihar) to 57.47 ± 2.51 ng/$m^3$ (Mukherjee Nagar) for gaseous-phase PAHs. Further, in the monsoon season, it ranged from 36.34 ± 2.80 (JNU) to 81.70 ± 5.84 ng/$m^3$ (Mukherjee Nager) for particulate-phase PAHs, whereas it ranged from 17.97 ± 2.25 (JNU) to 52.06 ± 6.51 ng/$m^3$ (Rohini) for gaseous-phase PAHs. The trend of the maximum concentration of the particulate phase was in the following order: Mukherjee Nagar > Anand Vihar > CP > Rohini > JNU during the winter season. Apart from the summer season, a pattern for the highest amount of the particulate phase was in the sequence of Rohini > Mukherjee Nagar > Anand Vihar > CP > JNU and that of gaseous-phase PAHs was in the sequence of Mukherjee Nagar > CP > JNU > Rohini > Anand Vihar. The mean TPAHs level at all monitoring stations has presented for summer, monsoon, and winter seasons in Figures 1, 2.

The level of particulate-phase PAHs was observed to be relatively higher at Mukherjee Nagar and Anand Vihar sites than at the other monitoring sites. The Anand Vihar site is considered to be an interstate bus terminal, which indicates higher vehicular emission sources. Additionally, other PAH emission sources in Delhi certainly had large seasonal variations, including residential biofuel burning and open burning of biomasses (62). Excessive traffic during the winter period due to fog and haze was also responsible for increasing the atmospheric level of PAHs during winter (63). The recorded TPAH concentration was low in summer due to photochemical degradation and dispersion of PAHs in Delhi (64), whereas

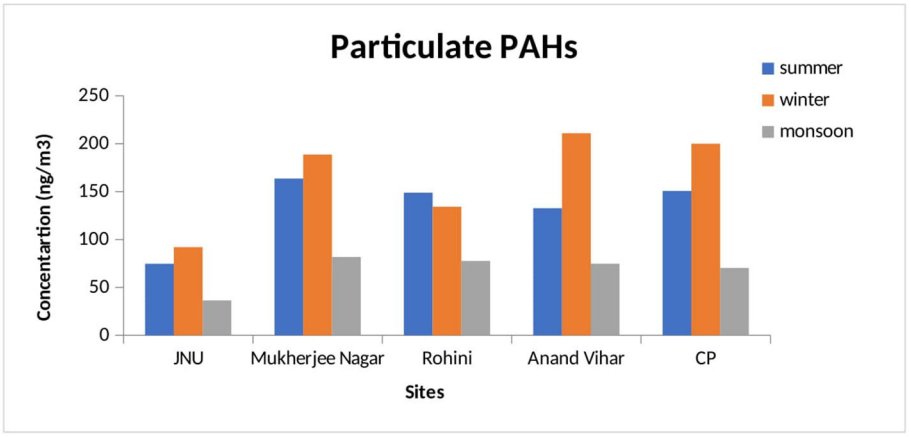


FIGURE 1
Seasonal variation of particulate PAHs at different monitoring stations.

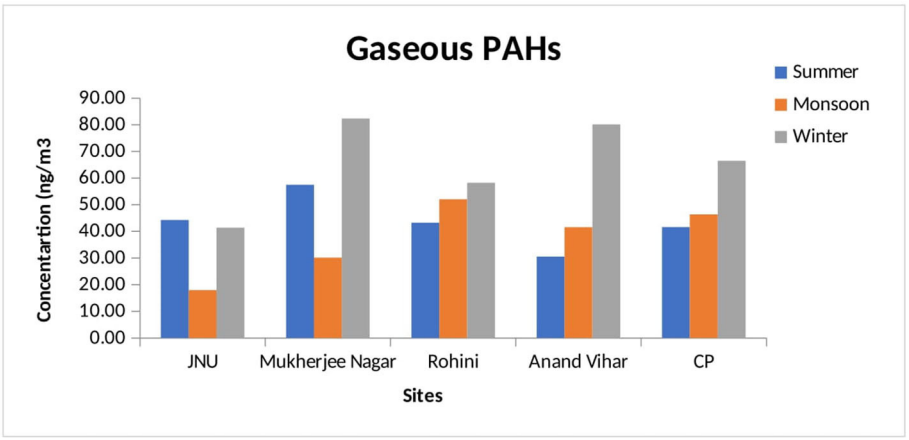


FIGURE 2
Seasonal variation of gaseous PAHs at different monitoring stations.

the highest concentration was observed in the winter season as a common phenomenon in many urban residential areas (65).

## PCA for annual PAHs

Principal component analysis for annual PAHs was calculated as a mean value for all seasons during the sampling period, as presented in Supplementary Tables 3, 4 for particulate- and gaseous-phase PAHs. Annually, for the particulate phase, six principal components (PCs) were extracted, while for the gaseous phase, three factors were extracted at different sites. In this study, a high factor loading for these PAHs was obtained in PC-1 for particulate-phase PAHs [B(a)P, B(k)f, B(g,h,i)P, and endo(cd)pyrene]. The present result indicated that PC-1 (eigenvalues 5.61) of particulate-phase PAHs represented gasoline sources. A similar result reported gasoline emission sources for B(a)P, B(k)F, B(g,h,i)P, and endo(cd)pyrene (66). Another study in east-central India reported higher PAH rings associated with diesel emission and coal combustion sources (57). Several researchers suggested that diesel emissions from vehicles had a high factor loading for fluorene, phenanthrene, anthracene, and pyrene (67), whereas Zhao et al. (68) proposed that fluorene and phenanthrene with a high factor loading of benzo (b & k) fluoranthene indicated diesel-driven vehicles. Several studies reported that diesel emissions from road traffic were associated with low and medium molecular weight (three to four rings) PAHs (69).

In this study, a high factor loading for these PAHs has been obtained in PC-4 for particulate-phase PAHs. Thus, it was witnessed that PC-4 of particulate-phase PAHs represented diesel-driven sources. Annual PCA revealed for the gaseous phase that Nap, Acy, Ace, and Flu were dominant species in the first factor, which indicated natural sources of emission for all seasons. The initial factor for most of the total variance (35.0%) was high loading with B(b)P, B(k)P, B(a)P, IcdP, DahA, and B(ghi)P for the particulate phase, whereas the gaseous phase accounted for the total variance (34.4%) with Nap, Acy, Ace, and Flu. The first factor with B(b)P and B(ghi)P confirmed that vehicle emission from traffic was one of the significant sources of the PAHs in all three seasons for the particulate phase (70). The second factor accounted for 23.17% of the total variance, where Anth and Pyr were identified. This factor accounted for natural gas sources (71). It reflected a substantial influence of low molecular weight PAHs with low rings (three to four rings PAHs). Several studies reported that high-loading Phe was associated with either unburned petroleum from vehicles or coal combustion (72, 73). A study was conducted on the gaseous phase reported that the first factor accounting for the majority of the total variance (25%) was highly loaded with BaP and DahA, while factor 2 was a high-loading factor with Phe and Flt (24).

## PCA for seasonal PAHs

Principal component analysis for particulate-phase PAHs extracted three factors for all seasons (summer, monsoon, and winter). The seasonal variations of PAHs accounted for more than 86.9%, 84.5%, and 94.5% for the summer, monsoon, and winter seasons, respectively, as a similar result in Changsha, China, was reported for 85.8% and 89.9% of the total data variance in the summer and autumn samples, respectively, for the particulate phase (74), while this study accounted for 83.6%, 75.5%, and 82.4% for gaseous phase samples in the three seasons. It was reported that similar PCA results in Japan accounted for 88.6% of the variance with a high loading of all PAHs, which indicated traffic emission (49).

In the summer season, for the particulate phase, the first factor illustrated 71.8% of the total variance, which indicated the loading of higher molecular weight PAHs, such as B(k)P B(a)P, DahA, and B(ghi)P. Transport was validated to be a significant contributor to higher PAHs. The loadings of lighter PAH (Acy, Ant, and Flu) for the particulate phase and Nap, Acy, and Flu for the gaseous phase were also higher for this factor, which accounted for natural gas sources (46). The second factor accounted for 18.4% of the total variance, with a finding of loading for Chry PAH as dominant, which may have been emitted from petrol and CNG vehicles for particulate-phase PAHs, whereas the gaseous phase accounted for 21.5% of the total variance and dominant species were Chry and B(a)P, which may have been emitted due to gasoline emission (75, 76).

During the monsoon season, the first factor demonstrated 51.7% of the total variance, which indicated the loading of higher PAH [such as DahA, BghiP, and B(a)P] for the particulate phase and PAHs such as Anth and Phen for the gaseous phase, respectively (Table 1). This study indicated that diesel and gasoline emission sources were significant sources (66). The second factor explained 17.8% and 24.0% of the total variance for particulate- and gaseous-phase PAHs, respectively, during the sampling period. The loading of higher PAHs Nap [B(a)P, and B(k)P] for the particulate phase and Nap, Acy, and Ace for the gaseous phase were the dominant species attributed to natural gas sources (24).

During the winter, the first factor accounted for 36.3% and 26.35% of the total variance for particulate- and gaseous-phase PAHs, respectively (Table 2). The higher molecular weight PAHs had reduced the loading concentration for gaseous-phase and particulate-phase PAHs. This factor was also dominated by Nap and Ace for gaseous-phase PAHs and Anth, Flt, and Chr for particulate-phase PAHs, which indicated a natural gas combustion source (71). The second factor accounted for 31.73% of the total variance for particulate-phase PAHs, and Phen and Pyr were dominant, which may have been emitted from diesel sources. The results obtained from PC-2 demonstrated that the low molecular weight (Phen) indicated a petrochemical source (77, 78). For the third factor, high molecular weight PAHs [B(b)F, B(a)P, and DahA] were dominant components, which accounted for 26.5% of the total variance for particulate-phase PAHs. Many researchers suggested that these species originated from vehicular sources, especially from diesel emissions (20, 79). Hence, the results of PCA revealed that the major source of PAHs was found to be vehicular emissions (diesel and gasoline) as well as wood burning (biomass burning).

## Correlation analysis for PAHs

Pearson's correlation was used to provide the correlation coefficients needed for data analysis, with a significant level of $p < 0.05$. The correlation of the total particulate- and gaseous-phase PAHs is presented in Tables 3, 4. A strong significant positive correlation was observed between B(ghi)P and DahA (0.92), B(a)P and IcdP (0.85), and B(a)P and DahA (0.821). The highest molecular weight was linked with particulate-phase PAHs and was released mainly from vehicular emissions. In addition to this, the correlation between Nap and Flu, Flu and Flt, and B(a)P and IcdP showed a moderate to high positive correlation ranging from 0.68 to 0.75 for particulate-phase PAHs. For the gaseous phase, a strong and positive correlation coefficient of 0.678 was observed between Acy and Nap, Nap and Ace. The lowest molecular weight emission was found in the gaseous phase as an indicator of petroleum sources (78). Furthermore, the correlation between Phe and Flu, Phe and Pyr, and Flu and Ant showed a low-to-moderate correlation

TABLE 1 Result of factor analysis with varimax rotation for particulate phase PAHs at different seasons.

| PAH | Summer | | | Monsoon | | | Winter | | |
|---|---|---|---|---|---|---|---|---|---|
| | 1 | 2 | 3 | 1 | 2 | 3 | 1 | 2 | 3 |
| Nap | −0.061 | 0.799 | −0.582 | 0.720 | −0.020 | −0.589 | −0.44 | −0.73 | 0.25 |
| Acy | 0.826 | 0.396 | −0.373 | – | – | – | – | – | – |
| Ace | −0.945 | 0.306 | 0.086 | – | – | – | – | – | – |
| Flu | 0.864 | −0.270 | 0.344 | 0.462 | −0.528 | – | – | – | – |
| Phe | −0.894 | 0.297 | −0.313 | −0.529 | 0.421 | 0.572 | 0.01 | **0.94** | 0.21 |
| Ant | 0.948 | 0.316 | 0.028 | 0.850 | 0.216 | 0.368 | **0.95** | −0.14 | −0.24 |
| Flt | 0.836 | 0.546 | −0.025 | 0.484 | −0.677 | 0.244 | **0.94** | −0.16 | −0.14 |
| Pyr | 0.708 | 0.590 | 0.349 | −0.789 | −0.280 | −0.182 | −0.45 | 0.86 | −0.10 |
| B(b)A | **0.971** | −0.050 | 0.114 | −0.170 | **0.810** | −0.086 | −0.87 | −0.06 | 0.46 |
| Chry | 0.192 | **0.908** | 0.366 | −0.960 | −0.021 | −0.238 | **0.89** | 0.04 | −0.37 |
| B(b)F | −0.763 | 0.482 | 0.430 | 0.319 | **0.807** | −0.398 | 0.02 | −0.69 | **0.70** |
| B(k)F | **0.996** | −0.038 | 0.043 | −0.286 | −0.122 | 0.825 | 0.31 | −0.94 | 0.11 |
| B(a)P | **0.981** | 0.050 | −0.182 | **0.917** | 0.287 | 0.132 | 0.07 | 0.19 | **0.97** |
| IcdP | **0.960** | −0.094 | −0.263 | −0.934 | 0.190 | −0.158 | 0.38 | −0.14 | **0.88** |
| DahA | **0.947** | −0.282 | −0.142 | **0.973** | 0.041 | 0.107 | 0.55 | 0.54 | 0.59 |
| BghiP | **0.972** | −0.081 | 0.201 | **0.928** | 0.112 | 0.121 | 0.66 | 0.46 | 0.57 |
| Initial Eigenvalues | 11.500 | 2.950 | 1.320 | 7.25 | 2.50 | 2.09 | 4.72 | 4.13 | 3.44 |
| % of variance | 71.88 | 18.47 | 8.25 | 51.7 | 17.83 | 14.90 | 36.29 | 31.74 | 26.48 |
| Cumulative % | 71.88 | 90.35 | 98.35 | 51.77 | 69.60 | 84.50 | 36.29 | 68.03 | 94.50 |

Bold values indicate a strong correlation.

ranging from 0.28 to 0.50 for gaseous-phase PAHs. A weak correlation of these gaseous-phase PAHs showed negligible sources of emissions.

## Toxicity of PAHs

Emission sources of air pollutants, especially PAHs, play a significant role in understanding and determining their potential in environmental and human health assessment. This study estimated the potential toxicity of human exposure to all selected sites in Delhi in terms of total TEFs. Total TEQ values at all sites were calculated to be 38.39 and 0.55 ng/m$^3$ for particulate- and gaseous-phase PAHs, respectively. The largest contributor to the total risk of particulate-phase PAHs was estimated to be D(ahA) (43.66–45.42%), followed by B(a)P (34.62–44.31%) at all sites, which was similar to the study conducted in Pakistan for D(ah)A (42.52–80.91%) followed by B(a)P (4.42–35.51%) in all cities (80). The maximum TEQ value for particulate-phase PAHS was attributed by D(ahA) at JNU (7.46), Mukherjee Nagar (20.94), Anand Vihar (18.99), and CP (18.28). Similar TEQ values at Anand Vihar and CP for particulate-phase PAHs were highly predominant in traffic areas, which indicated a similar source of emission driven by diesel- and gasoline-powered vehicles, whereas Mukherjee Nagar was considered to have a high population density and local emission sources such as wood and charcoal burning for cooking contributed to higher PAH concentrations. The current study focused on evaluating the health risk assessment in terms of LADD and cancer risk due to exposure to both particulate-phase and gaseous-phase PAHs. Average LADD values for children and adults were calculated as $3.17 \times 10^{-6}$, $1.65 \times 10^{-6}$ and $1.18 \times 10^{-6}$, $6.12 \times 10^{-6}$ for particulate-phase and gaseous-phase PAHs, respectively. In the gaseous phase, LADD values were reported to be relatively higher for adults than for children. The reason could be that gasoline was a significant source of gaseous-phase PAHs and adults are usually exposed to these for longer periods. In the particulate phase, the LADD value was higher for children, as a major source of particulate-phase PAHs was biomass burning, including wood burning in outdoor and indoor premises, to which children were more exposed. JNU observed minimum LADD values compared to other sites due to less movement of transport inside the campus. Cancer risk for children and adults at all sites was estimated for gaseous-phase and particulate-phase PAHs. The average value for cancer risk for children and adults were found to be $4.53 \times 10^{-6}$, $2.36 \times 10^{-5}$ and $1.22 \times 10^{-5}$,

TABLE 2 Result of factor analysis with varimax rotation for gaseous phase PAHs at different seasons.

| PAH | Summer | | | Monsoon | | | Winter | | |
|---|---|---|---|---|---|---|---|---|---|
| | 1 | 2 | 3 | 1 | 2 | 3 | 1 | 2 | 3 |
| Nap | 0.636 | −0.222 | 0.667 | −0.264 | **0.754** | 0.380 | 0.778 | 0.198 | 0.424 |
| Acy | 0.659 | −0.273 | 0.488 | −0.340 | **0.832** | −0.337 | 0.531 | 0.681 | −0.166 |
| Ace | 0.441 | −0.133 | 0.348 | −0.178 | **0.686** | −0.133 | 0.748 | 0.188 | 0.246 |
| Flu | 0.720 | −0.499 | −0.187 | 0.081 | 0.117 | 0.960 | 0.328 | 0.171 | −0.591 |
| Phen | 0.585 | 0.110 | −0.695 | **0.875** | 0.041 | −0.099 | 0.194 | 0.583 | −0.399 |
| Anth | 0.552 | −0.148 | −0.619 | **0.910** | 0.251 | −0.081 | −0.507 | 0.514 | 0.303 |
| Flt | −0.179 | 0.359 | 0.100 | 0.772 | 0.181 | 0.150 | −0.371 | 0.674 | −0.046 |
| Pyr | 0.593 | 0.553 | −0.175 | 0.677 | 0.281 | −0.106 | −0.374 | 0.393 | 0.670 |
| BaA | 0.280 | **0.789** | 0.212 | – | – | – | −0.124 | 0.175 | −0.013 |
| Chr | 0.332 | **0.815** | 0.139 | – | – | – | −0.700 | 0.207 | −0.332 |
| Initial Eigenvalues | 2.77 | 2.14 | 1.81 | 2.87 | 1.92 | 1.24 | 2.63 | 1.85 | 1.43 |
| % of variance | 27.69 | 21.45 | 18.10 | 35.89 | 24.01 | 15.58 | 26.33 | 18.53 | 14.30 |
| Cumulative % | 34.17 | 63.08 | 79.40 | 51.77 | 69.60 | 84.50 | 36.29 | 68.03 | 94.50 |

Bold values indicate a strong correlation.

$6.35 \times 10^{-5}$ for particulate-phase and gaseous-phase PAHs, respectively, which indicated that the values were found to be much higher than the prescribed standard ($1.0 \times 10^{-6}$). Similar results were reported for children and adults, with $3.5 \times 10^{-5}$ and $1.17 \times 10^{-5}$ for the hot season and $3.30 \times 10^{-5}$ and $1.10 \times 10^{-5}$, respectively, for the hot and cold seasons (7).

## Conclusion

This study analyzed seasonal variations, source identification, and toxicity of PAHs in urban sites. The concentration of TPAHs (particulate and gaseous phases) in all monitoring sites was higher in the winter season ($165.14 \pm 50.44$ and $65.73 \pm 16.84$ ng/m$^3$) than in the summer season ($134.08 \pm 35.0$ and $43.43 \pm 9.59$ ng/m$^3$), whereas in the monsoon season, the concentration was lower ($68.15 \pm 18.25$ and $37.63 \pm 13.62$ ng/m$^3$). The main source of PAH emission was manmade sources, including the burning of wood and stubble burning during the winter from the neighboring states like Punjab and Haryana. Some emission sources of PAHs in Delhi certainly had large seasonal variations, including residential biofuel burning and open burning of biomass. To identify the source apportionment of PAHs through statistical tools, this study used PCA analysis and revealed that natural gas combustion was significantly attributed to the particulate-phase PAHs during the winter season, followed by diesel-driven vehicles in the ambient atmosphere of Delhi. During the summer season, vehicular emission was a major contributor of particulate-phase PAHs, followed by gasoline. In the case of the gaseous phase, PAH dominant species B(a)P and Chry may have been emitted from gasoline emission. This study can contribute to a better understanding of the monitoring of both particulate- and gaseous-phase PAHs in the ambient atmosphere of the urban area.

The current study focused on evaluating the health risks in terms of LADD and cancer risk due to exposure to both particulate- and gaseous-phase PAHs. Average LADD values for children and adults were calculated to be $3.17 \times 10^{-6}$, $1.65 \times 10^{-6}$ and $1.18 \times 10^{-6}$, and $6.12 \times 10^{-6}$ for particulate- and gaseous-phase PAHs, respectively. The average value of cancer risk for particulate- and gaseous-phase PAHs were found to be $4.53 \times 10^{-6}$ and $2.36 \times 10^{-5}$ for children but $1.22 \times 10^{-5}$ and $6.35 \times 10^{-5}$ for men at all monitoring sites, respectively, which indicated much higher values than the prescribed standard ($1.0 \times 10^{-6}$) by CPCB. The carcinogenic health risk for this study was reported to be relatively higher than the prescribed standard values ($1.0 \times 10^{-6}$). This study confirmed that the PAH levels in the ambient atmosphere of Delhi could not be neglected, and this study would be enlightening among the scientists, researchers, and government to address the issues along with policy formulation. Furthermore, this study can enhance policymakers with appropriate scientific solutions, such as imposing a ban on the burning of steeples, examining the quality of petroleum (petrol and diesel), and setting antipollution measures, whereas the issue of health risk assessment and recognition of factors affecting pollution is crucial and essential. Further, more comprehensive studies are required in this area. Thus, the results of this study

TABLE 3 Correlation of PAH species in the particulate phase PAHs.

| | Nap | Acy | Ace | Flu | Phe | Ant | Flt | Pyr | B(a)A | Chry | B(b)F | B(k)F | B(a)P | IcdP | DahA | B(ghi)P |
|---|---|---|---|---|---|---|---|---|---|---|---|---|---|---|---|---|
| Nap | 1 | | | | | | | | | | | | | | | |
| Acy | 0.598** | 1 | | | | | | | | | | | | | | |
| Ace | 0.041 | −0.175 | 1 | | | | | | | | | | | | | |
| Flu | 0.688** | 0–0.734* | 0.210 | 1 | | | | | | | | | | | | |
| Phe | 0.079 | 0.088 | 0.010 | 0.414* | 1 | | | | | | | | | | | |
| Ant | −0.007 | 0.532** | 0.328 | −0.513** | −0.415** | 1 | | | | | | | | | | |
| Flt | 0.348* | 0.305 | 0.387 | 0.638** | 0.211 | 0.174 | 1 | | | | | | | | | |
| Pyr | −0.102 | 0.050 | 0.784 | −0.039 | 0.331* | −0.264 | −0.125 | 1 | | | | | | | | |
| B(a)A | −0.034 | −0.322 | 0.066 | −0.056 | −0.386** | −0.240 | −0.499** | 0.295* | 1 | | | | | | | |
| Chry | −0.191 | 0.510** | 0.838 | −0.385* | 0.196 | 0.038 | −0.013 | 0.275 | −0.079 | 1 | | | | | | |
| B(b)F | 0.029 | 0.397* | **0.989*** | −0.587** | −0.422** | 0.134 | −0.484** | 0.107 | 0.689** | 0.262 | 1 | | | | | |
| B(k)F | −0.120 | 0.351 | −0.246 | −0.512** | 0–0.718** | 0.305* | −0.155 | −0.248 | 0.450** | 0.215 | 0.637** | 1 | | | | |
| B(a)P | −0.233 | 0.056 | −0.466 | −0.463* | −0.552** | 0.078 | −0.304* | 0.310* | 0.620** | 0.205 | 0.614** | 0.731** | 1 | | | |
| IcdP | −0.241 | 0.336 | −0.751 | −0.515** | −0.331* | 0.026 | −0.224 | 0.259 | 0.425** | 0.507** | 0.523** | 0.756** | **0.851**** | 1 | | |
| DahA | −0.056 | 0.351 | −0.908 | −0.506** | −0.494** | 0.423** | −0.054 | 0.300* | 0.289* | 0.156 | 0.413** | 0.567** | **0.821**** | 0.638** | 1 | |
| B(ghi)P | −0.097 | 0.356 | 0.598 | −0.476* | −0.473** | 0.495** | −0.035 | 0.294* | 0.326* | 0.153 | 0.456** | 0.558** | **0.753**** | 0.591** | **0.922**** | 1 |

**Correlation is significant at the 0.01 level (two-tailed).

*Correlation is significant at the 0.05 level (two-tailed).

Bold values indicate a strong correlation.





10.3389/fpubh.2022.1070663

TABLE 4 Correlation of PAH species in the gaseous phase PAHs.

| | Nap | Acy | Ace | Flu | Phen | Anth | Flt | Pyr | BaA | Chr |
|---|---|---|---|---|---|---|---|---|---|---|
| Nap | 1 | | | | | | | | | |
| Acy | **0.619**** | 1 | | | | | | | | |
| Ace | **0.591**** | 0.481** | 1 | | | | | | | |
| Flu | 0.196 | 0.343** | 0.257* | 1 | | | | | | |
| Phen | −0.054 | 0.048 | 0.041 | 0.227 | 1 | | | | | |
| Anth | −0.057 | 0.129 | −0.132 | 0.258 | 0.462** | 1 | | | | |
| Flt | −0.066 | 0.076 | −0.162 | 0.078 | 0.124 | 0.293* | 1 | | | |
| Pyr | −0.115 | −0.165 | −0.080 | −0.197 | 0.351** | 0.301* | −0.015 | 1 | | |
| BaA | 0.056 | −0.011 | 0.017 | −0.032 | 0.129 | 0.170 | −0.100 | 0.011 | 1 | |
| Chr | −0.407** | −0.186 | −0.286 | −0.080 | 0.195 | 0.007 | 0.398* | 0.471** | 0.060 | 1 |

**Correlation is significant at the 0.01 level (two-tailed).
*Correlation is significant at the 0.05 level (two-tailed).
Bold values indicate a strong correlation.

emphasize the need for continuous monitoring of particulate- and gaseous-phase PAHs in the ambient air of Delhi, whereas the chances of exposure to the population are high for PAHs, which cause health risks such as cancer.

## Data availability statement

The original contributions presented in the study are included in the article/Supplementary material, further inquiries can be directed to the corresponding author.

## Author contributions

BS: conceptualization, analysis of the results and discussion, and visualization of graphs and tables. TZ: procurement of data. SA: frame the introduction section. AA-A: data curation and methodology. SR: conceptualization, results and discussion, and writing—review and editing. All authors contributed to the article and approved the submitted version.

## Funding

This research work was funded by the Institutional Fund Projects under grant no. (IFPDP-2-22). Therefore, authors gratefully acknowledge technical and financial support from Ministry of Education and the Deanship of Scientific Research (DSR), King Abdulaziz University (KAU), Jeddah, Saudi Arabia.

## Acknowledgments

BS thanks Saumya Kumari, Arathi Nair, Sweety Kumari, Kriti Mehra, and Khyati Chowdhary for their insightful discussion and valuable suggestions during the preparation of the manuscript.

## Conflict of interest

The authors declare that the research was conducted in the absence of any commercial or financial relationships that could be construed as a potential conflict of interest.

## Publisher's note



## Supplementary material

The Supplementary Material for this article can be found online at: https://www.frontiersin.org/articles/10.3389/fpubh.2022.1070663/full#supplementary-material

# References


1. Singh BP, Kumar A, Singh D, Punia M, Kumar K, Jain VK. An assessment of ozone levels, UV radiation and their occupational health hazard estimation during photocopying operation. *J Hazard Mater.* (2014) 275:55–62. doi: 10.1016/j.jhazmat.2014.04.049

2. Kumar A, Singh D, Singh BP, Singh M, Anandam K, Kumar K, et al. Spatial and temporal variability of surface ozone and nitrogen oxides in urban and rural ambient air of Delhi-NCR, India. *Air Qual Atmos Health.* (2015) 8:391–9. doi: 10.1007/s11869-014-0309-0

3. Pandey N, Singh BP, Singh M, Tyagi S. Diurnal variation of ozone levels in academic hostel in Delhi—a case study of JNU campus. *Int J Appl Environ Sci.* (2017) 12:1167–89.

4. Singh BP, Rana P, Mittal N, Kumar S, Athar M, Abduljaleel Z, et al. Variations in the Yamuna river water quality during the COVID-19 lockdowns. *Front Environ Sci.* (2022) 10:940640. doi: 10.3389/fenvs.2022.940640

5. Kumar A, Singh BP, Punia M, Singh D, Kumar K, Jain VK. Assessment of indoor air concentrations of VOCs and their associated health risks in the library of Jawaharlal Nehru University, New Delhi. *Environ Sci Pollut Res.* (2014) 21:2240–8. doi: 10.1007/s11356-013-2150-7

6. Kermani M, Jonidi Jafari A, Gholami M, Shahsavani A, Taghizadeh F, Arfaeinia H. Ambient air PM2. 5-bound PAHs in low traffic, high traffic, and industrial areas along Tehran, Iran. *Hum Ecol Risk Assess Int J.* (2019) 2019:1–18. doi: 10.1080/10807039.2019.1695194

7. Nadali A, Leili M, Bahrami A, Karami M, Afkhami A. Phase distribution and risk assessment of PAHs in ambient air of Hamadan, Iran. *Ecotoxicol Environ Saf.* (2021) 209:111807. doi: 10.1016/j.ecoenv.2020.111807

8. Singh BP, Kumari S, Nair A, Kumari S, Wabaidur SM, Avtar R, et al. Temporary reduction in VOCs associated with health risk during and after COVID-19 in Maharashtra, India. *J Atmos Chem.* (2022) 2022:1–24. doi: 10.1007/s10874-022-09440-5

9. Singh D, Kumar A, Kumar K, Singh B, Mina U, Singh BB, et al. Statistical modeling of O3, NOx, CO, PM2.5, VOCs and noise levels in commercial complex and associated health risk assessment in an academic institution. *Sci Total Environ.* (2016) 572:586–94. doi: 10.1016/j.scitotenv.2016.08.086

10. Singh BP, Kumar P. Spatio-temporal variation in fine particulate matter and effect on air quality during the COVID-19 in New Delhi, India. *Urban Clim.* (2021) 40. doi: 10.1016/j.uclim.2021.101013

11. Singh BP, Singh D, Kumar K, Jain VK. Study of seasonal variation of PM2. 5 concentration associated with meteorological parameters at residential sites in Delhi, India. *J Atmos Chem.* (2021) 78:161–76. doi: 10.1007/s10874-021-09419-8

12. Li R, Hua P, Zhang J, Krebs P. Effect of anthropogenic activities on the occurrence of polycyclic aromatic hydrocarbons in aquatic suspended particulate matter: evidence from Rhine and Elbe Rivers. *Water Res.* (2020) 179:115901. doi: 10.1016/j.watres.2020.115901

13. Mukhopadhyay S, Dutta R, Das P. A critical review on plant biomonitors for determination of polycyclic aromatic hydrocarbons (PAHs) in air through solvent extraction techniques. *Chemosphere.* (2020) 251:1–21. doi: 10.1016/j.chemosphere.2020.126441

14. Sharma D, Jain S. Impact of intervention of biomass cookstove technologies and kitchen characteristics on indoor air quality and human exposure in rural settings of India. *Environ Int.* (2019) 123:240–55. doi: 10.1016/j.envint.2018.11.059

15. Singh BP, Eldesoky GE, Kumar P, Chandra P, Islam MA, Rahman S. A Comparative study of particulate matter between New Delhi, India and Riyadh, Saudi Arabia during the COVID-19 lockdown period. *Front Environ Sci.* (2022) 9:784959. doi: 10.3389/fenvs.2021.784959

16. Avtar R, Rinamalo AV, Umarhadi DA, Gupta A, Khedher KM, Yunus AP, et al. Land use change and prediction for valuating carbon sequestration in viti Levu Island, Fiji. *Land.* (2022) 11:1274. doi: 10.3390/land11081274

17. Punia M, Nain S, Kumar A, Singh BP, Prakash A, Kumar K, et al. Analysis of temperature variability over north-west part of India for the period 1970–2000. *Nat Hazards.* (2015) 75:935–52. doi: 10.1007/s11069-014-1352-8

18. Zheng H, Kang S, Chen P, Li Q, Tripathee L, Maharjan L, et al. Sources and spatio-temporal distribution of aerosol polycyclic aromatic hydrocarbons throughout the Tibetan Plateau. *Environ Pollut.* (2020) 261:114144. doi: 10.1016/j.envpol.2020.114144

19. Zhu L, Lu H, Chen S, Amagai T. Pollution level, phase distribution and source analysis of polycyclic aromatic hydrocarbons in residential air in Hangzhou, China. *J Hazard Mater.* (2009) 162:1165–70. doi: 10.1016/j.jhazmat.2008.05.150

20. Wang XT, Miao Y, Zhang Y, Li YC, Wu MH, Yu G. Polycyclic aromatic hydrocarbons (PAHs) in urban soils of the megacity Shanghai: occurrence, source apportionment and potential human health risk. *Sci Total Environ.* (2013) 447:80–9. doi: 10.1016/j.scitotenv.2012.12.086

21. Jiao H, Wang Q, Zhao N, Jin B, Zhuang X, Bai Z. Distributions and sources of polycyclic aromatic hydrocarbons (PAHs) in soils around a chemical plant in Shanxi, China. *Int J Environ Res Public Health.* (2017) 14:1198. doi: 10.3390/ijerph14101198

22. Thang PQ, Kim SJ, Lee SJ, Ye J, Seo YK, Baek SO, et al. Seasonal characteristics of particulate polycyclic aromatic hydrocarbons (PAHs) in a petrochemical and oil refinery industrial area on the west coast of South Korea. *Atmos Environ.* (2019) 198:398–406. doi: 10.1016/j.atmosenv.2018.11.008

23. Katsoyiannis A, Sweetman AJ, Jones KC. PAH molecular diagnostic ratios applied to atmospheric sources: a critical evaluation using two decades of source inventory and air concentration data from the UK. *Environ Sci Technol.* (2011) 45:8897–906. doi: 10.1021/es202277u

24. Birgul A, Tasdemir Y. Concentrations, gas-particle partitioning, and seasonal variations of polycyclic aromatic hydrocarbons at four sites in Turkey. *Arch Environ Contam Toxicol.* (2015) 68:46–63. doi: 10.1007/s00244-014-0105-8

25. Bhardwaj P, Singh BP, Pandey AK, Jain VK, Kumar K. Characterization and morphological analysis of summer and wintertime PM 2.5 aerosols over urban-rural locations in Delhi-NCR. *Int J Appl Environ Sci.* (2017) 12:1009–30.

26. Birgul A, Tasdemir Y, Cindoruk SS. Atmospheric wet and dry deposition of polycyclic aromatic hydrocarbons (PAHs) determined using a modified sampler. *Atmos Res.* (2011) 101:341–53. doi: 10.1016/j.atmosres.2011.03.012

27. Bai L, He Z, Chen W, Wang Y. Distribution characteristics and source analysis of metal elements in indoor PM2.5 in high-rise buildings during the heating season in Northeast China. *Indoor Built Environ.* (2019) 29:1087–100. doi: 10.1177/1420326X19875495

28. Kumar A, Singh BP, Punia M, Singh D, Kumar K, Jain VK. Determination of volatile organic compounds and associated health risk assessment in residential homes and hostels within an academic institute, New Delhi. *Indoor Air.* (2014) 24:474–83. doi: 10.1111/ina.12096

29. Rengarajan T, Rajendran P, Nandakumar N, Lokeshkumar B, Rajendran P, Nishigaki I. Exposure to polycyclic aromatic hydrocarbons with special focus on cancer. *Asian Pac J Trop Biomed.* (2015) 5:182–9. doi: 10.1016/S2221-1691(15)30003-4

30. Bai L, Chen W, He Z, Sun S, Qin J. Pollution characteristics, sources and health risk assessment of polycyclic aromatic hydrocarbons in PM2.5 in an office building in northern areas, China. *Sustain Cities Soc.* (2020) 53:101891. doi: 10.1016/j.scs.2019.101891

31. Lu H, Zhu L, Zhu N. Polycyclic aromatic hydrocarbon emission from straw burning and the influence of combustion parameters. *Atmos Environ.* (2009) 43:978–83. doi: 10.1016/j.atmosenv.2008.10.022

32. Yang LX, Zhou XH, Wang Z. Airborne fine particulate pollution in Jinan, China: concentrations, chemical compositions and influence on visibility impairment. *Atmos Environ.* (2012) 55:506–14. doi: 10.1016/j.atmosenv.2012.02.029

33. Singh BP, Kumar K, Jain VK. Distribution of ring PAHs in particulate/gaseous phase in the urban city of Delhi, India: seasonal variation and cancer risk assessment. *Urban Clim.* (2021) 40:101010. doi: 10.1016/j.uclim.2021.101010

34. Tsai P, Shieh H, Lee W, Lai SO. Characteristics of exposure profiles for workers exposed to airbornr dusts and polycyclic aromatic hydrocarbons (PAHs) in the carbon black manufacturing industry. *J Occup Health.* (2001) 43:118–28. doi: 10.1539/joh.43.118

35. Singh BP, Kumar K, Jain VK. Source identification and health risk assessment associated with particulate- and gaseous-phase PAHs at residential sites in Delhi, India. *Air Qual Atmos Health.* (2021) 14:1505–21. doi: 10.1007/s11869-021-01035-5

36. Jörundsdóttir HÓ, Jensen S, Hylland K, Holth TF, Gunnlaugsdóttir H, Svavarsson J, et al. Pristine Arctic: background mapping of PAHs, PAH metabolites and inorganic trace elements in the North-Atlantic Arctic and sub-Arctic coastal environment. *Sci Total Environ.* (2014) 20:719–28. doi: 10.1016/j.scitotenv.2014.06.030

37. Rabha R, Ghosh S, Padhy PK. Indoor air pollution in rural north-east India: Elemental compositions, changes in haematological indices, oxidative stress and health risks. *Ecotoxicol Environ Saf.* (2018) 165:393–403. doi: 10.1016/j.ecoenv.2018.09.014

38. Tue NM, Suzuki G, Misaki K, Viet PH, Takahashi S, Tanabe S. Aryl hydrocarbon receptor mediated activities in road dust from a metropolitan area, Hanoi-Vietnam: contribution of polycyclic aromatic hydrocarbons (PAHs) and human risk assessment. *Sci Total Environ.* (2014) 2014:246–54. doi: 10.1016/j.scitotenv.2014.01.086

39. Agarwal T. Concentration level, pattern and toxic potential of PAHs in traffic soil of Delhi, India. *J Hazard Mater.* (2009) 171:894–900. doi: 10.1016/j.jhazmat.2009.06.081

40. Suman S, Sinha A, Tarafdar A. Polycyclic aromatic hydrocarbons (PAHs) concentration levels, pattern, source identification and soil toxicity assessment in urban traffic soil of Dhanbad, India. *Sci Total Environ.* 545–546:353–360. doi: 10.1016/j.scitotenv.2015.12.061

41. Moorthy B, Chu C, Carlin DJ. Polycyclic aromatic hydrocarbons: From metabolism to lung cancer. In: *Toxicological Sciences, Vol. 145*. Oxford University Press (2015). p. 515. doi: 10.1093/toxsci/kfv040

42. Hamid N, Syed JH, Junaid M. Elucidating the urban levels, sources and health risks of polycyclic aromatic hydrocarbons (PAHs) in Pakistan: implications for changing energy demand. *Sci Total Environ.* (2018) 619–620:165–75. doi: 10.1016/j.scitotenv.2017.11.080

43. Ji G, Gu A, Zhu P, Xia Y, Zhou Y, Hu F, et al. Joint effects of XRCC1 polymorphisms and polycyclic aromatic hydrocarbons exposure on sperm DNA damage and male infertility. *Toxicol Sci.* (2010) 116:92–8. doi: 10.1093/toxsci/kfq112

44. Clark JD, Serdar B, Lee DJ, Arheart K, Wilkinson JD, Fleming LE. Exposure to polycyclic aromatic hydrocarbons and serum inflammatory markers of cardiovascular disease. *Environ Res.* (2012) 117:132–7. doi: 10.1016/j.envres.2012.04.012

45. Mastral AM, Callén MS, García T, López JM. Benzo(a)pyrene, benzo(a)anthracene, and dibenzo(a, h)anthracene emissions from coal and waste tire energy generation at atmospheric fluidized bed combustion (AFBC). *Environ Sci Technol.* (2001) 35:2645–9. doi: 10.1021/es0015850

46. Lee JJ, Huang KL, Yu YY, Chen MS. Laboratory retention of vapour-phase PAHs using XAD adsorbents. *Atmos Environ.* (2004) 38:6185–93. doi: 10.1016/j.atmosenv.2004.07.024

47. NIOSH. Polynuclear aromatic hydrocarbons by GC: Method 5515. In: Eller PM, Cassinelli ME, editors. *NIOSH Manual of Analytical Methods (NMAM®). 4th ed*. Cincinnati, OH: National Institute for Occupational Safety and Health (1994).

48. Núñez-Alonso D, Pérez-Arribas LV, Manzoor S, Cáceres JO. Statistical tools for air pollution assessment: multivariate and spatial analysis studies in the Madrid region. *J Anal Methods Chem.* (2019) 2019:9753927. doi: 10.1155/2019/9753927

49. Xing W, Yang L, Zhang H, Zhang X, Wang Y, Bai P, et al. Variations in traffic-related polycyclic aromatic hydrocarbons in PM2.5 in Kanazawa, Japan, after the implementation of a new vehicle emission regulation. *J Environ Sci.* (2022) 121:38–47. doi: 10.1016/j.jes.2021.08.046

50. Yang HH, Chen CM. Emission inventory and sources of polycyclic aromatic hydrocarbons in the atmosphere at a suburban area in Taiwan. *Chemosphere.* (2004) 56:879–87. doi: 10.1016/j.chemosphere.2004.05.031

51. USEPA. *United States Environmental Protection Agency 2012.* Washington, DC: United States Environmental Protection Agency (2012). Available online at: http://www.epa.gov/reg3hwmd/risk/human (accessed December 20, 2012).

52. Chen SC, Liao CM. Health risk assessment on human exposed to environmental polycyclic aromatic hydrocarbons pollution sources. *Sci Total Environ.* (2006) 366:112–23. doi: 10.1016/j.scitotenv.2005.08.047

53. Peng C, Chen W, Liao X, Wang M, Ouyang Z, Jiao W, et al. Polycyclic aromatic hydrocarbons in urban soils of Beijing: Status, sources, distribution and potential risk. *Environ Pollut.* (2011) 159:802808. doi: 10.1016/j.envpol.2010.11.003

54. Bartoš T, Cupr P, Klánová J, Holoubek I. Which compounds contribute most to elevated airborne exposure and corresponding health risks in the Western Balkans? *Environ Int.* (2009) 35:1066–71. doi: 10.1016/j.envint.2009.06.005

55. USEPA. *Polycyclic Organic Matter*. Washington, DC: United States Environmental Protection Agency (2020). Available online at: http://www.epa.gov/ttn/atw/hlthef/polycycl.html (accessed June 20, 2020).

56. Singh DP, Gadi R, Manda TK. Characterization of gaseous and particulate polycyclic aromatic hydrocarbons in ambient air of Delhi, India. *Polycyclic Aromat. Compound.* (2012) 32:556-79. doi: 10.1080/10406638.2012.683230

57. Ambade B, Kumar A, Kumar A, Sahu LK. Temporal variability of atmospheric particulate-bound polycyclic aromatic hydrocarbons (PAHs) over central east India: sources and carcinogenic risk assessment. *Air Qual Atmos Health.* (2022) 15:115–30. doi: 10.1007/s11869-021-01089-5

58. Ravindra K, Bencs L, Wauters E, de Hoog J, Deutsch F, Roekens E, et al. Seasonal and site specific variation in vapor and aerosol phase PAHs over Flanders (Belgium) and their relation with anthropogenic activities. *Atmos Environ.* (2006) 40:771–85. doi: 10.1016/j.atmosenv.2005.10.011

59. Mellado D, Giuliani D, Demetrio PM, Sanchez EY, Porta A, Lerner JEC. Influence of vehicular emissions on the levels of polycyclic aromatic hydrocarbons (PAHs) in urban and industrial areas of La Plata, Argentina. *Environ Monit Assess.* (2022) 194:1–15. doi: 10.1007/s10661-022-10496-9

60. Khan M, Masiol M, Bruno C, Pasqualetto A, Formenton GM, Agostinelli C, et al. Potential sources and meteorological factors affecting PM2.5-bound polycyclic aromatic hydrocarbon levels in six main cities of northeastern Italy: an assessment of the related carcinogenic and mutagenic risks. *Environ Sci Pollut Res.* (2018) 25:31987–2000. doi: 10.1007/s11356-018-2841-1

61. Galán-Madruga D, Ubeda RM, Terroba JM, dos Santos SG, García-Cambero JP. Influence of the products of biomass combustion processes on air quality and cancer risk assessment in rural environmental (Spain). *Environ Geochem Health.* (2022) 44:2595–613. doi: 10.1007/s10653-021-01052-4

62. Lalchandani V, Srivastava D, Dave J, Mishra S, Tripathi N, Shukla AK, et al. Effect of biomass burning on PM2.5 composition and secondary aerosol formation during post-monsoon and winter haze episodes in Delhi. *J Geophys Res Atmos.* (2022) 127:e2021JD035232. doi: 10.1029/2021JD035232

63. Lakhani A. Source apportionment of particle bound polycyclic aromatic hydrocarbons at an industrial location in Agra, India. *Sci World J.* (2012) 2012:781291. doi: 10.1100/2012/781291

64. Sharma H, Jain VK, Khan ZH. Characterization and source identification of polycyclic aromatic hydrocarbons (PAHs) in the urban environment of Delhi. *Chemosphere.* (2007) 66:302–10. doi: 10.1016/j.chemosphere.2006.05.003

65. Park SS, Kim YJ, Kang CH. Atmospheric polycyclic aromatic hydrocarbons in Seoul, Korea. *Atmos Environ.* (2002) 36:2917–24. doi: 10.1016/S1352-2310(02)00206-6

66. Guo ZG, Sheng LF, Feng JL, Fang M. Seasonal variation of solvent extractable organic compounds in the aerosols in Qingdao, China. *Atmos Environ.* (2003) 37:1825–34. doi: 10.1016/S1352-2310(03)00064-5

67. Fang GC, Wu YS, Chang CN, Ho TT. A study of polycyclic aromatic hydrocarbons concentrations and source identifications by methods of diagnostic ratio and principal component analysis at Taichung chemical Harbor near Taiwan Strait. *Chemosphere.* (2006) 64:1233–42. doi: 10.1016/j.chemosphere.2005.11.031

68. Zhao T, Yang L, Huang Q, Zhang Y, Bie S, Li J, et al. PM2.5-bound polycyclic aromatic hydrocarbons (PAHs) and their derivatives (nitrated-PAHs and oxygenated-PAHs) in a road tunnel located in Qingdao, China: characteristics, sources and emission factors. *Sci Total Environ.* (2020) 720:137521. doi: 10.1016/j.scitotenv.2020.137521

69. Karavalakis G, Poulopoulos S, Zervas E. Impact of diesel fuels on the emissions of non-regulated pollutants. *Fuel.* (2012) 102:85–91. doi: 10.1016/j.fuel.2012.05.030

70. Zhou QY, Zhang LL, Yang L, Zhang X, Xing WL, Hu M, et al. Long-term variability of inorganic ions in TSP at a remote background site in Japan (Wajima) from 2005 to 2015. *Chemosphere.* (2021) 264:128427. doi: 10.1016/j.chemosphere.2020.128427

71. Callen MS, Cruz MT, de la López JM, Mastral AM. Carcinogenic character of PM10 samples and assessment of the energy generation impact. *Fuel Process Technol.* (2011) 92:176–82. doi: 10.1016/j.fuproc.2010.05.019

72. Kavouras IG, Koutrakis P, Tsapakis M, Lagoudaki E, Stephanou EG, Von Baer D, et al. Source apportionment of urban particulate aliphatic and polynuclear aromatic hydrocarbons (PAHs) using multivariate methods. *Environ Sci Technol.* (2001) 35:2288-94. doi: 10.1021/es001540z

73. Jang E, Alam MS, Harrison RM. Source apportionment of polycyclic aromatic hydrocarbons in urban air using positive matrix factorization and spatial distribution analysis. *Atmos Environ.* (2013) 79:271–85. doi: 10.1016/j.atmosenv.2013.06.056

74. Yang F, Zhai YB, Chen L, Li CT, Zeng GM, He Y, et al. The seasonal changes and spatial trends of particle-associated polycyclic aromatic hydrocarbons in the summer and autumn in Changsha city. *Atmos Res.* (2010) 96:122–30. doi: 10.1016/j.atmosres.2009.12.004

75. Zhang X, Tao S, Liu W, Yang Y, Zuo Q, Liu S. Source diagnostics of polycyclic aromatic hydrocarbons based on species ratios: a multimedia approach. *Environ Sci Technol.* (2005) 39:9109–14. doi: 10.1021/es0513741

76. Wang W, Huang M-J, Kang Y, Wang H-S, Leung AO, Cheung KC, et al. Polycyclic aromatic hydrocarbons (PAHs) in urban surface dust of Guangzhou, China: status, sources and human health risk assessment. *Sci Total Environ.* (2011) 409:4519–27. doi: 10.1016/j.scitotenv.2011.07.030

77. Abbasi S, Keshavarzi B. Source identification of total petroleum hydrocarbons and polycyclic aromatic hydrocarbons in PM10 and street dust of a hot spot for petrochemical production: Asaluyeh County, Iran. *Sustain Cities Soc.* (2019) 45:214–30. doi: 10.1016/j.scs.2018.11.015

78. Rovira J, Nadal M, Schuhmacher M, Domingo JL. Environmental impact and human health risks of air pollutants near a large chemical/petrochemical complex: case study in Tarragona, Spain. *Sci Total Environ.* (2021) 787:147550. doi: 10.1016/j.scitotenv.2021.147550

79. Yang B, Zhou L, Xue N, Li F, Li Y, Vogt RD, et al. Source apportionment of polycyclic aromatic hydrocarbons in soils of huanghuai plain, China: Comparison of three receptor models. *Sci Total Environ.* (2013) 443:31-9. doi: 10.1016/j.scitotenv.2012.10.094

80. Ishtiaq J, Syed JH, Jadoon WA, Hamid N, Iqbal Chaudhry MJ, Shahnawaz M, et al. Atmospheric polycyclic aromatic hydrocarbons (PAHs) at urban settings in Pakistan: spatial variations, sources and health risks. *Chemosphere.* (2021) 274:129811. doi: 10.1016/j.chemosphere.2021.129811

frontiers | Frontiers in Public Health

TYPE Original Research
PUBLISHED 19 January 2023
DOI 10.3389/fpubh.2023.1075262



OPEN ACCESS

EDITED BY
Dipesh Rupakheti,
Nanjing University of Information Science and Technology, China

REVIEWED BY
Kamal Jyoti Maji,
Georgia Institute of Technology, United States
Ming Liu,
Chang'an University, China
Chao He,
Yangtze University, China

*CORRESPONDENCE
Fuzhen Shen
✉ f.shen@fz-juelich.de
Michaela I. Hegglin
✉ m.i.hegglin@fz-juelich.de

SPECIALTY SECTION
This article was submitted to Environmental health and Exposome, a section of the journal Frontiers in Public Health

RECEIVED 20 October 2022
ACCEPTED 03 January 2023
PUBLISHED 19 January 2023

CITATION
Yuan Y, Zhang X, Zhao J, Shen F, Nie D, Wang B, Wang L, Xing M and Hegglin MI (2023) Characteristics, health risks, and premature mortality attributable to ambient air pollutants in four functional areas in Jining, China. *Front. Public Health* 11:1075262. doi: 10.3389/fpubh.2023.1075262



# Characteristics, health risks, and premature mortality attributable to ambient air pollutants in four functional areas in Jining, China

Yue Yuan[1], Xi Zhang[1], Jingfeng Zhao[1], Fuzhen Shen[2,3]*, Dongyang Nie[4], Bing Wang[5], Lei Wang[6], Mengyue Xing[7] and Michaela I. Hegglin[2,3]*

[1]Jining Meteorological Bureau, Shandong, China, [2]Institute of Energy and Climate Research, IEK-7: Stratosphere, Forschungszentrum Jülich, Jülich, Germany, [3]Department of Meteorology, University of Reading, Reading, United Kingdom, [4]School of Environmental Science and Engineering, Southern University of Science and Technology, Shenzhen, China, [5]Henley Business School, University of Reading, Reading, United Kingdom, [6]Jining Bureau of Ecology and Environment, Shandong, China, [7]Business School, Dalian University of Foreign Languages, Liaoning, China

Air pollution is one of the leading causes for global deaths and understanding pollutant emission sources is key to successful mitigation policies. Air quality data in the urban, suburban, industrial, and rural areas (UA, SA, IA, and RA) of Jining, Shandong Province in China, were collected to compare the characteristics and associated health risks. The average concentrations of $PM_{2.5}$, $PM_{10}$, $SO_2$, $NO_2$, and CO show differences of −3.87, −16.67, −19.24, −15.74, and −8.37% between 2017 and 2018. On the contrary, $O_3$ concentrations increased by 4.50%. The four functional areas exhibited the same seasonal variations and diurnal patterns in air pollutants, with the highest exposure excess risks (ERs) resulting from $O_3$. More frequent ER days occurred within the 25–30°C, but much larger ERs are found within the 0–5°C temperature range, attributed to higher $O_3$ pollution in summer and more severe PM pollution in winter. The premature deaths attributable to six air pollutants can be calculated in 2017 and 2018, respectively. Investigations on the potential source show that the ER of $O_3$ (*r* of 0.86) had the tightest association with the total ER. The bivariate polar plots indicated that the highest health-based air quality index (HAQI) in IA influences the HAQI in UA and SA by pollution transport, and thus can be regarded as the major pollutant emission source in Jining. The above results indicate that urgent measures should be taken to reduce $O_3$ pollution taking into account the characteristics of the prevalent ozone formation regime, especially in IA in Jining.

KEYWORDS

**air pollution, functional regions, health effect, potential source, premature mortality**

## 1. Introduction

Air pollution has attracted significant concern worldwide in recent decades, especially in China due to the highest ranking of death records across the world (1). Many previous studies have reported that exposure to both ambient and indoor air pollutants has a direct association with a significantly increased risk of cardiovascular, respiratory, and coronary heart diseases, and even can induce cancer (2–7). Moreover, numerous studies have demonstrated that no matter the long-term or short-term exposure, the varied risk and non-accident premature mortality could be attributed to exposure levels of different air pollutants [i.e., particulate matter with an aerodynamic diameter <2.5 and 10 μm ($PM_{2.5}$ and $PM_{10}$), nitrogen dioxide ($NO_2$), sulfur dioxide ($SO_2$), ozone ($O_3$), carbon monoxide (CO)] in one city or at the national scale (8–18).

Health impacts from different air pollutants are usually assessed by epidemiology, toxicology and clinical studies (19, 20). One of the popularly used approaches is the epidemiological statistics method, which can be used to calculate the coefficient of the exposure-response relationship based on the relative mortality risk of air pollutants (21), thus linking pollutants with health risks. At present, many health impact assessment studies have investigated the health risks or premature mortality attributable to a single air pollutant or adjusted for exposure to other pollutants globally or regionally (22–27). In China, numerous epidemiological literature concentrated on the association of single pollutants and population health has been designed by using various methods, which include time-series, cross-sectional, panel, case-crossover, cohort and intervention designs (28). To make an assessment of the short-term health effects of one single air pollutant, time-series studies coupled with Poisson regression or Generalized Additive Model (GAM) were conducted to explore the association of different air pollutants [like $NO_2$ (29), CO (30), $SO_2$ (31), $PM_{10}$ (32), $PM_{2.5}$ (33), and $O_3$ (34)] and daily mortality in large Chinese cities, including Beijing, Shanghai, Chongqing, Shenyang, and Wuhan (28). Because of the easier conducted research experiment and clearly interpretable result, single-pollutant air quality strategies are widely applicable to protect human health for policy-makers (35). However, the health effect of single-pollutant should be applied cautiously. Because of the certain correlation among different air pollutants, identifying the independent effects of single-pollutant become much more difficult (36). Moreover, the air that humans breathe at once is multiple pollutants. Therefore, exploring the joint effect associated with multi-pollutant should be taken into consideration urgently by scholars.

Currently, three typical approaches, including statistical regression models, the indicator approach, and the source identification methods, can be used to quantify the joint health risk from multi-pollutant (35). Generally, the indicator approach means that it is to use one pollutant to represent the total exposure to several pollutants. To evaluate the total health risks and premature mortalities attributed to different air pollutants (here including $PM_{2.5}$, $PM_{10}$, $SO_2$, $NO_2$, $O_3$, and CO), how to select an appropriate pollutant or construct a health risk index has become more significant. Currently, the air quality is characterized by the widely used Air Quality Index (AQI) system, an index implemented by the central government (like in the US or China) is determined by the primary pollutant rather than the overall air condition (37). To address the inadequacy of the single-pollutant-oriented AQI, the aggregate AQI (AAQI) (38) and air quality health index (AQHI) (39) have been developed and applied in practice. In a recent study, Hu et al. (40) using a novel index referred to as the health risk-based AQI (HAQI), investigated air quality in six representative Chinese cities and found that the total days in a given AQI category (either unhealthy or very unhealthy) were including days in HAQI categories that were equal or even higher than the respective AQI category (i.e., very unhealthy or hazardous). Shen et al. (41) applied the HAQI in 367 cities in China, showing high HAQI to be most prevalent in the North China Plain region (NCP). Zhou et al. (42) established the HAQI in 366 cities in China and found organics were driving $PM_{2.5}$-formation when $PM_{2.5}$ is at a lower level of health risk.

Here, we expand on these studies, which focused on atmospheric pollution at the city level (that is averaged over whole cities), to investigate multi-pollutant exposure health risks associated with different functional areas within a city. To this end, we applied the HAQI calculation to observations obtained from four functional areas in Jining city. Meanwhile, to identify which functional areas and air pollutants play the dominant role in Jining, we introduced the potential source contribution function (PSCF) model in this study as well. The PSCF is a conditional probability model by coupling the pollutant with an air mass arriving at the observational site after having passed through a specific geographical area (43). The PSCF value is determined by dividing the space up into certain grid cells and checking the back-trajectory endpoint to see if there was a sampling day commensurate with the trajectory. The PSCF analysis is widely applied to identify the potential source of any pollutant, like $SO_2$ (44), $NO_2$ (45), $PM_{2.5}$ (46), $PM_{10}$ (47), CO (48), and $O_3$ (48) black carbon particles (49), or a pollutant-related indicator (e.g., excess risk in section 2.4) (41).

At last, the results aim at providing a clear understanding of the regional distribution of health risks and to provide guidance to policy-makers for effective mitigation policies within Jining's city borders. In particular, Jining is located between the Beijing-Tianjin-Hebei region and the Yangtze River Delta, which is prone to air pollution under a zonal circulation and stable synoptic conditions (low wind and high relative humidity) aside from strong emissions of pollutants, especially in winter and spring. To evaluate the air quality expected over the 2017–2018 period and the associated feedback on health risks in four different functional regions in Jining city, this study aims to: (1) compare the air pollution levels across the four functional areas; (2) estimate the multi-pollutant exposure health risk in these functional areas; (3) evaluate all-cause premature mortalities attributable to all air pollutants, and (4) identify which functional areas and air pollutants are the major contributors to the health risk of Jining City.

## 2. Materials and methods

### 2.1. Site and data

The study region, Jining (116°26′-116°44′E, 35°08′-35°32′N), is located in the southwest of Shandong Province in eastern China (Figure 1A). The air sampling sites (colored stars) and meteorological stations (colored triangles) are located in the four different functional areas identified in Jining. Highways and industrial parks are found near the industrial (IA) site. For the urban (UA) site in the city center, the nearby road network is complex, with heavy traffic and high building density. The suburban (SA) site is located between the urban and rural areas, and the rural (RA) site is located by a farm and river and far away from the city center. The surrounding environment of each air quality sampling site is largely consistent with the basic characteristics of the functional areas. The meteorological stations were chosen to be as close as possible to the air pollutant sampling sites.

The hourly monitoring data of six pollutants and the hourly meteorological data at each site were obtained from the website of the Environmental Meteorological Platform of Shandong (http://10.76.10.119/) and the Jining Meteorological Bureau, respectively. The meteorology factors include temperature (°C), wind direction (WD), and wind speed (WS). Here, WS and WD were used to explore the potential source region of pollution. The temperature

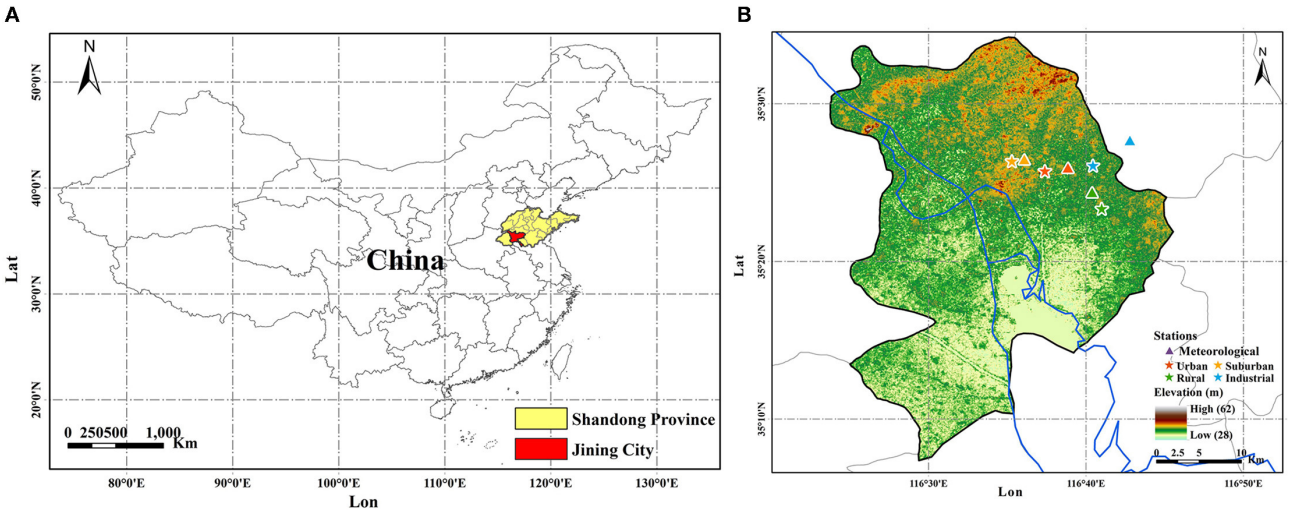


FIGURE 1
The location of Jining in Shandong Province **(A)**, and the meteorology and air quality stations **(B)** in Jining city. Colored stars and triangles represent air quality sites and meteorological site in four functional areas (Suburban: orange, Urban: red, Rural: green, Industry: blue).

was applied to investigate the impact on air pollutants, especially for $O_3$. Based on the daily minimum requirement for the validity of air pollutant concentration data (Chinese Ambient Air Quality Standard GB 3095-2012) (https://www.mee.gov.cn/ywgz/fgbz/bz/bzwb/dqhjbh/dqhjzlbz/201203/t20120302_224165.shtml), the daily and monthly data during 2017 (2018) reported in this study are valid for 362 (365) days and 12 (12) months, respectively. The other days in 1 year were deleted due to the sampling data being <20 h in a day. For the meteorology dataset, all the data used each day is valid according to China's Surface Meteorological Observation Standard (CSMOS) (https://www.cma.gov.cn/zfxxgk/gknr/flfgbz/bz/202209/t20220921_5099079.html). For precipitation and relative humidity, we did not explore the impact of the two meteorology factors on air pollution due to the large number of missing values.

## 2.2. The calculation method of excess risk and health-risk based AQI

The relative risk (RR) of each pollutant is expressed by an exponential-linear function as shown in Eq. 1 (40). Here, $\beta_i$ is the exposure-response relationship coefficient (which quantifies the additional health risk per unit increase of an air pollutant) with values of 0.038, 0.032, 0.081, 0.13, and 0.048% per $\mu g/m^3$ for $PM_{2.5}$, $PM_{10}$, $SO_2$, $NO_2$, and $O_3$, respectively, and 3.7% per $mg/m^3$ for CO (50). $C_i$ represents the mass concentration of a pollutant *i*. Meanwhile, a baseline concentration $C_{i,0}$ is also defined to determine the minimum risk of each pollutant *i*, meaning one pollutant has no health risk when its concentration is below or equal to $C_0$, that is, $RR_i = 1$. Here, the upper threshold values of Chinese Ambient Air Quality Standard (CAAQS) 24-h Grade II were regarded as the $C_{i,0}$ (Supplementary Table 1). The excess risk (ER) of pollutant *i* is written as in Eq. 2 and the total ER can be calculated by adding up the ER of each pollutant (Eq. 3). It should be noted that the ER added up linearly could over-estimate the assessment of total ER if those pollutants are highly correlated. Therefore, the total ER from six air pollutants can be regarded as an upper-bound estimation (40).

$$RR_i = exp\left[\beta_i\left(C_i - C_{i,0}\right)\right],\ C_i > C_{i,0} \quad (1)$$

$$ER_i = RR_i - 1 \quad (2)$$

$$ER_{total} = \sum_{i=1}^{n} ER_i = \sum_{i=1}^{n} (RR_i - 1). \quad (3)$$

After calculating the total ER, the combined multi-pollutant Relative Risk ($RR^*$) and an equivalent total concentration ($C_i^*$) of pollutant *i* (40) can be written as:

$$RR^* = ER_{total} + 1 = exp\left[\beta\left(C^* - C_0\right)\right] \quad (4)$$

$$C_i^* = \frac{ln\left(RR^*\right)}{\beta_i + C_{0,i.}} \quad (5)$$

Finally, $C_i^*$ is substituted for the $C_{i,m}$ in the AQI calculation to yield the HAQI (40), where the AQI calculation is as follows:

$$AQI_i = \frac{AQI_{i,j} - AQI_{i,j-1}}{\left(C_{i,j} - C_{i,j-1}\right)} \times \left(C_{i,m} - C_{i,j-1}\right) + AQI_{i,j-1},\ j > 1 \quad (6)$$

$$AQI_i = AQI_{i,1}\frac{C_{i,m}}{C_{i,1}},\ j = 1 \quad (7)$$

$$AQI = max\left(AQI_1, AQI_2 \ldots, AQI_n\right),\ n = 1,\ 2,\ \ldots,\ 6. \quad (8)$$

where $C_{i,m}$ is the measured concentration of pollutant *i*; *j* is the health category index; $C_{i,j}$ is the reference concentration for pollution

$i$ corresponding to the $j$-th health category. Accordingly, the HAQI calculation could be demonstrated as follows:

$$HAQI_i = \frac{HAQI_{i,j} - HAQI_{i,j-1}}{(C_{i,j} - C_{i,j-1})} \times (C_i^* - C_{i,j-1}) + HAQI_{i,j-1},\ j > 1, \quad (9)$$

$$HAQI_i = HAQI_{i,1} \frac{C_i^*}{C_{i,1}},\ j = 1 \quad (10)$$

$$HAQI = max\,(HAQI_1, HAQI_2 \ldots, HAQI_n),\ n = 1,\ 2,\ \ldots,\ 6. \quad (11)$$

## 2.3. Daily cause-specific mortality and health burden assessment

The annual all-cause mortality in Jining was obtained from the Jining Statistical Yearbooks 2017 and 2018. The daily mortality was then calculated by the annual mortality rate divided by the number of days per year. The estimated health burden owing to short-term exposure to air pollutants can be calculated as follows (51, 52):

$$M = \sum_i^n AF_i \times BM \quad (12)$$

$$AF_i = (RR_i - 1)/RR_i \quad (13)$$

where $M$ (total mortality due to atmospheric pollution), $n$ (total number of days), BM (daily baseline mortality), $AF_i$ (daily attributable fraction related to short-term exposure of air pollutant $i$).

## 2.4. Potential source contribution function analysis

In this study, back trajectory analyses were performed by using the Hybrid Single-Particle Lagrangian Integrated Trajectory HYSPLIT model (Version 4.9) (53). The 72 h back trajectories arriving at Jining city at a height of 300 m were calculated every 3-h from 2017 to 2018. Based on these back trajectories data, a potential source contribution function (PSCF) analysis (54) was executed with ZeFir, an Igor-based (Wavemetrics, USA) package (55). PSCF analyses are commonly used to investigate the origin of observed concentrations at a sampling site under a given criterion (here, the 75th percentile value).

$$PSCF_{i,j} = \frac{m_{i,j}}{n_{i,j}} \quad (14)$$

where $n_{i,j}$ and $m_{i,j}$ are the total count of endpoints and above-threshold endpoints located in the $i,jth$ air cell, respectively. A sigmoid weighting function (41) was used to reduce the influence of large differences between two air cells (see Eq. 15). Three values in this function are 10, 0.5, 0.1 for $a$, $b$, $c$ respectively (41). It is written as follows:

$$W = \frac{1}{(1+c)\left(1 + e^{-a(x-b)}\right)} + \frac{c}{1+c} \quad (15)$$

$$x = \log\left(n_{i,j} + 1\right) / \max_{log(n_{i,j}+1)} \quad (16)$$

After calculating the PSCF for each sampling site in one city individually, the combined PSCF over all the sampling sites in the city can be calculated by using a multi-site (MS) merging method:

$$MS_{i,j} = \frac{\sum_l m_{i,j}^l}{\sum_l n_{i,j}^l} \quad (17)$$

where $m^l$ and $n^l$ values indicate the $m$ and $n$ number counts of the sampling sites $l$ in Jining.

# 3. Results and discussion

## 3.1. Comparison of six pollutants in four functional areas

Figure 2 shows the annual mean mass concentrations of six pollutants in Jining during 2017 and 2018 at the city level. $PM_{2.5}$, $PM_{10}$, $SO_2$, $NO_2$, and CO all show lower values in 2018 than in 2017, indicating decreased emissions between the 2 years with 3.87% (from 57.11 to 54.89 $\mu g/m^3$), 16.67% (from 107.65 to 89.71 $\mu g/m^3$), 19.24% (from 26.27 to 21.21 $\mu g/m^3$), 15.74% (from 40.97 to 34.52 $\mu g/m^3$) and 8.37% (from 10.43 to 9.56 $mg/m^3$), respectively. Conversely, the mass concentration of $O_3$ was elevated by 4.5% (from 99.26 $\mu g/m^3$ to 103.72 $\mu g/m^3$). Elevated $O_3$ mass concentrations and decreased mass loadings of PM have become a generally observed phenomenon resulting from pollution control measures, indicating that fewer PM but more $O_3$ pollution events may also occur in Jining city in the future. Following many previous studies reports (56–59), this finding also stresses the key role of controlling $O_3$ pollution through a series of strategies, such as the reduction of anthropogenic emissions, adjustment of the temperature, and balanced NOx and VOC control, for the local government in the future.

The seasonal distributions of the six pollutants averaged over the 2 years were then compared among four functional areas: UA, SA, RA, and IA, with the results shown in Figure 3A. Overall, the mass loading of all pollutants (except for $O_3$) exhibited high (low) mass concentrations in winter and low (high) mass concentrations in summer. The seasonal patterns of all the air pollutants' mass loadings in Jining are consistent with that in almost all other cities across China (41, 42). The higher concentrations of the six air pollutants, except for ozone, in winter, can be explained by enhanced coal combustion, biomass burning, and unfavorable meteorological conditions, including low temperature (2.6°C), and boundary layer height (395 m) in winter (Supplementary Figure 1). The opposite behavior of the ozone concentrations, with the highest values during spring/summer is a well-known consequence of photochemistry, which is most active in these seasons.

After identifying the seasonal patterns of the six air pollutants in the four functional areas, the differences in the annual mean behavior (averaged over 2017 and 2018) of the mass loadings of the six air pollutants among UA, SA, RA, and IA are discussed. For PM ($PM_{10}$ and $PM_{2.5}$), the order of mass loading from high to low follows as: IA (105.00 and 60.37 $\mu g/m^3$) > RA (103.57 and 57.56 $\mu g/m^3$) > UA (98.52 and 54.49 $\mu g/m^3$) > SA (88.61 and 53.26 $\mu g/m^3$). With the contribution of fossil fuel combustion from plenty of power plants and the emissions from factories in this area, the IA had a higher

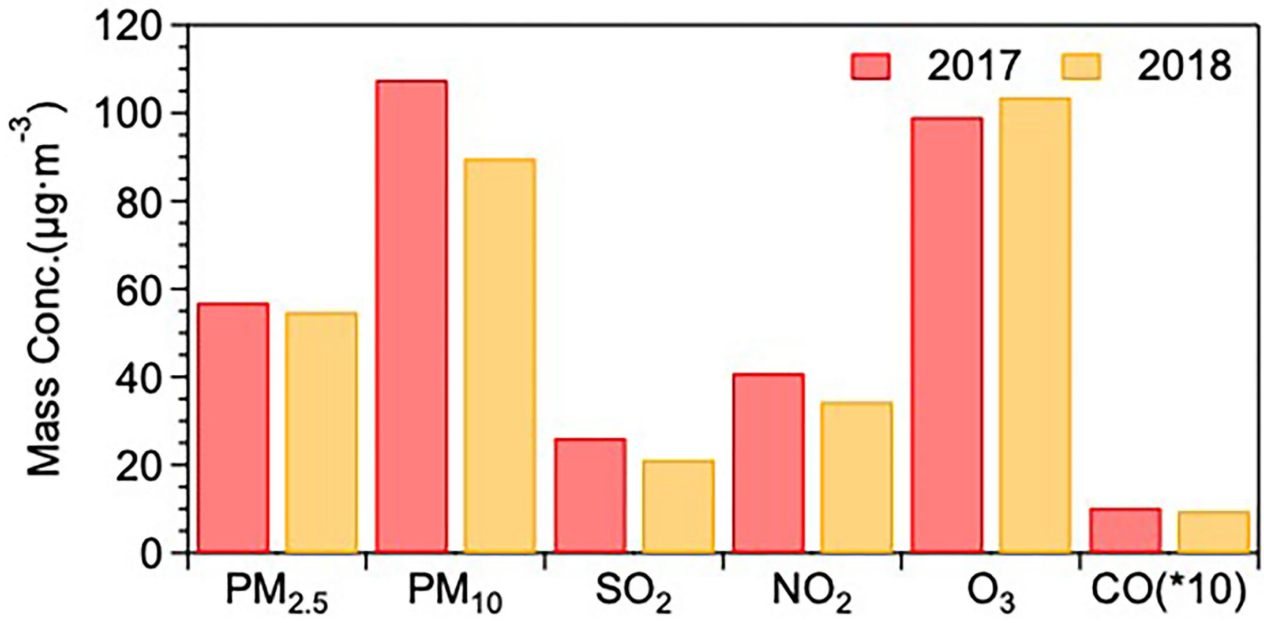


FIGURE 2
The annual mean mass concentrations of six pollutants in Jining during 2017 and 2018 [the unit of CO is mg/m$^3$, CO (*10) means the real CO mass concentration multiple 10].

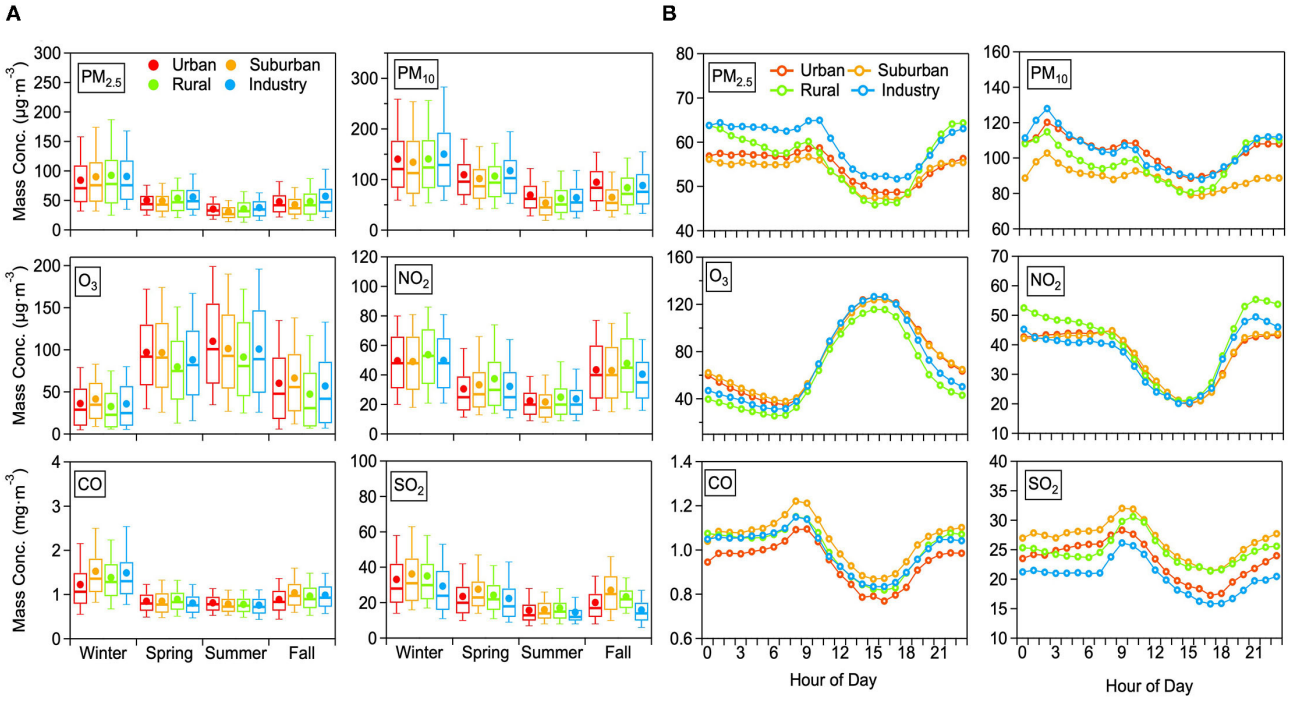


FIGURE 3
The seasonal **(A)** and diurnal **(B)** distributions of the six pollutants averaged over 2017 and 2018 for each of the functional areas (color-coded).

mass concentration of PM than in the other three areas in all four seasons (except for the $PM_{10}$ in summer and fall). The local source of high mass loading of PM in RA results mainly from residents cooking and straw burning. The higher $PM_{10}$ in UA compared to that in IA in summer and fall might be ascribed to the heavy traffic emissions and unfavorable pollution dilution conditions due to high building density. For $NO_2$ and $SO_2$, the mass concentrations in these areas followed the order of RA (41.02 μg/m$^3$) > UA (36.79 μg/m$^3$) > IA (36.61 μg/m$^3$) > SA (36.52 μg/m$^3$) and SA (26.74 μg/m$^3$) > RA (24.92 μg/m$^3$) > UA (23.13 μg/m$^3$) > IA (20.56 μg/m$^3$),

respectively. The mass concentrations of $NO_2$ and $SO_2$ were the highest in IA and SA, respectively. For CO, the mass loading was very similar during spring, summer, and fall. In winter, on the other side, the concentrations were decreasing following the order of SA (1.53 $mg/m^3$) > IA (1.49 $mg/m^3$) > RA (1.38 $mg/m^3$) > UA (1.23 $mg/m^3$). The SA and IA sites are located at the edge of the city and nearby the outside ring of a highway, therefore, higher traffic emissions of CO might be the main source in SA and IA. At last, for $O_3$, the mass loading ranked from high to low as: SA (76.61$\mu g/m^3$) ≈ UA (76.00 $\mu g/m^3$) > IA (70.49 $\mu g/m^3$) > RA (62.88 $\mu g/m^3$). Even though the average mass loading of $O_3$ in SA was almost equal to that in UA in all four seasons, the $O_3$ in UA was significantly higher than that in SA in summer, indicating a phenomenon that $O_3$ pollution has become an increasing concern for the urban residents in Jining. On the other hand, $O_3$ in RA was the lowest in all seasons.

Figure 3B illustrates the diurnal pattern of the six standard pollutants in the four functional areas. The different functional areas exhibit very similar diurnal cycles for the same pollutant. Overall, the mass loadings of $PM_{2.5}$ and $NO_2$ during night-time were stable but started to drop after 9:00 a.m. After reaching minimum values around 4:00 p.m., they began to increase until 11:00 p.m. For $PM_{10}$, the diurnal pattern is different to $PM_{2.5}$ and exhibits two peaks at 3:00 a.m. and 9:00 a.m. and a valley at 4:00 p.m. Overall, PM and $NO_2$ concentrations during night-time surpass daytime values and an obvious decrease appears in the afternoon, which could be interpreted by the strengthened emission (traffic emission, resident heating, etc.) during night-time and an elevated height of the planetary boundary layer (PBL) during the afternoon. Meanwhile, the decreased concentrations of gas pollutants, including $SO_2$ and CO, in the afternoon also can be explained by the increased height of PBL, which can dilute those gas pollutants. However, morning peaks (at 9:00 am) of PM, $SO_2$ and CO can be attributed to enhanced fossil fuel combustion.

## 3.2. Health risk in four functional areas

In the next step, the average AQI and HAQI values were calculated over the 2017–2018 time period based on the daily average values of pollutants (Figure 4). In the four functional areas, the mean value of AQI and HAQI in 2017–2018 decreases following the order: IA (AQI: 106.9 ± 47.0, HAQI: 121.3 ± 71.5) > UA (AQI: 103.6 ± 45.2, HAQI: 117.0 ± 68.2) > SA (AQI: 101.5 ± 47.1, HAQI: 112.5 ± 68.0) > RA (AQI: 99.1 ± 46.1, HAQI: 108.8 ± 65.0). For all functional areas, the mean values of HAQI are higher than the AQI value, which is consistent with the finding of studies concentrated on the comparison between AQI and HAQI (21, 40, 42). The main reason for higher HAQI than AQI is that the HAQI reflects comprehensive health risk rather than the single-pollutant oriented AQI.

It is interesting to also look at the total ERs needed as input to the HAQI calculation and which were calculated by using Eq. 3. It should be noted that $SO_2$ and CO concentrations were always below the threshold concentration and thus the two pollutants had no exposure health risk to the public people. The total ER in IA (Figure 5) was the highest with a value of 2.38%, followed by 2.35% in UA, 1.50% in SA, and 1.20% in RA, respectively. For total ERs in the four functional areas, ERs of $O_3$ (IA: 0.88%, UA: 1.05%, SA: 0.89%, RA: 0.41%) made the dominant contribution to total ERs. For the total ER in IA, the ER of $PM_{2.5}$ and $PM_{10}$ made an almost equal contribution (0.71% and 0.72%) after that of $O_3$, followed by the contribution of $NO_2$ (0.06%). In UA, the other total ER contributors amounted to 0.58% for $PM_{2.5}$, 0.68% for $PM_{10}$, and 0.04% for $NO_2$. In SA, the other three contributions to the total ER were 0.30% for $PM_{2.5}$, 0.24% for $PM_{10}$, and 0.07% for $NO_2$, respectively. Except for the ER of $O_3$, the ER of $PM_{2.5}$, $PM_{10}$, and $NO_2$ in RA were 0.29, 0.26, and 0.24%, respectively. For total ERs in RA, even though the major contributor of $O_3$ is rather low compared to the other functional areas, the highest ER for $NO_2$ can offset the contribution from $O_3$, leading to the not quite low HAQI in RA.

## 3.3. Premature mortality attributable to air pollutants

After evaluating the total ERs from six air pollutants in Jining, we can further investigate the premature mortality attributable to different air pollutants. Based on monitoring data of six pollutants in 2017 and 2018, the all-cause premature mortality by short-term exposure to air pollution in Jining was calculated here. The total premature mortality caused by air pollution for the 2 years was 6,072 and 2,145 for 2017 and 2018, respectively (Table 1). Specifically, the premature mortalities attributable to $NO_2$, $O_3$, $PM_{10}$, and $PM_{2.5}$ were 912, 1,755, 1,824, 1,581 for 2017 and 175, 666, 593, and 710 for 2018. For the number of premature mortality attributable to $PM_{2.5}$ in 2017, it is almost consistent with the death number of 1,488 in terms of the total population (1.5 million) (60). $PM_{10}$ was the dominant contributor to premature deaths in 2017, but its contribution decreased from 30.0% in 2017 to 27.7% in 2018. The relative contribution of $O_3$ increased from 28.9% in 2017 to 31.0% in 2018, exceeding the relative contribution of $PM_{10}$ in 2018. The changing contributions of $PM_{10}$ and $O_3$ to the total premature mortality between 2017 and 2018 are directly related to the opposed changes in their observed concentrations. Furthermore, the contribution of $NO_2$ decreased from 15.0% in 2017 to 8.2% in 2018. Note, the health effects of $SO_2$ and CO are not shown in the table because their concentrations are always under the threshold values and thus do not contribute to premature mortality.

Looking into the four functional areas separately, the number of $NO_2$-driven premature deaths in RA and IA was higher in 2017 than that in 2018, and their relative contributions decreased from 22.9% and 24.9% in 2017 to 7.2% and 15.8% in 2018, respectively. Note, the contribution of $NO_2$ to premature death was much lower and the inter-annual variation was not significant in the other two regions. Inspection of the contribution of $O_3$ to premature death in UA and SA reveals its significance in these areas, notably increasing from 43.5 and 40.1% in 2017 to 48.31 and 47.83% in 2018, respectively, and representing the main factor leading to premature death in UA and SA. In the other two regions, the contribution of $O_3$ to premature death was relatively low and the inter-annual variation was not significant.

The contributions of $PM_{10}$ and $PM_{2.5}$ to premature death in the four regions varied between 2017 and 2018. In RA, the contribution rates of $PM_{10}$ and $PM_{2.5}$ increased from 30.9 and 29.3% in 2017 to 38.2 and 42.8% in 2018, respectively. In SA

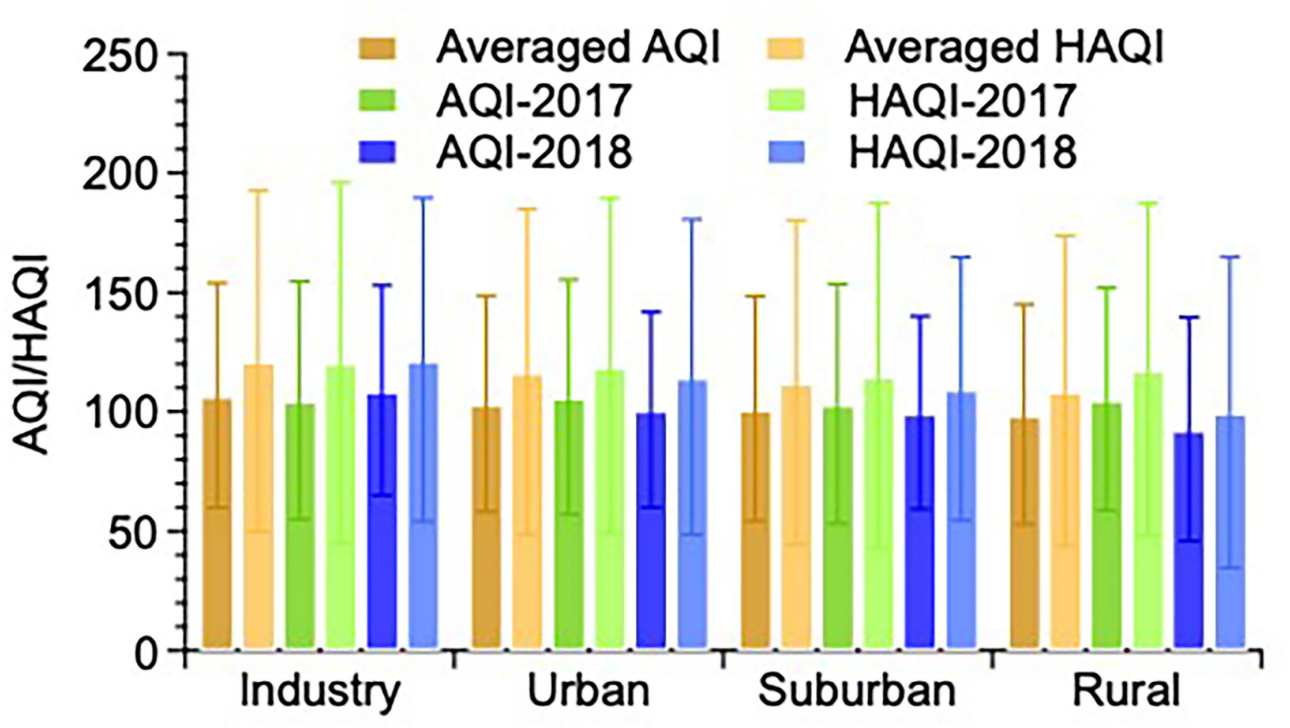


FIGURE 4
The mean AQI and HAQI average over 2017 and 2018 in four functional areas in Jining.

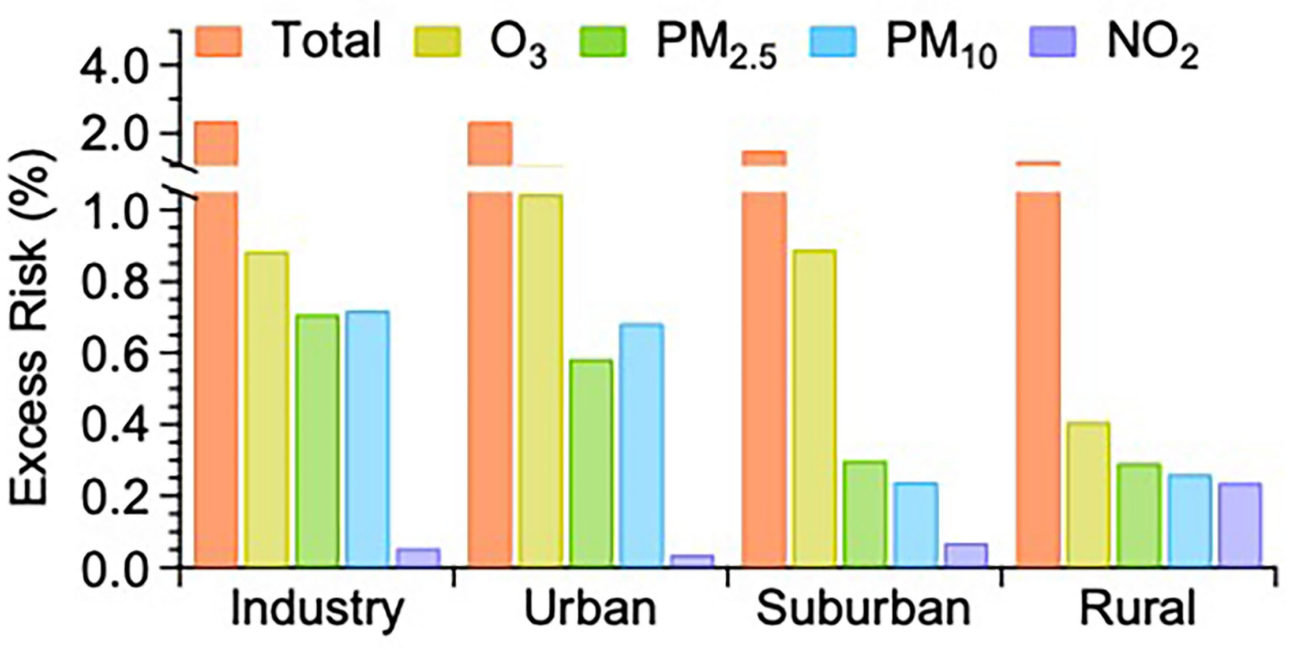


FIGURE 5
The comparison of excess risks (ERs) averaged over 2017 and 2018 attributable to the sum and individual air pollutants among the four functional areas in Jining.

and IA, the contribution rate of $PM_{10}$ decreased from 29.6 and 31.7% in 2017 to 19.5 and 23.6% in 2018, while $PM_{2.5}$ increased from 28.63 and 19.9% in 2017 to 31.2 and 36.2% in 2018, respectively. In RA, the trend of $PM_{10}$ and $PM_{2.5}$ contributions to premature death was thus different to that in the other functional areas.

10.3389/fpubh.2023.1075262

TABLE 1 Premature mortality attributable to short-term exposure to different air pollutants and their emission sources in 2017 and 2018, respectively.

| Air pollutant | 2017 | | | | 2018 | | | |
|---|---|---|---|---|---|---|---|---|
| | Premature death (person) | Urban | Contribution (%) | | Premature death (person) | Urban | Contribution (%) | |
| | | Suburban | | | | Suburban | | |
| | | Rural | | | | Rural | | |
| | | Industry | | | | Industry | | |
| $NO_2$ | **912** | 17 | **15.0** | 1.53 | **175** | 9 | **8.2** | 1.7 |
| | | 22 | | 1.7 | | 16 | | 1.4 |
| | | 392 | | 22.9 | | 34 | | 7.2 |
| | | 481 | | 24.9 | | 127 | | 15.8 |
| $O_3$_8h | **1,755** | 490 | **28.9** | 43.5 | **666** | 236 | **31.0** | 48.3 |
| | | 522 | | 40.1 | | 175 | | 47.8 |
| | | 288 | | 16.8 | | 57 | | 11.8 |
| | | 456 | | 23.6 | | 198 | | 24.5 |
| $PM_{10}$ | **1,824** | 298 | **30.0** | 26.4 | **593** | 147 | **27.7** | 30.1 |
| | | 385 | | 29.6 | | 71 | | 19.5 |
| | | 528 | | 30.9 | | 184 | | 38.2 |
| | | 613 | | 31.7 | | 191 | | 23.6 |
| $PM_{2.5}$ | **1,581** | 322 | **26.0** | 28.6 | **710** | 97 | **33.1** | 19.9 |
| | | 373 | | 28.6 | | 114 | | 31.2 |
| | | 501 | | 29.3 | | 206 | | 42.8 |
| | | 386 | | 19.9 | | 292 | | 36.2 |
| Total | **6,072** | 1,127 | **100** | 100 | **2,145** | 489 | **100** | 100 |
| | | 1,301 | | 100 | | 366 | | 100 |
| | | 1,708 | | 100 | | 482 | | 100 |
| | | 1,936 | | 100 | | 808 | | 100 |

Bold indicate total numbers, rows beside each total from top to bottom are numbers for UA, SA, RA, and IA.

## 3.4. Identify the contributions of air pollutants to health risk

The PSCF analysis (see methods in section 2.4) was used to identify which functional areas and air pollutants are the major contributors to the health risk in Jining (Figure 6). To this end, the total ER in each functional area is first calculated by adding up the ER of all six pollutants according to Eq. 3, and then the multi-site merging method (see Eq. 17) was applied for calculating the multi-site ER for the total (Figure 6A) and $PM_{2.5}$ (Figure 6B), $PM_{10}$ (Figure 6C), $O_3$ (Figure 6D), and $NO_2$ (Figure 6E) contributions in Jining, respectively. In Figure 6, the color scale represents the possibility of the ER source, while the areas of hot spots covered can be considered as the Potential Source Areas (PSA) for each pollutant. The information obtained from this analysis is expected to offer important information to the local government in Jining on which air regulation measures to implement to reduce public exposure to health risks depending on the different functional areas.

For the total ER in Jining, the dominant PSA are mainly located in the north and central of Shandong Province, including Jining city itself, and also expand to significant fractions of the southeast of Henan Province and the Anhui Province, and almost the total area of Yangtze River Delta (YRD). Besides, there was still a small part of PSA located in the northwest of Hubei Province and East China Sea extending from Henan Province and YRD, respectively. The hot spot areas in the north direction of ER for $PM_{2.5}$ was larger than that for $PM_{10}$, thus ER for $PM_{2.5}$ was considered as the major contributor of the total ER in the north direction. In the south direction, the contribution to the PSA of the total ER is mostly attributable to $O_3$, followed by that attributable to $PM_{2.5}$, $PM_{10}$, and $NO_2$. After identifying the PSA of the total ER in different directions, we further calculated the Pearson coefficient ($r$) and Spearman coefficient ($s$) between the PSA for ER of each pollutant and that for the total ER (Figure 7). From the results of the two coefficients, the ER of $O_3$ ($r$ of 0.86) had the tightest association with the total ER, followed by that of $PM_{2.5}$ ($r$ of 0.76), $PM_{10}$ ($r$ of 0.75), and $NO_2$ ($r$ of 0.42) when just considering the $r$. The ER of $NO_2$, on the other hand, was only weakly correlated with the total ER exhibiting the lowest $r$ of 0.4 and $s$ of 0.42. This finding stress that the local government in Jining should take urgent ways to reduce $O_3$ pollution as well as PM in the south direction and north direction of Jining City, respectively.

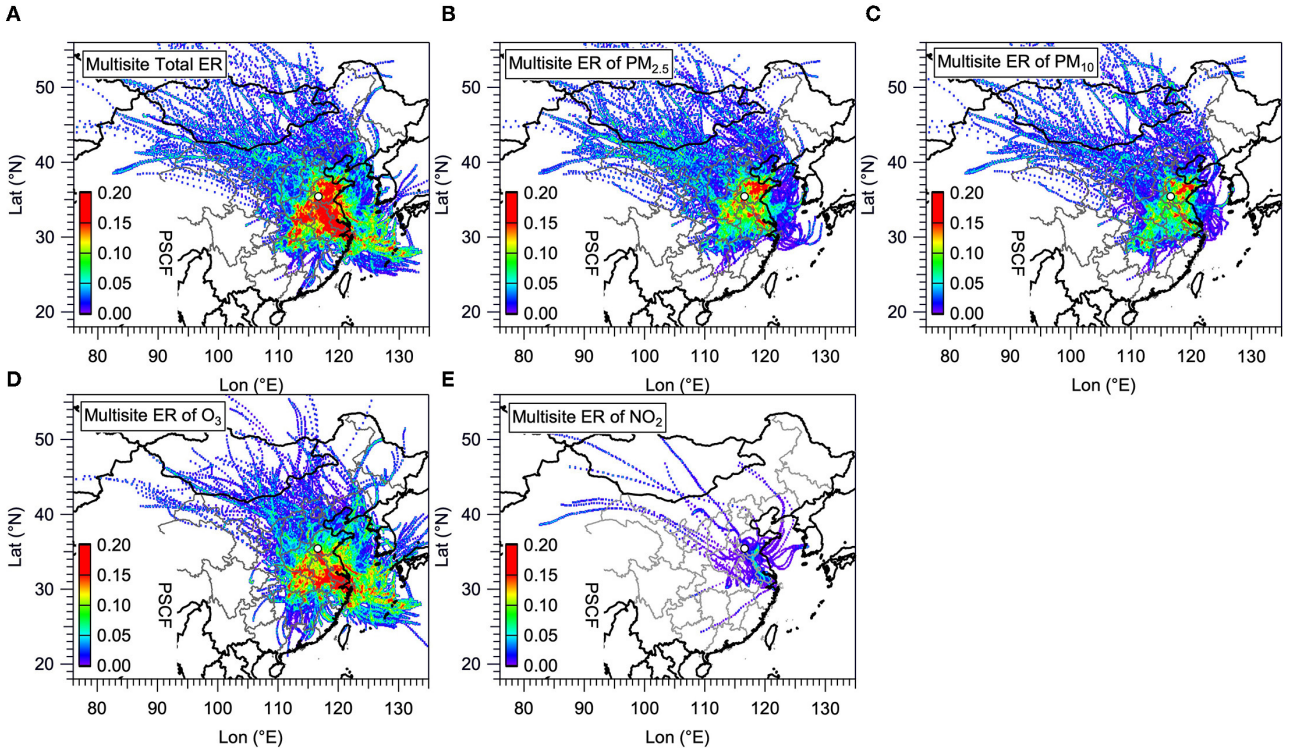


FIGURE 6
The potential source areas (PSA) of the excess risks (ERs) of air pollutants (based on CAAQS standards) in the four functional areas in Jining estimated based on multi-site emerging method. The color scale represents the possibility of the ER source, while the areas of hot spots covered can be considered as the PSA for each pollutant (**A**: Total; **B**: $PM_{2.5}$; **C**: $PM_{10}$; **D**: $O_3$; and **E**: $NO_2$).

## 3.5. Effects of meteorological factors on health risk

Figure 8 shows the bivariate polar plots of HAQI in four functional areas during 2017 and 2018. In Figure 8, the horizontal (W–E) and vertical (S–N) axes represent the wind directions, the length of the radial contours represents the wind speed, and the color bar scale indicates HAQI values. HAQI varied depending on the wind speed and wind direction. The layout of Figures 8A–D is displayed according to the actual geographic location of each functional site in Jining. For instance, the UA (Figure 8C) and RA (Figure 8D) sites are located in the west and south of the IA (Figure 8B) site, respectively. The SA (Figure 8A) site is on the west side of the UA. When the wind speed was low in IA and RA, the HAQIs were both higher indicating a local source leading to the high HAQI values. It also reveals high HAQIs for wind directions from the southeast and southwest suggesting two potential transport directions in IA. The RA site also had two potential transport directions in the southwest and northwest. Conversely, when the windspeed was higher at the UA and SA sites, the HAQI resulted in higher values, suggesting high HAQIs at these two sites can be attributed to transport from nearby pollution sources in the northeast and southeast directions. From the analysis above, IA has been identified as a likely source for increased health risk in UA and SA in situations with east wind direction.

Figure 9 illustrates the HAQI variation depending on the temperature in IA, UA, SA and RA (Figure 5a–d). At each site, the triangles (HAQI in 2017) and circles (HAQI in 2018) indicate the distribution of HAQI events in each temperature bin, with the circle size depending on the ER values and the circle color indicating the season during which the event occurred. Overall, in all four functional areas, more ER days (UA: 150, SA: 147, RA: 145, IA: 145) occurred in the temperature range of 25 to 30°C (that is primarily during summer), but higher averaged HAQI (UA: 134.7, SA: 140.28, RA: 139.66, IA: 149.24) presented in the temperature bin of 0 to 5°C (that is mostly during winter). High frequency of Ozone pollution days led to more ER days in summer, while less PM pollution days coupled with more severe pollution levels attributed to higher average HAQI in winter.

# 4. Policy implication

To better protect the public's health in Jining as well as in the whole of China, the local government should design certain policies and execute mitigation measures to tackle the threat to the public's health. Firstly, the multi-pollutant index should be considered when policymakers are developing relative regulations. Air quality standards are generally constructed based on the summary of the research evidence on the assessment of health impact attributable to each air pollutant separately. With the emergence of the multi-pollutant health index's framework and the increasing epidemiological evidence of the health effects, the future application of the multi-pollutant health index will become possible, even though there are still many uncertainties. Moreover, standards for multi-species air pollution levels should be built. If the multi-pollutant-oriented health risk assessment (including their statistical uncertainty) could be estimated with high reliability, then the air quality standards could be built on the base of the multi-species air

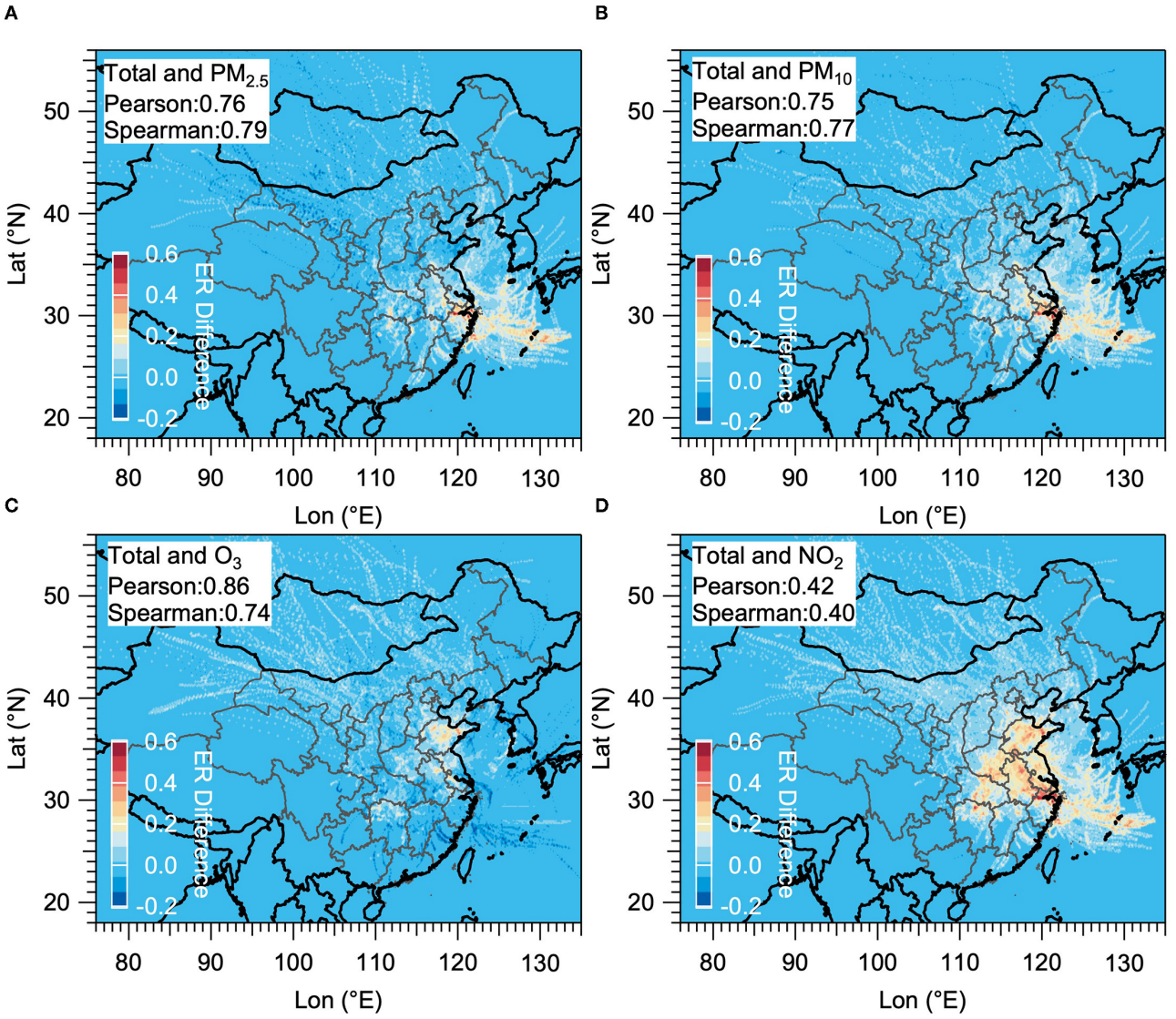


FIGURE 7
Distribution of the difference between total ER and ER from individual pollutant, and the Pearson coefficient and Spearman coefficient between the two in Jining. The color scale represents the difference between the total ER and ER from each air pollutant, the areas of hot spots covered can be considered as the PSA for each air pollutant (**A**: $PM_{2.5}$; **B**: $PM_{10}$; **C**: $O_3$; and **D**: $NO_2$).

pollution level. For example, this study in Jining city found that $PM_{10}$ was the dominant contributor to premature mortality but the $O_3$ pollution level increased simultaneously. Thus, it would be better to define a standard for $PM_{10}$ that considers the ozone pollution level. Finally, if the pollution source that leads to health risks for the humans is identified, the mitigation regulations could be designed such that it would account for the relative importance of the primary and secondary pollutants. For example, in Jining city, the ozone pollution level increased from 2017 to 2018, and control measures should be taken that yield a more balances control of the levels of VOC and NOx, which are the precursors of ozone.

## 5. Conclusion and remarks

In this study, four ambient air sampling sites in different functional areas, including urban, suburban, industrial, and rural areas, were selected to explore air pollution characteristics and the exposure health risk to the public in Jining. The spatiotemporal distribution, exposure health risks, and potential source areas of each functional area were compared for 2017 and 2018 in Jining. Overall, all average air pollutant concentrations in Jining decreased between 2017 and 2018, except for $O_3$, which showed an increase. The four functional areas showed the same seasonal and diurnal patterns among the six criteria air pollutants considered. The mass concentration of PM and $NO_2$ in IA and RA showed higher concentrations, respectively. The total premature deaths attributable to air pollution were 6,072 and 2,145 in 2017 and 2018 respectively, attributing to the decrease of air pollutants' concentrations and reflecting the benefits of controlling air pollution levels to human health in this region. Local pollutant emissions mainly contributed to high HAQI values in IA and RA, while high HAQI in UA and SA may instead be attributed to long-distance pollution transport. The ER of $O_3$ was with the highest *r*, reflecting the dominant contributor to the potential source area for total ER in the south, while PM was the main contributor to the potential source area

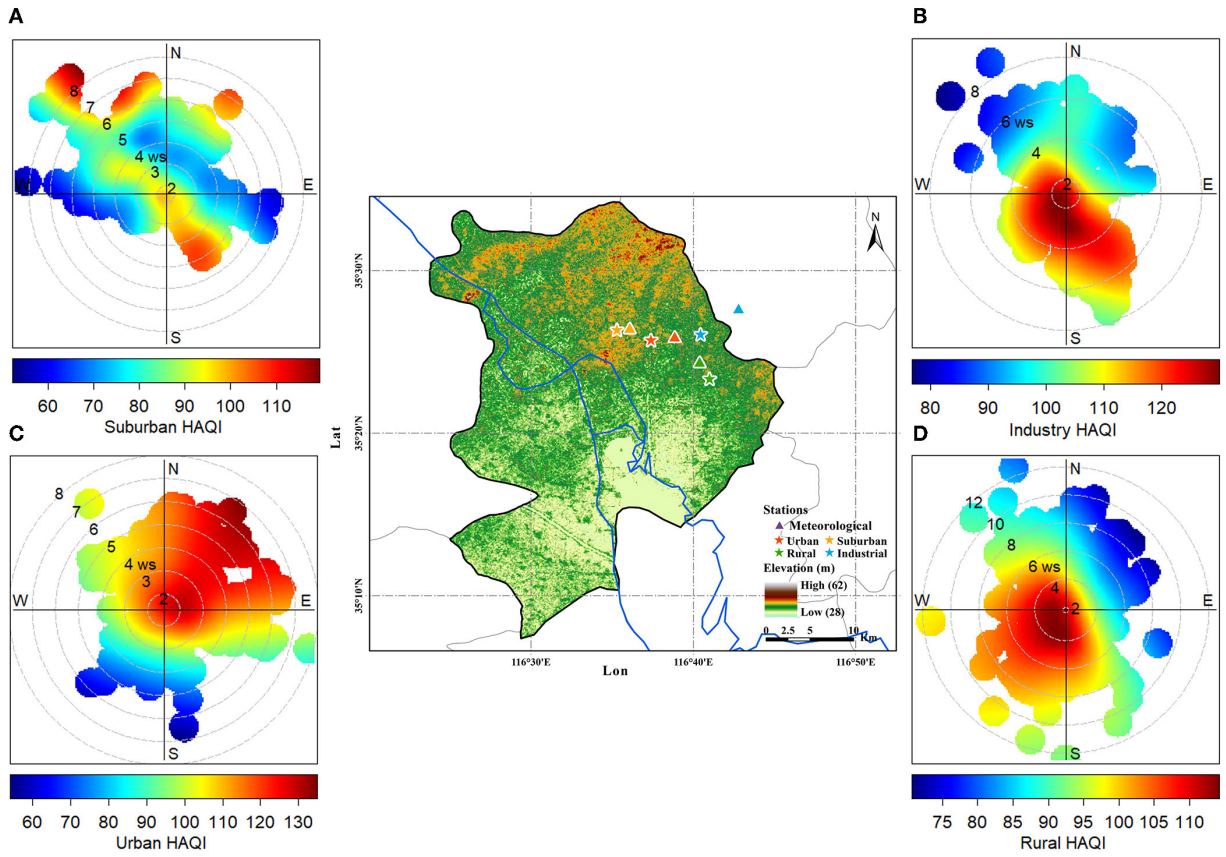


FIGURE 8
The bivariate polar plots of HAQI in suburban **(A)**, industry **(B)**, urban **(C)**, and rural **(D)** areas in Jining. The horizontal (W–E) and vertical (S–N) axes in the bivariate polar plots represent the wind directions, the length of the radial contours represents the wind speed, and the color bar scale indicates HAQI values.

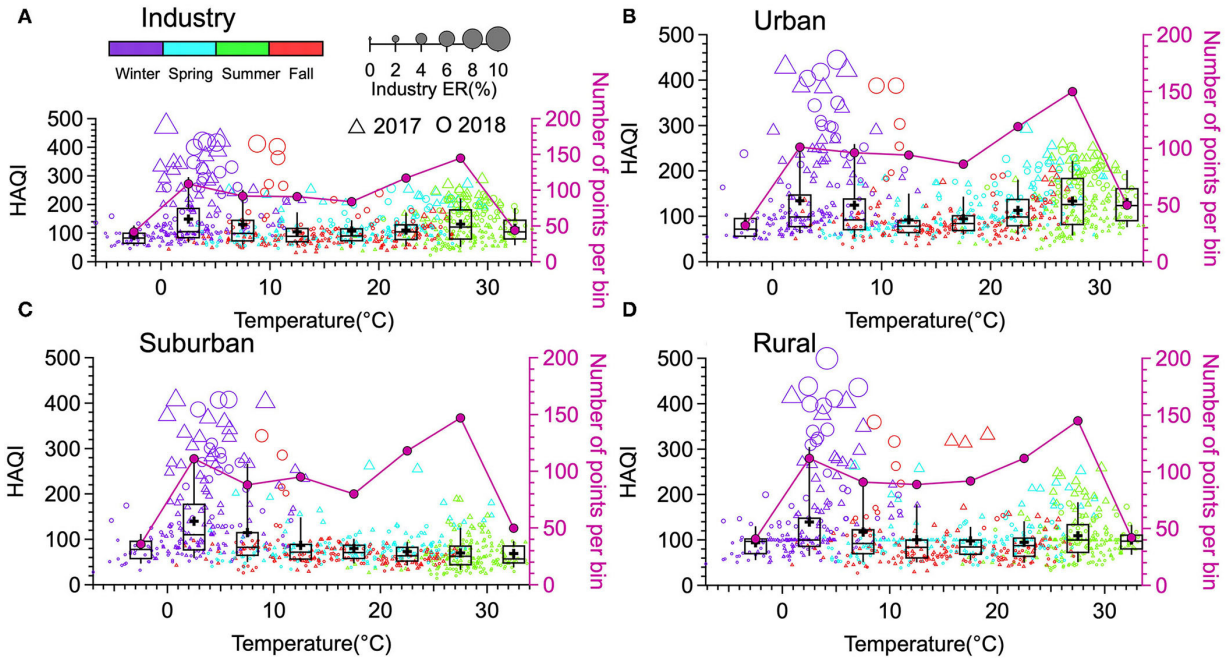


FIGURE 9
The HAQI variation depends on the temperature in the four functional areas (**A**: Industry; **B**: Urban; **C**: Suburban; **D**: Rural) in Jining. The triangles (HAQI in 2017) and circles (HAQI in 2018) indicate the distribution of HAQI events in each temperature bin, with the circle size depending on the ER values and the circle color indicating the season.

of total ER in the north. Overall, these results highlight that IA is the main local pollution source and that the most urgent measures should be taken to reduce $O_3$ pollution and particulate matter (PM), especially in industrial and urban areas to improve public health.

Results demonstrated in this study imply that $O_3$ rather than PM might become the primary threat to the public's health and urgent measures should be taken in the IA region in Jining city. However, it should be noted that this health assessment includes uncertainties due to various factors such as the ER calculation, measurement errors, and degree of correction between pollutants etc. More epidemiologic studies are required in the future to validate whether or not the HAQI is reliable to represent the multi-pollutant's health risk. Simultaneously, more attention should be paid on how to select the baseline concentration and ER coefficients since the results are sensitive to these measures as well.

## Data availability statement

The original contributions presented in the study are included in the article/Supplementary material, further inquiries can be directed to the corresponding authors.

## Author contributions

YY: conceptualization, methodology, software, data curation, writing—original draft, software, and validation. XZ, JZ, DN, BW, LW, and MX: data curation. FS: conceptualization, methodology, software, writing—original draft, supervision, software, validation, and writing—review and editing. MH: conceptualization, methodology, supervision, software, validation, and writing—review and editing. All authors contributed to the article and approved the submitted version.

## Funding

This work was supported by the Meteorological Science and Technology Research Project of the Jining Meteorological Bureau (2019JNZL06 and 2022JNZL09) and Guided project of Shandong Meteorological Burea (2021SDYD27).

## Acknowledgments

The authors gratefully acknowledge the Jining Meteorological Bureau for providing the air quality monitoring data and meteorological factor data.

## Conflict of interest

The authors declare that the research was conducted in the absence of any commercial or financial relationships that could be construed as a potential conflict of interest.

## Publisher's note



## Supplementary material

The Supplementary Material for this article can be found online at: https://www.frontiersin.org/articles/10.3389/fpubh.2023.1075262/full#supplementary-material

## References

1. HEI. *State of Global Air 2020*. Boston, MA: Health Effects Institute (2020).

2. Achakulwisut P, Brauer M, Hystad P, Anenberg SC. Global, national, and urban burdens of paediatric asthma incidence attributable to ambient $NO_2$ pollution: estimates from global datasets. *Lancet Planet Health.* (2019) 3:e166–78. doi: 10.1016/S2542-5196(19)30046-4

3. Fu P, Guo X, Cheung FMH, Yung KKL. The association between PM2.5 exposure and neurological disorders: a systematic review and meta-analysis. *Sci Tot Environ.* (2019) 655:1240–8. doi: 10.1016/j.scitotenv.2018.11.218

4. Lelieveld J, Pozzer A, Pöschl U, Fnais M, Haines A, Münzel T. Loss of life expectancy from air pollution compared to other risk factors: a worldwide perspective. *Cardiovasc Res.* (2020) 116:1910–7. doi: 10.1093/cvr/cvaa025

5. Shin J, Choi J, Kim KJ. Association between long-term exposure of ambient air pollutants and cardiometabolic diseases: a 2012 Korean Community Health Survey. *Nutr Metab Cardiovasc Dis.* (2019) 29:144–51. doi: 10.1016/j.numecd.2018.09.008

6. Shou Y, Huang Y, Zhu X, Liu C, Hu Y, Wang H. A review of the possible associations between ambient PM2.5 exposures and the development of Alzheimer's disease. *Ecotoxicol Environ Saf.* (2019) 174:344–52. doi: 10.1016/j.ecoenv.2019.02.086

7. Yuan Y, Wu Y, Ge X, Nie D, Wang M, Zhou H, et al. *In vitro* toxicity evaluation of heavy metals in urban air particulate matter on human lung epithelial cells. *Sci Tot Environ.* (2019) 678:301–8. doi: 10.1016/j.scitotenv.2019.04.431

8. Diao B, Ding L, Zhang Q, Na J, Cheng J. Impact of urbanization on PM2.5-related health and economic loss in China 338 cities. *Int J Environ Res Public Health.* (2020) 17:990. doi: 10.3390/ijerph17030990

9. Sohrabi S, Zietsman J, Khreis H. Burden of disease assessment of ambient air pollution and premature mortality in urban areas: the role of socioeconomic status and transportation. *Int J Environ Res Public Health.* (2020) 17:1166. doi: 10.3390/ijerph17041166

10. Wang Q, Wang J, He MZ, Kinney PL, Li T. A county-level estimate of PM2.5 related chronic mortality risk in China based on multi-model exposure data. *Environ Int.* (2018) 110:105–12. doi: 10.1016/j.envint.2017.10.015

11. Zhu G, Hu W, Liu Y, Cao J, Ma Z, Deng Y, et al. Health burdens of ambient PM2.5 pollution across Chinese cities during 2006–2015. *J Environ Manag.* (2019) 243:250–6. doi: 10.1016/j.jenvman.2019.04.119

12. Cibella F, Cuttitta G, Della Maggiore R, Ruggieri S, Panunzi S, et al. Effect of indoor nitrogen dioxide on lung function in urban environment. *Environ Res.* (2015) 138:8–16. doi: 10.1016/j.envres.2015.01.023

13. Chen T-M, Kuschner WG, Gokhale J, Shofer S. Outdoor air pollution: nitrogen dioxide, sulfur dioxide, and carbon monoxide health effects. *Am J Med Sci.* (2007) 333:249–56. doi: 10.1097/MAJ.0b013e31803b900f

14. Kim CS, Alexis NE, Rappold AG, Kehrl H, Hazucha MJ, Lay JC, et al. Lung function and inflammatory responses in healthy young adults exposed to 0.06 ppm ozone for 6.6 hours. *Am J Respir Crit Care Med.* (2011) 183:1215–21. doi: 10.1164/rccm.201011-1813OC

15. Kim J, Han Y, Seo SC, Lee JY, Choi J, Kim KH, et al. Association of carbon monoxide levels with allergic diseases in children. *Allergy Asthma Proc.* (2016) 37:e1–7. doi: 10.2500/aap.2016.37.3918

16. Jiang Y, Niu Y, Xia Y, Liu C, Lin Z, Wang W, et al. Effects of personal nitrogen dioxide exposure on airway inflammation and lung function. *Environ Res.* (2019) 177:108620. doi: 10.1016/j.envres.2019.108620

17. Goudarzi G, Geravandi S, Idani E, Hosseini SA, Baneshi MM, Yari AR, et al. An evaluation of hospital admission respiratory disease attributed to sulfur dioxide ambient concentration in Ahvaz from 2011 through 2013. *Environ Sci Pollut Res.* (2016) 23:22001–7. doi: 10.1007/s11356-016-7447-x

18. Nuvolone D, Petri D, Voller F. The effects of ozone on human health. *Environ Sci Pollut Res.* (2018) 25:8074–88. doi: 10.1007/s11356-017-9239-3

19. Kim K-H, Jahan SA, Kabir E. A review on human health perspective of air pollution with respect to allergies and asthma. *Environ Int.* (2013) 59:41–52. doi: 10.1016/j.envint.2013.05.007

20. Krzyzanowski M, Cohen A, Anderson R. Quantification of health effects of exposure to air pollution. *Occup Environ Med.* (2002) 59:791. doi: 10.1136/oem.59.12.791

21. Luo H, Guan Q, Lin J, Wang Q, Yang L, Tan Z, et al. Air pollution characteristics and human health risks in key cities of northwest China. *J Environ Manage.* (2020) 269:110791. doi: 10.1016/j.jenvman.2020.110791

22. Maji KJ, Dikshit AK, Arora M, Deshpande A. Estimating premature mortality attributable to PM2.5 exposure and benefit of air pollution control policies in China for 2020. *Sci Tot Environ.* (2018) 612:683–93. doi: 10.1016/j.scitotenv.2017.08.254

23. Hu J, Huang L, Chen M, Liao H, Zhang H, Wang S, et al. Premature mortality attributable to particulate matter in china: source contributions and responses to reductions. *Environ Sci Technol.* (2017) 51:9950–9. doi: 10.1021/acs.est.7b03193

24. Shaddick G, Thomas ML, Mudu P, Ruggeri G, Gumy S. Half the world's population are exposed to increasing air pollution. *NPJ Clim Atmos Sci.* (2020) 3:23. doi: 10.1038/s41612-020-0124-2

25. Chowdhury S, Pozzer A, Haines A, Klingmüller K, Münzel T, Paasonen P, et al. Global health burden of ambient PM2.5 and the contribution of anthropogenic black carbon and organic aerosols. *Environ Int.* (2022) 159:107020. doi: 10.1016/j.envint.2021.107020

26. Maji KJ, Namdeo A. Continuous increases of surface ozone and associated premature mortality growth in China during 2015–2019. *Environ Pollut.* (2021) 269:116183. doi: 10.1016/j.envpol.2020.116183

27. Wang C, Wang Y, Shi Z, Sun J, Gong K, Li J, et al. Effects of using different exposure data to estimate changes in premature mortality attributable to PM2.5 and O3 in China. *Environ Pollut.* (2021) 285:117242. doi: 10.1016/j.envpol.2021.117242

28. Kan H, Chen R, Tong S. Ambient air pollution, climate change, and population health in China. *Environ Int.* (2012) 42:10–9. doi: 10.1016/j.envint.2011.03.003

29. Chen R, Samoli E, Wong C-M, Huang W, Wang Z, Chen B, et al. Associations between short-term exposure to nitrogen dioxide and mortality in 17 Chinese cities: the China Air Pollution and Health Effects Study (CAPES). *Environ Int.* (2012) 45:32–8. doi: 10.1016/j.envint.2012.04.008

30. Chen R, Pan G, Zhang Y, Xu Q, Zeng G, Xu X, et al. Ambient carbon monoxide and daily mortality in three Chinese cities: the China Air Pollution and Health Effects Study (CAPES). *Sci Tot Environ.* (2011) 409:4923–8. doi: 10.1016/j.scitotenv.2011.08.029

31. Chen R, Huang W, Wong C-M, Wang Z, Thach TQ, Chen B, et al. Short-term exposure to sulfur dioxide and daily mortality in 17 Chinese cities: the China air pollution and health effects study (CAPES). *Environ Res.* (2012) 118:101–6. doi: 10.1016/j.envres.2012.07.003

32. Wu R, Zhong L, Huang X, Xu H, Liu S, Feng B, et al. Temporal variations in ambient particulate matter reduction associated short-term mortality risks in Guangzhou, China: a time-series analysis (2006–2016). *Sci Tot Environ.* (2018) 645:491–8. doi: 10.1016/j.scitotenv.2018.07.091

33. Chen C, Xu D, He MZ, Wang Y, Du Z, Du Y, et al. Fine particle constituents and mortality: a time-series study in Beijing, China. *Environ Sci Technol.* (2018) 52:11378–86. doi: 10.1021/acs.est.8b00424

34. Yang C, Yang H, Guo S, Wang Z, Xu X, Duan X, et al. Alternative ozone metrics and daily mortality in Suzhou: the China Air Pollution and Health Effects Study (CAPES). *Sci Tot Environ.* (2012) 426:83–9. doi: 10.1016/j.scitotenv.2012.03.036

35. Dominici F, Peng RD, Barr CD, Bell ML. Protecting human health from air pollution: shifting from a single-pollutant to a multi-pollutant approach. *Epidemiology.* (2010) 21:187. doi: 10.1097/EDE.0b013e3181cc86e8

36. Zhu Y, Wang Y, Xu H, Luo B, Zhang W, Guo B, et al. Joint effect of multiple air pollutants on daily emergency department visits in Chengdu, China. *Environ Pollut.* (2020) 257:113548. doi: 10.1016/j.envpol.2019.113548

37. Shen F, Ge X, Hu J, Nie D, Tian L, Chen M. Air pollution characteristics and health risks in Henan Province, China. *Environ Res.* (2017) 156:625–34. doi: 10.1016/j.envres.2017.04.026

38. Swamee PK, Tyagi A. Formation of an air pollution index. *J Air Waste Manag Assoc.* (1999) 49:88–91. doi: 10.1080/10473289.1999.10463776

39. Stieb DM, Burnett RT, Smith-Doiron M, Brion O, Shin HH, Economou V. A new multipollutant, no-threshold air quality health index based on short-term associations observed in daily time-series analyses. *J Air Waste Manag Assoc.* (2008) 58:435–50. doi: 10.3155/1047-3289.58.3.435

40. Hu J, Ying Q, Wang Y, Zhang H. Characterizing multi-pollutant air pollution in China: comparison of three air quality indices. *Environ Int.* (2015) 84:17–25. doi: 10.1016/j.envint.2015.06.014

41. Shen F, Zhang L, Jiang L, Tang M, Gai X, Chen M, et al. Temporal variations of six ambient criteria air pollutants from 2015 to 2018, their spatial distributions, health risks and relationships with socioeconomic factors during 2018 in China. *Environ Int.* (2020) 137:105556. doi: 10.1016/j.envint.2020.105556

42. Zhou W, Chen C, Lei L, Fu P, Sun Y. Temporal variations and spatial distributions of gaseous and particulate air pollutants and their health risks during 2015–2019 in China. *Environ Pollut.* (2021) 272:116031. doi: 10.1016/j.envpol.2020.116031

43. Biegalski S, Hopke P. Total potential source contribution function analysis of trace elements determined in aerosol samples collected near Lake Huron. *Environ Sci Technol.* (2004) 38:4276–84. doi: 10.1021/es035196s

44. Boichu M, Favez O, Riffault V, Petit JE, Zhang Y, Brogniez C, et al. Large-scale particulate air pollution and chemical fingerprint of volcanic sulfate aerosols from the 2014–2015 Holuhraun flood lava eruption of Bárð*arbunga volcano (Iceland). *Atmos Chem Phys.* (2019) 19:14253–87. doi: 10.5194/acp-19-14253-2019

45. Liu H, Liu C, Xie Z, Li Y, Huang X, Wang S, et al. A paradox for air pollution controlling in China revealed by "APEC Blue" and "Parade Blue". *Sci Rep.* (2016) 6:34408. doi: 10.1038/srep34408

46. Zhao N, Wang G, Li G, Lang J, Zhang H. Air pollution episodes during the COVID-19 outbreak in the Beijing–Tianjin–Hebei region of China: an insight into the transport pathways and source distribution. *Environ Pollut.* (2020) 267:115617. doi: 10.1016/j.envpol.2020.115617

47. Dimitriou K, Grivas G, Liakakou E, Gerasopoulos E, Mihalopoulos N. Assessing the contribution of regional sources to urban air pollution by applying 3D-PSCF modeling. *Atmos Res.* (2021) 248:105187. doi: 10.1016/j.atmosres.2020.105187

48. Guo H, Huang S, Chen M. Air pollutants and asthma patient visits: indication of source influence. *Sci Tot Environ.* (2018) 625:355–62. doi: 10.1016/j.scitotenv.2017.12.298

49. Zhang L, Shen F, Gao J, Cui S, Yue H, Wang J, et al. Characteristics and potential sources of black carbon particles in suburban Nanjing, China. *Atmos Pollut Res.* (2020) 11:981–91. doi: 10.1016/j.apr.2020.02.011

50. Shang Y, Sun Z, Cao J, Wang X, Zhong L, Bi X, et al. Systematic review of Chinese studies of short-term exposure to air pollution and daily mortality. *Environ Int.* (2013) 54:100–11. doi: 10.1016/j.envint.2013.01.010

51. Nie D, Shen F, Wang J, Ma X, Li Z, Ge P, et al. Changes of air quality and its associated health and economic burden in 31 provincial capital cities in China during COVID-19 pandemic. *Atmos Res.* (2021) 249:105328. doi: 10.1016/j.atmosres.2020.105328

52. Tian X, Dai H, Geng Y, Wilson J, Wu R, Xie Y, Hao H. Economic impacts from PM2.5 pollution-related health effects in China's road transport sector: a provincial-level analysis. *Environ Int.* (2018) 115:220–9. doi: 10.1016/j.envint.2018.03.030

53. Draxler R, Stunder B, Rolph G, Stein A, Taylor A. *HYSPLIT4 User's Guide, Version 4, Report*. Silver Spring, MD: NOAA (2012).

54. Polissar AV, Hopke PK, Paatero P, Kaufmann YJ, Hall DK, Bodhaine BA, et al. The aerosol at Barrow, Alaska: long-term trends and source locations. *Atmos Environ.* (1999) 33:2441–58. doi: 10.1016/S1352-2310(98)00423-3

55. Petit JE, Favez O, Albinet A, Canonaco F. A user-friendly tool for comprehensive evaluation of the geographical origins of atmospheric pollution: wind and trajectory analyses. *Environ Model Softw.* (2017) 88:183–7. doi: 10.1016/j.envsoft.2016.11.022

56. Wang F, Qiu X, Cao J, Peng L, Zhang N, Yan Y, et al. Policy-driven changes in the health risk of PM2.5 and O3 exposure in China during 2013–2018. *Sci Tot Environ.* (2021) 757:143775. doi: 10.1016/j.scitotenv.2020.143775

57. Wu J, Zhang Y, Wang T, Qian Y. Rapid improvement in air quality due to aerosol-pollution control during 2012–2018: an evidence observed in Kunshan in the Yangtze River Delta, China. *Atmos Pollut Res.* (2020) 11:693–701. doi: 10.1016/j.apr.2019.12.020

58. Xiao K, Wang Y, Wu G, Fu B, Zhu Y. Spatiotemporal characteristics of air pollutants (PM10, PM2.5, SO2, NO2, O3, and CO) in the Inland Basin City of Chengdu, Southwest China. *Atmosphere.* (2018) 9:74. doi: 10.3390/atmos9020074

59. Zhao S, Yin D, Yu Y, Kang S, Qin D, Dong L. PM2.5 and O3 pollution during 2015–2019 over 367 Chinese cities: SPATIOTEMPORAL variations, meteorological and topographical impacts. *Environ Pollut.* (2020) 264:114694. doi: 10.1016/j.envpol.2020.114694

60. Zheng S, Schlink U, Ho KF, Singh RP, Pozzer A. Spatial distribution of PM2. 5-related premature mortality in China. *GeoHealth.* (2021) 5:e2021GH000532. doi: 10.1029/2021GH000532

frontiers | Frontiers in Public Health

TYPE Hypothesis and Theory
PUBLISHED 26 January 2023
DOI 10.3389/fpubh.2023.1073902



OPEN ACCESS

EDITED BY
Parth Sarathi Mahapatra,
Deutsche Gesellschaft für Internationale Zusammenarbeit (GIZ) GmbH, India

REVIEWED BY
Sagar Adhikari,
International Centre for Integrated Mountain Development, Nepal
Pankaj Sadavarte,
Duke University, United States

*CORRESPONDENCE
Qingyong Lei
✉ Jluktz123@163.com

SPECIALTY SECTION
This article was submitted to Environmental health and Exposome, a section of the journal Frontiers in Public Health

RECEIVED 19 October 2022
ACCEPTED 10 January 2023
PUBLISHED 26 January 2023

CITATION
Guo H, Li S, Pan C, Xu S and Lei Q (2023) Analysis of spatial and temporal characteristics of carbon emission efficiency of pig farming and the influencing factors in China. *Front. Public Health* 11:1073902. doi: 10.3389/fpubh.2023.1073902



# Analysis of spatial and temporal characteristics of carbon emission efficiency of pig farming and the influencing factors in China

Hongpeng Guo, Shi Li, Chulin Pan, Shuang Xu and Qingyong Lei*

College of Biological and Agricultural Engineering, Jilin University, Changchun, China

Pig farming has been a crucial contribution to China's food security although intestinal fermentation and its excrement during pig breeding are major sources of greenhouse gas emissions. In this paper, we measured the carbon emission efficiency of pig farming in 30 provinces (autonomous regions and municipalities) from 2010 to 2020 by using the non-expected output Slack-Based Measure (SBM) model and analyzed the spatial characteristics of the carbon emission efficiency of pig farming in China. We also examined and analyzed the factors influencing the carbon emission efficiency of pig farming by using the limited dependent variable model (Tobit). The results show that: the carbon emission efficiency of pig farming in China shows an M-shaped upward trend over time by comparing the carbon emission efficiency longitudinally during the study period and the carbon emission efficiency of pig farming shows a decreasing trend in the east, central and west regions of China by comparing the carbon emission efficiency of different regions horizontally. It's also shown that regions with low- and extremely-low-efficiency transfer from the east to the central and west regions and the central and regions with high-efficiency transfer to the east. The regression analysis of the factors influencing the carbon emission efficiency of pig breeding shows that the comparative advantage of the pig industry and transportation accessibility is positively correlated with the carbon emission efficiency of pig breeding, whereas the proportion of food resources and market scale is negatively correlated with the carbon emission efficiency of pig breeding. At the same time, the production layout index has no significant influence on the carbon emission efficiency of pig breeding. The research results provide a theoretical basis for regional differentiation of carbon emission management from pig farming, optimizing the layout of the pig industry and reducing environmental pollution.

KEYWORDS

**carbon emission efficiency, SBM model, distribution characteristics of carbon emission efficiency, Tobit model, factors affecting carbon emission efficiency**

## 1. Introduction

Carbon emissions from livestock and poultry farming have been one of the most significant sources of greenhouse gas emissions in China (1). Statistics from the Food and Agriculture Organization of the United Nations (FAO) show that pigs, cattle, sheep, and poultry account for 18% of overall greenhouse gas emissions. China is not only a major pig-producing country but also a major pork-consuming country. In China, both pig rearing and pork consumption account for half of the world's total. The pig farming industry pollutes water, air, and soil, making the rural ecological environment more fragile and limiting the sustainable development of the

industry (2). The carbon emission from pig farming has become the second largest type of carbon emission from livestock farming in China, second only to that from cattle farming. The carbon emission from pig farming has become one of the major difficulties in the management of agricultural surface pollution in China (3). It is very important to get higher profits with lesser carbon emissions and carbon emission efficiency has been used to measure this index. By referring to other scholars' definitions of carbon emission efficiency (4–6), this paper defines the carbon emission efficiency of pig breeding as low carbon emission to obtain maximum benefits in the process of pig breeding with certain input factors.

Livestock production accounts for a significant share of the global greenhouse gas (GHG) balance, including carbon dioxide ($CO_2$), methane ($CH_4$), ammonia ($NH_3$), and nitrous oxide ($N_2O$) released into the atmosphere (7). There are many calculation and assessment methods to study carbon emission efficiencies, such as the stochastic frontier model, regression model, data envelopment analysis (DEA) method, and unexpected output (Slack-Based Measure) model (8–11). Most studies have adopted the unexpected output (Slack-Based Measure) model to calculate carbon emission efficiency. For example, Zhao et al. (12) used the Slack-Based Measure (SBM) model to measure the agricultural eco-efficiency of 31 provinces in China during 2010–2019 and analyzed the spatial-temporal differences (12). Wang and Du (13) also used the Slack-Based Measure (SBM) model to measure the carbon emission efficiency and environmental efficiency of 14 cities in Hunan Province in China from 2010 to 2016 and analyzed the spatial differences.

Domestic and foreign scholars have carried out a large number of studies on the influencing factors of carbon emissions from pig farming. Due to the differences in the farming environment, mode of farming as well as fecal waste treatment methods at home and abroad, the influencing factors of carbon emissions from pig farming also vary. Some developed countries mainly adopt intelligent management systems, automatic phased feeding systems, pig farm environmental monitoring systems, and other modern techniques to carry out real-time feeding and testing of pig breeding, reducing carbon emissions through the improvement of technical means (14). Domestic scholars mainly study the influencing factors of carbon emissions from animal husbandry, including economic development, breeding scale, industrial structure, agricultural technical conditions, education level, scales of the agricultural labor force, urbanization level, etc., (15–19).

With the current national emphasis on environmental pollution control, most scholars have measured and evaluated the carbon emission efficiency of agriculture and animal husbandry in the context of environmental pollution (20–22). However, scholars have not studied the carbon emission efficiency of a single industry, and the relationship between the change in pig industry layout and the carbon emission efficiency of pig farming and the influencing factors are still unknown. Based on the above studies, this paper uses the non-expected output Slack-Based Measure (SBM)model to measure the carbon emission efficiency of pig breeding in 30 provinces (autonomous regions and municipalities) in China and combines the Tobit model to test and analyze its influencing factors. It provides the government with theoretical references and policy guidance on the layout of the pig industry and how to improve the carbon emission efficiency of pig farming to reduce pollution.

TABLE 1 Carbon emission efficiency measurement index of pig farming.

| Category | Indicators | Metrics |
|---|---|---|
| Input elements | Capital Investment<br>Labor input | Pig farming cost<br>Number of employees in the pig industry |
| Output elements | Expected output<br>Non-desired outputs | Pig production value<br>Carbon emissions from pig farming |

## 2. Materials and methodology

### 2.1. Spatial and temporal characteristics of carbon emission efficiency of pig farming

#### 2.1.1. Data sources

The data required for this paper were obtained from the 2010–2020 China Statistical Yearbook[1] and the China Rural Statistical Yearbook[2], as well as provincial and municipal statistical yearbooks and statistical bulletins on national economic and social development. Due to the unavailability of data, Hong Kong, Macau, Tibet and Taiwan have not been included in the study.

#### 2.1.2. Indicator construction

Through reviewing a large amount of literature, this study selected pig farming capital, and labor (23) as input indicators, pig production value (1), and carbon emission (24) as desired output indicators and non-desired output indicators, respectively (Table 1).

#### 2.1.3. Costs of pig farming

The total costs of pig farming in each province and city were obtained by calculating the product of the cost per pig farmed and the annual pig slaughter volume in each province and city by reviewing the literature and referring to the China Rural Statistical Yearbook[3] and the statistical yearbooks of each province and city.

#### 2.1.4. Number of employees in the pig industry

Due to the lack of accurate data on the number of employees in the pig industry, by reviewing the literature, we refer to the methods and ideas of Zhang et al. (23) to calculate the amount of investment in fixed assets and the number of employees in the livestock industry. The formula for calculating the number of employees in the pig industry is shown below.

$$PE_k^t = XE_k^t \frac{POV_k^t}{XOV_k^t} \quad (1)$$

In the formula: $PE$ is the number of employees in the pig industry, $XE$ is the number of employees in the livestock industry, $POV$ is the

1 "China Statistical Yearbook" (https://data.cnki.net/yearbook/Single/N2022110021).

2 "China Rural Statistical Yearbook" (https://data.cnki.net/yearbook/Single/N2021120010).

3 "China Rural Statistical Yearbook" (https://data.cnki.net/yearbook/Single/N2021120010).

output value of pigs, *XOV* is the output value of livestock, k is the region, and t is the period.

### 2.1.5. Carbon emissions from pig farming

After reviewing the literature, it is found that the carbon emissions of pig farming mainly come from methane ($CH_4$) produced by the intestinal fermentation process of pigs, $CH_4$ (1 t $CH_4$ = 6.82 carbon), and nitrous oxide ($N_2O$, 1 t = $N_2O$ = 81.27 t carbon) from manure emissions. Referring to the IPCC Greenhouse Gas Emissions Inventory Guidelines 2019, carbon emissions are calculated as follows:

$$C = \sum_{i=1}^{1} C_k^t = \sum_{i=1}^{1} [6.82 \times \lambda_k^t \times (\mu_i + \nu_i) + 81.27 \times \lambda_k^t \times \omega_i] \quad (2)$$

Where: $C$ is the total carbon emission, $C_k^t$ is the carbon emission from pig farming in year t in region $k$, $\lambda_k^t$ is the average feeding capacity of pigs in year t in region $k$ [see Equation (4) for the calculation of the average feeding capacity], $\mu_i$, $\nu_i$, $\omega_i$ are the $CH_4$ and $N_2O$ emission coefficients of pigs, and by referring to the IPCC Guidelines for Greenhouse Gas Emission Inventories 2019, we know that the emission coefficient of $CH_4$ from enteric fermentation of pigs ($\mu_i$) is 1, the emission coefficient of $CH_4$ from manure emissions from $CH_4$ ($\nu_i$) is 3.5 and $N_2$ O ($\omega_i$) is 0.53, respectively.

$$\begin{cases} \lambda_k^t = \phi_k^t \times \frac{\varphi_k^t}{365} & \gamma \geq 1 \\ \lambda_k^t = \frac{\tau_k^t + \sigma_k^t}{2} & \gamma < 1 \end{cases} \quad (3)$$

Where: λ is the average stocking, Φ is the average annual growth cycle, ϕ is the annual slaughter, $\gamma$ is the slaughter rate (where the slaughter rate of pigs and poultry is $\geq$ 1, and the average annual growth cycle is 200 d and 55 d, respectively), $\tau$ is the stocking at the end of the previous year, $\sigma$ is the stocking at the end of the current year, $k$ is the region, and $t$ is the period.

### 2.1.6. Non-desired output SBM model

Modern production methods have increased labor productivity, which not only facilitates the increasing trade and economic activities between countries, but it also improves people's living standards with the privilege of having abundant and cheap industrial products. At the same time, industrial production inevitably produces large amounts of pollutants such as wastewater, waste gas, and solid waste, which are commonly referred to as undesired outputs.

Furthermore, it leads to a series of problems such as haze and global warming. Therefore, green production methods which reduce waste have become a crucial goal in every production area. If non-desired outputs are being considered, we do not want to produce more industrial waste, no matter what the input is. Therefore, the most efficient production method in today's society is the green production method, producing more desired outputs with fewer inputs as well as fewer undesired outputs. Tone proposed the undesired output Slack-Based Measure (SBM) model in 2003. The model is based on the Slack-Based Measure (SBM) model proposed by Tone in 2001 (23).

Suppose there are $n$ decision units, each of which contains three elements: three vectors of inputs $X$, desired outputs $Y^g$ and non-desired outputs (production emissions such as wastewater, $CO_2$, soot etc.) $Y^b$, which can be expressed as

$$\begin{aligned} X &= [x_1, \ldots, x_n] \in R^{m \times n} \\ Y^g &= \left[y_1^g, \ldots, y_n^g\right] \in R^{s_1 \times n} \\ Y^b &= \left[y_1^b, \ldots, y_n^b\right] \in R^{s_2 \times n} \end{aligned} \quad (4)$$

Where: $X$, $Y^g$, $Y^b > 0$, $R$ is the set of real vectors, $m$, $s_1$, $s_2$ are the number of factors of input, desired output, and non-desired output, respectively. The SBM model for non-desired outputs can be expressed as

$$\begin{cases} \rho^* = \dfrac{1 - \frac{1}{m}\sum_j^m \frac{S_i^-}{x_{i_0}}}{1 + \frac{1}{s_1+s_2}\left(\sum_{r=1}^{s_1} \frac{S_r^g}{y_{r_0}^g} + \sum_{r=1}^{s_2} \frac{S_r^b}{y_{r_0}^b}\right)} \\ s.t.\ x_0 = X\lambda + s^-, y_0^g = Y^g\lambda - s^g, y_0^b = Y^g\lambda + s^b \end{cases} \quad (5)$$

In this model $\rho^*$ is the carbon emission efficiency value, and $s^-$, $s^g$ and $s^b$ are the slack amounts of input, desired output, and non-desired output, respectively. When $\rho^* = 1$, the decision unit is valid, i. e., there is a Pareto optimum; when $\rho^* > 0 \sim < 1$, it is in an invalid state, and the efficiency can be improved by optimizing the input and output. Efficiency is specifically divided into four levels: very low efficiency ($0 < \rho^* \leq 0.3$), low efficiency ($0.3 < \rho^* \leq 0.6$), medium efficiency ($0.6 < \rho^* \leq 0.9$), and high efficiency ($\rho^* > 0.9$) (25).

### 2.1.7. Carbon emission efficiency values

In this paper, Equations (1)–(5) and Matlab software are used to measure the carbon emission efficiency values of 30 provinces (autonomous regions and municipalities) in China from 2010 to 2020, and the results are shown in Table 2.

## 2.2. Analysis of factors affecting carbon emission efficiency of pig farming

### 2.2.1. Data sources

The data required for this paper are obtained from the carbon emission efficiency values calculated in the previous sections, those from the China Statistical Yearbook and the China Rural Statistical Yearbook for 2010–2020, as well as from provincial and municipal statistical yearbooks and statistical bulletins on national economic and social development. Due to the lack of availability of data, Hong Kong, Macau, Tibet and Taiwan have not been included in the study.

### 2.2.2. Introduction to the Tobit model

The national carbon emission efficiency values from pig farming obtained from the efficiency evaluation are all >0, which are truncated data. The Tobit model is a model in which the dependent variable is continuous but subject to some restrictions on its value. Therefore, it's also known as a restricted dependent variable model. The Tobit model focuses on the analysis of how continuous variables change under a certain choice of behaviors. The general form of the model is shown below:

$$\begin{aligned} y_i &= \beta^T X_i + \varepsilon_i, i = 1, 2, \ldots, n, \varepsilon_i \sim N\left(0, \sigma^2\right) \\ &\begin{cases} y^* \leq 0, & y_i = 0 \\ y^* \geq 0, & y_i = y^* \end{cases} \end{aligned} \quad (6)$$

10.3389/fpubh.2023.1073902

TABLE 2 Carbon emission efficiency values of pig farming in 30 provinces, cities, and autonomous regions nationwide, 2010–2020.

| Region | 2010 | 2011 | 2012 | 2013 | 2014 | 2015 | 2016 | 2017 | 2018 | 2019 | 2020 |
|---|---|---|---|---|---|---|---|---|---|---|---|
| Beijing | 0.862 | 0.847 | 0.905 | 0.938 | 0.882 | 0.776 | 0.438 | 0.794 | 0.953 | 0.114 | 1.000 |
| Tianjin | 0.413 | 1.000 | 1.000 | 1.000 | 1.000 | 1.000 | 1.000 | 1.000 | 1.000 | 1.000 | 1.000 |
| Hebei | 0.397 | 0.447 | 0.408 | 0.468 | 0.437 | 0.470 | 0.296 | 0.298 | 0.465 | 0.309 | 0.467 |
| Shanxi | 0.414 | 0.370 | 0.307 | 0.304 | 0.296 | 0.323 | 0.240 | 0.296 | 0.291 | 0.214 | 0.379 |
| Inner Mongolia | 0.398 | 0.408 | 0.377 | 0.439 | 0.447 | 0.485 | 0.279 | 0.416 | 0.399 | 0.417 | 0.483 |
| Liaoning | 0.472 | 0.701 | 0.536 | 0.617 | 0.534 | 0.544 | 0.288 | 0.315 | 0.318 | 0.183 | 0.129 |
| Jilin | 1.000 | 0.715 | 0.718 | 0.650 | 0.716 | 0.727 | 1.000 | 0.445 | 0.554 | 0.274 | 0.414 |
| Heilongjiang | 1.000 | 1.000 | 1.000 | 1.000 | 1.000 | 1.000 | 1.000 | 1.000 | 0.893 | 1.000 | 1.000 |
| Shanghai | 1.000 | 1.000 | 1.000 | 1.000 | 1.000 | 1.000 | 1.000 | 1.000 | 1.000 | 0.508 | 1.000 |
| Jiangsu | 0.424 | 0.539 | 0.537 | 0.592 | 0.531 | 0.545 | 0.347 | 0.716 | 0.844 | 0.449 | 0.608 |
| Zhejiang | 0.418 | 0.698 | 0.635 | 0.693 | 0.690 | 0.839 | 0.828 | 1.000 | 1.000 | 0.585 | 0.833 |
| Anhui | 0.462 | 0.458 | 0.453 | 0.439 | 0.429 | 0.471 | 0.493 | 1.000 | 0.706 | 0.314 | 0.747 |
| Fujian | 0.522 | 0.652 | 0.594 | 0.633 | 0.623 | 0.687 | 0.476 | 0.703 | 0.903 | 0.516 | 1.000 |
| Jiangxi | 0.346 | 0.408 | 0.380 | 0.415 | 0.422 | 0.467 | 0.196 | 0.192 | 0.207 | 0.218 | 0.264 |
| Shandong | 0.556 | 0.635 | 0.582 | 0.604 | 0.579 | 0.657 | 0.532 | 0.615 | 0.677 | 0.446 | 0.382 |
| Henan | 0.322 | 0.427 | 0.411 | 0.422 | 0.421 | 0.448 | 0.238 | 0.280 | 0.479 | 0.236 | 0.318 |
| Hubei | 1.000 | 0.553 | 0.472 | 0.535 | 0.563 | 0.596 | 0.551 | 0.577 | 0.783 | 0.491 | 0.679 |
| Hunan | 0.315 | 0.385 | 0.338 | 0.370 | 0.335 | 0.383 | 0.246 | 0.283 | 0.376 | 0.360 | 0.591 |
| Guangdong | 0.340 | 0.410 | 0.410 | 0.443 | 0.431 | 0.449 | 0.215 | 0.418 | 0.467 | 0.329 | 0.373 |
| Guangxi | 0.309 | 0.317 | 0.348 | 0.330 | 0.308 | 0.343 | 0.213 | 0.436 | 0.360 | 0.259 | 0.189 |
| Hainan | 0.492 | 0.736 | 0.680 | 0.673 | 0.630 | 0.788 | 0.766 | 0.998 | 0.984 | 1.000 | 0.780 |
| Chongqing | 0.188 | 0.199 | 0.237 | 0.271 | 0.239 | 0.238 | 0.166 | 0.178 | 0.206 | 0.214 | 0.412 |
| Sichuan | 0.332 | 0.357 | 0.333 | 0.370 | 0.353 | 0.460 | 0.200 | 0.227 | 0.266 | 0.324 | 0.432 |
| Guizhou | 0.184 | 0.189 | 0.191 | 0.220 | 0.254 | 0.377 | 0.550 | 1.000 | 1.000 | 0.506 | 0.386 |
| Yunnan | 0.241 | 0.266 | 0.303 | 0.369 | 0.322 | 0.352 | 0.417 | 0.430 | 0.504 | 0.257 | 0.370 |
| Shaanxi | 1.000 | 0.615 | 0.602 | 0.639 | 0.584 | 0.649 | 1.000 | 0.819 | 0.787 | 0.457 | 0.570 |
| Gansu | 0.288 | 0.261 | 0.241 | 0.266 | 0.273 | 0.306 | 0.229 | 0.226 | 0.282 | 0.197 | 0.198 |
| Qinghai | 0.231 | 0.285 | 0.261 | 0.303 | 0.294 | 0.256 | 0.204 | 0.344 | 0.441 | 0.250 | 0.209 |
| Ningxia | 0.283 | 0.293 | 0.328 | 0.342 | 0.325 | 0.335 | 0.377 | 0.327 | 0.414 | 0.241 | 0.328 |
| Xinjiang | 0.515 | 0.578 | 0.346 | 0.493 | 0.647 | 0.806 | 0.590 | 0.478 | 0.750 | 0.524 | 0.847 |

In Equation (6), $y_i$ is the explained variable, $X_i$ is the explanatory variable, $\beta^T$ is the parameter vector, and $\varepsilon_i$ denotes the random error term of the model equation that follows a normal distribution. Tobit model is an intercept regression model, where the explanatory variable $X_i$ takes actual observations and the explained variable $y_i$ takes values in a restricted manner: when $y^* \geq 0$, $y_i$ takes actual observations, and when $y^* \leq 0$, $y_i$ takes values of 0.

### 2.2.3. Selection of indicators

For pig farming, the change of various influencing factors triggers the change of production layout through the change of the number of pigs in each region, which will lead to the change in the carbon emission efficiency of pig breeding in each region. Microscopically, the change in pig farming layout in China is formed by the change in the scale of the feeding of many pig farmers. At the same time, the change in pig farming layout will also lead to the industrial shift of pig farming and thus the change in carbon emission efficiency in each region. Therefore, any change of factors leading to the change of pig farmers' feeding scale will become a factor affecting the change of pig farming layout in China. The formation of the regional layout of pigs is the product of natural, economic, and social interaction at a certain stage of development. According to the theory of agricultural regional factor formation developed based on location theory, there are many factors affecting the carbon emission efficiency of pig farming. This study selects the carbon emission efficiency of pig farming as the dependent variable and, by referring to the research results of other scholars, we select the proportion of grain resources

(26), production layout index (27), market size (26), transportation accessibility (28) and comparative advantage of pig industry (2) as independent variables. Hence we construct the model as below:

$$PE_k^t = \alpha_k^t + \beta_1 LS_k^t + \beta_2 PLI_k^t + \beta_3 SG_k^t + \beta_4 BS_k^t + \beta_5 JT_k^t + \varepsilon_k^t \quad (7)$$

Where: $PE$ is the carbon emission efficiency generated by pig farming, $LS$ is the share of food resources, $PLI$ is the production layout index, $SG$ is the market size, $BS$ is thcomparativedvantage, $JT$ is the transportation accessibility, $\beta_1 \sim \beta_5$ are the estimation coefficients, $\varepsilon$ is the disturbance term, $k$ is the region, and $t$ is the period.

### 2.2.4. Interpretation of indicators

#### 2.2.4.1. Share of food resources

Grain, as the main type of feed for pigs, has an important impact on pig farming. The amount of grain production directly determines whether farmers have enough grain to convert into feed grain for pig farming in addition to their subsistence needs. Hence, it has an impact on the behavioral choice of whether to engage in pig farming. Generally speaking, farmers who have resources of grain to convert into feed grain will continue or expand pig farming scale, whereas farmers who do not have grain to convert into feed grain will face two choices of either withdrawing from production or purchasing feed grain. The latter option translates to increased breeding costs (29). Therefore, the abundance or scarcity of grain resources, especially corn and soybean resources, directly affects the pig farming scale of farmers.

#### 2.2.4.2. Production layout index

The production layout index can better reflect the regional distribution and scale of pig farming, and the regional distribution and scale of pig farming affect the change of carbon emission efficiency in each region. In this paper, the production layout index is measured by the proportion of pig farming in each region to the national pig farming in that specific year (27).

#### 2.2.4.3. Market size

Supply and demand theory suggests that an increase in demand leads to an increase in supply, which in turn makes the equilibrium quantity rise and demand is the most direct factor affecting the change in supply. The market size has an important impact on the distribution of live pig farming (27). The larger the market size is, the more people will consume pigs and the more pigs are being kept in the nearby area. The increase in the number of pigs kept will also have an impact on the carbon emission efficiency of the area.

#### 2.2.4.4. Comparative advantage of the pig industry

If pig farming in each region has obvious advantages over agriculture, it will push more farmers and enterprises to enter the pig-producing industry. that the reality is that major agricultural and animal husbandry enterprises are entering the pig industry and expanding their production capacity drastically. The more obvious the comparative advantage of pig breeding, the greater the potential and space for pig farming (30). The greater the pig farming potential and space, the more likely other regions will have a large pig farming potential and space for transfer, and the carbon emission efficiency will change accordingly.

#### 2.2.4.5. Transportation accessibility

The distance between the place of consumption and the origin of pigs determines the source of pork in that individual market. Without considering the differences in pork quality, transportation costs become the most substantial cost factor when the differences in pig farming costs between regions are small. In addition to the distance from the market, the transportation cost is largely related to the transportation systems and conditions of the region. The more developed the transportation systems and conditions are, the easier it is for pig farming to form a scale, which generates more carbon emissions, and, as a consequence, the carbon emission efficiency will change (26).

### 2.2.5. Variable description

To interpret the model variable data more effectively, this study provides descriptive statistics on the variables and explains the measures of the independent variables in Table 3.

## 3. Results

### 3.1. Spatial and temporal characteristics of carbon emission efficiency of pig farming

#### 3.1.1. Analysis of time-series characteristics of carbon emission efficiency of pig farming in China

Due to the vast geographic landscape of China, there are obvious differences in resource endowment and support policies in pig farming across the country. To analyze the spatial and temporal differences in the carbon emission efficiency of pig farming in different regions, the 30 provinces (autonomous regions and municipalities) in China were divided into three major regions, eastern, central, and western regions for analysis, as shown in Figure 1.

To better analyze the differences and trends of carbon emission efficiency of pig farming in different regions from 2010 to 2020, the average values of carbon emission efficiency in the eastern region, central region, western region, and the whole country were calculated. The results are shown in Table 4. A line graph was also drawn, which is shown in Figure 2.

Looking into three different regions, the carbon emission efficiency value of pig farming shows a trend of "East > Central > West." The efficiency value of the eastern region increased from 0.536 in 2010 to 0.688 in 2020, with an increase of 28.4% realizing the transformation from a low to medium efficiency zone. The carbon emission efficiency value of the central region decreased from 0.607 in 2010 to 0.549 in 2020, with a decline of 10% changing from a medium to a low-efficiency zone. Carbon emission efficiency in the western region, on the other hand, increased from 0.361 in 2010 to 0.402 in 2020, with an increase of 11.4%. It remains in the low-efficiency zone.

From 2010 to 2020, the carbon emission efficiency of pig farming in China generally showed an M-shaped upward fluctuating trend. Although the nationwide carbon emission efficiency was still at a low-efficiency level in 2020, the carbon emission efficiency value has increased from 0.491 to 0.549. The value was close to the medium efficiency level, indicating that the ratio of input to output is more harmonious, which improves the carbon emission efficiency. From 2010 to 2014, the carbon emission efficiency of pig farming in China

TABLE 3 Descriptive statistics of variables.

| Variables | Observed values | Average value | Standard deviation | Minimum value | Maximum value | Metrics |
|---|---|---|---|---|---|---|
| PE | 330 | 0.5200 | 0.25600 | 0.11400 | 1.00000 | Carbon efficiency of pig farming |
| LS | 330 | 0.33200 | 0.02800 | 0.00434 | 0.11410 | Grain production by region/total national grain for the year |
| PLI | 330 | 2.05100 | 3.22800 | 0.00033 | 18.6868 | Pig slaughter volume by region/national pig slaughter volume of the year |
| SG | 330 | 0.33200 | 0.02000 | 0.00420 | 0.08940 | Total population by region/year-end national population of the same period |
| BS | 330 | 0.38300 | 0.16100 | 0.02850 | 0.75670 | Output value of pig industry by region/total output value of livestock industry |
| JT | 330 | 0.96200 | 0.51500 | 0.08900 | 2.23400 | Total road and rail mileage by region/land area |

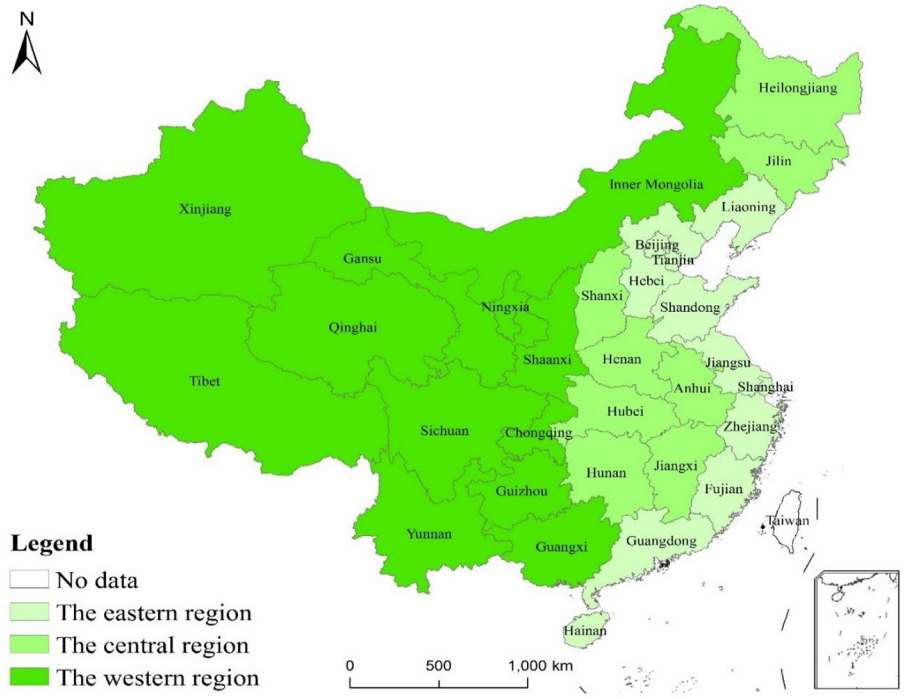


FIGURE 1
Spatial characteristics of the three major regions in China.

showed a relatively steady change and fluctuated up and down around 0.5. The first high and first low-value points of "M" appeared in 2015 and 2016 respectively but the difference between the high and low-value points of efficiency was not significant. From 2016 to 2018, the carbon emission efficiency of Chinese pig farming showed a significant upward trend and reached a medium efficiency level in 2018. The efficiency value dropped deeply in 2019 followed by a rebound in 2020, probably due to the downward adjustment of inputs and outputs caused by the epidemic.

The carbon emission efficiency values of the three regions from 2010 to 2020 were generally consistent with the national trend. The carbon emission efficiency values of the eastern region were at the medium efficiency level in all years except for 2010 and 2019 when they were at a low-efficiency level. The central region only reached a medium efficiency level in 2010 with all the other years at a low-efficiency level. The carbon emission efficiency of the western region was at a low-efficiency level during the period of study.

### 3.1.2. Spatial characteristics analysis of carbon emission efficiency of pig farming in China

According to the carbon emission efficiency values of pig farming in China from 2010 to 2020, ArcGIS was used to draw the spatial distribution of carbon emission efficiency of pig farming in 30 provinces (autonomous regions and municipalities) nationwide, as shown in Figures 3A–D.

In 2010, Shanghai and Beijing in the eastern region were in the high and medium-efficiency zones respectively, while all other cities were in the low-efficiency zone. In the central region, Jilin,

10.3389/fpubh.2023.1073902

TABLE 4 The average value of carbon emission efficiency of pig farming in China, 2010–2020.

| Region | 2010 | 2011 | 2012 | 2013 | 2014 | 2015 | 2016 | 2017 | 2018 | 2019 | 2020 |
|---|---|---|---|---|---|---|---|---|---|---|---|
| Eastern region | 0.536 | 0.697 | 0.663 | 0.696 | 0.667 | 0.705 | 0.563 | 0.714 | 0.783 | 0.495 | 0.688 |
| Central region | 0.607 | 0.539 | 0.510 | 0.517 | 0.523 | 0.552 | 0.495 | 0.509 | 0.536 | 0.388 | 0.549 |
| Western region | 0.361 | 0.342 | 0.324 | 0.367 | 0.368 | 0.419 | 0.384 | 0.444 | 0.492 | 0.331 | 0.402 |
| Nationwide | 0.491 | 0.525 | 0.498 | 0.528 | 0.519 | 0.559 | 0.479 | 0.560 | 0.610 | 0.406 | 0.546 |

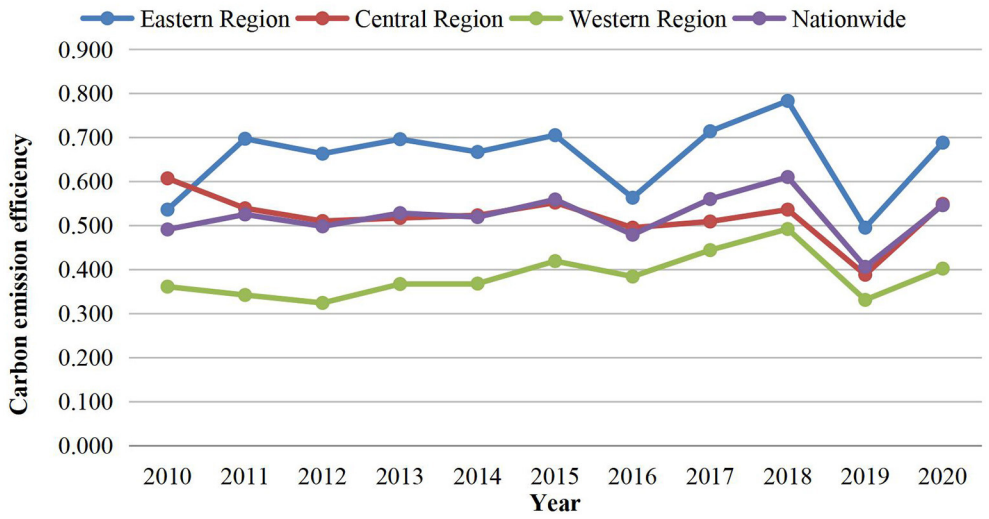


FIGURE 2
The trend of carbon emission efficiency of pig farming in China, 2010–2020.

Heilongjiang, and Hubei were in the high-efficiency zone, while other cities were in the low-efficiency zone. In the western region, no city was in the medium-efficiency zone, with only Inner Mongolia, Xinjiang, Sichuan, and Shaanxi in the low-efficiency zone. All the other cities in the region were in a very low-efficiency zone. In 2014, the number of provinces in medium-efficiency zones increased from 1 to 5, and Xinjiang, Zhejiang, Fujian, and Hainan underwent a shift from low-efficiency zone to medium-efficiency zone. In the eastern region, the number of high-efficiency zones increased by one and the carbon emission efficiency of Tianjin went from a low-efficiency zone to a high-efficiency zone. The number of medium-efficiency zones also increased by four provinces, whereas the others were still located in the low-efficiency zones. In the central region, only Heilongjiang remained in the high-efficiency zone while other provinces were still in the low-efficiency zone. Jilin in the central region changed from the high-efficiency zone to the medium-efficiency zone and Hubei in the central region also changed from the high-efficiency zone to the low-efficiency zone.

From 2014 to 2017, the number of provinces in the medium efficiency zone increased from 5 to 6, while the number of provinces in the very low-efficiency zone increased from 6 to 9. Most of them were in the central and western regions, such as Sichuan, Hunan, Jiangxi, Henan, etc. In the eastern region, except for Hebei, Liaoning, and Guangdong which were in the very low-efficiency and low-efficiency zones, the remaining provinces were located in the medium and high-efficiency zones. It's also worth mentioning that the number of provinces in the high-efficiency zone reached five, so the efficiency of the eastern region has been improving faster. Sichuan, Hunan, Jiangxi, and Henan in the central region changed from low-efficiency areas to very low-efficiency areas in 2014, while Anhui province in the central region evolved from low-efficiency areas to high-efficiency areas. In 2020, the eastern region still has the highest number of provinces with high efficiency, while the central region has no province in high-efficiency areas. In the central region, there were two provinces, Anhui and Hubei in medium-efficiency areas and only Jiangxi with a very low-efficiency. Although the carbon emission efficiency of the western region was not as high as that of the eastern and central regions, the overall carbon emission efficiency has improved. For example, Xinjiang has changed from a low-efficiency area to a high-efficiency area, while Sichuan and Chongqing have changed from a very low-efficiency area to a low-efficiency area.

From 2010 to 2020, the carbon emission efficiency of pig breeding in China has improved to a certain extent and we have seen the trend of "East > Middle > West." The number of areas with very low efficiency increased first followed by a decrease. From 2010 to 2017, the number of areas with very low efficiency increased from 6 to 9 and in 2020, the number dropped back to 6, which transferred to the Great Northwest and the Great Southwest comprehensive economic zones. From 2010 to 2020, the number of low-efficiency areas decreased from 16 to 13 and we have seen a shift from the eastern to the central and western regions, from the south to the north. During the same period, the number of areas with medium efficiency increased from 1 to 6 and we have seen a shift to Beijing, Tianjin, and South China water network areas. High-efficiency areas showed a

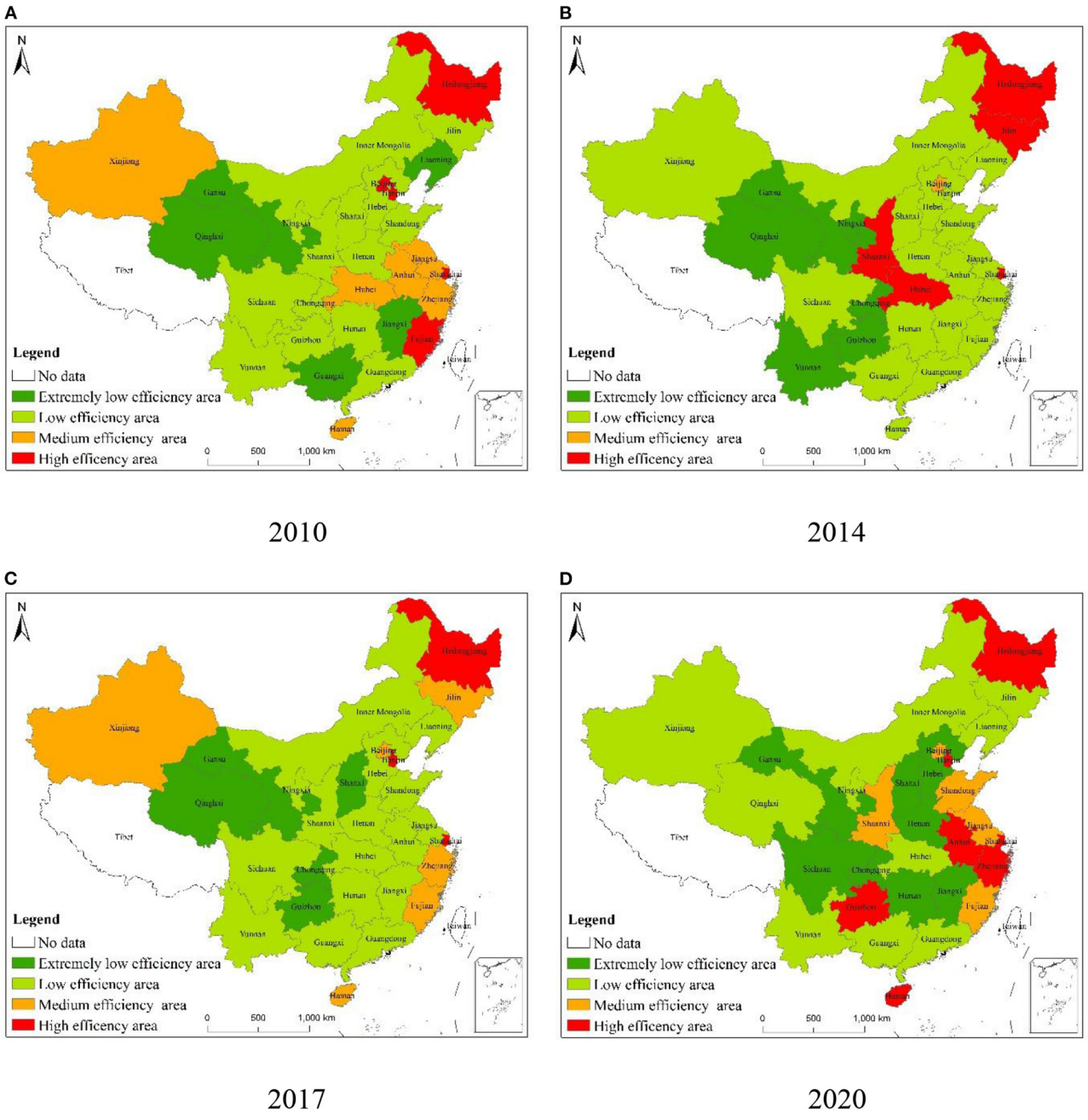


FIGURE 3
Spatial distribution of carbon emission efficiency of pig farming in China in some years **(A–D)**.

trend of "decrease—increase—decrease" pattern and transferred to Beijing, Tianjin, Shanghai, and other areas with higher economic development levels.

## 3.2. Regression analysis of factors affecting carbon emission efficiency of pig farming

The mixed Tobit regression and random panel Tobit regression scores were applied to the model using STATA 14 software and the random panel Tobit model was selected by LR test to determine the direction of influence and the degree of influence of each influencing factor. The results are shown in Table 5.

From the regression results, the regression coefficient value of food resources is −0.736 and it shows a significance at 0.05 level, implying that food resources have a significant negative correlation with carbon emission efficiency. For every one-unit increase in food resources, the carbon emission efficiency of pig farming will decrease by 0.736 units. The regression coefficient value of the production layout index is 0.00564 and the *p*-value is 0.507, implying that the production layout index has a non-significant positive influence on carbon emission efficiency. The carbon emission efficiency increases by 0.00113 units for each unit of increase in production layout index,

TABLE 5 Tobit model estimation results.

| Variables | Hybrid Tobit regression | | Stochastic panel Tobit regression | |
|---|---|---|---|---|
| | Estimated coefficient | *p*-value | Estimated coefficient | *p*-value |
| *LS* | 2.77000 | 0.18500 | −0.73600** | 0.67600 |
| *PLI* | −0.00451 | 0.40200 | 0.00564 | 0.50700 |
| *SG* | −7.40300* | 0.09600 | −5.04100* | 0.05400 |
| *BS* | 0.15700 | 0.20500 | 0.35500*** | 0.00100 |
| *JT* | 0.23300** | 0.03100 | 0.21100** | 0.00200 |
| *C* | 0.41600*** | 0.00000 | 0.33100*** | 0.00000 |
| *LR* 244.11 ($p = 0.000$) | | | | |

*, **, ***indicate significance at the 10, 5, and 1% levels, respectively; *C* is the constant term, and *LR* is the likelihood ratio test value.

the regression coefficient value of market size is −5.401 and it shows a significance of 0.1 level, implying that market size has a significant negative influence on carbon emission efficiency.

The regression coefficient value of the comparative advantage of the pig industry is 0.355 and it shows a significance at 0.01 level, which means that the comparative advantage of the pig industry has a significant positive influence on the carbon emission efficiency. With each unit increase in the comparative advantage of the pig industry, the carbon emission efficiency will increase by 0.355 units. The regression coefficient value of transportation accessibility is 0.211 and it shows a significance at 0.05 level, implying that transportation accessibility has a significant positive influence on carbon emission efficiency. With every one unit of increase in transportation accessibility, the carbon emission efficiency will increase by 0.211 units.

# 4. Discussion

## 4.1. Spatial and temporal characteristics of carbon emission efficiency of pig farming

### 4.1.1. Time-series characteristics of carbon emission efficiency of pig farming in China

From 2010 to 2020, the carbon emission efficiency of pig farming in China roughly exhibited an "M" type growth trend with three different stages. From 2010 to 2015, the fluctuation of carbon emission efficiency of pig farming in China was in a stable and slow growth state, with little changes in the ratio of input to output. From 2015 to 2020, the carbon emission efficiency of China's pig farming showed an inverted M-shape trend. In 2015, the State promulgated the Regulations on Prevention and Control of Pollution from Livestock and Poultry Farming, which have put forward the requirement that the livestock and poultry farming industry should achieve sustainable development and minimize environmental pollution caused by livestock and poultry farming. As a result, various provinces (autonomous regions and municipalities) have actively responded to the national policies and they have taken measures to improve carbon emission efficiency and the ecological environment.

Although the carbon emission efficiency of China's pig farming decreased from 2015 to 2016, it rose back sharply from 2016 to 2018. In 2018, the outbreak of African swine fever (ASF) led to a significant decline in the number of pig farms. Hence the income of pig farmers and the number of people engaged in pig farming have also been severely impacted. The significant reduction in the supply of pigs led to an imbalance of demand and supply in the pork market, leading to a sharp rise in the price of pork. When the price of pork rose, consumers reduced their consumption of pork, resulting in a decline in output value and a significant decline in input and output. From 2018 to 2019, the carbon emission efficiency of pig farming in China decreased significantly from 0.601 to 0.406. After ASF was effectively controlled, the carbon emission efficiency of China's pig breeding in 2019–2020 improved somehow, but the improvement was not very significant due to the outbreak of COVID-19.

### 4.1.2. Spatial characteristics of carbon emission efficiency of pig farming in China

Overall, the carbon emission efficiency of pig farming in all provinces (autonomous regions and municipalities) has improved to a certain extent from 2010 to 2019 and the local government of all provinces (autonomous regions and municipalities) have taken corresponding measures to improve carbon emission efficiency at source by implementing the concept of green development. From the regional perspective, the carbon emission efficiency value of China's pig farming showed a trend of "East > Middle > West" during 2010–2019. Moreover, a trend has been seen that the distribution of very low-efficiency areas and low-efficiency areas has transformed from eastern to central and western China. Also, the same trend has been seen from the southern part to the northern part of China with medium high-efficiency areas shifting to the eastern and southern parts of China.

The eastern region is mostly in the front of the country in terms of economic development state and potential, high degree of pig industry intensification, early development of pig scale, rich talent resources and mature production and breeding technology, high degree of effective transformation of animal husbandry resources, and large output to input ratio. At the same time, the development of pig farming in economically developed areas happened much earlier and the environmental regulation policies have been implemented earlier and more strictly. Hence, the pollutant emission management ability is stronger and the carbon emission efficiency is higher. With economic development, pork production is more influenced by the regional economic level, and economically developed areas gradually

reduce pig farming. Traditional pig breeding areas, such as Zhejiang and Guangdong, have moved to Sichuan, Hubei, and Guizhou, which are the main producing areas of pig breeding currently.

In the central region, Henan is one of the ten main pig farming areas in China. Besides Henan, the traditional pig breeding areas are in the southern water network as well as Jilin and Heilongjiang in the northeast. These regions have a lower level of economic development with a more developed livestock industry, less intensive pig industry, lower level of pig breeding technology know-how, and less capability in pollution management. As a result, the carbon emission efficiency of pig breeding is lower than that of the eastern region. The central region is rich in grain resources and Henan, as the main producing area of corn and wheat, has abundant feed resources. That translates to low production cost, high scale and organization of pig farming, and a relatively developed pig processing industry, which has gathered many well-known domestic meat processing enterprises such as Shuanghui, Delis, and Jinluo. Jilin and Heilongjiang provinces are also China's main grain-producing areas, the agricultural labor force is rich in these two provinces and their breeding technology has certain capital and geographic advantages. These advantages will attract external investment in the pig industry from Beijing, Tianjin, and Shanghai, the Yangtze River Delta, and the Pearl River Delta.

However, the pig breeding technology in the central region is not mature and the pollution emissions in the breeding process have not been well-controlled, resulting in low carbon emission efficiency (31). The western region is greatly influenced by the level of economic development (32). Moreover, the development mode of animal husbandry is scattered and small with poor scale efficiency. As a result, the pollution surface is wide and scattered and governance is difficult (2, 33), leading to a low level of carbon emission efficiency.

## 4.2. Analysis of factors affecting carbon emission efficiency of pig farming

Since ancient times, there has been an old saying that "pigs and grains secure the world," which shows that in the process of national economic development, pig farming and grain industry as two basic industries play an important role (34). As a grain-consuming industry, pig farming is based on grain production (especially corn industry and soybean industry), and from the perspective of the industrial chain, one of the most crucial constraints to the development of pig farming is the supply of upstream feeding materials (35). Therefore, pig farming and grain production are closely related. Pig farming is a grain-consuming livestock industry, which consumes a large amount of corn and other grain crops. The introduction of a market mechanism makes it possible to allocate resources to maximize production efficiency and concentrate on areas with rich grain resources. The more abundant the food resources are, the easier it is to become the main production area for pig farming. However, the economic development level of those areas is relatively low generally. The result is, for those more developed areas of the livestock industry, there're more carbon emissions from pig farming so the carbon emission efficiency is relatively low.

The pig production layout index is the performance of regional centralization and concentration of pig farming, which integrally reflects the regional distribution and the changes in the scale of pig farming. The production layout index of pigs is also subject to various factors, such as non-agricultural employment opportunities, science and technology, and economic factors. The higher the production layout index of pigs in a region, the more concentrated pig farming in the region is. Hence, it's much easier for pig farming to form an economy of scale. However, the results of the model regression show that the effect on carbon emission efficiency is not significant, indicating that the production layout index of pigs does not have a significant effect on the carbon emission efficiency of pig farming.

With the continuous promotion of market-oriented reform, the market gradually becomes the decisive force for resource allocation so the market demand is becoming more and more obvious for the development of pig farming. China is the world's number one pork-consuming country and pork is the most consumed meat product. With the improvement of income level, people will further increase the consumption of pork, thus stimulating farmers to increase the amount and scale of pig slaughter, which will constantly affect the layout and change of pig farming areas. Regions with large market scales will have more demand for the consumption of pork than those in other regions. As a result, it stimulates more farmers to increase the breeding of pigs. Through regression analysis, market scale and carbon emission efficiency show a negative correlation, and regions with large market scale will have higher breeding volume and lower carbon emission efficiency than those regions with small market scale.

If the benefits generated by pig farming in each region have obvious advantages over agricultural production, more farmers and enterprises will be attracted to increase their investment in scaling up pig farming as well as technological advancement. Through the regression results, the comparative advantage of the pig industry has a positive influence over carbon emission efficiency, which indicates that regions with obvious comparative advantage in the pig industry attract more capital and technology to that region. The introduction of technology can improve pig breeding, pig rearing environment, feed, and grain types, hence improving pig rearing efficiency and reducing carbon emissions generated in the pig breeding process. At the same time, the introduction of capital can make farmers increase their investment in the intestinal fermentation and manure excretion aspects of the pig breeding process, thus reducing carbon emissions and improving carbon emission efficiency.

The separation of pig farmers and consumers and the differentiation of production and consumption areas require convenient transportation facilities to ease the contradiction between supply and demand and to reduce transportation costs. Through transportation facilities, modern production factors such as capital, technology, and information can also be quickly transferred to producers, thus improving production efficiency. Convenient transportation conditions have a great positive impact on the distribution of regional feeds, transportation, and sales of pigs. Developed transportation systems not only facilitate sales, but also transfers information and technology to pig farmers timely, which facilitates farmers to understand relevant technical know-how to improve pig farming technology. Hence the carbon emission can be better controlled in the pig farming process, thus improving carbon emission efficiency (31).

# 5. Conclusions

By comparing the spatial and temporal characteristics of the carbon emission efficiency of pig farming in 30 provinces

(autonomous regions and municipalities) in China during the study period, it was found that the carbon emission efficiency of pig farming in China showed an M-shape growth trend. Moreover, the trends of the three regions identified were the same as the changing trend of carbon emission efficiency of pig farming in China. Through horizontal comparison, we found that the carbon emission efficiency of the three regions of the eastern, middle, and western parts of China showed the trend of "East > Middle > West" and the very low-efficiency areas and low-efficiency areas shifted from eastern to middle and western part of China. At the same time, areas with middle and high efficiency shifted to the east.

For pig farming, changes in various influencing factors will contribute to changes in the carbon emission efficiency of pig farming. The regression analysis found that the comparative advantage of the pig industry and transportation accessibility had a significant positive influence on the carbon emission efficiency of pig farming. The proportion of food resources and market size had a significant negative correlation on carbon emission efficiency. The production layout index had no significant influence on the carbon emission efficiency generated by pig farming.

## Data availability statement

The original contributions presented in the study are included in the article/supplementary material, further inquiries can be directed to the corresponding author.

## Author contributions

Conceptualization, resources, writing—original draft, project administration, and funding acquisition: HG. Methodology, software, validation, formal analysis, and investigation: HG and SL. Data curation: SL. Writing—review and editing: SL, HG, and SX. Visualization: CP. Supervision: QL. All authors have read and agreed to the published version of the manuscript.

## Conflict of interest

The authors declare that the research was conducted in the absence of any commercial or financial relationships that could be construed as a potential conflict of interest.

## Publisher's note



## References

1. Yang T, Li F, Du M, Wang Y, Sun Z. Measuring pollutant emissions of cattle breeding and its spatial–temporal variation in China. *J Environ Manag.* (2021) 299:3615. doi: 10.1016/j.jenvman.2021.113615

2. Wang H, Qiao J. An economic analysis of the changes in the distribution of pig production in China. *Econ Geography.* (2017) 37:129–36. doi: 10.15957/j.cnki.jjdl.2017.08.017

3. Tian W, Yu H, Wu X. Estimation of the scale of moderate pig breeding from the perspective of pollution control cost: based on the survey of Sichuan pig transfer county. *Rural Economy.* (2019) 3:122–7.

4. Ma D, Chen Z, Wang L. Spatial econometrics research on inter–provincial carbon emissions efficiency in China. *China Pop Res Environ.* (2014) 25:67–77.

5. Zhou P, Ang BW, Han JY. *Total Factor Carbon Emission Performance: A Malmquist Index Analysis*. Guangzhou, Guangdong: China National Natural Science Foundation of China (2010). doi: 10.1016/j.eneco.2009.10.003

6. Wang Q, Zhou P, Zhou D. Research on dynamic carbon dioxide emissions performance, regional disparity, and affecting factors in China. *China Indust Econ.* (2010) 1:45–54. doi: 10.19581/j.cnki.ciejournal.2010.01.004

7. Chmielowiec-Korzeniowska A, Tymczyna L, Pyrz M, Trawińska B, Abramczyk K, Dobrowolska M. Occupational exposure level of pig facility workers to chemical and biological pollutants. *Annals Agricult Environ Med.* (2018) 25:262–7. doi: 10.26444/aaem/78479

8. Shi R, Irfan M, Liu G, Yang X, Su X. Analysis of the impact of livestock structure on carbon emissions of animal husbandry: a sustainable way to improving public health and green environment. *Front Public Health.* (2022) 10:5210. doi: 10.3389/fpubh.2022.835210

9. Cai T, Yang D, Zhang X, Xia F, Wu R. Study on the vertical linkage of greenhouse gas emission intensity change of the animal husbandry sector between China and its provinces. *Sustainability.* (2018) 10:2492. doi: 10.3390/su10072492

10. Chen Y, Shang J. Disconnect analysis and influence factors of animal husbandry in China. *China Pop Res Environ.* (2014) 24:101–7.

11. Chen Y. Evaluation of greenhouse gas emission efficiency of Chinese regional livestock industry based on DEA. *Heilongjiang Animal Sci Vet Med.* (2016) 8:41–4. doi: 10.13881/j.cnki.hljxmsy.2016.0649

12. Zhao J, Dang G, Tang X. Spatial–temporal differences and influencing factors of agricultural eco–efficiency in China based on SBM–Tobit model. *J Southwest Forestry University.* (2022) 6:10–8.

13. Wang Z, Du Y. Spatial–temporal differences and influencing factors of carbon emission efficiency in Hunan Province based on SBM–DEA model. *Scient Geographica Sinica.* (2019) 39:797–806. doi: 10.13249/j.cnki.sgs.2019.05.011

14. Zhou J, Yan H. Environmental justice of hog CAFOs: experience and enlightenment from North Carolina in the United States. *Stud Dialect Nat.* (2019) 35:71–7. doi: 10.19484/j.cnki.1000-8934.2019.02.013

15. Zhao Y. Influence factors and trend prediction on dynamic change of agricultural carbon emissions in Jiangsu Province. *Chin J Agricult Res Reg Plann.* (2018) 39:97–102.

16. Jiang L. *Environmental Impact Assessment of Pig Breeding in Hunan Province*. [dissertation/master's thesis] Hunan: Hunan Agricultural University (2016).

17. He X, Chen X, Pang J. Analysis on the status and influencing factors of agricultural carbon emissions in Lanzhou based on LMDI. *J China Agricult Univ.* (2018) 23:150–8.

18. Wang S, Zhao RQ, Yang QL, Xiao LG, Yang WJ, Yu J. Agricultural production efficiency and spatial pattern under carbon emission constraint: based on 65 villages of Henan province. *J Nat Res.* (2020) 35:2092–104. doi: 10.31497/zrzyxb.20200905

19. Wu X, Zhang J. Provincial agricultural carbon emissions in China: growth dominance and emission reduction decoupling. *J Agricult Tech Econ.* (2017) 5:27–36. doi: 10.13246/j.cnki.jae.2017.05.003

20. Zha J, Tang F. Research on static level, dynamic change and affecting factors of industrial carbon emissions performance. *J Shanxi Finance Econ Univ.* (2012) 34:71–80. doi: 10.13781/j.cnki.1007-9556.2012.03.010

21. Wang Q, Zhou D, Zhou P. Regional carbon dioxide emission performance and its reduction potential based on environmental production technology: the case of main industrial provinces in China. *Stud Sci Scien.* (2011) 29:868–75. doi: 10.16192/j.cnki.1003-2053.2011.06.011

22. Duan Q. Comparative analysis on performance of carbon emission in provincial regions of China: based on method of Malmquist Index. *Technol Econ.* (2012) 31:68–74.

23. Zhang X, Ma D, Wang T. Study on carbon emission efficiency and influencing factors of animal husbandry in Heilongjiang Province. *Heilongjiang Animal Sci Vet Med*. (2020) 4:7–12. doi: 10.13881/j.cnki.hljxmsy.2019.07.0017

24. Yao C, Qian S, Mao Y, Li Z. Decomposition of impacting factors of animal husbandry carbon emissions change and its spatial differences in China. *Transact Chin Soc Agricult Engin*. (2017) 33:10–19.

25. Zhou Y, Liu W, Lv X, Chen X, Shen M. Investigating interior driving factors and cross–industrial linkages of carbon emission efficiency in China's construction industry: based on Super–SBM DEA and GVAR model. *J Clean Prod*. (2019) 241:8322. doi: 10.1016/j.jclepro.2019.118322

26. Tang M. *Study on the Change and Optimization of Pig Production Layout in China*. [dissertation/master's thesis] [Sichuan]: Sichuan Agricultural University (2014).

27. Zhang Z, Qiao, J. An empirical study on influence factor of pig production layout in China: based on the panel data of provinces. *Stat Inform Forum*. (2011) 26:61–7.

28. Wang R, Fang Y, Liu J. The spatio–temporal evolution characteristics and the influencing factors of China's hog industry. *Research of Agricultural Modernization*. (2020) 41:852–62. doi: 10.13872/j.1000-0275.2020.007

29. Hu H, Ying R, Liu J. An economic analysis of the movement of live pig producing Area in China—The transition from natural layout to economic layout. *China's Rural Econ*. (2005) 12:46–52.

30. Chen J. Study on Regional Optimal Layout of planting industry in Sichuan Province. [dissertation/master's thesis] [Sichuan]: Sichuan Agricultural University (2009).

31. Zhao JW, Chen YF, Yu L, Yin CB. Spatial–Temporal characteristics and affecting factors of swine breeding industry in China. *Economic Geography*. (2019) 39:180–9. doi: 10.15957/j.cnki.jjdl.2019.02.022

32. Zhong S, Li J, Chen X, Wen H. Study on regional comparative advantages and influencing factors of pig industry in Southwest China. *Heilongjiang Animal Sci Vet Med*. (2022) 3:180. doi: 10.13881/j.cnki.hljxmsy.2022.04.0180

33. Hu Y, Wang D. A study on evolvement and influencing factors of pig production layout in China: analysis based on provincial panel data. *J Zhejiang Sci–Tech University*. (2017) 38:195–202.

34. Pan G, Long F. Analysis on fluctuation cycle of hog production in Hunan. *Technol Econ*. (2011) 30:76–80.

35. Huang Y, Wang J. Changes of the relationship between live pig production and grain production in China. *Xinjiang Agricult Sci*. (2007) S2:212–216.

frontiers | Frontiers in Public Health

TYPE Original Research
PUBLISHED 07 March 2023
DOI 10.3389/fpubh.2023.1123594



OPEN ACCESS

EDITED BY
Juliana Jalaludin,
Universiti Putra Malaysia, Malaysia

REVIEWED BY
Tao Liu,
Jinan University, China
Agnieszka Pac,
Jagiellonian University Medical College, Poland

*CORRESPONDENCE
Xiaojun Zhou
✉ xiaojuncqfy@163.com
Jin Cheng
✉ chengjin_126@126.com

†These authors have contributed equally to this work

SPECIALTY SECTION
This article was submitted to Environmental health and Exposome, a section of the journal Frontiers in Public Health

RECEIVED 14 December 2022
ACCEPTED 15 February 2023
PUBLISHED 07 March 2023

CITATION
Zhou W, Ming X, Yang Y, Hu Y, He Z, Chen H, Li Y, Cheng J and Zhou X (2023) Associations between maternal exposure to ambient air pollution and very low birth weight: A birth cohort study in Chongqing, China. *Front. Public Health* 11:1123594. doi: 10.3389/fpubh.2023.1123594



# Associations between maternal exposure to ambient air pollution and very low birth weight: A birth cohort study in Chongqing, China

Wenzheng Zhou[1,2†], Xin Ming[1,2†], Yunping Yang[1,2], Yaqiong Hu[1,2], Ziyi He[1,2], Hongyan Chen[1,2], Yannan Li[1,2], Jin Cheng[3*] and Xiaojun Zhou[1,2*]

[1]Department of Quality Management Section, Women and Children's Hospital of Chongqing Medical University, Chongqing, China, [2]Department of Quality Management Section, Chongqing Health Center for Women and Children, Chongqing, China, [3]Institute of Toxicology, College of Preventive Medicine, Army Medical University (Third Military Medical University), Chongqing, China

**Introduction:** There have been many researches done on the association between maternal exposure to ambient air pollution and adverse pregnancy outcomes, but few studies related to very low birth weight (VLBW). This study thus explores the association between maternal exposure to ambient air pollutants and the risk of VLBW, and estimates the sensitive exposure time window.

**Methods:** A retrospective cohort study analyzed in Chongqing, China, during 2015–2020. The Generalized Additive Model were applied to estimate exposures for each participant during each trimester and the entire pregnancy period.

**Results:** For each 10 $\mu g/m^3$ increase in $PM_{2.5}$ during pregnancy, the relative risk of VLBW increased on the first trimester, with RR = 1.100 (95% CI: 1.012, 1.195) in the single-pollutant model. Similarly, for each 10 $\mu g/m^3$ increase in $PM_{10}$, there was a 12.9% (RR = 1.129, 95% CI: 1.055, 1.209) increase for VLBW on the first trimester in the single-pollutant model, and an 11.5% (RR = 1.115, 95% CI: 1.024, 1.213) increase in the multi-pollutant model, respectively. The first and second trimester exposures of $NO_2$ were found to have statistically significant RR values for VLBW. The RR values on the first trimester were 1.131 (95% CI: 1.037, 1.233) and 1.112 (95% CI: 1.015, 1.218) in the single-pollutant model and multi-pollutant model, respectively; The RR values on the second trimester were 1.129 (95% CI: 1.027, 1.241) and 1.146 (95% CI: 1.038, 1.265) in the single-pollutant model and multi-pollutant model, respectively. The RR of O3 exposure for VLBW on the entire trimester was 1.076 (95% CI: 1.010–1.146), and on the second trimester was 1.078 (95% CI: 1:016, 1.144) in the single-pollutant model.

**Conclusion:** This study indicates that maternal exposure to high levels of $PM_{2.5}$, $PM_{10}$, $NO_2$, and $O_3$ during pregnancy may increase the risk of very low birth weight, especially for exposure on the first and second trimester. Reducing the risk of early maternal exposure to ambient air pollution is thus necessary for pregnant women.

KEYWORDS

**very low birth weight, air pollution, risk assessment, environmental exposure, China**

# 1. Introduction

Nowadays, considerable literatures on epidemiology and clinical medicine has reported the association and adverse effects of ambient air pollution on adverse pregnancy outcomes (1, 2). Low birth weight (LBW), defined as weight at birth <2,500 g, is a major neonatal adverse outcome that is strongly related to infant mortality and even producing adverse effects on children's health in adulthood (3). Very low birth weight (VLBW) is defined as weight at birth <1,500 g (4). Many researchers have explored the association between maternal exposure to ambient air pollution and low birth weight or preterm birth (5–8). Among these significant results, it has been suggested ambient air pollution may increase the risk of low birth weight. However, few studies have yet specifically focused on the association between ambient air pollution and very low birth weight. Probably because of the low incidence of VLBW, these studies can be limited by sample size (9). However, further specific research is still essential to explore the ongoing risk of air pollutants on very low birth weight.

Many scholars in China have studied and published the relationship between exposure to air pollutants and birth outcomes (10–12); however, the association between exposure to ambient air pollutants and very low birth weight has been rarely reported. Chongqing is the largest municipality in China and is located along the Yangtze River. It is a huge industrial city with 40 districts and a permanent population of 31 million. From 2014 to the present, the air quality of Chongqing has greatly improved through years of efforts by local governments. These special air quality change trends in Chongqing offer a unique research environment for studying the effects of air pollution exposure on birth outcomes that is quite different from the environments found in Europe, America, Africa, and other countries and regions.

Given that few studies have explored the potential relationship between ambient air pollution and VLBW, this study sought to estimate the association between maternal exposure to ambient air pollutants ($PM_{2.5}$, $PM_{10}$, $SO_2$, $O_3$, $NO_2$, and CO) and the risk of VLBW in Chongqing, China. In doing so, it focused on the sensitive exposure time window of air pollutants for VLBW with a large sample size and also *via* precise individual exposure assessment.

# 2. Materials and methods

## 2.1. The study population

Research data for this study was gathered from a large retrospective cohort of live births from 2015 to 2020, in Chongqing, China, which was consistent with our previously published paper (13), all birth data were extracted from the birth certificate system database for Chongqing. This database contains maternal age, maternal residence address, date of birth, birth weight, gestational age, etc. We only used part of this information for our scientific research.

To facilitate a comparison of this study to previous studies, the subset of births used for this analysis was limited to singleton live births among women with 20–42 completed gestation weeks. We used the date of birth and gestational age to establish the start and end dates of gestational exposure and estimate the exposure time during the entire pregnancy and each trimester. Trimesters were defined as the 1–13, 14–27, and 28 weeks until birth (14). Cases were excluded if they had missing data for birth outcome variables. We also excluded births for any of the following: Extremely low birth weight where the value was <500 g; and a multi-fetal gestation; the mother lived ≥10 km from the nearest monitor station; and exposure data were not available for all three trimesters.

This study was approved by the Institutional Ethical Committee Board of the Chongqing Health Center for Women and Children.

## 2.2. Assessment of air pollution exposure

All ambient air pollutant concentrations, including $PM_{2.5}$, $PM_{10}$, $SO_2$, CO, $NO_2$, and $O_3$, were obtained from the Chinese National Urban Air Quality Monitoring Platform (https://air.cnemc.cn:18007/) for 17 ground-based monitoring stations in nine main districts of Chongqing, China, from January 1, 2015, to December 31, 2020.

Air pollution exposure assessment was carried out using the same method as our published paper (13) mentioned above. Based on the detailed residence address of every researched pregnant woman and the location of air monitoring stations, we calculated the distance between each maternal residence and the monitoring sites using ArcGIS (version 10.2). The benefit from this process is that we were able to assign exposure values at an individual level, rather than compiling only our distinct-level measurements from the raw data (11). The proximity principle from the nearest air quality monitoring stations was applied with a cut-off distance of 10 km, which is consistent with the related research literatures (15, 16). The pregnancy exposure time started with the date of conception, according to the date of the gestational week and the last menstruation of the individual woman (17).

Daily average relative humidity and temperature were available from the China Greenhouse Data Sharing Platform (http://data.sheshiyuanyi.com). Input of any missing data was done using multiple linear interpolation based on other monitoring values.

## 2.3. Statistical analysis

To evaluate the association between ambient air pollutant exposure and the risk of VLBW in each exposure period, we performed a Generalized Additive Model (GAM), also consistent with our previously published paper (13). The effects were examined for both single-pollutant and multiple-pollutant models. The single-pollutant model was adjusted for mean temperature and humidity, the age of the mother and father, week of gestational age; further, the multi-pollutant model was adjusted for covariates that included mean temperature and humidity, age of the mother and father, week of gestational age, and additionally adjusted for other air pollutant exposure. The basic model can be described as follows:

$$Log\left[E\left(Y_t\right)\right] = \alpha + \beta Z_t + S\left(time, df\right) + S\left(temperature, df\right) + S\left(relativehumidity, df\right) + as.factor(Dow)$$

10.3389/fpubh.2023.1123594

TABLE 1 Descriptive summary of the general characteristics of live birth data.

| Variables | LBW ($n$ = 24,497, 4.28%) | VLBW ($n$ = 1,725, 0.3%) | Non-VLBW ($n$ = 570,381, 99.7%) | Total ($n$ = 572,106) | $p$-value |
|---|---|---|---|---|---|
| **Gestational age** | 35.15 ± 2.61 | 30.02 ± 2.55 | 38.75 ± 1.41 | 38.73 ± 1.49 | <0.001 |
| Preterm birth | | | | | |
| Yes | 16,421 (67.01%) | 1,706 (98.90%) | 31,961 (5.60%) | 33,667 (5.88%) | <0.001 |
| No | 8,086 (32.99%) | 19 (1.10%) | 538,420 (94.40%) | 538,439 (94.12%) | |
| **Maternal age** | 29.58 ± 5.15 | 30.18 ± 5.16 | 28.84 ± 4.95 | 28.84 ± 4.95 | <0.001 |
| <20 years | 416 (1.7%) | 22 (1.28%) | 8,184 (1.43%) | 8,206 (1.42%) | <0.001 |
| 20–24 years | 3,589 (14.65%) | 203 (11.77%) | 97,075 (17.02%) | 97,278 (17.11%) | |
| 25–29 years | 8,536 (34.85%) | 578 (33.51%) | 229,341 (40.21%) | 229,919 (40.43%) | |
| 30–34 years | 7,837 (31.99%) | 575 (33.33%) | 163,020 (28.58%) | 163,595 (28.44%) | |
| ≥35 years | 4,092 (16.7%) | 346 (20.06%) | 72,265 (12.67%) | 72,611 (12.51%) | |
| Missing | 27(0.11%) | 1 (0.05%) | 496 (0.08%) | 497 (0.08%) | |
| **Father age** | 31.90 ± 5.96 | 32.76 ± 5.98 | 31.13 ± 5.62 | 31.14 ± 5.62 | <0.001 |
| <20 years | 76 (0.31%) | 4 (0.23%) | 1,736 (0.30%) | 1,740 (0.30%) | <0.001 |
| 20–24 years | 1,842 (7.52%) | 77 (4.46%) | 48,907 (8.57%) | 48,984 (8.56%) | |
| 25–29 years | 7,021 (28.66%) | 423 (24.52%) | 191,604 (33.59%) | 192,027 (33.57%) | |
| 30–34 years | 8,101 (33.07%) | 563 (32.64%) | 183,848 (32.23%) | 184,411 (32.23%) | |
| ≥35 years | 6,702 (27.36%) | 525 (30.43%) | 132,639 (23.25%) | 133,164 (23.28%) | |
| Missing | 755 (3.08%) | 133 (7.71%) | 11,647 (2.04%) | 11,780 (2.05%) | |
| Conception season | | | | | |
| Spring | 5,850 (23.88%) | 416 (24.12%) | 134,931 (23.66%) | 135,347 (23.66%) | <0.001 |
| Summer | 6,062 (24.75%) | 411 (23.83%) | 135,916 (23.83%) | 136,327 (23.83%) | |
| Autumn | 6,324 (25.82%) | 448 (25.97%) | 154,892 (27.16%) | 155,340 (27.15%) | |
| Winter | 6,261 (25.56%) | 450 (26.09%) | 144,642 (25.36%) | 145,092 (25.36%) | |

The $p$-value stands for the comparison of VLBW and non-VLBW.

where $Log[]$ is a link function; t is the observation day; $\alpha$ is the model intercept; $\beta$ is the factor for each pollutant; $Y_t$ is the concentration of pollutants in day t; $S()$ is the natural spline function; and Dow is dummy variable for day of week; $S(time, df)$ is the conception time.

We estimated attributable risk percent (ARP) to explore the increased risk of VLBW caused by exposure to air pollutants. ARP indicates that the air concentration in Chongqing is higher than the national standard concentration. The standard leads to an increased proportion of VLBW occurring, which is Proportion of increased risk attributed to higher concentrations of air pollutants. In order to facilitate calculation and calculation of confidence interval, Levin's formula is applied, and the formula is as follows:

$$ARP = \frac{P_e \times (RR - 1)}{P_e \times (RR - 1) + 1} \times 100\%$$

In the formula, $P_e$ is the incidence of very low birth weight in Chongqing at present when the air pollutant exposure is higher than the national level I standard concentration. $RR$ means that the air concentration in Chongqing is higher than the national level I standard concentration due to this study.

Sensitivity analysis were undertaken by changing the degree of freedom (df) for the time (6–8 df/year) by minimizing the Akaike information criterion (18). Finally, we selected the df of time, temperature, and relative humidity in the spline function, which were 7, 3, and 3 in the model, respectively. The GAM models were employed using R software (Version 4.1.0) with the "splines" and "mgcv" packages.

# 3. Results

## 3.1. Descriptive statistics of the research objects

In this study, a total number of 572,106 mother-newborn pairs were finally analyzed. The descriptive summary of the general characteristics of live birth data is shown in Table 1. The ages of the mothers ranged from 18 to 37 years, with an average age of 28.84 ± 4.95. The mean gestational age was 38.73 ± 1.49 weeks. Among them, 24,497 (4.28%) were LBW and 1,725 (0.3%) were VLBW.

10.3389/fpubh.2023.1123594

TABLE 2 Descriptive summary of air pollutants and meteorological factors in the study area.

| Pollutants ($\mu g/m^3$) | Mean | SD | Min | Max | Percentiles | | |
|---|---|---|---|---|---|---|---|
| | | | | | 25th | 50th | 75th |
| $PM_{2.5}$ | 41.62 | 10.01 | 17.82 | 83.65 | 34.39 | 42.69 | 47.50 |
| $PM_{10}$ | 66.39 | 12.61 | 28.79 | 121.46 | 59.12 | 67.30 | 73.66 |
| $NO_2$ | 38.95 | 6.46 | 10.78 | 68.19 | 35.50 | 38.35 | 41.15 |
| CO ($mg/m^3$) | 1.02 | 0.18 | 0.54 | 1.52 | 0.89 | 1.01 | 1.14 |
| $SO_2$ | 9.73 | 3.14 | 3.21 | 22.11 | 7.32 | 9.12 | 11.27 |
| $O_3$ | 38.45 | 13.34 | 8.27 | 105.65 | 30.24 | 39.07 | 47.38 |
| Temperature (°C) | 20.25 | 2.73 | 13.13 | 29.09 | 18.43 | 20.42 | 21.86 |
| Relative humidity (%) | 75.25 | 2.17 | 66.89 | 80.37 | 73.85 | 75.21 | 76.81 |

Period for January 1, 2015, to December 31, 2020.

## 3.2. Air pollutants descriptive statistics

The characteristics of air pollution and their meteorological factors are summarized in Table 2. The mean concentration of $PM_{2.5}$ during a whole pregnancy was 41.62 $\mu g/m^3$, and the mean concentration of $PM_{10}$ at the same time was 66.39 $\mu g/m^3$. The mean concentrations were 38.95 $\mu g/m^3$ for $NO_2$, 1.02 $mg/m^3$ for CO, 9.73 $\mu g/m^3$ for $SO_2$, 38.45 $\mu g/m^3$ for $O_3$, 20.25°C for the apparent mean temperature, and 75.25% for relative humidity during the entire study period.

The correlation between most pollutant correlations were positive except $O_3$. In addition, except for O3 and temperature, CO and humidity, the correlation between other air pollutants and meteorological factors was mostly negative. A positive correlation between $PM_{2.5}$ and $PM_{10}$ ($r$ = 0.910), and a negative correlation between $PM_{2.5}$ and average daily temperature ($r$ =-0.244) were observed. The correlation analysis results between air pollutants and meteorological factors are shown in Figure 1.

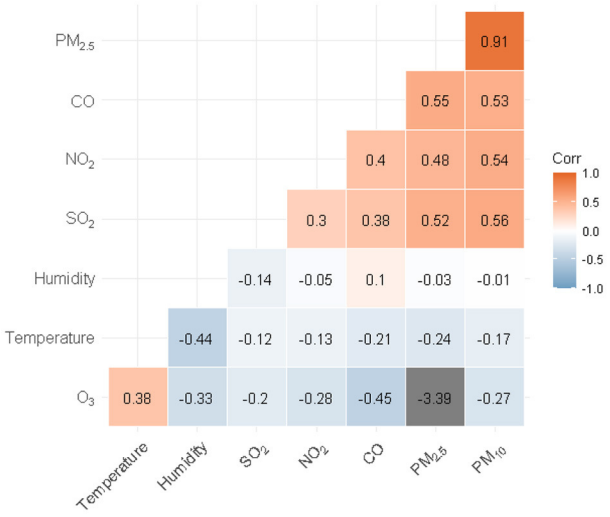


FIGURE 1
Correlation analysis results for air pollutants and meteorological factors.

## 3.3. Associations between air pollutants and VLBW

The associations found between Air pollutants and VLBW were calculated using the GAM models. The adjusted relative risks (RRs) and corresponding 95% confidence intervals (CIs) for VLBW to maternal exposure to air pollutants by pregnancy trimester are given in Table 3.

We observed that for each 10 $\mu g/m^3$ increase in $PM_{2.5}$ during pregnancy, the relative risk of VLBW increased on the first trimester, with RR=1.100 (95% CI: 1.012, 1.195) in the single-pollutant model. Similarly, for each 10 $\mu g/m^3$ increase in $PM_{10}$, there was a 12.9% (RR = 1.129, 95% CI: 1.055, 1.209) increased risk for VLBW on the first trimester in the single-pollutant model, and an 11.5% (RR = 1.115, 95% CI: 1.024, 1.213) increase in the multi-pollutant model, respectively.

The first and second trimester exposures of $NO_2$ were found to have statistically significant RR values for VLBW. The RR values on the first trimester were 1.131 (95% CI: 1.037, 1.233) and 1.112 (95% CI: 1.015, 1.218) in the single-pollutant model and the multi-pollutant model, respectively; The RR values on the second trimester were 1.129 (95% CI: 1.027, 1.241) and 1.146 (95% CI: 1.038, 1.265) in the single-pollutant model and the multi-pollutant model, respectively.

The RR of $O_3$ exposure for VLBW on the entire trimester was 1.076 (95% CI: 1.010, 1.146), and on the second trimester was 1.078 (95% CI: 1:016, 1.144) in the single-pollutant model. As shown in Table 3, No statistically significant RR was found for $SO_2$ and CO in each trimester of pregnancy.

Overall, the association with statistical significance between maternal exposure to air pollutants and VLBW was concentrated in PM2.5, PM10, and $NO_2$. Exposure at different stages of pregnancy had different results, particularly the risk of early pregnancy exposure was relatively higher. Forest plots of the RR values and 95% CIs for VLBW associated with maternal exposure to six pollutants during the different stages of pregnancy are shown in Figure 2.

TABLE 3 Adjusted relative risks (RRs) and corresponding 95% confidence intervals (CIs) from GAM models for VLBW maternal exposure to air pollutants by trimester of pregnancy.

| Pollutant | Model | Trimester 1 | | Trimester 2 | | Trimester 3 | | Entire pregnancy | |
|---|---|---|---|---|---|---|---|---|---|
| | | *RR* | *95% CI* | *RR* | *95% CI* | *RR* | *95% CI* | *RR* | *95% CI* |
| $PM_{2.5}$ | Model 1 | **1.100** | **(1.012, 1.195)** | 0.968 | (0.883, 1.062) | 1.017 | (0.965, 1.072) | 1.018 | (0.908, 1.141) |
| | Model 2 | 1.070 | (0.972, 1.176) | 0.934 | (0.836, 1.045) | 1.041 | (0.978, 1.108) | 1.034 | (0.891, 1.200) |
| $PM_{10}$ | Model 1 | **1.129** | **(1.055, 1.209)** | 1.048 | (0.978, 1.124) | 1.007 | (0.970, 1.045) | 1.050 | (0.962, 1.145) |
| | Model 2 | **1.115** | **(1.024, 1.213)** | 1.041 | (0.955, 1.135) | 1.028 | (0.980, 1.078) | 1.100 | (0.975, 1.242) |
| $SO_2$ | Model 1 | 1.198 | (0.921, 1.562) | 1.234 | (0.946, 1.610) | 0.961 | (0.760, 1.216) | 1.199 | (0.878, 1.641) |
| | Model 2 | 1.062 | (0.785, 1.438) | 1.257 | (0.928, 1.701) | 0.945 | (0.731, 1.222) | 1.080 | (0.739, 1.577) |
| $NO_2$ | Model 1 | **1.131** | **(1.037, 1.233)** | **1.129** | **(1.027, 1.241)** | 0.962 | (0.897, 1.032) | 1.069 | (0.967, 1.182) |
| | Model 2 | **1.112** | **(1.015, 1.218)** | **1.146** | **(1.038, 1.265)** | 0.944 | (0.872, 1.022) | 1.071 | (0.964, 1.190) |
| $O_3$ | Model 1 | 1.013 | (0.952, 1.077) | **1.078** | **(1.016, 1.144)** | 0.995 | (0.952, 1.037) | **1.076** | **(1.010, 1.146)** |
| | Model 2 | 1.036 | (0.967, 1.110) | 1.069 | (0.996, 1.146) | 0.996 | (0.952, 1.041) | 1.083 | (0.998, 1.175) |
| CO | Model 1 | 0.993 | (0.958, 1.030) | 0.974 | (0.939, 1.010) | 0.999 | (0.971, 1.028) | 0.960 | (0.923, 0.998) |
| | Model 2 | 1.002 | (0.962, 1.044) | 0.999 | (0.960, 1.041) | 0.998 | (0.967, 1.029) | 0.987 | (0.940, 1.036) |

The bold face indicates statistical significance established at $p < 0.05$ in the above three models. Model 1: single-pollutant model, adjusted for covariates including mean temperature and humidity, age of mother and father, and age of gestation; Model 2: multi-pollutant model, adjusted for covariates including mean temperature and humidity, age of mother and father, weight of birth, and additionally adjusted for other air pollutants.

### 3.4. Attribution analysis of maternal exposure to air pollutants and VLBW

In this study, we calculated the attributable risk percentage (ARP) of $PM_{2.5}$ for VLBW throughout the entire pregnancy according to the Chinese Class I Standard of $PM_{2.5} < 35$ μg/m$^3$. We adjusted for the covariates including mean temperature and mean humidity, parental age, and gestational age. We estimated the ARP of $PM_{2.5}$ for VLBW that was attributable to $PM_{2.5}$ exposure concentration to be higher than the Chinese Class I Standard after adjusting for covariates. The ARP was 17.89% (95% CI: 10.5%, 24.26%). Similarly, the attributable risk percentage (ARP) of $PM_{10}$ for VLBW was calculated using the Chinese Class I Standard of $PM_{10} < 50$ μg/m$^3$. Lastly, the ARP of $PM_{10}$ for VLBW was 36.81% (95% CI: 25.69%, 46.01%).

## 4. Discussion

In this study, we used a generalized additive model (GAM) to analyze the exposure-response association of air pollutants on the risk of very low birth weight. It revealed that maternal exposure to $PM_{2.5}$ and $PM_{10}$ in the first trimester of pregnancy was associated with increased risk of VLBW. In addition, a positive association with VLBW was linked to $NO_2$ exposure during the first and second trimesters of pregnancy. These results are a valuable supplement to the few previous association researches for maternal exposure to ambient air pollution and the risk of very low birth weight (19). Especially in China, such similarly related research is quite rare.

There are a lot of studies that have demonstrated that maternal exposure to fine ambient air pollution increases the risk of preterm birth and low birth weight (2, 20–22). Ghosh et al. (23) conducted a meta-regression and analysis related association of $PM_{2.5}$ pollution and adverse perinatal outcomes for 204 countries and territories. Its pooled estimates indicated 22 grams (95% UI: 12, 32) lower birth weight, and 11% greater risk of LBW (1.11, 95% UI: 1.07, 1.16) per 10 μg/m$^3$ increment in ambient $PM_{2.5}$. Globally, an estimated 15.6% (95% UI: 15.6, 15.7) of all LBW infants were attributable to total $PM_{2.5}$ in 2019. A meta-analysis by Bekkar et al. (2) reported that positive associations between exposure to air pollution and LBW were found across all US geographic regions. Exposure to $PM_{2.5}$ or ozone was associated with an increased risk of LBW in 25 of 29 studies (86%). Niu et al. (24) carried out a cohort study in Los Angeles, California, and found early pregnancy to mid-pregnancy exposures to $PM_{2.5}$, $PM_{10}$, and $NO_2$ were associated with lower birth weight. Their result is highly consistent with our research. Still, some studies have suggested that the sensitive exposure period for $NO_2$ is throughout all of a pregnancy (12, 25). Although the stages of a sensitive window to air pollution exposure varied in the different literatures, the basic consensus is that maternal exposure to air pollution, particularly during the critical windows of pregnancy, significantly do increases the risk of LBW.

Over the past decade, numerous studies have been published on air pollutant exposure and low birth weight in China (12, 26, 27). The study by Yuan et al. (28) reported critical windows of gestational exposure to $PM_{2.5}$ were identified as 31st−34th gestational weeks for reduced birth weight, and 38th−42nd weeks for LBW, respectively. Liang et al. (29) conducted a study on 1,455,026 singleton births during 2014–2017 in nine cities of Guangdong, China, and found $PM_{2.5}$ was significantly associated with LBW in every trimester of pregnancy stage, with stronger effects on the first and third trimester for each 10 μg/m$^3$ increase in $PM_{2.5}$ concentrations. The results of a cohort study performed in Changsha, China, further showed term LBW was significantly associated with exposure to ambient PM during pregnancy, with OR = 1.47 (95% CI: 1.00, 2.14) for per IQR increase after

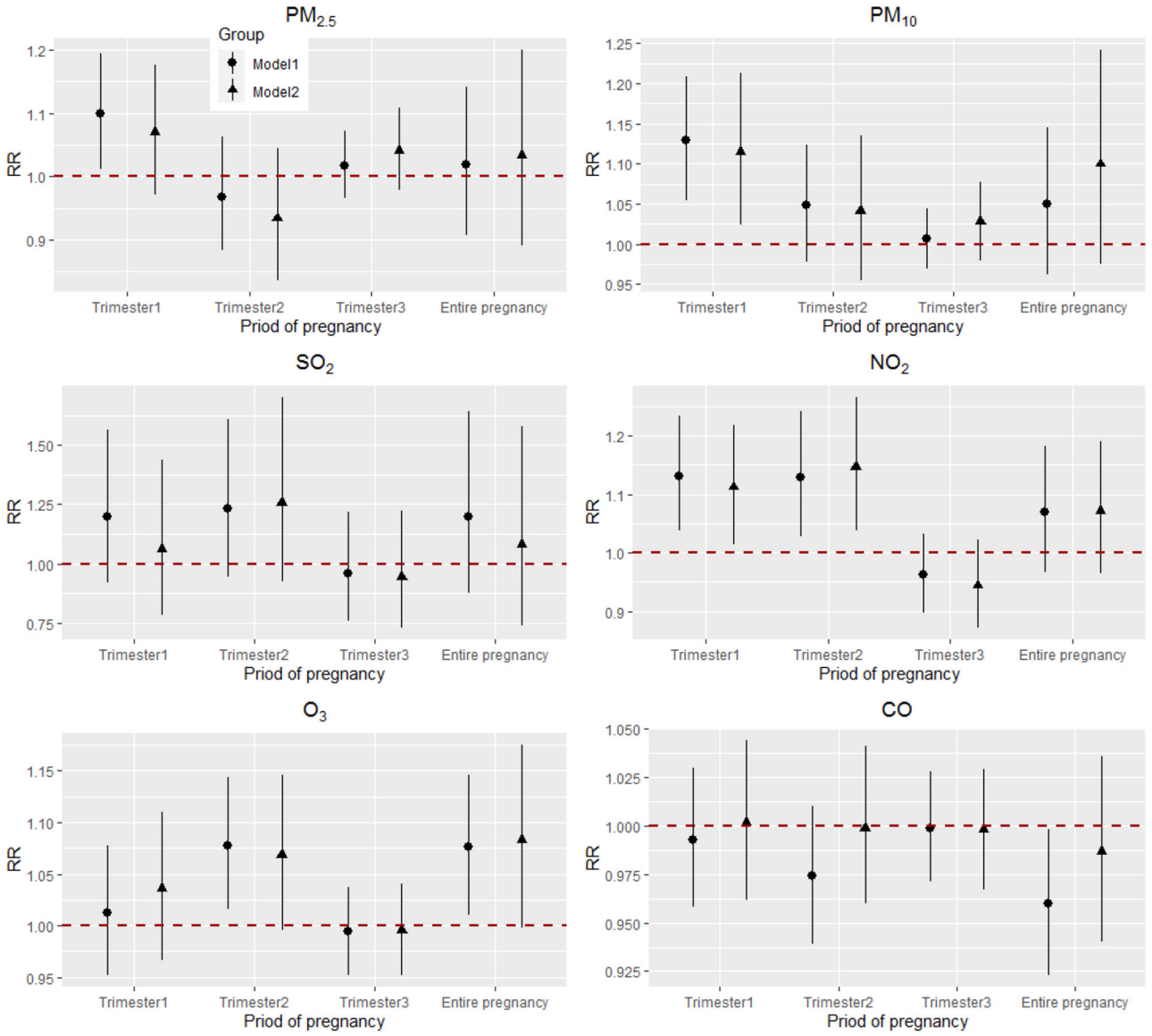


FIGURE 2
Adjusted RRs (95% CIs) for VLBW associated with air pollutants during the different stages of pregnancy in Model 1 and Model 2. Model 1: single-pollutant model, adjusted for covariates including mean temperature and humidity, age of mother and father, and age of gestation, as represented by a circle; Model 2: multi-pollutant model, adjusted for covariates including mean temperature and humidity, age of mother and father, weight of birth, and additionally adjusted for other air pollutants, as represented by a triangle.

adjustment for the covariates and home environmental factors (3). Specifically, the authors identified a significant association in the early phase of pregnancy including conception month and the first trimester. Zou et al. (26) performed a retrospective observational study on 2,527 preschoolers in Shanghai, China, and indicated that exposure to $NO_2$ was a risk factor for LBW and T-LBW. The difference when compared to this study is that effects of exposures could be greater during early periods than during later periods of gestation.

Related studies have suggested different sensitive windows worldwide. The differences may be due to study design, air pollution level, regional disparity, components of PM, and sample size, etc. However, most of the sensitive time windows are concentrated in the first trimester. For example, in a study of seven states in the U.S. (30) for associations between maternal exposure to $PM_{2.5}$ and the risk of LBW, showed a statistically significant correlation during the entire stage of pregnancy and all specific trimesters in New York, for the full gestation, the first and third trimesters in Minnesota, and for the entire pregnancy and first trimester in New Jersey.

The current study focused on associations between maternal exposure to ambient air pollution and VLBW, which was unique to our study. We observed that the first trimester may be the sensitive window for $PM_{2.5}$ and $PM_{10}$, consistent with a few previous studies on LBW (29, 31). Meanwhile, the first and second trimesters constituted the susceptible exposure window for $NO_2$. On the other hand, a few studies have shown different staging methods with consequently different results. For example, several

researchers divided pregnancy into months or weeks to evaluate the relationship between exposure and outcomes. Our large sample size and the exposure evaluation mode of individual assessment allowed us to reliably estimate the associations. However, the effect of exposure sensitive time does need to be further explored, and personal exposure measurements need to be more widely utilized.

Few studies have evaluated the disease burdens of PM exposure on LBW worldwide. We found 17.89% (95% CI: 10.5%, 24.26%) of VLBW was attributable to a higher $PM_{2.5}$ exposure ($PM_{2.5} \geq 35\ \mu g/m^3$) relative to the Chinese Class I Standard after adjusting for covariates. The ARP of $PM_{10}$ for VLBW was 36.81% (95% CI: 25.69%, 46.01%), calculated for $PM_{10}$ exposure concentration higher than 50 $\mu g/m^3$. These results were statistically sufficient to demonstrate the harmful effects of high PM exposure on very low birth weight. Liu et al. (4) estimated the LBW burden caused by outdoor $PM_{2.5}$ exposure in Shanghai, China, in 2013, according to Shanghai's Class I Standard (15 $\mu g/m^3$). Those results showed that 23.36% (95%CI: 3.86%, 40.02%) of LBW could be attributed to $PM_{2.5}$ exposure. Our results provided a particular estimate of attribution analysis of PM exposure on VLBW in China.

There are several possible biologic mechanisms through which ambient air pollution can cause LBW (32, 33). Yet, no studies have specifically focused on the mechanisms that cause very low birth weight. Current research reports mainly include systemic oxidative stress and inflammatory response that induces premature birth; maternal endocrine disorder; the release of inflammatory factors and entering into the placenta; direct toxicity to the placenta or fetus, etc. (7, 34, 35). Studies on the effects of different components of $PM_{2.5}$ on birth outcomes have shown that the component elements of carbon, calcium, copper, nickel, titanium, zinc, aluminum, and antimony are associated with low birth weight (36). The toxicological effects of metal components are inferred as well, mainly by increasing oxidative stress (37). The biological mechanisms related to VLBW, however, need to be further investigated and explored in the future.

This study did have some limitations. First, due to the large sample size, it was difficult to obtain comprehensive and complete information. Some potential risk factors were not considered in this study, such as maternal nutritional status, pregnancy complications, and life behaviors, genetic information, etc. These factors may have confounded the association results. However, previous similar studies have found little change in efficacy estimates based on whether or not these factors are adjusted (33). Second, as with most related studies, exposure measurement errors were inevitable. The type of area, proximity of green/blue area and the "quality" of neighborhood can also be important in assessment of exposure level. However, due to the absence of these variables in the original data, we did not conduct further analysis about this. The proximity principle from nearby air quality monitoring stations was applied to serve as the estimates of individual air pollution exposure. Moreover, we limited the exposure concentration assessment to within 10 km of the monitoring station. We did not assess the movement of pregnant women during pregnancy. Fortunately, the large sample size used for this study balanced that situation to some extent. Third, the composition of PM is complex, and that composition was not obtained and analyzed in this study. It is possible that different pollutant components can have inconsistent effects on VLBW. The risk effects caused by specific components will be explored in subsequent relevant studies.

## 5. Conclusions

In conclusion, this study provides special evidence on the associations between air pollutant exposure during pregnancy and VLBW using a retrospective birth cohort study. We estimated that maternal exposure to high levels of $PM_{2.5}$, $PM_{10}$, $NO_2$, and $O_3$ during pregnancy may increase the risk of very low birth weight. The sensitive period for that exposure window is likely to be the first and second trimesters. Reducing the risk of early maternal exposure to ambient air pollution is thus necessary for pregnant women.

## Data availability statement

The raw data supporting the conclusions of this article will be made available by the authors, without undue reservation.

## Author contributions

WZ, XM, JC, and XZ: conceptualization. XM and JC: methodology. YY: software. YY and YH: validation. ZH: formal analysis. XM and HC: investigation. WZ: resources, project administration, and funding acquisition. HC and YL: data curation. WZ and XM: writing—original draft preparation. JC and XZ: writing—review and editing. XM and ZH: visualization. JC: supervision. All authors have read and agreed to the published version of the manuscript.

## Funding

This work was supported by the Chongqing Science and Technology Bureau Project [grant number: cstc2018jscx-mszdX0021] and the Association Between Exposure to Ambient Air Pollution and Premature Birth and Low Birth Weight Outcomes in Chongqing Based on Birth Cohort [grant number: cstc2020jcyj-msxmX0511].

## Conflict of interest

The authors declare that the research was conducted in the absence of any commercial or financial relationships that could be construed as a potential conflict of interest.

## Publisher's note

# References


1. Brumberg HL, Karr CJ. Ambient air pollution: Health hazards to children. *Pediatrics.* (2021) 147:51484. doi: 10.1542/peds.2021-051484

2. Bekkar B, Pacheco S, Basu R, DeNicola N. Association of air pollution and heat exposure with preterm birth, low birth weight, and stillbirth in the US a systematic review. *J Am Med Assoc Netw Open.* (2020) 3:8243. doi: 10.1001/jamanetworkopen.2020.8243

3. Lu C, Zhang WS, Zheng XR, Sun JC, Chen L, Deng QH. Combined effects of ambient air pollution and home environmental factors on low birth weight. *Chemosphere.* (2020) 240:124836. doi: 10.1016/j.chemosphere.2019.124836

4. Liu AN, Qian NS, Yu HT, Chen RJ, Kan HD. Estimation of disease burdens on preterm births and low birth weights attributable to maternal fine particulate matter exposure in Shanghai, China. *Sci Total Environ.* (2017) 609:815–21. doi: 10.1016/j.scitotenv.2017.07.174

5. Chen J, Fang J, Zhang Y, Xu Z, Byun HM, Li PH, et al. Associations of adverse pregnancy outcomes with high ambient air pollution exposure: Results from the Project ELEFANT. *Sci Total Environ.* (2021) 761:143218. doi: 10.1016/j.scitotenv.2020.143218

6. Yang Y, Liang ZJ, Ruan ZL, Zhang SY, Zhao QG, Lin HL. Estimating the attributable burden of preterm birth and low birth weight due to maternal ozone exposure in nine Chinese cities. *Atmos Environ.* (2020) 222:117169. doi: 10.1016/j.atmosenv.2019.117169

7. Simoncic V, Enaux C, Deguen S, Kihal-Talantikite W. Adverse birth outcomes related to $NO_2$ and PM exposure: European systematic review and meta-analysis. *Int J Env Res Pub He.* (2020) 17:218116. doi: 10.3390/ijerph17218116

8. Rodríguez-Fernández A, Ramos-Castillo N, Ruiz-De la Fuente M, Parra-Flores J, Maury-Sintjago E. Association of prematurity and low birth weight with gestational exposure to PM(25) and PM(10) particulate matter in chileans newborns. *Int J Environ Res Public Health.* (2022) 19:106133. doi: 10.3390/ijerph19106133

9. Conforti A, Mascia M, Cioffi G, De Angelis C, Coppola G, De Rosa P, et al. Air pollution and female fertility: A systematic review of literature. *Reprod Biol Endocrinol.* (2018) 16:117. doi: 10.1186/s12958-018-0433-z

10. Fang J, Kang CM, Osorio-Yanez C, Barrow TM, Zhang R, Zhang Y, et al. Prenatal PM25 exposure and the risk of adverse births outcomes: Results from Project ELEFANT. *Environ Res.* (2020) 191:110232. doi: 10.1016/j.envres.2020.110232

11. Guo P, Miao HZ, Chen YL, Fu Y, Wu YT, Zhao QG, et al. Maternal exposure to gaseous ambient air pollutants increases the risk of preterm birth in the Pearl River Delta, China 2014-2017. *Sci Total Environ.* (2019) 671:959–70. doi: 10.1016/j.scitotenv.2019.03.375

12. Huang HJ, Yu QY, Zheng T, Wang SS, Yang XJ. Associations between seasonal ambient air pollution and adverse perinatal outcomes: A retrospective cohort study in Wenzhou, China. *Environ Sci Pollut Res Int.* (2022) 29:59903–14. doi: 10.1007/s11356-022-20084-6

13. Zhou W, Ming X, Yang Y, Hu Y, He Z, Chen H, et al. Association between maternal exposure to ambient air pollution and the risk of preterm birth: A birth cohort study in Chongqing, China, 2015-2020. *Int J Environ Res Public Health.* (2022) 19:42211. doi: 10.3390/ijerph19042211

14. Xiao QY, Chen HY, Strickland MJ, Kan HD, Chang HH, Klein M, et al. Associations between birth outcomes and maternal PM25 exposure in Shanghai: A comparison of three exposure assessment approaches. *Environ Int.* (2018) 117:226–36. doi: 10.1016/j.envint.2018.04.050

15. Guo P, Chen YL, Wu HS, Zeng J, Zeng ZS, Li WP, et al. Ambient air pollution and markers of fetal growth: A retrospective population-based cohort study of 2.57 million term singleton births in China. *Environ Int.* (2020) 135:105410. doi: 10.1016/j.envint.2019.105410

16. Wang L, Liu C, Meng X, Niu Y, Lin Z, Liu Y, et al. Associations between short-term exposure to ambient sulfur dioxide and increased cause-specific mortality in 272 Chinese cities. *Environ Int.* (2018) 117:33–9. doi: 10.1016/j.envint.2018.04.019

17. Leiser CL, Hanson HA, Sawyer K, Steenblik J, Al-Dulaimi R, Madsen T, et al. Acute effects of air pollutants on spontaneous pregnancy loss: A case-crossover study. *Fertil Steril.* (2019) 111:341–7. doi: 10.1016/j.fertnstert.2018.10.028

18. Li C, Xu JJ, He YC, Chen L, Dennis CL, Huang HF, et al. Effects of acute ambient pollution exposure on preterm prelabor rupture of membranes: A time-series analysis in Shanghai, China. *Environ Pollut.* (2021) 276:116756. doi: 10.1016/j.envpol.2021.116756

19. Uwak I, Olson N, Fuentes A, Moriarty M, Pulczinski J, Lam J, et al. Application of the navigation guide systematic review methodology to evaluate prenatal exposure to particulate matter air pollution and infant birth weight. *Environ Int.* (2021) 148:106378. doi: 10.1016/j.envint.2021.106378

20. Liu Y, Xu JH, Chen D, Sun P, Ma X. The association between air pollution and preterm birth and low birth weight in Guangdong, China. *BMC Public Health.* (2019) 19:7. doi: 10.1186/s12889-018-6307-7

21. Fleischer NL, Merialdi M, van Donkelaar A, Vadillo-Ortega F, Martin RV, Betran AP, et al. Outdoor air pollution, preterm birth, and low birth weight: Analysis of the world health organization global survey on maternal and perinatal health. *Environ Health Perspect.* (2014) 122:425–30. doi: 10.1289/ehp.1306837

22. Wu H, Jiang BF, Geng XY, Zhu P, Liu Z, Cui LL, et al. Exposure to fine particulate matter during pregnancy and risk of term low birth weight in Jinan, China, 2014-2016. *Int J Hyg Envir Heal.* (2018) 221:183–90. doi: 10.1016/j.ijheh.2017.10.013

23. Ghosh R, Causey K, Burkart K, Wozniak S, Cohen A, Brauer M. Ambient and household PM25 pollution and adverse perinatal outcomes: A meta-regression and analysis of attributable global burden for 204 countries and territories. *PLoS Med.* (2021) 18:e1003718. doi: 10.1371/journal.pmed.1003718

24. Niu Z, Habre R, Chavez TA, Yang T, Grubbs BH, Eckel SP, et al. Association between ambient air pollution and birth weight by maternal individual- and neighborhood-level stressors. *J Am Med Assoc Netw Open.* (2022) 5:e2238174. doi: 10.1001/jamanetworkopen.2022.38174

25. Dong S, Abu-Awad Y, Kosheleva A, Fong KC, Koutrakis P, Schwartz JD. Maternal exposure to black carbon and nitrogen dioxide during pregnancy and birth weight: Using machine-learning methods to achieve balance in inverse-probability weights. *Environ Res.* (2022) 211:112978. doi: 10.1016/j.envres.2022.112978

26. Zou Z, Liu W, Huang C, Cai J, Fu Q, Sun C, et al. Gestational exposures to outdoor air pollutants in relation to low birth weight: A retrospective observational study. *Environ Res.* (2021) 193:110354. doi: 10.1016/j.envres.2020.110354

27. Hao J, Peng L, Cheng P, Li S, Zhang C, Fu W, et al. time series analysis of ambient air pollution and low birth weight in Xuzhou, China. *Int J Environ Health Res.* (2022) 32:1238–47. doi: 10.1080/09603123.2020.1867828

28. Yuan L, Zhang Y, Wang W, Chen R, Liu Y, Liu C, et al. Critical windows for maternal fine particulate matter exposure and adverse birth outcomes: The Shanghai birth cohort study. *Chemosphere.* (2020) 240:124904. doi: 10.1016/j.chemosphere.2019.124904

29. Liang Z, Yang Y, Qian Z, Ruan Z, Chang J, Vaughn MG, et al. Ambient PM25 and birth outcomes: Estimating the association and attributable risk using a birth cohort study in nine Chinese cities. *Environ Int.* (2019) 126:329–35. doi: 10.1016/j.envint.2019.02.017

30. Hao YP, Strosnider H, Balluz L, Qualters JR. Geographic variation in the association between ambient fine particulate matter (PM25) and term low birth weight in the United States. *Environ Health Persp.* (2016) 124:250–5. doi: 10.1289/ehp.1408798

31. Lavigne E, Burnett RT, Stieb DM, Evans GJ, Godri Pollitt KJ, Chen H, et al. Fine particulate air pollution and adverse birth outcomes: Effect modification by regional nonvolatile oxidative potential. *Environ Health Perspect.* (2018) 126:77012. doi: 10.1289/EHP2535

32. Wang Q, Miao H, Warren JL, Ren M, Benmarhnia T, Knibbs LD, et al. Association of maternal ozone exposure with term low birth weight and susceptible window identification. *Environ Int.* (2021) 146:106208. doi: 10.1016/j.envint.2020.106208

33. Gong C, Wang J, Bai Z, Rich DQ, Zhang Y. Maternal exposure to ambient PM(25) and term birth weight: A systematic review and meta-analysis of effect estimates. *Sci Total Environ.* (2022) 807:150744. doi: 10.1016/j.scitotenv.2021.150744

34. Zhang J, Chen G, Liang S, Liu J, Zhang J, Shen H, et al. PM(25) exposure exaggerates the risk of adverse birth outcomes in pregnant women with pre-existing hyperlipidemia: Modulation role of adipokines and lipidome. *Sci Total Environ.* (2021) 787:147604. doi: 10.1016/j.scitotenv.2021.147604

35. Shao X, Cheng H, Zhou J, Zhang J, Zhu Y, Yang C, et al. Prenatal exposure to ambient air multi-pollutants significantly impairs intrauterine fetal development trajectory. *Ecotoxicol Environ Saf.* (2020) 201:110726. doi: 10.1016/j.ecoenv.2020.110726

36. Iodice S, Hoxha M, Ferrari L, Carbone IF, Anceschi C, Miragoli M, et al. Particulate air pollution, blood mitochondrial DNA copy number, and telomere length in mothers in the first trimester of pregnancy: Effects on fetal growth. *Oxid Med Cell Longev.* (2018) 2018:1–9. doi: 10.1155/2018/5162905

37. Zhao N, Wu W, Feng Y, Yang F, Han T, Guo M, et al. Polymorphisms in oxidative stress, metabolic detoxification, and immune function genes, maternal exposure to ambient air pollution, and risk of preterm birth in Taiyuan, China. *Environ Res.* (2021) 194:110659. doi: 10.1016/j.envres.2020.110659

frontiers | Frontiers in Public Health

TYPE Original Research
PUBLISHED 09 March 2023
DOI 10.3389/fpubh.2023.1134516



OPEN ACCESS

EDITED BY
Juliana Jalaludin,
Universiti Putra Malaysia, Malaysia

REVIEWED BY
Zhijing Lin,
Anhui Medical University, China
Arthit Phosri,
Mahidol University, Thailand

*CORRESPONDENCE
Weihong Chen
✉ wchen@mails.tjmu.edu.cn
Xiaokang Zhang
✉ zhangxiaokaju@163.com

†These authors have contributed equally to this work

SPECIALTY SECTION
This article was submitted to Environmental health and Exposome, a section of the journal Frontiers in Public Health

RECEIVED 30 December 2022
ACCEPTED 20 February 2023
PUBLISHED 09 March 2023

CITATION
You X, Cao X, Guo Y, Wang D, Qiu W, Zhou C, Zhou M, Chen W and Zhang X (2023) Associations between short-term $PM_{2.5}$ exposure and daily hospital admissions for circulatory system diseases in Ganzhou, China: A time series study.
*Front. Public Health* 11:1134516.
doi: 10.3389/fpubh.2023.1134516



# Associations between short-term $PM_{2.5}$ exposure and daily hospital admissions for circulatory system diseases in Ganzhou, China: A time series study

Xiaojie You[1,2], Xiuyu Cao[1,2], You Guo[3,4,5], Dongming Wang[1,2], Weihong Qiu[1,2], Chuanfei Zhou[3,4,5], Min Zhou[1,2], Weihong Chen[1,2*†] and Xiaokang Zhang[3,4,5*†]

[1]Department of Occupational and Environmental Health, School of Public Health, Tongji Medical College, Huazhong University of Science and Technology, Wuhan, Hubei, China, [2]Key Laboratory of Environment and Health, Ministry of Education and Ministry of Environmental Protection, and State Key Laboratory of Environmental Health (Incubating), School of Public Health, Tongji Medical College, Huazhong University of Science and Technology, Wuhan, Hubei, China, [3]First Affiliated Hospital, Gannan Medical University, Ganzhou, China, [4]Key Laboratory of Prevention and Treatment of Cardiovascular and Cerebrovascular Diseases, Ministry of Education, Gannan Medical University, Ganzhou, China, [5]School of Public Health and Health Management, Gannan Medical University, Ganzhou, China

**Objective:** Previous epidemiological studies have shown that both long-term and short-term exposure to fine particulate matters ($PM_{2.5}$) were associated with the morbidity and mortality of circulatory system diseases (CSD). However, the impact of $PM_{2.5}$ on CSD remains inconclusive. This study aimed to investigate the associations between $PM_{2.5}$ and circulatory system diseases in Ganzhou.

**Methods:** We conducted this time series study to explore the association between ambient $PM_{2.5}$ exposure and daily hospital admissions for CSD from 2016 to 2020 in Ganzhou by using generalized additive models (GAMs). Stratified analyses were also performed by gender, age, and season.

**Results:** Based on 201,799 hospitalized cases, significant and positive associations were found between short-term PM2.5 exposure and hospital admissions for CSD, including total CSD, hypertension, coronary heart disease (CHD), cerebrovascular disease (CEVD), heart failure (HF), and arrhythmia. Each 10 $\mu g/m^3$ increase in $PM_{2.5}$ concentrations was associated with a 2.588% (95% confidence interval [CI], 1.161%–4.035%), 2.773% (95% CI, 1.246%–4.324%), 2.865% (95% CI, 0.786%–4.893%), 1.691% (95% CI, 0.239%–3.165%), 4.173% (95% CI, 1.988%–6.404%) and 1.496% (95% CI, 0.030%–2.983%) increment in hospitalizations for total CSD, hypertension, CHD, CEVD, HF, and arrhythmia, respectively. As $PM_{2.5}$ concentrations rise, the hospitalizations for arrhythmia showed a slow upward trend, while other CSD increased sharply at high $PM_{2.5}$ levels. In subgroup analyses, the impacts of $PM_{2.5}$ on hospitalizations for CSD were not materially changed, although the females had higher risks of hypertension, HF, and arrhythmia. The relationships between $PM_{2.5}$ exposure and hospitalizations for CSD were more significant among individuals aged ≤65 years, except for arrhythmia. $PM_{2.5}$ had stronger effects on total CSD, hypertension, CEVD, HF, and arrhythmia during cold seasons.

**Conclusion:** $PM_{2.5}$ exposure was positively associated with daily hospital admissions for CSD, which might provide informative insight on adverse effects of $PM_{2.5}$.

KEYWORDS

**circulatory system diseases, $PM_{2.5}$, hospital admissions, air pollution, generalized additive model (GAM), time series study**

# 1. Introduction

The development of modern industrialization has made air pollution one of the leading public health concerns worldwide (1). According to the latest Global Burden of Disease (GBD) Survey, ambient air pollution could be responsible for 6.7 million deaths in 2019 (2). Accumulating studies have shown that exposure to air pollutants, whether both short- or long-term, may damage human health on multiple levels (3).

$PM_{2.5}$, named particulate matter with aerodynamic diameter below 2.5 μm, is considered the most sensitive indicator of air quality (4). Ambient $PM_{2.5}$ mainly comes from natural conditions (volcanic eruptions and dust storms) and human activities such as industrial production, and traffic exhaust emissions (5). $PM_{2.5}$ has become an environmental problem and has attracted global public health concerns because of its adverse effects on multiple organs (6). Previous studies suggested that $PM_{2.5}$ exposure might lead to increased risks of respiratory diseases (7), circulatory system diseases (CSD) (8), neurological diseases (9), and metabolic diseases (10). In fact, the impact of $PM_{2.5}$ on CSD has been extensively reported in previous studies (11–13). However, epidemiologic studies regarding the relationships of short-term exposure to $PM_{2.5}$ and CSD remain inconclusive. According to a national study containing 379,133 participants, there was a 0.12% (95% CI, 0.001–0.25%) elevation in cardiovascular disease mortality with a 10-μg/m$^3$ increase in $PM_{2.5}$ levels on the same day (14). However, a study (15) including over 286 million hospitalizations in England and Wales found little evidence of $PM_{2.5}$ exposure with increased risk of cardiovascular admissions, and even in many cases, $PM_{2.5}$ was related to decrease risks of cardiovascular hospitalization. More studies are warranted to evaluate the impacts of short-term $PM_{2.5}$ exposure on CSD risks.

Ganzhou, a city with 9.8402 million population in 2021 and located in southern China, enjoys a typical subtropical monsoon climate. In recent years, great measures were conducted to reduce urban ambient pollution in China and the air quality of Ganzhou has gradually improved in last 10 years. In 2021, the mean concentration of $PM_{2.5}$ in Ganzhou was 23 μg/m$^3$, 34.3% lower than the that (35 μg/m$^3$) in 168 Chinese cities in the same year. To evaluate potential effects of $PM_{2.5}$ on the onset of CSD in Ganzhou is also helpful to understand adverse health effects caused by relatively low levels of $PM_{2.5}$ in China.

In this study, daily concentrations of air pollutants in Ganzhou were collected from China National Environmental Monitoring Center (CNEMC), and hospital admission data for CSD from 2016 to 2020 were extracted from the biggest hospital in Ganzhou. This time-series analysis was conducted to evaluate the relationships of ambient $PM_{2.5}$ exposure with daily hospitalizations for CSD. The effects of co-exposure to other air pollutants on above relationships were also analyzed.

# 2. Materials and methods

## 2.1. Daily hospital admissions data

Daily hospital admissions data of CSD from Jan.1, 2016 to Dec.31, 2020 were extracted from the hospital's admission case registry system in the biggest hospital of Ganzhou. The patient information included gender, age, residential address, date of admission, and principal diagnosis. The CSD in present study were encoded according to *the 10th version of the International Classification of Diseases* (ICD-10) as follows: total circulatory disease (I00-I99), hypertension (I10-I15), coronary heart disease (CHD, I20-I25), cerebrovascular diseases (CEVD, I60-I69), heart failure (HF, I50), and arrhythmia (I47-I49).

## 2.2. Ambient air pollutants and meteorological data

The 24-h average concentrations of $PM_{2.5}$, $NO_2$, $PM_{10}$, $SO_2$, and CO, and the maximum 8-h mean concentrations of $O_3$ from January 1, 2016 to December 31, 2020 were obtained from the National Real-Time Air Quality Monitoring Data Publishing Platform developed by CNEMC (http://www.cnemc.cn/). Daily average meteorological data including daily average temperature, relative humidity, and wind speed during the 5 years were obtained from the National Meteorological Information Center (http://data.cma.cn/). Present study did not involve/include any personally identifiable information and Institutional Review Board approval was not applicable.

## 2.3. Statistical analysis

Descriptive statistical analyses were performed to reveal the features of daily circulatory hospital admissions, ambient air pollutants and meteorological factors from January 1, 2016 to December 31, 2020. Spearman's rank correlation test was used to evaluate the bivariate associations between air pollutants and meteorological variables. To address the associations between $PM_{2.5}$ and hospitalization for CSD, the quasi-Poisson regression method in generalized additive models (GAMs) based on time series was applied. In this model, spline smoothing functions of time trend, daily mean temperature and relative humidity were introduced into the GAMs to exclude the potential confounding effects of long-term time trend and meteorological variables. Besides, the day of the week (DOW) and holiday were also considered as potential confounders. The model finally used was as follows:

$$\begin{aligned} Log\left[E\left(Yt\right)\right] = {} & \alpha + \beta Xt + s\left(time,\ df = 14\ per\ year\right) \\ & + s\left(Temp,\ df = 3\right) + s\left(RH,\ df = 3\right) \\ & + as.factor\left(DOW\right) + as.factor(Holiday) \end{aligned}$$

Where $t$ is the day of observation; $Yt$ denotes daily count of hospital admissions for CSD at day t; $Xt$ is the daily mean concentration of $PM_{2.5}$ at day t; $\beta$ is the regression coefficient which represents the log-relative rate of hospital admissions for CSD with a 10 μg/m$^3$ increase of $PM_{2.5}$ concentration; $DOW$ means the day of the week; $df$ is degree of freedom whose value is determined based on the Quasi-Akaike information criterion (QAIC); $\alpha$ is the model intercept.

TABLE 1 Characteristics of meteorological variables, ambient air pollutants, and hospital admissions in Ganzhou (2016–2020).

| | *N* (%) | Mean ± Sd | Min | P25 | P50 | P75 | Max |
|---|---|---|---|---|---|---|---|
| **Meteorological factors** | | | | | | | |
| Temperature (°C) | – | 20.54 ± 8.09 | 1 | 13.69 | 21.7 | 27.79 | 33.5 |
| Relative Humidity (%) | – | 75.21 ± 12.00 | 35.5 | 66.3 | 75.5 | 84.5 | 99 |
| **Air pollutants** | | | | | | | |
| $PM_{2.5}$ ($\mu g/m^3$) | – | 37.38 ± 20.8 | 6 | 23 | 33 | 47 | 184 |
| $PM_{10}$ ($\mu g/m^3$) | – | 60.06 ± 33.60 | 11 | 36 | 52 | 75 | 246 |
| $NO_2$ ($\mu g/m^3$) | – | 22.75 ± 12.60 | 4 | 14 | 19 | 28 | 84 |
| $SO_2$ ($\mu g/m^3$) | – | 18.73 ± 11.18 | 2 | 11 | 16 | 23 | 73 |
| CO ($mg/m^3$) | – | 1.24 ± 0.32 | 0.6 | 1 | 1.2 | 1.43 | 2.9 |
| $O_3$ ($\mu g/m^3$) | – | 90.52 ± 39.09 | 7 | 62.5 | 88 | 116 | 224 |
| **Hospital admissions** | | | | | | | |
| Total | 201,799 (100) | 110.0 ± 45.10 | 18 | 77 | 103 | 139 | 308 |
| Male | 114,671 (56.8) | 62.76 ± 26.70 | 9 | 44 | 58 | 79 | 177 |
| Female | 87,101 (43.2) | 47.67 ± 19.90 | 6 | 33 | 45 | 60 | 131 |
| ≤65 years old | 99,921 (49.5) | 54.69 ± 24.30 | 6 | 37 | 51 | 69 | 150 |
| >65 years old | 101,878 (50.5) | 55.76 ± 23.10 | 7 | 38 | 52 | 71 | 160 |
| Cold | 100,711 (49.91) | 111.0 ± 44.98 | 18 | 79 | 105 | 138 | 308 |
| Warm | 101,088 (50.09) | 109.0 ± 45.17 | 25 | 77 | 102 | 139 | 281 |
| **CSD** | | | | | | | |
| Total | 201,799 (100) | 110.0 ± 45.10 | 18 | 77 | 103 | 139 | 308 |
| Hypertension | 94,844 (47.0) | 51.91 ± 22.00 | 8 | 36 | 49 | 65 | 155 |
| CHD | 28,597 (14.2) | 15.00 ± 7.36 | 0 | 10 | 15 | 20 | 49 |
| CEVD | 42,120 (20.9) | 23.05 ± 8.79 | 2 | 16 | 22 | 29 | 57 |
| HF | 21,636 (10.7) | 11.84 ± 6.73 | 0 | 7 | 10 | 16 | 40 |
| Arrhythmia | 14,602 (7.2) | 7.99 ± 4.93 | 0 | 4 | 7 | 11 | 29 |

N, number; Sd, standard deviation; P, percentile; CSD, circulatory system diseases; CEVD, Cerebrovascular Disease; CHD, Coronary Heart Disease; HF, Heart Failure.

It is universally accepted that ambient air pollutants have persistent and hysteresis effects on health outcomes (16). We considered both single-day lags (lag0–lag14) and multiday lags (lag01–lag014) to evaluate delayed effects of $PM_{2.5}$. Lag0 refers to the impact of $PM_{2.5}$ on hospitalizations for CSD on the same day and Lag01 shows the effect of $PM_{2.5}$ in the current and the previous days. Additionally, stratified analyses were performed to determine whether the associations differed by age (≤65 and >65 years old), gender, season (May-October, warm season; December-April, cold season).

To exclude the potential confounding effect of other pollutants, a series of co-pollutant models were developed in addition to the single-pollutant model. Notably, to avoid collinearity, pollutants with correlation coefficients >0.6 were not incorporated into co-pollutant models simultaneously.

In the sensitivity analysis, we adjust the dfs of calendar time to 7 per year to test the stability of the associations, according to relevant studies (17–19). In addition, previous studies have shown that COVID-19 might have impacts on circulatory system (20). In this study, in order to control the impact of COVID-19 on the associations, we also included the occurrence of COVID-19 in the model for sensitivity analysis.

All results were given as percent changes and 95% confidence intervals (CIs) in daily hospitalizations for CSD per 10 $\mu g/m^3$ increment in $PM_{2.5}$ levels. All statistical analyses were performed in R version 4.1.2 with the "mgcv" and "tsModel" packages. *P*-value $< 0.05$ was considered as statistically significant (2-sided).

## 3. Results

The descriptive statistics of daily air pollutants, meteorological variables, and hospitalizations for CSD during the 5 years were shown in Table 1. A total of 201,799 hospitalizations for CSD (daily average: 110 hospital admissions) in Ganzhou were included in the analysis. Among all the records, 50.5% were older than 65 years old, and 56.8% were males. As for disease subtypes, hypertension accounted for 47.0% of total CSD, followed by cerebrovascular diseases (20.9%), coronary heart disease (14.2%), heart failure (10.7%) and arrhythmia (7.2%).

10.3389/fpubh.2023.1134516

The average daily concentrations of $PM_{2.5}$, $PM_{10}$, $NO_2$, $SO_2$ and CO during research period were 37.38 μg/m$^3$, 60.06 μg/m$^3$, 22.75 μg/m$^3$, 18.73 μg/m$^3$, 1.24 mg/m$^3$, respectively, while the 8-hour average concentration of $O_3$ was 90.52 μg/m$^3$. On average, the daily temperature was 20.54°C and the relative humidity was 75.21 %.

As shown in the time series plots, the levels of $PM_{2.5}$ in Ganzhou decreased slowly and gradually during the study period (Supplementary Figure 1). The levels of $PM_{10}$, $NO_2$, $SO_2$ and CO also showed similar trends, except that $O_3$ levels increased. During the same period, hospital admissions for total CSD and five specific subtypes fluctuated and rose steadily (Supplementary Figure 2).

The Spearman's correlation coefficients for exposure variables were given in Figure 1. $PM_{2.5}$ was highly correlated with $PM_{10}$ and $SO_2$, and $NO_2$ ($r > 0.6$ and $P < 0.05$), moderately correlated with CO and $O_3$ ($r = 0.44$ and 0.33, respectively, $P < 0.05$). However, $PM_{2.5}$ was negatively correlated with relative humidity ($r = -0.21$, $P < 0.05$) and temperature ($r = -0.22$, $P < 0.05$).

Positive linear exposure-response relationships between $PM_{2.5}$ concentrations and daily hospitalizations for total and cause-specific CSD were observed (Figure 2). Hospitalizations for total CSD, hypertension, CHD, CEVD, and HF increased rapidly at high levels of $PM_{2.5}$, except for arrhythmia, which showed a slowly linear rise. In single-pollutant models, significantly positive associations were observed between $PM_{2.5}$ levels and hospital admissions for studied CSD in both single-day (lag1–lag14) and cumulative-day (lag01–lag014) lag structures (Table 2). The largest single day effect of $PM_{2.5}$ was at lag6 for total CSD, hypertension, CHD, lag4 for CEVD, and lag1 for HF and arrhythmia. The greatest cumulative day effect for total CSD, hypertension, CHD and HF were observed at lag014. The effect of $PM_{2.5}$ on hospitalizations for CEVD peaked at lag011. Every 10 μg/m$^3$ increment of ambient $PM_{2.5}$ concentrations was associated with a 2.588% [95% confidence interval (CI), 1.161–4.035%], 2.773% (95% CI, 1.246–4.324%),

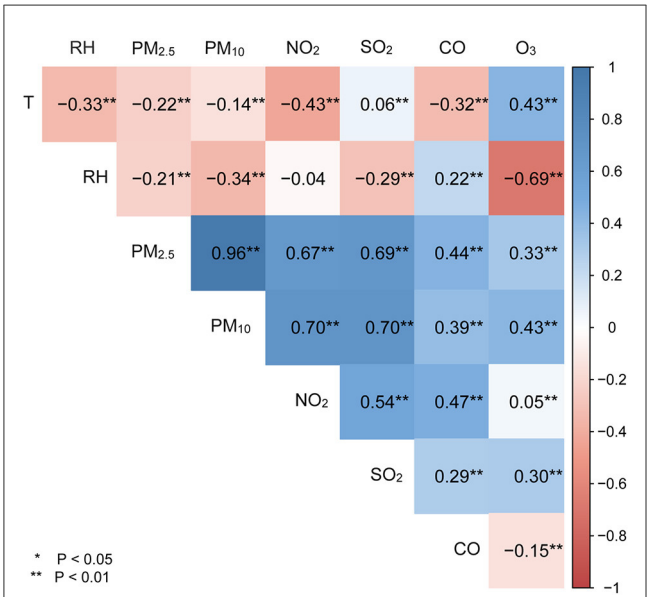


FIGURE 1
Spearman's rank correlations of meteorological variables with ambient air pollutants. T represents temperature; RH denotes relative humanity; *means $P < 0.05$, **means $P < 0.01$.

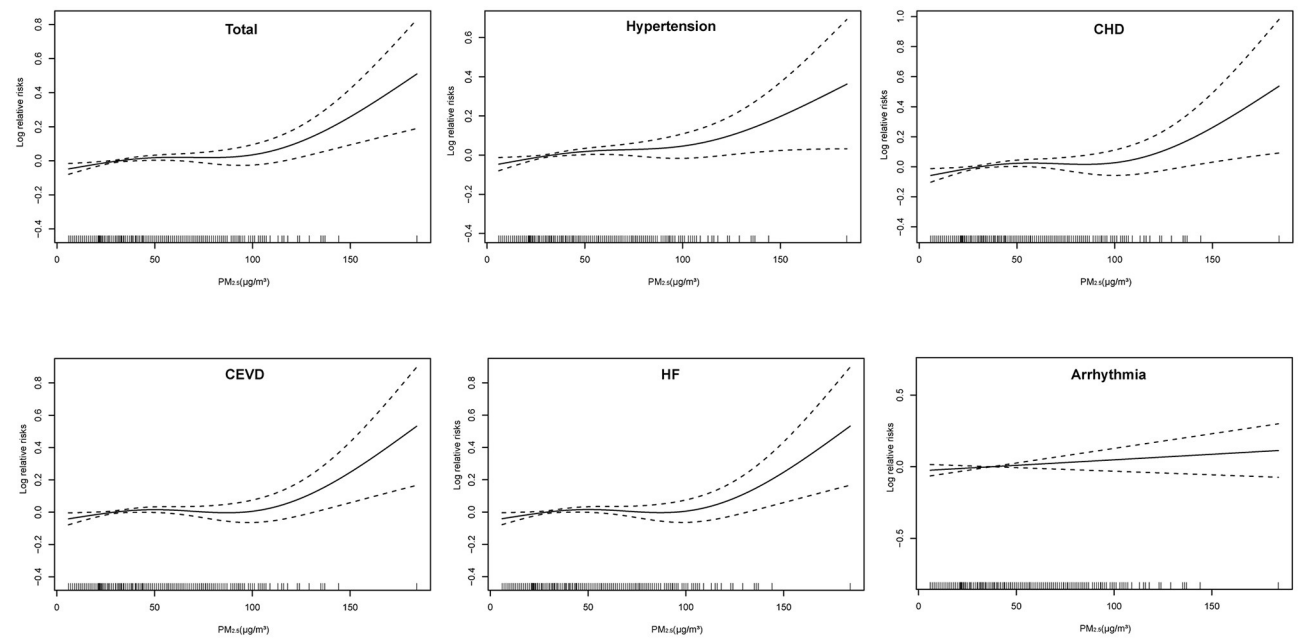


FIGURE 2
Exposure-response relationships of $PM_{2.5}$ concentrations with daily hospital admissions for total and cause-specific circulatory system diseases. CEVD, Cerebrovascular Disease; CHD, Coronary Heart Disease; HF, Heart Failure. The concentration response curve is the solid line and the 95% CI is presented by the dotted line.

TABLE 2 Percent changes and 95% confidence intervals (CIs) of daily hospital admissions for total and cause-specific circulatory system diseases by each 10 $\mu g/m^3$ increase of $PM_{2.5}$ concentrations at different lag structures in the single-pollutant model.

| Lag Type | Lag day | Total CSD | Hypertension | CHD | CEVD | HF | Arrhythmia |
|---|---|---|---|---|---|---|---|
| Single-lag | 0 | 0.245 (−0.495, 0.990) | 0.134 (−0.660, 0.935) | 0.402 (−0.632, 1.446) | −0.125 (−0.972, 0.730) | **1.436 (0.326, 2.558)** | 0.804 (−0.541, 2.168) |
| | 1 | **0.880 (0.157, 1.609)** | 0.758 (−0.017, 1.538) | 0.840 (−0.180, 1.870) | 0.443 (−0.380, 1.274) | **2.277 (1.172, 3.393)** | **1.638 (0.320, 2.972)** |
| | 2 | 0.560 (−0.147, 1.272) | 0.586 (−0.170, 1.348) | 0.349 (−0.649, 1.356) | 0.279 (−0.526, 1.091) | **1.655 (0.571, 2.750)** | 0.557 (−0.736, 1.866) |
| | 3 | 0.305 (−0.394, 1.01) | 0.442 (−0.308, 1.198) | −0.084 (−1.072, 0.914) | 0.132 (−0.667, 0.937) | 0.898 (−0.167, 1.974) | 0.359 (−0.918, 1.653) |
| | 4 | **0.691 (0.001, 1.386)** | **0.822 (0.080, 1.569)** | 0.378 (−0.600, 1.365) | **0.873 (0.083, 1.670)** | 0.462 (−0.585, 1.520) | 0.562 (−0.700, 1.84) |
| | 5 | **0.935 (0.250, 1.624)** | **1.134 (0.397, 1.875)** | 0.667 (−0.304, 1.647) | **0.858 (0.072, 1.651)** | **1.079 (0.042, 2.127)** | 0.395 (−0.859, 1.664) |
| | 6 | **1.099 (0.421, 1.782)** | **1.129 (0.399, 1.864)** | **1.185 (0.223, 2.156)** | 0.767 (−0.015, 1.555) | **1.934 (0.904, 2.975)** | 0.774 (−0.474, 2.038) |
| | 7 | **0.912 (0.233, 1.595)** | **1.084 (0.354, 1.820)** | 0.804 (−0.159, 1.776) | 0.692 (−0.088, 1.479) | **1.336 (0.305, 2.378)** | 0.206 (−1.040, 1.468) |
| | 8 | **0.711 (0.029, 1.398)** | **0.925 (0.190, 1.665)** | 0.597 (−0.370, 1.573) | 0.555 (−0.229, 1.345) | 0.747 (−0.282, 1.788) | 0.114 (−1.133, 1.376) |
| | 9 | **0.747 (0.070, 1.429)** | **0.973 (0.244, 1.707)** | 0.735 (−0.225, 1.704) | 0.558 (−0.222, 1.344) | 0.562 (−0.459, 1.594) | 0.254 (−0.981, 1.505) |
| | 10 | **0.689 (0.009, 1.374)** | 0.690 (−0.043, 1.429) | **1.060 (0.095, 2.034)** | 0.784 (0.000, 1.575) | 0.423 (−0.597, 1.453) | 0.252 (−0.986, 1.506) |
| | 11 | 0.488 (−0.196, 1.176) | 0.584 (−0.153, 1.327) | 0.965 (−0.007, 1.946) | 0.179 (−0.607, 0.971) | 0.228 (−0.795, 1.261) | 0.347 (−0.899, 1.608) |
| | 12 | 0.504 (−0.184, 1.196) | 0.475 (−0.267, 1.223) | **1.277 (0.299, 2.266)** | 0.029 (−0.760, 0.824) | 0.528 (−0.501, 1.567) | 0.708 (−0.545, 1.978) |
| | 13 | 0.219 (−0.470, 0.913) | 0.246 (−0.498, 0.996) | 0.720 (−0.261, 1.711) | −0.252 (−1.041, 0.544) | 0.533 (−0.498, 1.575) | 0.177 (−1.079, 1.448) |
| | 14 | 0.223 (−0.466, 0.916) | 0.207 (−0.537, 0.957) | 0.473 (−0.506, 1.461) | −0.24 (−1.030, 0.556) | 0.522 (−0.511, 1.566) | 0.958 (−0.304, 2.236) |
| Cumulative-lag | 01 | 0.697 (−0.111, 1.512) | 0.555 (−0.310, 1.427) | 0.758 (−0.376, 1.905) | 0.198 (−0.723, 1.128) | **2.305 (1.077, 3.547)** | **1.496 (0.030, 2.983)** |
| | 02 | 0.820 (−0.051, 1.698) | 0.717 (−0.211, 1.655) | 0.766 (−0.453, 1.999) | 0.290 (−0.697, 1.287) | **2.632 (1.301, 3.981)** | 1.441 (−0.134, 3.041) |
| | 03 | 0.836 (−0.091, 1.772) | 0.798 (−0.190, 1.796) | 0.631 (−0.666, 1.944) | 0.310 (−0.740, 1.371) | **2.670 (1.247, 4.113)** | 1.385 (−0.290, 3.089) |
| | 04 | **1.020 (0.039, 2.011)** | 1.024 (−0.022, 2.081) | 0.699 (−0.672, 2.089) | 0.639 (−0.471, 1.761) | **2.538 (1.032, 4.066)** | 1.509 (−0.261, 3.311) |
| | 05 | **1.279 (0.249, 2.320)** | **1.339 (0.240, 2.449)** | 0.858 (−0.580, 2.317) | 0.921 (−0.243, 2.099) | **2.751 (1.170, 4.356)** | 1.517 (−0.338, 3.408) |
| | 06 | **1.599 (0.526, 2.685)** | **1.642 (0.497, 2.801)** | 1.254 (−0.244, 2.774) | 1.139 (−0.075, 2.368) | **3.324 (1.677, 4.998)** | 1.700 (−0.234, 3.671) |
| | 07 | **1.802 (0.688, 2.929)** | **1.894 (0.703, 3.098)** | 1.439 (−0.115, 3.018) | **1.266 (0.009, 2.539)** | **3.631 (1.919, 5.371)** | 1.654 (−0.353, 3.702) |
| | 08 | **1.954 (0.797, 3.125)** | **2.101 (0.864, 3.353)** | 1.574 (−0.038, 3.213) | **1.379 (0.074, 2.701)** | **3.709 (1.930, 5.518)** | 1.640 (−0.445, 3.769) |
| | 09 | **2.122 (0.921, 3.338)** | **2.327 (1.042, 3.628)** | **1.760 (0.088, 3.460)** | **1.488 (0.136, 2.859)** | **3.766 (1.921, 5.645)** | 1.667 (−0.496, 3.878) |
| | 010 | **2.280 (1.033, 3.541)** | **2.476 (1.143, 3.827)** | **2.024 (0.290, 3.788)** | **1.675 (0.272, 3.097)** | **3.804 (1.892, 5.752)** | 1.704 (−0.538, 3.997) |
| | 011 | **2.383 (1.092, 3.691)** | **2.601 (1.218, 4.002)** | **2.256 (0.458, 4.085)** | **1.691 (0.239, 3.165)** | **3.795 (1.816, 5.812)** | 1.780 (−0.542, 4.156) |
| | 012 | **2.501 (1.165, 3.856)** | **2.699 (1.268, 4.151)** | **2.574 (0.712, 4.470)** | **1.682 (0.181, 3.207)** | **3.916 (1.870, 6.003)** | 1.961 (−0.442, 4.422) |
| | 013 | **2.543 (1.160, 3.945)** | **2.742 (1.261, 4.244)** | **2.744 (0.818, 4.708)** | **1.590 (0.041, 3.164)** | **4.042 (1.927, 6.202)** | 1.994 (−0.492, 4.542) |
| | 014 | **2.588 (1.161, 4.035)** | **2.773 (1.246, 4.324)** | **2.865 (0.876, 4.893)** | 1.508 (−0.089, 3.129) | **4.173 (1.988, 6.404)** | 2.240 (−0.329, 4.874) |

Bold font indicates statistical significance.

CSD, circulatory system diseases; CEVD, Cerebrovascular Disease; CHD, Coronary Heart Disease; HF, Heart Failure.





10.3389/fpubh.2023.1134516

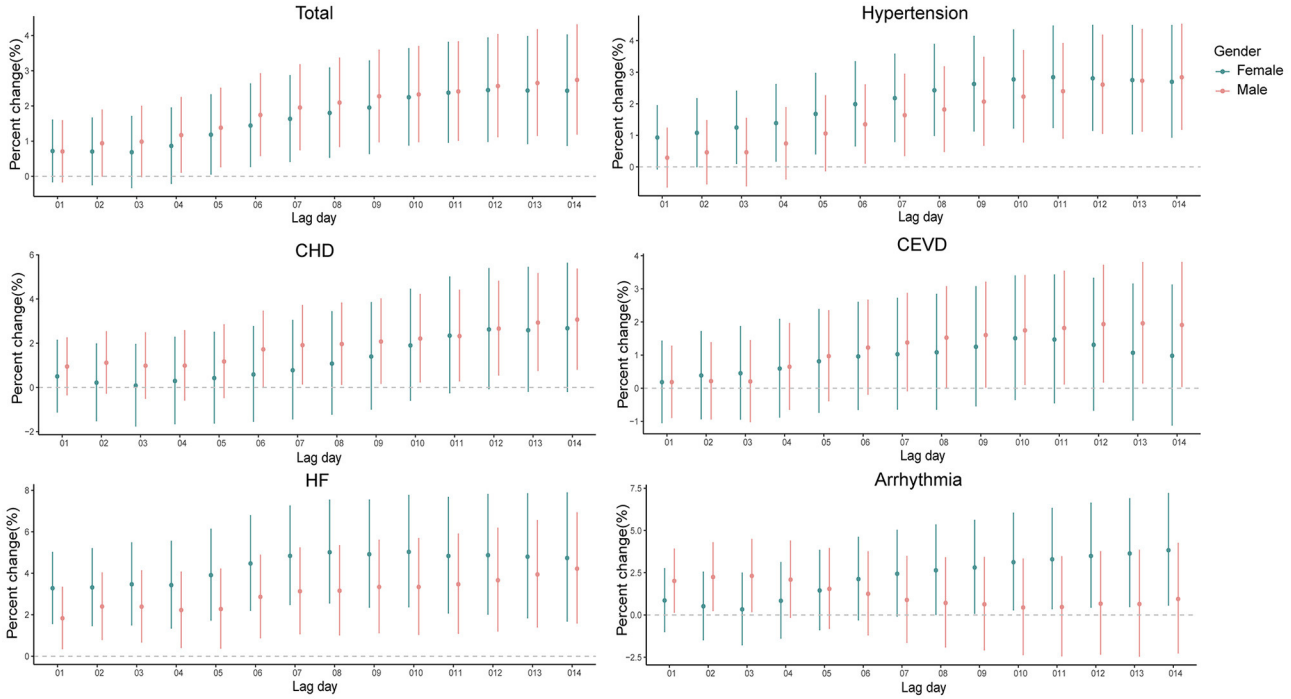


FIGURE 3
Percent changes and 95% confidence intervals (CIs) of daily hospital admissions for total and cause-specific circulatory system diseases by each 10 $\mu g/m^3$ increase of $PM_{2.5}$ concentrations stratified by gender at the cumulative-day lag models. HBP, hypertension; CHD, Coronary Heart Disease; CEVD, Cerebrovascular Disease; HF, Heart Failure.

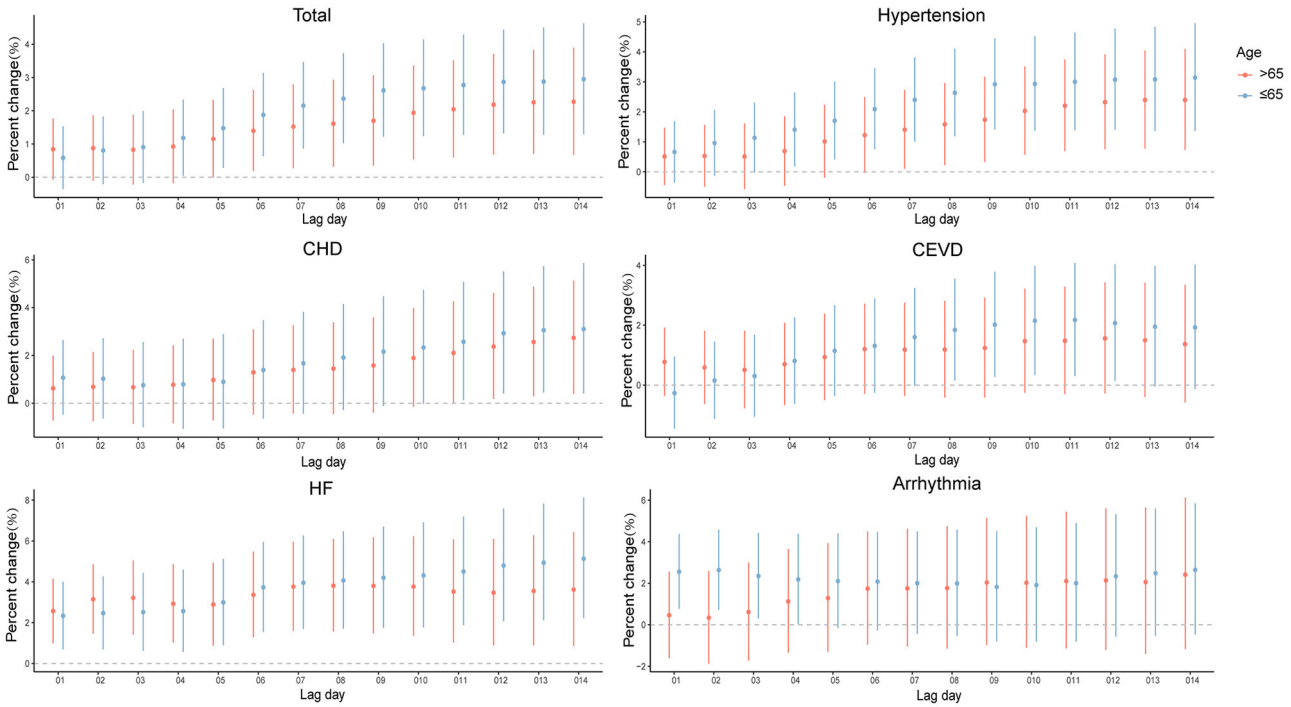


FIGURE 4
Percent changes and 95% confidence intervals (CIs) of daily hospital admissions for total and cause-specific circulatory system diseases by each 10 $\mu g/m^3$ increase of $PM_{2.5}$ concentrations stratified by age in the cumulative-day lag models. HBP, hypertension; CHD, Coronary Heart Disease; CEVD, Cerebrovascular Disease; HF, Heart Failure.

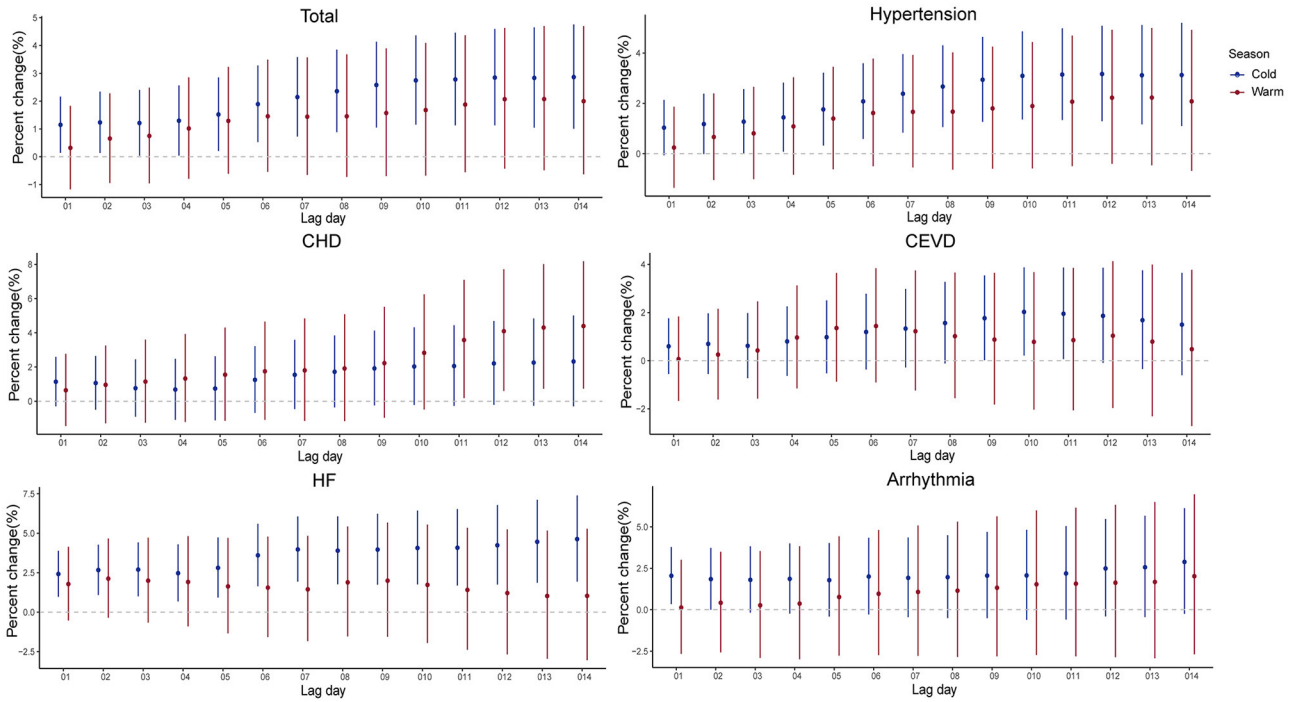


FIGURE 5
Percent changes and 95% confidence intervals (CIs) of daily hospital admissions for total and cause-specific circulatory system diseases by each 10 μg/m$^3$ increase of $PM_{2.5}$ concentrations stratified by season in the cumulative-day lag models. HBP, hypertension; CHD, Coronary Heart Disease; CEVD, Cerebrovascular Disease; HF, Heart Failure.

2.865% (95% CI, 0.786–4.893%), 1.691% (95% CI, 0.239–3.165%), 4.173% (95% CI, 1.988–6.404%) and 1.496% (95% CI, 0.030–2.983%) increment in hospitalizations for total CSD, hypertension, CHD, CEVD, HF, and arrhythmia, respectively.

The risk of hospital admissions seems to be higher in males for total CSD, CHD, and CEVD, and in females for hypertension, HF, and arrhythmia (Supplementary Figure 3 and Figure 3).

When analyses were stratified by age (≤65 and >65 years old), the results were not materially changed. In the elderly (>65 years old), significantly positive associations were observed of $PM_{2.5}$ exposure with all the outcomes of interest in present study (Supplementary Figure 4 and Figure 4), slightly different from those in the younger (≤65 years old). As for the young people, $PM_{2.5}$ levels were significantly associated with hospitalizations for CSD, except for arrhythmia.

The impacts of $PM_{2.5}$ on hospitalizations for CSD in cold seasons were stronger than those in warm seasons (Supplementary Figure 5 and Figure 5). In cold seasons, positive associations were observed in at least one exposure lag structure in present study, except for CHD. In warm seasons, hospitalizations for CHD and HF increased 2.618% (95% CI, 0.725–4.546%) and 2.769% (95% CI, 0.493–5.097%) per 10 μg/m$^3$ elevation in $PM_{2.5}$ levels, while there were no significant increases observed for total CSD, hypertension, CEVD, and arrhythmia.

The results of co-pollutant models were shown in Table 3. The associations remained largely unchanged when additionally adjusted for CO or/and $O_3$, and were similar with additionally adjusted for all major air pollutants. Moreover, the results were similar when we changed the df for secular time (Supplementary Tables 1, 2 and Supplementary Figures 6–11) and adjusted the effect of COVID-19 (Supplementary Table 3), which illustrated the robustness of our findings.

## 4. Discussion

In this study, we found that short-term exposure to $PM_{2.5}$ was positively associated with hospitalizations for CSD, including total CSD, hypertension, CHD, CEVD, HF and arrhythmia, with significant lag effects. When analyses were stratified by age, gender, and season, there were no material changes of our findings, although the risk of hospitalizations seems to be higher among young people and cold seasons. Our results kept robust in the co-exposure models.

Though previous studies have reported relationships of $PM_{2.5}$ with the risks of CSD, the results were largely inconsistent. Most studies found positive relationships of $PM_{2.5}$ with increased risk of CSD. A multi-country time series study including 30 countries reported that every 10-μg/m$^3$ elevation in $PM_{2.5}$ concentrations was significantly relevant to a 0.12%, 0.42%, and 0.17% increase in cardiovascular diseases (CVD), acute myocardial infarction (AMI), and CHD on the same day (14). Furthermore, another study conducted in Beijing found that increasing $PM_{2.5}$ levels were associated with hospitalizations for total CVD, CHD and atrial fibrillation (AF) (21). However, a few studies argued that there were no significantly associations of $PM_{2.5}$ exposure with the risks of CSD (12, 15). Notably, the case data in above studies mainly came from government

10.3389/fpubh.2023.1134516

departments, which means that the data might be incomplete. Moreover, the confounding effect of time was not considered. Here, this time-series study based on more complete data were conducted and significantly positive associations of $PM_{2.5}$ exposure with hospitalizations for CSD were observed, which was keeping with most studies.

The delayed effect of $PM_{2.5}$ was also inconsistent in previous studies. Some studies across different countries showed that the impacts of $PM_{2.5}$ on CSD mortality were peaked on the current day (22) and lag03 (13, 23, 24). A study in Kraków, Poland reported the delayed effects of $PM_{2.5}$ levels on the risk of Myocardial Infarction (MI) admissions were observed at lag4 and lag6 (11). In our study, the earliest positive association between $PM_{2.5}$ and hospitalizations for total CSD was at lag1 and peaked at lag6, as well as lag04 and lag014 in the cumulative-day lag model, which were longer than the hysteresis of other studies. The potential underlying reasons are as follows. First of all, the air quality of Ganzhou city is relatively good, and the average levels of $PM_{2.5}$ from 2016 to 2020 was 37.38 $\mu g/m^3$, which was significantly lower than that in other studies (21, 25). According to previous toxicological studies, $PM_{2.5}$ exposure could lead to chronic systemic inflammation (26, 27), oxidative stress (28), stress hormone secretion (29–31) and vascular endothelial disfunction (32, 33), thereby causing to cardiovascular system damage. It takes several days from $PM_{2.5}$ exposure to symptoms and hospitalization. Therefore, we speculated that exposure to higher levels of $PM_{2.5}$ might have an acute effect on circulatory system health, while relatively low levels of $PM_{2.5}$ tended to have delayed effects. Further studies are definitely needed to verify the hypothesis. Besides, in present study, hypertension and CHD accounted for relatively higher proportion of 47.0% and 14.2% in total CSD, respectively (Table 1). Worthy of note was that patients with hypertension and CHD are more inclined to self-medicate rather than to be hospitalized until their conditions worsen, which might be responsible for longer days' lag and underestimations of the impacts of $PM_{2.5}$.

In this study, the cumulative-day lag model generally has higher estimates than the single-day lag model, with the greatest effects observed at lag 014. Similar results have been observed in other studies (34–36). The health effects of air pollutants usually last for several days, therefore, a cumulative lag model might be more accurate than a single-day lag model in assessing the health effects of air pollutants.

Our results regarding the positive associations of $PM_{2.5}$ with CSD were correspondent with current mainstream understanding of the damage effects of $PM_{2.5}$ on the circulatory system. Previous toxicological studies (28) have shown that $PM_{2.5}$ is inhaled into lung through respiration, causing lung inflammation. The particles and inflammatory mediators released by alveolar macrophages could also enter the blood circulation system directly through the capillaries in the lungs and cause systemic inflammation and vascular endothelial dysfunction (37). These responses may underlie PM-induced circulatory system damage. $PM_{2.5}$ could also activate the hypothalamic–pituitary–adrenal (HPA) axis, triggering an increase of stress hormones release, thereby causing vasoconstriction, increased blood pressure and a series of pathological reactions (29). However, full details regarding the biological mechanisms remain largely unclear and warrant further study.

TABLE 3 Percent changes and 95% CIs of hospital admissions associated with every 10 $\mu g/m^3$ increase of $PM_{2.5}$ under co-pollutant models.

| Model Type | [a]Total(PC, 95% CI, %) | [a]HBP (PC, 95% CI, %) | [a]CHD (PC, 95% CI, %) | [b]CVD (PC, 95% CI, %) | [a]HF (PC, 95% CI, %) | [a]ARR (PC, 95% CI, %) |
|---|---|---|---|---|---|---|
| $PM_{2.5}$ | 2.588 (1.161, 4.035)* | 2.773 (1.246, 4.324)* | 2.865 (0.876, 4.893)* | 1.691 (0.239, 3.165)* | 4.170 (1.988, 6.404)* | 2.240 (−0.329, 4.874) |
| $PM_{2.5}$ + CO | 2.480 (0.997, 3.985)* | 2.730 (1.132,4.354)* | 2.781 (0.697,4.909)* | 1.800 (0.279,3.345)* | 3.867 (1.637,6.147)* | 1.557 (−1.057,4.240) |
| $PM_{2.5}$ + $O_3$ | 2.626 (1.197, 4.075)* | 2.804 (1.273,4.358)* | 2.917 (0.927,4.946)* | 1.664 (0.207,3.143)* | 4.260 (2.068,6.498)* | 2.425 (−0.149,5.066) |
| $PM_{2.5}$ + CO + $O_3$ | 2.494 (1.011, 3.999)* | 2.739 (1.138,4.364)* | 2.788 (0.705,4.914)* | 1.782 (0.258,3.329)* | 3.936 (1.702,6.219)* | 1.658 (−0.966,4.352) |
| ALL | 2.729 (1.227, 4.254)* | 2.974 (1.344,4.629)* | 3.055 (0.941,5.212)* | 2.014 (0.455,3.596)* | 3.979 (1.721,6.287)* | 1.784 (−0.890,4.530) |

PC, Percent change; HBP, Hypertension; CEVD, Cerebrovascular Disease; CHD, Coronary Heart Disease; HF, Heart Failure; ARR, arrhythmia.

[a]The peak lag effect of $PM_{2.5}$ was lag014 in the cumulative lag models.

[b]The peak lag effect of $PM_{2.5}$ was lag011 in the cumulative lag models.

*Means $P < 0.05$.

The associations between $PM_{2.5}$ and hospitalizations for CSD were not materially changed in different gender subgroups. The impacts of $PM_{2.5}$ on the hospitalizations for arrhythmia seemed to be stronger in females compared with males, consistent with some studies (35–37), which might be attributable to more vulnerable biological systems of females.

In age subgroups, we found that younger people (≤65 years old) showed greater sensitivity to $PM_{2.5}$ exposure in total CSD, hypertension, CHD, CEVD, and heart failure. In addition to air pollution, numerous factors such as occupational exposure (38), lifestyles (39), and even social status (40) and psychological factors (8) could also affect the health of circulatory system. Compared with the elderly, younger people tend to spend more time outdoors and are more vulnerable to harmful ambient hazards and occupational factors, such as industrial dust, chemicals, and noise (41), which can explain why younger people are more susceptible to $PM_{2.5}$. Overall, more researches are warranted to probe the potential modifiers in age and sex on associations of $PM_{2.5}$ exposure with the risks of CSD.

In our study, the impacts of $PM_{2.5}$ on the CSD, except for CHD, dominated during the cold seasons. The differences in $PM_{2.5}$ levels and compositions might be accounted for the seasonal variations in the relationships of $PM_{2.5}$ exposure with hospitalizations for CSD. The mean levels of $PM_{2.5}$ during cold seasons from 2016 to 2020 in Ganzhou is 43.62 $\mu g/m^3$, significantly higher than that in warm seasons (31.22 $\mu g/m^3$), shown in Supplementary Table 2. Furthermore, some constituents in $PM_{2.5}$, including polycyclic aromatic hydrocarbons (PAHs) and metals, which were acknowledged to cause damage to the circulatory system (42, 43), increased significantly compared with warm seasons according to related studies (44, 45).

Profound elucidation for the exposure-response relationship is essential for public health policy formulation regarding the limit for $PM_{2.5}$. In this study, the exposure-response curves were approximately linear with relatively steeper increases at higher concentrations of PM2.5 (>110 $mg/m^3$ for HF, >100 $mg/m^3$ for other circulatory system diseases). A series of previous studies also reported similar linear exposure-response relationships (21, 36, 46–50). For example, a study in Beijing found that the hospitalizations for ischemic stroke had a stable increase at lower concentrations (<100 $\mu g/m^3$) and a steeper increment at higher concentrations of $PM_{2.5}$ (46).

Notably, the average 24h concentration of $PM_{2.5}$ in Ganzhou from 2016 to 2020 was 37 $\mu g/m^3$, lower than current National Ambient Air Quality Standard (NAAQS) for $PM_{2.5}$ (75 $\mu g/m^3$) (51). However, significantly positive associations of $PM_{2.5}$ and hospitalizations for CSD were still observed. Our findings were consistent with some studies. In a study of 200 Chinese cities (52), which included 58.52 million hospital admissions, the positive relationships of $PM_{2.5}$ with hospitalizations were observed when the daily levels met the current NAAQS (75 $\mu g/m^3$). Furthermore, a recent analysis of Europe (53) also revealed that long-term low levels of $PM_{2.5}$ exposure was related to the morbidity of stroke and CHD. Additionally, a study in USA (54) also reported the deleterious effects of $PM_{2.5}$ at levels below the specified limits. From the perspective of public health, our study suggests that more stringent $PM_{2.5}$ standard limits than current NAAQS should be established to minimize the harmful effects of ambient $PM_{2.5}$.

In the co-pollutant models, after adjusting CO or/and $O_3$, and other major pollutants, the hospitalizations for CSD per 10-$\mu g/m^3$ elevation of $PM_{2.5}$ still significantly increased, indicating that the impacts of $PM_{2.5}$ on the risks of CSD were robust, in keeping with most studies (21, 23, 55).

There are several strengths in the current study. Firstly, this study estimated the associations between $PM_{2.5}$ levels and the risk of hospitalizations for CSD in Ganzhou for the first time. Besides, hospital admission data was selected as the effect indicator, which was more sensitive than mortality and has great public health implications.

However, several limitations should also be considered. First, using outdoor air pollution measured at outdoor fixed sited monitors as a proxy for individual exposure levels might lead to the misestimation of the exposure assessment. Secondly, our case data were only collected from one hospital in Ganzhou, which was inevitably to the ecological fallacy and the extrapolation of our research results were limited, to a certain extent. In addition, confounding factors such as smoking, alcohol consumption, occupation and education levels were not considered in the analysis due to lack of information. Finally, we were unable to evaluate the long-term influence of $PM_{2.5}$ on the CSD under the time-series analysis design. Therefore, more well-designed studies are needed to explore the short-term and long-term impacts of $PM_{2.5}$ exposure on the incidence of CSD in depth.

## 5. Conclusion

In this study, we found significantly positive associations of relatively low $PM_{2.5}$ exposure with daily hospitalizations for total and cause-specific CSD in Ganzhou. And the associations varied in age, gender, and season subgroups. Our findings provide substantial insight regarding the effects of $PM_{2.5}$ exposure on CSD, which may provide evidence of stricter limits on $PM_{2.5}$ concentrations and help local policymakers to formulate or promulgate prevention policies.

## Data availability statement

The raw data supporting the conclusions of this article will be made available by the authors, without undue reservation.

## Author contributions

XY contributed to conception, the design of the study, data analysis, and wrote the first draft of the manuscript. XC contributed to data analysis and the design of the study. YG, DW, WQ, CZ, and MZ contributed to manuscript revision. WC and XZ contributed to conception, the design of the study, funding acquisition, and project administration. All authors contributed to manuscript revision, read, and approved the submitted version.

## Funding

This study was supported by Doctoral Fund of Gannan Medical University (No. QD201901) and Science and Technology Project Founded by the Education Department of Jiangxi Province (No. GJJ190786).

## Acknowledgments

We sincerely appreciated all participants recruited in the study and the support from the study team.

## Conflict of interest

The authors declare that the research was conducted in the absence of any commercial or financial relationships that could be construed as a potential conflict of interest.

## Publisher's note

All claims expressed in this article are solely those of the authors and do not necessarily represent those of their affiliated organizations, or those of the publisher, the editors and the reviewers. Any product that may be evaluated in this article, or claim that may be made by its manufacturer, is not guaranteed or endorsed by the publisher.

## Supplementary material

The Supplementary Material for this article can be found online at: https://www.frontiersin.org/articles/10.3389/fpubh.2023.1134516/full#supplementary-material

## References

1. Kampa M, Castanas E. Human health effects of air pollution. *Environ Pollut.* (2008) 151:362–7. doi: 10.1016/j.envpol.2007.06.012

2. Safiri S, Carson-Chahhoud K, Noori M, Nejadghaderi SA, Sullman MJM, Ahmadian Heris J, et al. Burden of chronic obstructive pulmonary disease and its attributable risk factors in 204 countries and territories, 1990-2019: results from the Global Burden of Disease Study 2019. *Bmj.* (2022) 378:e069679. doi: 10.1136/bmj-2021-069679

3. Hankey S, Marshall JD. Urban form, air pollution, and health. *Curr Environ Health Rep.* (2017) 4:491–503. doi: 10.1007/s40572-017-0167-7

4. van den Elshout S, Léger K, Heich H. CAQI Common air quality index–update with PM(2.5) and sensitivity analysis. *Sci Total Environ.* (2014) 488–9:461–8. doi: 10.1016/j.scitotenv.2013.10.060

5. Liang CS, Duan FK, He KB, Ma YL. Review on recent progress in observations, source identifications and countermeasures of PM2.5. *Environ Int.* (2016) 86:150–70. doi: 10.1016/j.envint.2015.10.016

6. Feng S, Gao D, Liao F, Zhou F, Wang X. The health effects of ambient PM2.5 and potential mechanisms. *Ecotoxicol Environ Safety.* (2016) 128:67–74. doi: 10.1016/j.ecoenv.2016.01.030

7. Xing YF, Xu YH, Shi MH, Lian YX. The impact of PM2.5 on the human respiratory system. *J Thorac Dis.* (2016) 8:E69–74. doi: 10.3978/j.issn.2072-1439.2016.01.19

8. Kivimäki M, Steptoe A. Effects of stress on the development and progression of cardiovascular disease. *Nat Rev Cardiol.* (2018) 15:215–29. doi: 10.1038/nrcardio.2017.189

9. Kioumourtzoglou MA, Schwartz JD, Weisskopf MG, Melly SJ, Wang Y, Dominici F, et al. Long-term PM2.5 exposure and neurological hospital admissions in the Northeastern United States. *Environ Health Perspect.* (2016) 124:23–9. doi: 10.1289/ehp.1408973

10. Rajagopalan S, Park B, Palanivel R, Vinayachandran V, Deiuliis JA, Gangwar RS, et al. Metabolic effects of air pollution exposure and reversibility. *J Clin Invest.* (2020) 130:6034–40. doi: 10.1172/JCI137315

11. Konduracka E, Niewiara Ł, Guzik B, Kotynia M, Szolc P, Gajos G, et al. Effect of short-term fluctuations in outdoor air pollution on the number of hospital admissions due to acute myocardial infarction among inhabitants of Kraków, Poland. *Pol Arch Intern Med.* (2019) 129:88–96. doi: 10.20452/pamw.4424

12. Moein N, Garakyaraghi M, Shafie D, Rabiei K, Hosseini SM, Jafari-Koshki T, et al. The association between particulate matter 2.5 and hospitalization and mortality rates of heart failure: The CAPACITY study. *ARYA Atheroscler.* (2019) 15:253–9. doi: 10.22122/arya.v15i6.1825

13. Sicard P, Khaniabadi YO, Perez S, Gualtieri M, De Marco A. Effect of O(3), PM(10) and PM(2.5) on cardiovascular and respiratory diseases in cities of France, Iran and Italy. *Environ Sci Pollut Res Int.* (2019) 26:32645–65. doi: 10.1007/s11356-019-06445-8

14. Chen C, Zhu P, Lan L, Zhou L, Liu R, Sun Q, et al. Short-term exposures to PM(2.5) and cause-specific mortality of cardiovascular health in China. *Environ Res.* (2018) 161:188–94. doi: 10.1016/j.envres.2017.10.046

15. Milojevic A, Wilkinson P, Armstrong B, Bhaskaran K, Smeeth L, Hajat S. Short-term effects of air pollution on a range of cardiovascular events in England and Wales: case-crossover analysis of the MINAP database, hospital admissions and mortality. *Heart.* (2014) 100:1093–8. doi: 10.1136/heartjnl-2013-304963

16. Loxham M, Davies DE, Holgate ST. The health effects of fine particulate air pollution. *Bmj.* (2019) 367:l6609. doi: 10.1136/bmj.l6609

17. Tian Y, Liu H, Zhao Z, Xiang X, Li M, Juan J, et al. Association between ambient air pollution and daily hospital admissions for ischemic stroke: a nationwide time-series analysis. *PLoS Med.* (2018) 15:e1002668. doi: 10.1371/journal.pmed.1002668

18. Wang L, Liu C, Meng X, Niu Y, Lin Z, Liu Y, et al. Associations between short-term exposure to ambient sulfur dioxide and increased cause-specific mortality in 272 Chinese cities. *Environ Int.* (2018) 117:33–9. doi: 10.1016/j.envint.2018.04.019

19. Yin P, Chen R, Wang L, Meng X, Liu C, Niu Y, et al. Ambient ozone pollution and daily mortality: a nationwide study in 272 Chinese cities. *Environ Health Perspect.* (2017) 125:117006. doi: 10.1289/EHP1849

20. Liu F, Liu F, Wang L. COVID-19 and cardiovascular diseases. *J Mol Cell Biol.* (2021) 13:161–7. doi: 10.1093/jmcb/mjaa064

21. Amsalu E, Wang T, Li H, Liu Y, Wang A, Liu X, et al. Acute effects of fine particulate matter (PM(2.5)) on hospital admissions for cardiovascular disease in Beijing, China: a time-series study. *Environ Health.* (2019) 18:70. doi: 10.1186/s12940-019-0506-2

22. Shah AS, Lee KK, McAllister DA, Hunter A, Nair H, Whiteley W, et al. Short term exposure to air pollution and stroke: systematic review and meta-analysis. *BMJ.* (2015) 350:h1295. doi: 10.1136/bmj.h1295

23. Zhou X, Wang C, Chen P, Chen Y, Yin L, Du W, et al. Time series analysis of short-term effects of particulate matter pollution on the circulatory system disease mortality risk in Lishui District, China. *Environ Sci Pollut Res Int.* (2022) 29:17520–9. doi: 10.1007/s11356-021-17095-0

24. Kim H, Bell ML, Lee JT. Multi-dimensional community characteristics in linking particulate matter pollution and cause-specific mortality: 72 communities of South Korea. *Environ Res.* (2021) 196:110989. doi: 10.1016/j.envres.2021.110989

25. Guan M, Sun C, Tang D, Kang H, Chen F. A time-series analysis on the association between fine particulate matter and daily mortality - Shijiazhuang City, Hebei Province, China, 2015-2020. *China CDC Wkly.* (2022) 4:226–31.

26. Guan L, Geng X, Stone C, Cosky EEP Ji Y, Du H, et al. PM(2.5) exposure induces systemic inflammation and oxidative stress in an intracranial atherosclerosis rat model. *Environ Toxicol.* (2019) 34:530–8. doi: 10.1002/tox.22707

27. Yue W, Tong L, Liu X, Weng X, Chen X, Wang D, et al. Short term Pm2.5 exposure caused a robust lung inflammation, vascular remodeling, and exacerbated

transition from left ventricular failure to right ventricular hypertrophy. *Redox Biol.* (2019) 22:101161. doi: 10.1016/j.redox.2019.101161

28. Zhao T, Qi W, Yang P, Yang L, Shi Y, Zhou L, et al. Mechanisms of cardiovascular toxicity induced by PM(2.5): a review. *Environ Sci Pollut Res Int.* (2021) 28:65033–51. doi: 10.1007/s11356-021-16735-9

29. Li H, Cai J, Chen R, Zhao Z, Ying Z, Wang L, et al. Particulate matter exposure and stress hormone levels: a randomized, double-blind, crossover trial of air purification. *Circulation.* (2017) 136:618–27. doi: 10.1161/CIRCULATIONAHA.116.026796

30. Nääv Å, Erlandsson L, Isaxon C, Åsander Frostner E, Ehinger J, Sporre MK, et al. Urban PM2.5 Induces Cellular Toxicity, Hormone Dysregulation, Oxidative Damage, Inflammation, and Mitochondrial Interference in the HRT8 Trophoblast Cell Line. *Front Endocrinol.* (2020) 11:75. doi: 10.3389/fendo.2020.00075

31. Liu C, Yang J, Guan L, Zhu Y, Geng X. Filtered air intervention reduces inflammation and hypothalamus-pituitary-adrenal axis activation in adult male and female rats after PM 2.5 exposure. *Environ Sci Pollut Res Int.* (2020) 27:35341–8. doi: 10.1007/s11356-020-09564-9

32. Münzel T, Gori T, Al-Kindi S, Deanfield J, Lelieveld J, Daiber A, et al. Effects of gaseous and solid constituents of air pollution on endothelial function. *Eur Heart J.* (2018) 39:3543–50. doi: 10.1093/eurheartj/ehy481

33. Liang S, Zhang J, Ning R, Du Z, Liu J, Batibawa JW, et al. The critical role of endothelial function in fine particulate matter-induced atherosclerosis. *Part Fibre Toxicol.* (2020) 17:61. doi: 10.1186/s12989-020-00391-x

34. Qiu X, Wei Y, Wang Y, Di Q, Sofer T, Awad YA, et al. Inverse probability weighted distributed lag effects of short-term exposure to PM(2.5) and ozone on CVD hospitalizations in New England Medicare participants - Exploring the causal effects. *Environ Res.* (2020) 182:109095. doi: 10.1016/j.envres.2019.109095

35. Andersen ZJ, Olsen TS, Andersen KK, Loft S, Ketzel M, Raaschou-Nielsen O. Association between short-term exposure to ultrafine particles and hospital admissions for stroke in Copenhagen, Denmark. *Eur Heart J.* (2010) 31:2034–40. doi: 10.1093/eurheartj/ehq188

36. Ren Z, Liu X, Liu T, Chen D, Jiao K, Wang X, et al. Effect of ambient fine particulates (PM(2.5)) on hospital admissions for respiratory and cardiovascular diseases in Wuhan, China. *Respir Res.* (2021) 22:128. doi: 10.1186/s12931-021-01731-x

37. Xie W, You J, Zhi C, Li L. The toxicity of ambient fine particulate matter (PM2.5) to vascular endothelial cells *J Appl Toxicol.* (2021) 41:713–23. doi: 10.1002/jat.4138

38. Davis-Lameloise N, Philpot B, Janus ED, Versace VL, Laatikainen T, Vartiainen EA, et al. Occupational differences, cardiovascular risk factors and lifestyle habits in South Eastern rural Australia. *BMC Public Health.* (2013) 13:1090. doi: 10.1186/1471-2458-13-1090

39. Mechanick JI, Zhao S, Garvey WT. The adipokine-cardiovascular-lifestyle network: translation to clinical practice. *J Am Coll Cardiol.* (2016) 68:1785–803. doi: 10.1016/j.jacc.2016.06.072

40. Piedra LM, Andrade FCD, Hernandez R, Perreira KM, Gallo LC, González HM, et al. Association of subjective social status with life's simple 7s cardiovascular health index among hispanic/latino people: results from the HCHS/SOL. *J Am Heart Assoc.* (2021) 10:e012704. doi: 10.1161/JAHA.119.012704

41. Scarselli A, Corfiati M, Di Marzio D, Marinaccio A, Iavicoli S. Gender differences in occupational exposure to carcinogens among Italian workers. *BMC Public Health.* (2018) 18:413. doi: 10.1186/s12889-018-5332-x

42. Nickel NP, Yuan K, Dorfmuller P, Provencher S, Lai YC, Bonnet S, et al. Beyond the lungs: systemic manifestations of pulmonary arterial hypertension. *Am J Respir Crit Care Med.* (2020) 201:148–57. doi: 10.1164/rccm.201903-0656CI

43. Chowdhury R, Ramond A, O'Keeffe LM, Shahzad S, Kunutsor SK, Muka T, et al. Environmental toxic metal contaminants and risk of cardiovascular disease: systematic review and meta-analysis. *BMJ.* (2018) 362:k3310. doi: 10.1136/bmj.k3310

44. Ma WL, Sun DZ, Shen WG, Yang M, Qi H, Liu LY, et al. Atmospheric concentrations, sources and gas-particle partitioning of PAHs in Beijing after the 29th Olympic Games. Environ Pollut. (2011) 159:1794–801. doi: 10.1016/j.envpol.2011.03.025

45. Trusz A, Ghazal H, Piekarska K. Seasonal variability of chemical composition and mutagenic effect of organic PM2.5 pollutants collected in the urban area of Wrocław (Poland). *Sci Total Environ.* (2020) 733:138911. doi: 10.1016/j.scitotenv.2020.138911

46. Tian Y, Xiang X, Wu Y, Cao Y, Song J, Sun K, et al. Fine particulate air pollution and first hospital admissions for ischemic stroke in Beijing, China. *Sci Rep.* (2017) 7:3897. doi: 10.1038/s41598-017-04312-5

47. Lee S, Lee W, Kim D, Kim E, Myung W, Kim SY, et al. Short-term PM(2.5) exposure and emergency hospital admissions for mental disease. *Environ Res.* (2019) 171:313–20. doi: 10.1016/j.envres.2019.01.036

48. Dominici F, Peng RD, Bell ML, Pham L, McDermott A, Zeger SL, et al. Fine particulate air pollution and hospital admission for cardiovascular and respiratory diseases. *Jama.* (2006) 295:1127–34. doi: 10.1001/jama.295.10.1127

49. Li M, Wu Y, Tian YH, Cao YY, Song J, Huang Z, et al. Association between PM(2.5) and daily hospital admissions for heart failure: a time-series analysis in Beijing. *Int J Environ Res Public Health.* (2018) 15:2217. doi: 10.3390/ijerph15102217

50. Yao C, Wang Y, Williams C, Xu C, Kartsonaki C, Lin Y, et al. The association between high particulate matter pollution and daily cause-specific hospital admissions: a time-series study in Yichang, China. *Environ Sci Pollut Res Int.* (2020) 27:5240–50. doi: 10.1007/s11356-019-06734-2

51. Wu R, Song X, Bai Y, Chen J, Zhao Q, Liu S, et al. Are current Chinese national ambient air quality standards on 24-hour averages for particulate matter sufficient to protect public health? *J Environ Sci.* (2018) 71:67–75. doi: 10.1016/j.jes.2018.01.017

52. Tian Y, Liu H, Liang T, Xiang X, Li M, Juan J, et al. Fine particulate air pollution and adult hospital admissions in 200 Chinese cities: a time-series analysis. *Int J Epidemiol.* (2019) 48:1142–51. doi: 10.1093/ije/dyz106

53. Wolf K, Hoffmann B, Andersen ZJ, Atkinson RW, Bauwelinck M, Bellander T, et al. Long-term exposure to low-level ambient air pollution and incidence of stroke and coronary heart disease: a pooled analysis of six European cohorts within the ELAPSE project. *Lancet Planet Health.* (2021) 5:e620–e32. doi: 10.1016/S2542-5196(21)00195-9

54. Makar M, Antonelli J, Di Q, Cutler D, Schwartz J, Dominici F. Estimating the causal effect of low levels of fine particulate matter on hospitalization. *Epidemiology.* (2017) 28:627–34. doi: 10.1097/EDE.0000000000000690

55. Last JA. Global atmospheric change: potential health effects of acid aerosol and oxidant gas mixtures. *Environ Health Perspect.* (1991) 96:151–7. doi: 10.1289/ehp.9196151

frontiers | Frontiers in Public Health

TYPE Original Research
PUBLISHED 06 April 2023
DOI 10.3389/fpubh.2023.1122139



OPEN ACCESS

EDITED BY
Xiaodong Yang,
Xinjiang University, China

REVIEWED BY
Chenyang Yu,
Guangzhou University, China
Chuanwang Sun,
Xiamen University, China
Yang Yu,
Hainan University, China
Yantuan Yu,
Guangdong University of Foreign Studies, China
Zhou Liang,
Shanghai Jiao Tong University, China

*CORRESPONDENCE
Shilei Hu
✉ yiruodongchuan@163.com

SPECIALTY SECTION
This article was submitted to Environmental health and Exposome, a section of the journal Frontiers in Public Health

RECEIVED 12 December 2022
ACCEPTED 06 March 2023
PUBLISHED 06 April 2023

CITATION
Feng Y, Gao Y, Zhu Y and Hu S (2023) How does national development zone policy affect carbon emissions in China? New evidence from a quasi-natural experiment. *Front. Public Health* 11:1122139. doi: 10.3389/fpubh.2023.1122139



# How does national development zone policy affect carbon emissions in China? New evidence from a quasi-natural experiment

Yanchao Feng[1], Yue Gao[1], Yuehua Zhu[1] and Shilei Hu[2]*

[1]Business School, Zhengzhou University, Zhengzhou, China, [2]School of Economics and Management, Harbin Institute of Technology, Weihai, China

The expansion of China's development zones has made great contributions to economic development, as well as provided practical guidance for other developing countries to implement development zone policies. However, in the context of global advocacy of low carbon, literature about how the development zone policy affect carbon emissions is poor, especially in China at the urban level. Therefore, this study takes China's development zone policy as a quasi-natural experiment, using the panel data of 285 cities in China from 2003 to 2020, and adopting the DID model to analyze its impact on carbon emissions. After a series of robustness tests including placebo test, dynamic test (all independent variables are lagged by one period), endogeneity test, and parallel trend test, the results are basically robust. The findings show that the development zone policy indeed significantly reduces carbon emissions. In addition, we find that cities with higher resource endowments, cities in the eastern and central regions, and other larger cities across the country have better carbon emissions reduction effects. To a certain extent, the research in this paper fills the gap of theoretical research on carbon emissions in terms of the development zone policy, and provides some practical basis for future research in the field of carbon emissions.

KEYWORDS

**national development zone policy, carbon emissions, spatial difference-in-differences model, quasi-natural experiment, spatial heterogeneity**

## 1. Introduction

The world's first special economic zone can be traced back to 1959, when the development zone in Shannon, Ireland, was established. Establishing the development zone has brought prosperity to the Irish economy (1). Since then, many countries worldwide have established various special economic zones similar to the development zone [(2–5); Frick et al., 2022]. In particular, China's first batch of national-level development zones was launched in 1984, which has rapidly promoted economic growth due to its unique advantages in management mechanisms, innovative elements, and preferential policies (6). It is widely known that China has the second largest economic system in the world (7), while there is no consensus on the factors driving sustainable economic development, especially in the field of policy evaluation (8). In fact, it is commonly known that national development zone strategy promotes economic development (9). The global economy has slumped in recent years due to the COVID-19 pandemic, and China's economy has also been significantly impacted at the same time, thus the outlook for export commerce situation is not promising. Fortunately, since China's population base is large and is located in a development zone, the Chinese people can alleviate the effects of the pandemic there,

allowing China's economy to continue to grow steadily despite the ongoing decline of the world economy (10–12).

Despite the fact that China has experienced significant economic growth in the recent decades (13), the rise in carbon emissions year after year casts doubt on this broad progress (14). China now ranks among the countries with the highest global carbon emissions (15). In contrast, China's carbon emissions in 2017 made up 28% of all carbon emissions worldwide (16). In addition, global carbon dioxide emissions increased in 2021 compared to 2020 by 4.8% (17). Global warming, caused by the recent rapid surge in carbon emissions, poses a serious threat to human sustainability (18). Therefore, the main challenge facing the Chinese government is to find solutions to balance the issues of economic development and environmental conservation (19). Against this background, in order to accept the international duty and foster the development of "a community with a shared destiny for mankind", Chinese President Xi proposes the program of "strive to peak carbon dioxide emissions by 2030 and strive to achieve carbon neutrality by 2060" in September 2020 (20).

The available literature on the effects of national development zone policy may generally be split into three categories including economy, society, and environment. As for the economy, the development zone has a significant economic impact on the city's technological innovation (21), and it may foster the growth of high-tech enterprises, encourage investment benefits, and broaden the region's economic base (22). In terms of social welfare, the development zone's economic expansion will unavoidably encourage regional growth, raise residents' quality of life, and further the completion of sanitary infrastructure (23). In addition, the level of employment, wealth, and happiness of the populace will rise locally (24). However, the development zone resembles an industrial cluster in terms of ecology. Sulfur dioxide, nitrogen dioxide, and industrial waste water, will be released as a result of mass production, which will take a lot of energy and fuel and which will cause serious damage to the ecological environment (25). At this time, the research how development zone policies affect carbon emissions is limited, which forms the initial incentive of this study, that is, to fill the research gap.

Has the implementation of the development zone policy reduced total carbon emissions? Evidence from a quasi-natural experiment in China. Research on the impact of development zone policies on carbon emissions based on DID model; Study the lagging effect of development zone policies; Analyze whether the effect of implementing development zone policies in different regions, cities of different sizes and different resource types in China is consistent; Study the spatial effects of development zone policies between pilot and non-pilot cities. Through the above correlation analysis, the mechanism of how the implementation of development zone policies and similar policies affects the total carbon emissions is systematically elaborated. It aims to provide guiding advice to developing countries like China. According to existing research findings, the DID model and its derivatives are frequently employed in the field of policy assessment due to their benefits in avoiding issues with endogeneity and omitted variable bias (26, 27). Due to China's unique characteristics, including its huge landmass and wealth of natural resources (28), there may be disparities in the extent of the effects of the development zone policy's implementation in various areas and cities. Additionally, the city's resource endowment will influence how the development zone policy performs (29). Moreover, this work takes into account the effect of policy upgrading or superposition on carbon emissions in order to further illustrate the research scenario (30). In order to examine the effects of development zone policies on urban carbon emissions, this study seeks to arrange development zone policies as a collection of quasi-natural experiments, and employs the DID model as a benchmark regression approach (31). The propensity score matching DID model (PSM-DID model) (32) is used to around the DID model's limitations. Furthermore, the spatial difference model (SDID) is also employed to detect the probable existence of spatial spillover effects (33).

Two characteristics of this study can be used to infer its key contributions (33). Theoretically, research on the effects of development zone rules now focuses majorly on the effects on the economic scale and economic development of the city, while the research on the impacts of the policies on the urban environment is uncommon. In order to conceptually fill the gap left by the absence of this module. We put the development zone policy and carbon emissions into a research framework, and comprehensively analyzed the relationship between the development zone policy and carbon emissions from both static and dynamic perspectives by using various methods. This research has significant worldwide guiding relevance for other emerging nations as well as significant practical meanings for the creation and optimization of development zones including high-tech zones and economic development zones, etc. Practically, this study divided the entire sample into subgroups according to geographic location, urban scale, and resource endowment of the city, which enriches the application value of policy recommendations.

The remainder of the study is organized as follows to maintain its integrity. Section 2 presents and summarizes earlier related studies in a concise manner, and constructs the theoretical mechanism. Section 3 describes the economic model and related variables. Section 4 examines the empirical results and some robustness tests. Section 5 covers the diversity of city location, scale and resource donation, and tests the SDID model and policy upgrading and superposition effects. Section 6 summarizes the research results, offers guidance, and identifies future directions for further study.

## 2. Literature review and theoretical mechanism

The literature review is divided into four sections: The first part provides an overview of the current literature on carbon emissions; The second part analyzes the literature on the economic effects of development zone policies; The third part provides a brief summary of the research literature on the environmental effects of development zone policies; The forth part, through the research of relevant literature, the theoretical mechanisms of the development zone policy's effect on carbon emission are sorted out.

## 2.1. Literature on carbon emissions

As is common knowledge, energy use and carbon emissions are intimately correlated with human activity. Especially, population mobility has a major negative impact on carbon emissions in regions where people live (34, 35). Mobility of the population will unavoidably result in frequent use of transportation, which uses a lot of fossil fuels and raises carbon emissions. In the transportation sector, intelligent mobility can significantly reduce carbon emissions (36). Economic manufacturing will raise carbon emissions in cities, which is another significant element affecting China's industrial development. Some academics contend that while economic progress aids in the rationalization of industrial structure and carbon emissions, the upgrading and optimization of industrial structure has a detrimental effect on carbon emissions (19, 37).

China has a significant agricultural sector, thus its influence on carbon emissions cannot be understated. Research on the steadily rising rural carbon emissions in China's provinces discovered that the provinces closest to the ministry created the most emissions (38). Numerous academics have studied how the use of science and technology in diverse areas influences carbon emissions in light of China's tremendous advancement. Some academics state that China's total carbon emissions are somewhat increasing due to low innovation efficacy of green technology (39, 40). Also, some scholars think that the advancement of green technology benefits the research and creation of renewable resources. Eventually, it has a major detrimental influence on carbon emissions, but has less of an effect in the short term (41). Science and technology advancements encourage the development of digital technology, and these advancements can decrease carbon emissions as a result of their positive knock-on effects (42). According to the study, China's embedded carbon emissions from 2002 to 2017 were significantly impacted negatively by factors relating to the production structure of the digital economy (43).

## 2.2. Literature on the influence of development zone policy on the economy

We can assume that when we talk about the development zone, we are talking about development-related information. Therefore, the focus of this research material is on the development and economic development zones, as well as on how these development zones impact affect the local economy. According to some academics, the creation of development zones can, in some cases, encourage industrial agglomeration, boost industrial productivity, and boost exports. Also, the upgrading strategy policy of development zones influences both imports and exports (44). Moreover, China's development zones have a variety of repercussions, the most notable of which is a considerable impact on nearby manufacturing businesses (45). The creation of the economic development zone serves as a foundation for improving the organization of the industrial land, maximizing its use, and providing a solid land guarantee for the industrial transfer of the manufacturing industry (46).

Development zones can boost investment effectiveness, increase financial openness, and enhance the region's overall economic growth in terms of fostering regional economy (47). Development initiatives strategies has considerably significant spillover and driving impacts and serves as a launchpad for communities to pursue innovation-driven development initiatives (46). Over time, the spillover impacts will differ in numerous ways, largely depending on the special zone's strategic development and policy objectives (48). By distributing resources fairly, the spillover effect can effectively encourage regional economic growth, and help close the economic development gap between regions (22). By maximizing the arrangement of public service facilities, the high-tech zone diversifies urban public service goals in order to better the city as a whole (49). At the macro level, it encourages regional economic growth, and at the micro level, it benefits business performance and the improvement of individual performance (50, 51).

## 2.3. Literature on the impact of development zone policies on the environment

Development zones influence our ecological environment to varied degrees in addition to having an effect on our economic development. Theoretically, the establishment of the development zone will attract a large number of industries to settle in these cities, since industrial manufacturing is an indispensable real economy in a city. Unfortunately, it contaminated the environment of the city in the process of creating the economy. According to Guo et al. (52), the industrial pollution index records an initial decline and a gradual rise with time. Furthermore, the research shows that industrial production will produce a large amount of polluting gases, the most important of which are sulfur dioxide and nitrogen dioxide (52). Simultaneously, the production of heavy industry produces a large amount of industrial wastewater. Palani et al. (53) explain that improper treatment of wastewater will cause pollution of water resources, and the long-term consequence is the decline in the quality of the ecological environment.

Arguably, developing digital industries and sustainable industries are critical skills that can be used to solve this problem. Some researchers hold that developing the digital economy will significantly reduce the industrial pollution (35). The argument is that the high-tech sector puts emphasis on progressing science and technology (54). Consequently, the upgrading of science and technology will improve the efficiency and quality of environmental pollution treatment (55). Because of the varying stages of development zones, the pollution situation after implementation is also very different. The formation of provincial-level development zones further aggravated China's contamination intensity, but rising to the national level, they no longer play the same role (56). Likewise, concerning the smog pollution in the nation, the provincial development zone policies significantly increased smog pollution. On the other hand, the national development zone policies have no significant effect (57).

Contrasting the development zones, the establishment of high-tech zones can improve the environment, and the increase of green patents and economic agglomeration are the mechanisms by which high-tech zones can improve the environment (47).

## 2.4. Theoretical mechanism

From the perspective of technological innovation, on the one hand, the establishment and construction of the development zone will attract a large number of high-tech enterprises (22), and at the same time, it will encourage local enterprises to carry out technological innovation activities and increase investment in innovative scientific research (26). High and new technology will improve the efficiency of production and manufacturing, meanwhile, it will increase the utilization rate of raw materials, promoting production efficiency and reducing the consumption of production resources and power resources (58), to achieve the effect of reducing carbon dioxide emissions. On the other hand, the establishment of the development zone will promote the development of emerging green industries such as high-end equipment manufacturing, new energy industries, and lead the direction of urban industrial transformation (59). With the acceleration of the industrial structure upgrading process led by the establishment of the development zone, the living space of the traditional "three high" industries in the city has been further reduced, and the vacated development space will be more occupied by strategic emerging green industries, which makes pollution-free, Clean and green production factors have been widely gathered and applied (60), it can also reduce carbon dioxide emission intensity and improve urban air quality.

From the perspective of resource allocation, on the one hand, the lower land price inside the development zone and related policy grants enable enterprises in the park to enjoy low supply of factors and ensure the continuity of normal production activities of enterprises (13, 61), to promote the efficiency of enterprise factor utilization. In addition, the complete infrastructure of the national development zone has successfully attracted foreign high-quality innovation capital, creating conditions for the emergence and development of high-end productive services (61). On the other hand, the high-end production factors attracted by the development zone can fully replace traditional production factors, promote the development of resource-intensive industries, and gradually reduce environmental pollution (62). To sum up, the optimization of resource allocation caused by the establishment of national development zones will help reduce undesired outputs in the industrial production process (63), and accordingly reduce carbon dioxide emissions.

From the perspective of the city's own conditions, under the background of the establishment of national development zones, there are large differences between different cities in terms of economic scale, innovation factor agglomeration capacity, resource allocation efficiency, and industrial policy formulation and implementation capacity (46). Generally speaking, regional economic development lags behind that of central cities (64). Under the guidance of the construction of ecological civilization, compared with other cities, the central city with stronger agglomeration ability of innovation elements can give full play to its advantages in terms of policy pilot, economic development scale and innovation element agglomeration, so as to achieve the transformation of economic development model (65). And the first-mover advantage of industrial structure adjustment, promote the full release of the potential of urban environmental improvement (66). Due to the relatively poor elements to promote the upgrading of the industrial structure and the poor external environment for industrial development, other cities have great potential and latecomer advantages in terms of environmental improvement capabilities (67). Through the construction of national-level development zone, such cities can obtain the technological spillover effect and high-end production factor agglomeration associated with the establishment of development zones, and fully release the vitality of urban industrial transformation (68), thereby enhancing the city's ability to improve environmental quality by adjusting its industrial structure.

From the perspective of spatial effects, in view of the spatial agglomeration and spatial differences in my country's environmental policies, institutional environment and energy structure, when examining the impact of the establishment of national development zones on local carbon dioxide emissions, the carbon emissions of neighboring cities should also be taken into account (69). In other words, we should fully consider the spatial spillover effect of policy. With the rapid development of country's digital information technology, cloud computing platform, and big data applications, industries in different cities are more closely connected (70). The development zone policy can not only rely on the transformation of the local energy structure to enhance the green total factor productivity and improve the quality of the urban environment (63), but also have a significant impact on the carbon dioxide emissions of adjacent cities (71). Namely, although the local carbon dioxide emissions have been reduced, their cost may be higher energy consumption in neighboring cities and lower urban environmental quality. In particular, to reveal the theoretical mechanism vividly, we have draw the framework of empirical steps and reported in Figure 1.

# 3. Empirical model

## 3.1. Empirical framework

After the creation of the initial group of development zones, the nation's policies have always maintained development as an essential objective. Pilot areas of development zones across China were the large-scale cities. It is clear that the development brought to the cities caused economic growth and betterment of science and technology. Consumption of resources is another causal factor for economic growth, the consumption of resources is at the expense of the environment, which will bring large emissions of greenhouse gases, such as the total carbon emissions of cities. Research holds that the development of science and technology can ease this occurrence. Theoretically, the use of advanced technology will lower the total carbon emissions of the city. In this regard, this paper considers development zone policies as a set of quasi-natural experiments. The paper also relies on the DID model to assess how development zone policies impact carbon emissions. For this

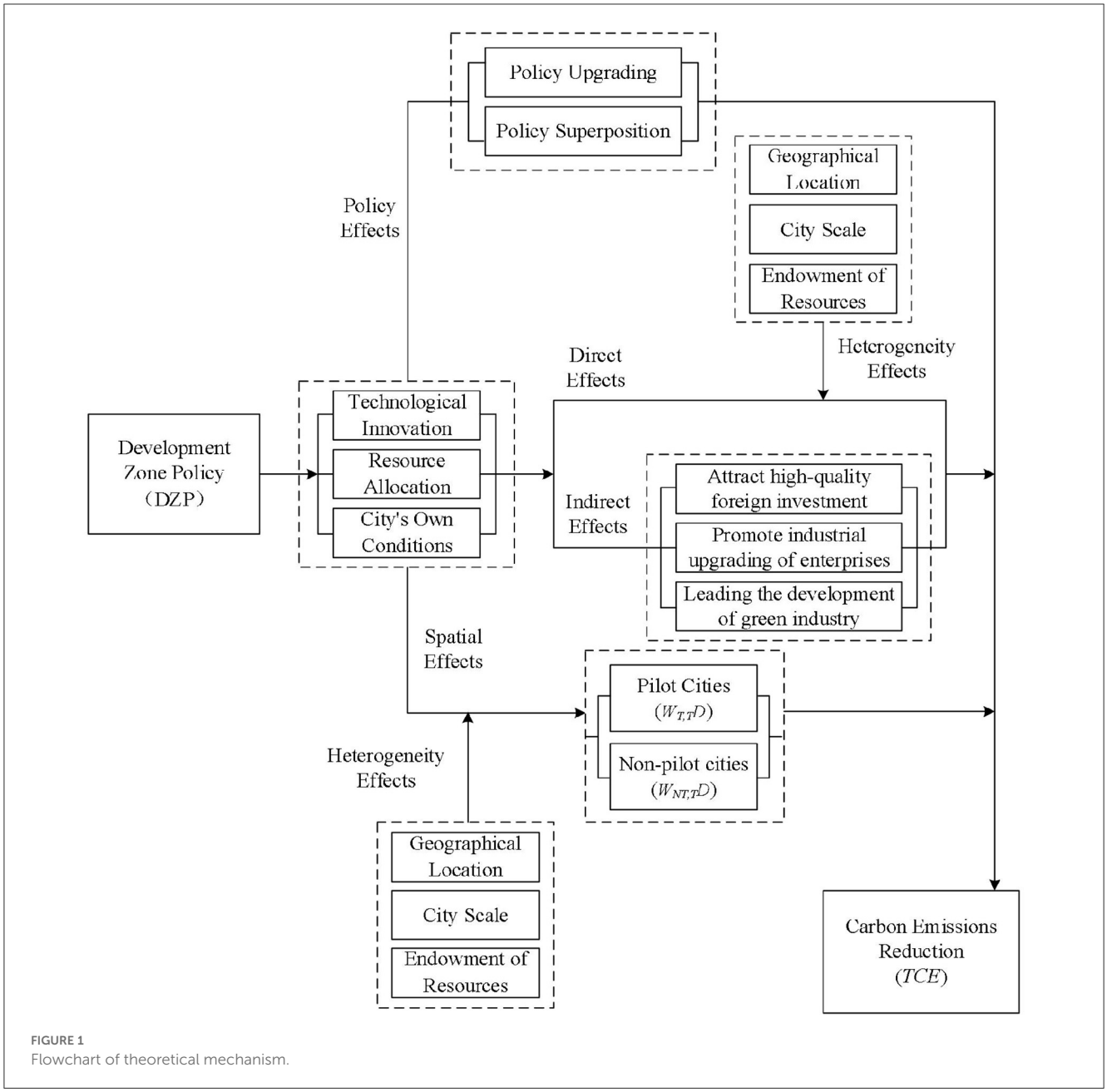


FIGURE 1
Flowchart of theoretical mechanism.

research, pilot cities were listed as the experimental group while the non-pilot cities were the control group. Since the development zone pilots are conducted in different years, a multi-phase DID model will be used. The following is the formula for the multi-period DID model:

$$TCE_{it} = \alpha_0 + \alpha_1 DZP_{it} + \beta X_{it} + \lambda_i + \lambda_t + \mu_{it} \quad (1)$$

Where the subscripts $i$ and $t$ represent city and year, $TCE$ is the total carbon emissions of the city, $DZP$ represents the dummy variable about the status of the policy implementing, $X$ is a series of control variables, $\lambda_i$ denotes the individual effect, $\lambda_t$ denotes the time fixed effect, $\alpha_1$ is the DID estimator, indicating the net effect of policy on total carbon emissions, $\beta$ is the coefficient of control variables, $\mu$ is the random disturbance term, $\alpha_0$ is the constant term. $DZP_{it}$ is the dummy variable, representing a city's development zone policy implementing status. More specifically, $DZP_{it}$= 1 if city $i$ implemented the development zone policy during the sample period, and 0 otherwise.

In addition, we constructed a PSM-DID model for correlation robustness checks because the DID model is not ideal in addressing the problem of sample selection bias. In addition, the model can make the more actual test in line with the theory. Using the model, we can more accurately measure if development zone policies can effectively affect the city's total carbon emissions. The specific theoretical model is as follows:

$$TCE_{it}^{PSM} = \alpha_0 + \alpha_1 DZP_{it} + \beta X_{it} + \lambda_i + \lambda_t + \mu_{it} \quad (2)$$

Furthermore, a spatially extended form of the DID model to SDID model based on Equation (1) was used to analyze the spatial spillover effects of policy further. The following is the formulated form of this extended model:

$$TCE_{it} = \alpha_0 + \alpha_1 DZP_{it} + \beta X_{it} + \beta_1 \times W_{T,T} D_{it} + \beta_2 \times W_{NT,T} D_{it} + \beta_3 \times W \times X_{it} + \lambda_i + \lambda_t + \mu_{it} \quad (3)$$

Where $W$ is the spatial weight matrix, $W_{T,T}D_{it}$represents the spatial spillover effects among pilot cities, $W_{NT,T}D_{it}$designates the spatial spillover result of pilot cities on non-pilot cities which neighbor pilot cities, $W \times X_{it}$ is the spillover effects of control variables. $\beta_1$ is the spatial coefficient of $W_{T,T}D_{it}$, $\beta_2$ is the spatial coefficient of $W_{NT,T}D_{it}$, and $\beta_3$ is the spatial coefficient of $W \times X_{it}$.

Last but not least, it should be pointed out that the DID model satisfies the parallel trend test. In other words, levels of carbon emission from pilot and non-pilot cities must not differ systematically over time. According to the approach of Jacobson and Sullivan (72), by constructing a series of temporal dummy variables, a temporal analysis research framework is used to analyze the dynamic influence of the application of development zone policies on urban carbon emissions. Consequently, we create a dynamic analysis model as formulated below:

$$TCE_{it} = \alpha_0 + \sum_{t\text{-}5}^{t+5} \alpha_t DZP_{it} + \beta X_{it} + \lambda_i + \lambda_t + \mu_{it} \quad (4)$$

Among them, *DZP* represents the dummy variable of the years before and after the realization of the development zone policy. $DZP_0$ is the dummy variable of the year when the city enforces the development zone policy; $DZP_{t-n}$ is the dummy variable of $n$ years before the implementation of the development zone policy; $DZP_{t+n}$ is the dummy variable of $n$ years after the enforcement of the development zone policy; other variables are constant as in the case of Equation (1).

## 3.2. Data and variables

Panel datasets and IPE research reports of 285 cities in China provide the sample data. The data period was scanning from 2003 to 2020. Other data sources included several official national statistical documents like the China Urban Construction Statistical Yearbook, the China Urban Yearbook, and the China Statistical Yearbook. After the disruption, all minor indicators are adjusted to the constant price in 2003 as per the provincial price index.

### 3.2.1. Dependent variable

The total carbon emissions is the dependent variable. To prevent double counting, the annual consumption of various types of energy in each city was subtracted from the input and loss of energy processing and conversion process and industrial production as raw materials, and the net consumption of 285 cities was obtained. As per the regulations stipulated in the 2006 IPCC Guidelines for National Greenhouse Gas Inventories issued by the IPCC Panel on Climate Change (IPCC), carbon emissions from fossil fuel combustion are projected from the amount of fuel burned and default emission factors. When calculating urban carbon emissions as explained by Zhang et al. (73), the consumption of three energy sources is mainly considered. These energy sources are liquefied petroleum gas (*LPG*) represented by $LCO_2$, natural gas (*NGas*) represented by $NCO_2$, and electricity (*ET*) represented by $ECO_2$. Below is the formula for calculating the total carbon emissions:

$$CO_2 = LCO_2 + NCO_2 + ECO_2 = \sigma_1 LPG + \sigma_2 NGas + \sigma_3 (k \times ET) \quad (5)$$

Where $\sigma_1$ represents the carbon emission factor of LPG with a value of 3.1013 kg/m$^3$; $\sigma_2$ stands for the carbon emission factor of *NGas* with a value of 2.1622 kg/m$^3$; $\sigma_3$ represents the carbon emission factor of the coal-fired fuel chain, equal to 1.3023 kg/kW carbon emissions; $\kappa$ is the ratio of coal-fired power generation to total power generation.

### 3.2.2. Key independent variable

In this study, we chose $DZP_{it}$ as the key dependent variable, which is a dummy variable that describes the application status of development zone policies in pilot cities. When $DZP_{it}$= 1, it means that the ith pilot city began to implement the development zone policy in t, and the rest of the cases are 0. Specifically, from 2008 to 2012, a total of 113 cities implemented the development zone policy. After 2013, by 2020, a total of 7 cities implementing the development zone policy will be added, for a total of 120 pilot cities. Due to the non-uniform nature of policy timing points, multi-period DID was used for correlation analysis.

### 3.2.3. Control variables

Studies conducted previously by other researchers (74, 75), explain that to prevent omission of small variables related to the level of total carbon emissions, we need various control variables. For this study, the control variables are: (1) Foreign direct investment (*FDI*): expressed by the ratio of foreign direct investment to GDP. (2) Urban rate (*UR*): expressed by the ratio of the urban population to the total population of the city (3) Per capita GDP (*PGDP*): expressed by logarithmic form of per capita GDP; (4) Finance Decentralization (*FD*): expressed by the form of the ratio of fiscal expenditure to fiscal revenue; (5) Population density (*DENSTY*): expressed by logarithmic form of the ratio of the total urban population to the urban administrative area; (6) Industrial upgrading (*IU*): expressed by the ratio of the total industrial value of the secondary industry to GDP and the ratio of the total output value of the tertiary industry to GDP.

This paper gives relevant statistical descriptions of independent variables, dependent variables and control variables. The number of valid samples is 5,130, and the mean, standard deviation, minimum and maximum values of each variable are statistically described. The specific details are shown in Table 1.

10.3389/fpubh.2023.1122139

TABLE 1 Descriptive statistics.

| Variables | Observations | Mean | S.D. | Min | Max |
|---|---|---|---|---|---|
| *TCE* | 5,130 | 25.988 | 23.617 | 1.529 | 230.712 |
| *DZP* | 5,130 | 0.472 | 0.499 | 0.000 | 1.000 |
| *lnPGDP* | 5,130 | 10.252 | 0.837 | 7.545 | 13.056 |
| *lnDENSITY* | 5,130 | 5.726 | 0.916 | 1.547 | 7.923 |
| *FD* | 5,130 | 2.814 | 1.869 | 0.649 | 18.399 |
| *IU* | 5,130 | 0.933 | 0.512 | 0.094 | 5.348 |
| *UR* | 5,130 | 0.495 | 0.174 | 0.078 | 1.000 |
| *FDI* | 5,130 | 0.022 | 0.025 | 0.000 | 0.376 |

TABLE 2 Benchmark regression results.

| Variables | TCE | |
|---|---|---|
| | (1) | (2) |
| *DZP* | −1.390** | −1.057* |
| | (0.603) | (0.553) |
| *lnPGDP* | | −0.469 |
| | | (1.346) |
| *lnDENSITY* | | 12.252*** |
| | | (4.387) |
| *FD* | | −0.651*** |
| | | (0.156) |
| *IU* | | 2.024*** |
| | | (0.739) |
| *UR* | | 8.132** |
| | | (3.497) |
| *FDI* | | −30.376*** |
| | | (11.613) |
| City fixed | Yes | Yes |
| Year fixed | Yes | Yes |
| Observations | 5,130 | 5,130 |
| R-squared | 0.966 | 0.968 |

Robust standard errors in parentheses, ***, **, and * indicate significance at the 1, 5, and 10% levels, respectively.

# 4. Empirical analysis

## 4.1. Benchmark regression test

It is important to note the regression analysis is conducted on the primary variables first then other overall variables in the results of the regression analysis are shown in Table 2. From column (1), it is found that the coefficient of the key variable *DZP* is −1.390. The coefficient reaches a significant level of 5%, indicating that the implementation of the development zone policy is conducive to the reduction of the total carbon emissions of the pilot cities. Column (2) of the table indicates that with the upsurge of the control variables, the coefficient of *DZP* and the significance test do not change considerably. These results mean that control variables have the very minimal effect on the total carbon emissions of the pilot cities. This conclusion is consistent with Gao et al. (76), whose research on the impact of development zones on carbon emissions, and the establishment of development zones has a positive impact on the city's carbon emission performance. Table 2 also shows that in the control variables, *FD*, *FDI* and the total carbon emissions of the pilot cities have the positive relationship of change. On the other hand, *lnPGDP*, *lnDENSITY*, *IU*, *UR* and the total carbon emissions of the pilot cities have an inverse relationship of change relating to the total carbon emissions of the pilot cities.

## 4.2. Robustness test

Several robustness tests were necessary to demonstrate the robustness of the results gotten from the regression tests on the core results. These robustness tests included PSM-DID model evaluation, endogeneity test, dynamic effect analysis, parallel trend test, placebo test, and other test removing municipalities that can prove robustness of regression analysis. Based on the results from a series of analysis the core results have strong robustness. In other words, the effect of development zone policies in pilot cities on the total carbon emissions is very significant.

### 4.2.1. Parallel trend test

According to the parallel trend test of carbon emissions related to special economic zones by existing scholars (50), he believes that after the establishment of new special economic zones, the trend of per capita carbon emissions is consistent with that before the policy impact. This means that the assumption of parallel trends is valid. After the impact of relevant policies, carbon emissions show a significant downward trend, which further indicates that the establishment of new special economic zones will have a negative impact on the carbon emissions of cities. As a kind of special economic zone, whether the development zone has the same parallel trend of carbon emissions. This paper also conducts a parallel trend test for this problem. The test results are shown in the following figure.

The horizontal axis in Figure 2 represents the years before and after the implementation of the development zone policy. On the other hand, the vertical axis on the same figure depicts its correlation coefficient. For example, $t$-4 represents the 4th year before the policy implementation, and $t$+4 represents the 4th year after the policy implementation.

In Figure 2, from year $t$-5 to year $t$ of the policy execution, the coefficients all contain 0 values within the 95% confidence interval. These results indicate that the development zone policy when implemented and not enforced in the cities have the same time trend and that the effect of the policy on the carbon emissions is insignificant From year $t$+1 to year $t$+5 of the policy execution, all coefficient values in the 95% confidence interval are $<0$. Likewise, this nature shows that enforcing the development zone policy in pilot cities and non-enforced cities share the same trend. Consequently, carbon emissions decreased significantly during

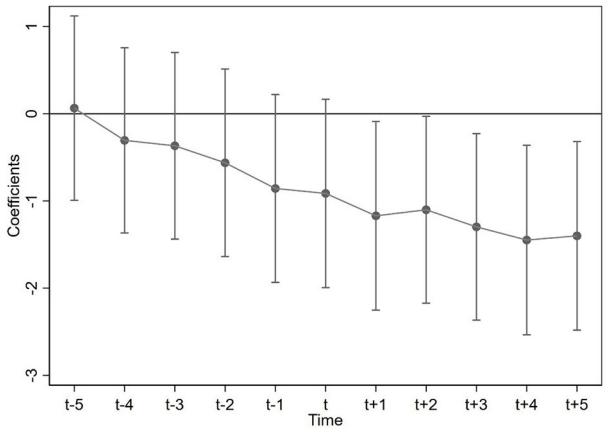


FIGURE 2
Parallel trend test chart.

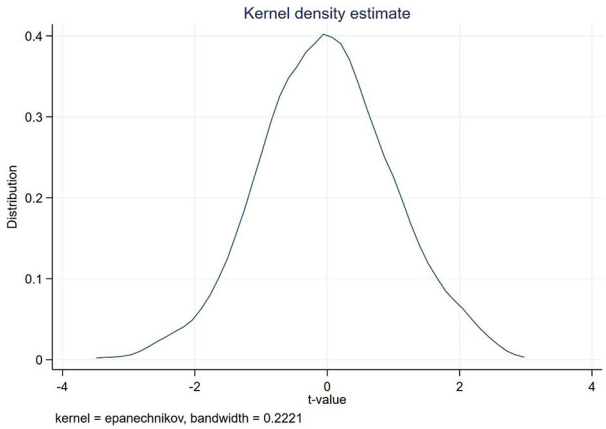


FIGURE 3
Placebo test chart.

this time period because of the enactment of the development zone policy in the cities. Thus, this test holds and satisfies the parallel trend hypothesis of this study. Over the period of 5 years after implementation of the development zone policy in these cities, there was a gradual decrease of the coefficient value for key independent variable. Before the policy was implemented, the coefficient value was smaller showing that the implementation of the development zone policy has a significant inhibitory effect on the total carbon emissions.

## 4.2.2. Placebo test

Referring to the placebo test conducted by scholars (77) on the impact of national independent innovation demonstration zones on urban carbon emissions, according to the number of pilot cities launched each year, the same number of cities were randomly selected as the experimental group to construct a dummy variable baseline model. Perform 1,000 and 2,000 repeated regressions on the data. This article discusses how development zone policies affect carbon emissions. We adopted the placebo test to try and evade situations like sample selection bias (38). Specifically, there were 113 cities from 2008 to 2012, that executed the development zone policy. Later in 2013, 7 cities were added in 2020 year, for a total of 120 pilot cities for the study. Through the period from 2008 to 2020, there are 5,130 – 1,525 = 3,605 data samples in the control group and 113 × 5 + 120 × 8 = 1,525 data samples in all experimental groups. We randomly selected 113 cities that implemented the development zone policy from 2008–2020 to collect data. To collect data from the second group of cities, we also randomly selected 7 cities that did not implement the development zone policy from 2013 to 2020 as cities that implemented the development zone policy. In total, 120 cities were randomly selected as the treatment group for the placebo experiment. As shown in Figure 3, the vertical axis represents the corresponding *p*-value while the horizontal axis represents the t value of the development zone policy. The overall figure shows that the distribution is roughly centered at 0. Most of the *p*-values are >0.1, and the absolute value of the corresponding *t*-value is <2. Results from this test analysis support that the effect of our development zone policy on the total carbon emissions is not affected by the omitted variables.

TABLE 3 PSM-DID regression results.

| Variables | TCE | |
|---|---|---|
| | (1) | (2) |
| *DZP* | −1.739*** | −1.693*** |
| | (−6.237) | (−6.144) |
| Control variables | No | Yes |
| City fixed | Yes | Yes |
| Year fixed | Yes | Yes |
| Observations | 4,695 | 4,695 |
| R-squared | 0.942 | 0.945 |

Robust standard errors in parentheses, *** indicates significance at the 1% level.

## 4.2.3. PSM-DID assessment

During this study, we relied on research methods of existing literature and use PSM-DID to conduct robustness tests. This approach allowed us to avoid systematic differences among cities that do not implement policies and cities that implement policies by reducing the estimation bias of the key variable *DZP*. The primary stages are as follows: first, conduct logit regression on the control variables in the baseline model to get propensity scores; After that, use the non-pilot cities with the most alike propensity scores as the paired objects for the pilot cities; third, use the DID model to approximate the paired sample cities. As shown in Table 3, from the approximation results, the coefficients before the key variable *DZP* are all negative, from the comparison of the (1) and (2) columns, the coefficient values are very approximative when considering and not considering the control variables. These results indicate that the application of the development zone policy has successfully lowered the total carbon emissions. Conclusively, we hold that the core results have strong robustness.

TABLE 4 Dynamic test results.

| Variables | TCE | |
|---|---|---|
| | (1) | (2) |
| *L.DZP* | −1.122** | −0.845* |
| | (0.523) | (0.482) |
| Control variables | No | Yes |
| City fixed | Yes | Yes |
| Year fixed | Yes | Yes |
| Observations | 4,845 | 4,845 |
| R-squared | 0.973 | 0.974 |

Robust standard errors in parentheses, ** and * indicate significance at the 5 and 10% levels, respectively.

TABLE 5 Endogenous test results.

| Variables | DZP | TCE |
|---|---|---|
| | (1) | (2) |
| *IV* | −0.002*** | |
| | (−2.981) | |
| *DZP* | | −54.703*** |
| | | (−3.210) |
| Control variables | Yes | Yes |
| City fixed | Yes | Yes |
| Year fixed | Yes | Yes |
| Observations | 5,130 | 5,130 |
| R-squared | 0.732 | – |

Robust standard errors in parentheses, *** indicates significance at the 1% level.

### 4.2.4. Dynamic effect test

Because economic and social development have a certain inertia, the impact on economic operation after the implementation of the policy will not be immediate. It is probable that the impact of applying the development zone policy will be many periods or a one-period lag. For this study we only factor the likely effect of the policy with one-period lag on the total carbon emissions of the city. In essence, we considered the dynamic effect for the research. So, we set the one-period lagged core variable as *LDZP* and re-regressed it in the study with all control variables with one-period lag. Results of these modifications are displayed in Table 4. According to the test data of the core variable *LDZP*, the application of the development zone policy still affects the total carbon emissions in the cities. Through the comparison of Tables 2, 4, it is found that majority of the independent variable coefficients still have high consistency, and their significance is slightly different, and it is obvious that the lagging policy effect is not significant.

### 4.2.5. Endogeneity test

To alleviate endogeneity problems, this paper conducts research using the instrumental variable (*IV*) approach. For the assortment of the instrumental variable, refer to the research ideas as discussed by Zhang et al. (78). Ming Dynasty post stations were the national postal and postal transportation system in ancient times. These stations have unique benefits in logistics transportation and information transmission while simultaneously bringing prosperity to the regional economy and development of the nation. It follows that the layout of post stations and the number of these stations have an effect on the economic development of the region, and may also have a relationship with the existing economic development. Consequently, it conforms to the endogenous principle. It is worth noting that there is no direct relationship between the post stations in the Ming Dynasty and the current carbon emissions. Because the Ming Dynasty post station has a long time span, and there is no reasonable relationship between the Ming Dynasty post station and carbon emissions. In this sense, Ming Dynasty post stations satisfy the principle of exogenous assumptions. Keeping in mind that the Ming Dynasty Post Station is already an existing and unchanging historical data, it cannot be directly inserted into the panel baseline model. To overcome this problem, we introduced the number of modern taxis in the city as an instrumental variable and sets the interactive term of the number of post stations in the Ming Dynasty and, denoted by *IV*. The following formulas are established based on Equations (1) and (2):

$$\begin{aligned} DZX_{it} &= \omega_0 + \omega_1 IV + \omega_2 x_{it} + \gamma_i + \gamma t + \varepsilon_{it} TCE_{it} \\ &= \varphi_0 + \varphi_1 \widetilde{DZP}_{it} + \varphi_2 X_{it} + \nu_i + \nu_t + \xi_{it} \end{aligned} \quad (6)$$

Equation (6) is the regression of the first stage. The core explanatory variable is represented by *DZP* represents while the instrumental variable is represented by *IV*; Equation (7) is the final regression result. The *DZP* with a wavy line is a new variable column fitted by the first-stage regression. It combines the instrumental variable and the original core explanatory variable. Table 5 shows the final regression results. From the table, it is clear that the instrumental variable has no direct linkages with the total carbon emissions in the cities. As a result, these results are constant with the exogenous hypothesis. From the table, the absolute value implicated with the core variable *DZP* is small. Nonetheless, the absolute value still maintains a significant effect on the core variable *DZP* at the 1% significance level. In this regard, these results align with the endogeneity hypothesis analysis successfully tested endogeneity using carefully selected instrumental variables. However, these results do not show a direct relationship between the dependent variable and an instrumental variable. At the same time, there is an indirect impact on the dependent variable through the core variable *DZP*.

### 4.2.6. Other related test

Because of the different administrative levels from one city to the next, there is a need to eliminate the differential impact. We achieved it by eliminating the municipalities in the original sample cities, and using the remaining cities as a new sample (the four municipalities of Beijing, Shanghai, Tianjin, and Chongqing were excluded in the new sample). After that, the regression analysis as stipulated in the DID model is used to test data from the new

TABLE 6 Regression results for samples that remove municipalities.

| Variables | TCE | |
|---|---|---|
| | (1) | (2) |
| *DZP* | −1.420** | −1.080* |
| | (0.603) | (0.554) |
| Control variables | No | Yes |
| City fixed | Yes | Yes |
| Year fixed | Yes | Yes |
| Observations | 5,058 | 5,058 |
| R-squared | 0.954 | 0.957 |

Robust standard errors in parentheses, ** and * indicate significance at the 5 and 10% levels, respectively.

sample. Results of these tests are depicted Table 6. *DZP*, as the primary variable, remains consistent with the core results, while the absolute value of the coefficient is slightly smaller. These results support the fact that application of the development zone policies in cities result in a decline in total carbon emissions in these regions.

# 5. Further analysis

## 5.1. Heterogeneity test

According to relevant literature (32, 79), it is found that China's industrial carbon dioxide emissions have different emission standards due to different local policies and environmental requirements. Therefore, it is important to note that development zone policies may have varying effects from one city to the next. This phenomenon is caused by factors like large differences in the resource endowments of cities, different urban scales and different geographic locations. These variances are shown in Table 7, columns (1), (2), and (3) show the effect on the total carbon emissions after enforcing the development zone policy in the eastern, central and western pilot cities, respectively. Based on the analysis, development in the central region is balanced and implementation of the development zone policy at this point causes more effect on the decline of carbon emissions. The eastern region in China is relatively developed and the development zone policy is implemented early. Despite these efforts, the marginal effect of the policy is fading, from the current stage, the policy effect is not ideal. The western region in the country is least developed in terms of economy, science and technology, making it too backward in comparison. Therefore, it is essential to hasten the development of these sectors and eventual implementation of the development zone policy. As shown in the table, the implementation of the policy resulted in the slight increase in urban carbon emissions. Columns (4) represents the impact of the implementation of the development zone policy on the total carbon emissions in small cities, column (5) represents the impact of the implementation of the development zone policy on the total carbon emissions in medium cities and column (6) represents the impact of the implementation of the development zone policy on the total carbon emissions in large cities. The conclusion we made is that the larger the city scale, the more beneficial it is to reduce the total carbon emissions. Columns (7) represents the impact of the implementation of development zone policies in resource-based cities on the total carbon emissions. Column (8) represents the impact of the implementation of development zone policies in non-resource-based cities on the total carbon emissions. Conclusively, the enforcement of the development zone policy in non-resource-based cities has a very obvious effect on lowering the total carbon emissions of the city. Conversely, implementing the development zone policy increases the total carbon emissions in resource-based cities.

## 5.2. SDID test analysis

Possibly, there is a spatial connection between carbon emissions and neighboring cities. Neglecting this spatial correlation may cause inconsistent findings when comparing the theoretical results and actual results of the study. To prevent this inconsistency, the spatial impact of implementing development zone policy pilots and the spatial dependence of carbon emissions were taken into account in the model, and the SDID model was used for analysis. The results are shown in Table 8.

Column (1) and column (2) prove that the application of the development zone policy has a spatial effect on the total carbon emissions of neighboring cities. Absolute values of the coefficients of variables $W_{NT,T}D$, $W_{T,T}D$, and *DZP*, are very large and they all reach the 1% significance level. From column (1), it is conclusive that regardless of whether control variables are considered, the development zone policy has the spatial effect of the total carbon emissions of surrounding cities. On the other hand, the coefficient of *DZP* is significantly negative. In other words, the development zone policies can significantly reduce the total carbon emissions. The coefficient of $W_{NT,T}D$ is significantly negative, indicating that the spatial effect of the development zone policy pilot cities reduces total carbon emissions in neighboring non-pilot cities. On the other hand, the coefficient of $W_{T,T}D$ is significantly positive, indicating that the spatial effect of the pilot cities of development zone policy increases the total carbon emissions of the neighboring pilot cities. This condition may be implicated with the variances in economic scale, the policy implementation and the administrative levels between pilot cities and non-pilot cities. According to Guo et al. (52), whose research stands there are indeed geographical proximity effects and spatial spillover effects between cities in China. This effect is more pronounced between cities that are spatially closer.

## 5.3. Effect test about upgrading and superposition of the policy

To further improve the accuracy of the study, we factored if the upgrading and superposition of policies will still have the same impact on the total carbon emissions as the core results. The results of the regression analysis are shown in Table 9. The policy upgrading effect of the pilot city's upgrading to the national high-tech zone policy from the provincial high-tech zone policy is Column (1). *DZP_up*1 represents the core

TABLE 7 Heterogeneity test results.

| Variables | TCE | | | | | | | |
|---|---|---|---|---|---|---|---|---|
| | Geographical location | | | City scale | | | Endowment of resources | |
| | Eastern | Central | Western | Small | Medium | Large | Resource | Non-resource |
| | (1) | (2) | (3) | (4) | (5) | (6) | (7) | (8) |
| *DZP* | −0.784 | −1.933** | 0.061 | 0.472 | 0.539 | −2.241** | 1.130 | −2.223*** |
| | (0.946) | (0.771) | (1.021) | (0.961) | (0.526) | (0.871) | (0.733) | (0.689) |
| City fixed | Yes | Yes | Yes | Yes | Yes | Yes | Yes | Yes |
| Year fixed | Yes | Yes | Yes | Yes | Yes | Yes | Yes | Yes |
| Control variables | Yes | Yes | Yes | Yes | Yes | Yes | Yes | Yes |
| Observations | 1,818 | 1,800 | 1,512 | 896 | 1,801 | 2,397 | 2,070 | 3,060 |
| R-squared | 0.976 | 0.953 | 0.961 | 0.948 | 0.976 | 0.978 | 0.956 | 0.974 |

Robust standard errors in parentheses, *** and ** indicate significance at the 1 and 5% levels, respectively.

TABLE 8 The regression results are based on the SDID model.

| Variables | TCE | |
|---|---|---|
| | (1) | (2) |
| *DZP* | −5.804*** | −5.033*** |
| | (1.165) | (1.052) |
| $W_{T,T}D$ | 5.252*** | 4.759*** |
| | (1.618) | (1.478) |
| $W_{NT,T}D$ | −3.888*** | −3.441*** |
| | (1.248) | (1.197) |
| Control variables | No | Yes |
| City fixed | Yes | Yes |
| Year fixed | Yes | Yes |
| Observations | 5,130 | 5,130 |
| R-squared | 0.968 | 0.970 |

Robust standard errors in parentheses, *** indicates significance at the 1% level.

TABLE 9 Policy upgrade and superposition test results.

| Variables | TCE | | | |
|---|---|---|---|---|
| | P to N | P to N | N plus N | N plus N |
| | (1) | (2) | (3) | (4) |
| *DZP_up*1 | −2.891** | | | |
| | (1.426) | | | |
| *DZP_up*2 | | −0.131 | | |
| | | (0.962) | | |
| *DZP_sp*1 | | | −2.745* | |
| | | | (1.439) | |
| *DZP_sp*2 | | | | −0.665 |
| | | | | (0.761) |
| Control variables | Yes | Yes | Yes | Yes |
| City fixed | Yes | Yes | Yes | Yes |
| Year fixed | Yes | Yes | Yes | Yes |
| Observations | 3,030 | 2,881 | 2,423 | 2,423 |
| R-squared | 0.953 | 0.948 | 0.981 | 0.981 |

Robust standard errors in parentheses, ** and * indicate significance at the 5 and 10% levels, respectively.

variable with its coefficient being −2.891 and a significance level of 5%. These results show that upgrading the high-tech zone policy considerably helps to lessen the total carbon emissions. The second column is the policy upgrading effect of the pilot cities' upgrading to the national-level economic development zone policy from the provincial-level economic development zone policy. *DZP_up*2 represents the core variable and its coefficient is −0.131. These results show that upgrading the economic development zone policy causes a minor decrease in the total carbon emissions.

The policy superposition effect of the pilot cities is Column (3). The superposition effect first applies to the national economic development zone policy and then to the national high-tech zone policy. *DZP_sp*1 represents the core variable. Its coefficient is −2.745 with a 10% significance level. These figures show that the superposition of such policies has a relatively clear lessening impact on the total carbon emissions of the pilot cities. Column (4) is the policy superposition effect of the pilot cities first executing the national high-tech zone policy and then executing the national economic development zone policy. The core variable is represented by *DZP_sp*2, and its coefficient is −0.665. These figures support that the superposition of such policies has a feeble impact on the total carbon emissions in the cities. Contrasting column (1), (2), (3), and (4), shows that the high-tech zone policy has more effect than the economic development zone policy in the cities. Contrasting the two columns (1) and (2), shows that the upgrade of the high-tech zone policy has a more significant and clear impact in terms of reducing the total carbon emissions compared to the upgrade of the economic development zone policy. Comparing the two columns (3) and (4), shows that shifting to a national high-tech zone from a national economic development zone can decrease the total carbon emissions of pilot cities more

than shifting to a national economic development zone from a national high-tech zone.

# 6. Conclusions and research prospects

## 6.1. Conclusions

By analyzing the results of the study, five main conclusions can be drawn: first, the implementation of the development zone policy can effectively reduce the total carbon emissions of the city; Second, the development zone policy that lags behind a single cycle can still significantly reduce the total carbon emissions of cities; Third, the implementation of development zone policies for cities, larger cities and non-resource cities in the central region has a better effect on carbon reduction than other cities; Fourth, there is a spatial effect on the impact of development zone policies on carbon emissions. Its spatial effect reduces the total carbon emissions of neighboring non-pilot cities and increases the total carbon emissions of neighboring pilot cities. Fifth, there are upgrading and overlapping effects in the implementation of relevant policies. Whether it is upgrading or superimposing, the carbon reduction effect of the high-tech zone policy is better than that of the economic development zone.

## 6.2. Policy implications

The following policy suggestions are put forward based on the above discussions: First, the development zone policy can effectively reduce the total carbon emissions, which means that the formulation of relevant policies can successfully achieve a balance between the ecological environment and economic development, which is a positive measure toward optimizing the ecological environment. Therefore, developing countries similar to China that face similar environmental optimization in the process of urbanization can vigorously promote the construction of development zones. Second, there is a single-period lag effect in the implementation of the development zone policy, which means that there is a single-cycle buffer time for the implementation of relevant policies. Therefore, the government should fully consider the time inconsistency of the policy and the final policy results when formulating relevant policies. The third suggestion is the selection of development zone policies suitable for local cities while considering the city's scale, resource endowment, and geographical location while promoting the inclusive development of the local cities in a targeted manner to evade the variance in the effect of development zone policies on carbon emissions. The western region of China is comparatively backward in technology. However, this region has abundant natural resources and a large urban area. The country's western development project has been advancing in recent years and it is arguable that the region is more conducive for the development zone policies. Science technology and natural resources are ample in the central region of China, thus it is necessary to choose and implement appropriate high-tech zone policies to coordinate the overall development and balance the requirements of development and economy. In the eastern part of China, there is a high population density, technological development and advanced economic development. Moreover, the majority of cities in eastern China are closer to the sea, hence, development of foreign trade is a primary advantage for these urban areas. With this in mind, local economic and technological development is arguably reliant on the development zone policies. Forth, the local government should try to reduce the impact of the spatial effect in the implementation of the development zone policy in response to the spatial effect among cities. The central government is responsible for strictly checking the policy effect of each region, establishing strict regulated rules, and issuing relevant deployment documents. The local governments are implicated with conducting implementations of the policies to categorize regional responsibilities and interests, further preventing any pollution transfer. Finally, according to the research results, the central government should vigorously support the construction of high-tech economic development zones in local areas as much as possible, take innovation as the driving force for sustainable development, and create a win-win development pattern of economic development and ecological protection.

## 6.3. Research prospects

Some of the limitations discovered during the research of this paper may encourage future research on relating subjects. To begin with, bias may have arose during the calculations of industrial carbon emissions because of the limited data on the subject. The aim is to attain an inclusive measure of the environmental efficiency. Thus, we included industrial carbon emissions as one of the undesirable outputs. Nonetheless, as per the "China Urban Statistical Yearbook", we can only analyze the carbon dioxide emissions from three energy sources, that is, natural gas, electricity and liquefied petroleum gas. And so, the results can be altered or protracted in the future using newer or alternative data sources. The second limitation is that the endogeneity analysis lacked some sample data for the tests. The instrumental variable consists of the number of stations in a city and the product of the number of taxis. Unfortunately, we only managed to collect data for most cities, while we could not get data from other cities because of the limited data collection methods available and limited research. In other words, in all the 285 sample cities used for this study, there are missing data. It follows that this missing data needs to be collected to facilitate supplementary verification. Lastly, we use the dummy variable *DZP* to represent the core variable because the PITI (pollution source supervision information disclosure index) standard used by the 113 pilot cities from 2008 to 2012 is different from the PITI standard used by the 120 pilot cities from 2013 to 2020. The variance in PITI intensity between the two times is not definitely distinguished in terms of treatment. In future, more unified and reliable standards can enhance the study of the effect of national development zone policy on carbon emissions.

# Data availability statement

The raw data supporting the conclusions of this article will be made available by the authors, without undue reservation.

## Author contributions

YF: conceptualization, methodology, and formal analysis. YG: data curation, writing—original draft, visualization, and investigation. SH: writing—review and editing, supervision, and resources. YZ: software, data, and variables. All authors contributed to the article and approved the submitted version.

## Funding

This research was supported by the youth program of the high-end science and technology innovation think tank of the Chinese Association for Science and Technology (Grant No. 2021ZZZLFZB1207131), the Program for Science and Technology Innovation Talents in the Universities of the Henan Province (Grant No. 2021-CX-018), and the Postdoctoral Research Foundation of China (Grant No. 2022M720131).

## Acknowledgments

The authors are grateful to the editor and reviewers for their critical suggestions of this manuscript.

## Conflict of interest

The authors declare that the research was conducted in the absence of any commercial or financial relationships that could be construed as a potential conflict of interest.

## Publisher's note



## References

1. Zeng DZ. The past, present, and future of special economic zones and their impact. *J Int Econ Law.* (2021) 24:259–75. doi: 10.1093/jiel/jgab014

2. Kusago T, Tzannatos Z. *Export Processing Zones: A Review in Need of Update*. Social Protection Group, Human Development Network. Washington, DC: The World Bank (1998).

3. Ritchie BK. Coalitional politics, economic reform, and technological upgrading in Malaysia. *World Dev.* (2005) 33:745–61. doi: 10.1016/j.worlddev.2005.01.006

4. Alkon M. Do special economic zones induce developmental spillovers? Evidence from India's states. *World Dev.* (2018) 107:396–409. doi: 10.1016/j.worlddev.2018.02.028

5. Rodríguez-Pose A, Bartalucci F, Frick SA, Santos-Paulino AU, Bolwijn R. The challenge of devel Special Economic Zones in Africa: evidence and lessons learnt. *Regional Sci Policct.* (2022) 14:456–81. doi: 10.1111/rsp3.12535

6. Yang L, Luo X, Ding Z, Liu X. Restructuring for growth in development zones, China: a syste literature and policy review (1984–2022). *Land.* (2022) 11:97 doi: 10.3390/land11070972

7. Jenkins R. *How China Is Reshaping the Global Economy*. Oxford: Oxford University Press (2022).

8. Fang X, Zou J, Wu Y, Zhang Y, Zhao Y. Evaluation of the sustainable development of an island "Blue Economy": a case study of Hainan, China. *Sustainable Cities Soc.* (2021) 66:102662. doi: 10.1016/j.scs.2020.102662

9. Deng X, Liang L, Wu F, Wang Z. A review of the balance of regional development in China from the perspective of development geography. *J Geogr Sci.* (2022) 32:3–22. doi: 10.1007/s11442-021-1930-0

10. Yan Y, Wang X. Global contraction and local strengthening of firms' supply and sales logistics netwon the context of covid-19: evidence from the development zones in weifang, china. *PRS Int J Geo Information.* (2021) 10:477. doi: 10.3390/ijgi10070477

11. Wang X, Wang L, Zhang X, Fan F. The spatiotemporal evolution of COVID-19 in China and its impacurban economic resilience. *China Econ Rev.* (2022) 74:10 doi: 10.1016/j.chieco.2022.101806

12. Yang G, Zhang F, Zhang F, Ma D, Gao L, Chen Y, et al. Spatiotemporal changes in efficiency and influg factors of China's industrial carbon emissions. *Environ Sci Pollut Res.* (202136288–302. doi: 10.1007/s11356-021-13003-8

13. Xi Q, Sun R, Mei L. The impact of special economic zones on producer services productivity: evidence from China. *China Econ Rev.* (2021) 65:101558. doi: 10.1016/j.chieco.2020.101558

14. Wu L, Zhu Q. Impacts of the carbon emission trading system on China's carbon emission peak: a new data-driven approach. *Natural Hazards.* (2021) 107:2487–515. doi: 10.1007/s11069-020-04469-9

15. Liu J, Yu Q, Chen Y. The impact of digital technology development on carbon emissions: a spatial effect analysis for China. *Resources Conserv Recycling.* (2022) 185:106445. doi: 10.1016/j.resconrec.2022.106445

16. Zhang J. Environmental Kuznets curve hypothesis on CO2 emissions: evidence for China. *J Risk Financ Manage.* (2021) 14:93. doi: 10.3390/jrfm14030093

17. Liu Z, Deng Z, Davis SJ, Giron C, Ciais P. Monitoring global carbon emissions in 2021. *Nat Rev Earth Environ.* (2022) 3:217–9. doi: 10.1038/s43017-022-00285-w

18. Banerjee S, Sharma H, Hazra S. *Green Energy Solution to Combat Global Warming//Bio-Clean Energy Technologies*, Vol. 2. Singapore: Springer (2022). p. 1–11.

19. Feng J, Wang N, Sun G. Measurement of innovation-driven development performance of large-scale environmental protection enterprises investing in public–private partnership projects based on the hybrid method. *Sustainability.* (2022) 14:5096. doi: 10.3390/su14095096

20. Xiong Y, Luo Y. Will green development increase the cost of debt financing for heavily polluting companies? *Modern Econ.* (2022) 13:545–65. doi: 10.4236/me.2022.134029

21. Jia L, Hu X, Zhao Z, He B. How environmental regulation, digital development and technological innovation affect China's green economy performance: evidence from dynamic thresholds and system GMM panel data approaches. *Energies.* (2022) 15:884. doi: 10.3390/en15030884

22. Wang Z, Yang Y, Wei Y. Has the construction of national high-tech zones promoted regional economic growth?-Empirical research from prefecture-level cities in China. *Sustainability.* (2022) 14:6349. doi: 10.3390/su14106349

23. Wang G. Evaluation and analysis of high quality economic development indicators by the Analytic Hierarchy Process Model. *Sci Program.* (2022). doi: 10.1155/2022/1042587

24. Yi X, Jue W, Huan H. Does economic development bring more livability? Evidence from Jiangsu province, China. *J Clean Prod.* (2021) 293:126187. doi: 10.1016/j.jclepro.2021.126187

25. Wu G. *Practice of Water Pollution Control in Small Watershed—Taking Taiping River, Shuangqiao Economic Development Zone, Chongqing, China as an Example* (2022). Available online at: scholar.archive.org

26. Yu H, Jiang Y, Zhang Z, Shang WL, Han C. The impact of carbon emission trading policy on firms' green innovation in China. *Financ Innovat.* (2022) 8:55. doi: 10.1186/s40854-022-00359-0

27. Yu X, Wan K. How does the selection of national development zones affect urban green innov?-Evidence from China. *PLoS ONE.* (2022) 17:e01. doi: 10.1371/journal.pone.0268111

28. Wang R, Zhao X, Zhang L. Research on the impact of green finance and abundance of natural resouon China's regional eco-efficiency. *Resources Policy.* (2022) 76:10 doi: 10.1016/j.resourpol.2022.102695

29. Qian Y, Liu J, Cheng Z, Forrest JYL. Does the smart city policy promote the green growth of the urban economy? Evidence from China. *Environ Sci Pollut Res.* (2021) 28:66709–23. doi: 10.1007/s11356-021-15120-w

30. Guo X, Xiao B, Song L. Emission reduction and energy-intensity enhancement: The expected and unexpected consequences of China's coal consumption constraint policy. *J Clean Prod.* (2020) 271:122691. doi: 10.1016/j.jclepro.2020.122691

31. Zhou G, Liu C, Luo S. Resource allocation effect of green credit policy: based on DID model. *Mathematics.* (2021) 9:159. doi: 10.3390/math9020159

32. Wang Z, Wu M, Li S. The effect evaluation of China's energy-consuming right trading policy: empirical analysis based on PSM-DID. *Sustainability.* (2021) 13:11612. doi: 10.3390/su132111612

33. Li C, Zhang J, Lyu Y. Does the opening of China railway express promote urban total factor produty? New evidence based on SDID and SDDD model. *Socioecon Plann Sci.* (2022) 80:10 doi: 10.1016/j.seps.2022.101269

34. Bu Y, Wang E, Qiu Y. Impact assessment of population migration on energy consumption and carbon emissions in China: a spatial econometric investigation. *Environ Impact Assess Rev.* (2022) 93:106744. doi: 10.1016/j.eiar.2022.106744

35. Chen L, Li X, Yang Y, Wang M. Analyzing the features of energy consumption and carbon emissions in the upper Yangtze river economic zone. *Greenhouse Gases Sci. Technol.* (2021) 11:573–89. doi: 10.1002/ghg.2067

36. Zhao C, Wang K, Dong X. Is smart transportation associated with reduced carbon emissions? The case of China. *Energy Econ.* (2022) 105:105715. doi: 10.1016/j.eneco.2021.105715

37. Feng Y, Wu H. How does industrial structure transformation affect carbon emissions in China: the mting effect of financial development. *Environ Sci Pollut Res.* (2022) 29:1377. doi: 10.1007/s11356-021-16689-y

38. Zhang H, Li S. Carbon emissions' spatial-temporal heterogeneity and identification from rural energy consumption in China. *J Environ Manage.* (2022) 304:114286. doi: 10.1016/j.jenvman.2021.114286

39. Yu Y, Zhang N. Environmental regulation and innovation: evidence from China. *Global Environ Change.* (2022) 76:102587. doi: 10.1016/j.gloenvcha.2022.102587

40. Zeng S, Li G, Wu S, Dong Z. The impact of green technology innovation on carbon emissions in the context of carbon neutrality in China: evidence from spatial spillover and nonlinear effect analysis. *Int J Environ Res Public Health.* (2022) 19:730. doi: 10.3390/ijerph19020730

41. Kuang H, Akmal Z, Li F. Measuring the effects of green technology innovations and renewable energy investment for reducing carbon emissions in China. *Renewable Energy.* (2022) 197:1–10. doi: 10.1016/j.renene.2022.06.091

42. Liu Z, Deng Z, He G, Wang H, Zhang X, Lin J, et al. Challenges and opportunities for carbon neutrality in China. *Nat Rev Earth Environ.* (2022) 3:141–55. doi: 10.1038/s43017-021-00244-x

43. Wang J, Dong X, Dong K. How digital industries affect China's carbon emissions? Analysis of the d and indirect structural effects. *Technol Soc.* (2022) 68:10 doi: 10.1016/j.techsoc.2022.101911

44. Ouyang X, Mao X, Sun C. Industrial energy efficiency and driving forces behind efficiency improvement: evidence from the Pearl River Delta urban agglomeration in China. *J Clean Prod.* (2019) 220:899–909. doi: 10.1016/j.jclepro.2019.02.206

45. Wang Y. Development zone spillover effect: the externality of the gathering of manufacturing enterprises//E3S Web of Conferences. *EDP Sci.* (2021) 251:01006. doi: 10.1051/e3sconf/202125101006

46. Yang S, Liu W, Zhang Z. The dynamic value of China's high-tech zones: direct and indirect influence on urban ecological innovation. *Land.* (2022) 11:59. doi: 10.3390/land11010059

47. Kong Q, Li R, Peng D. High-technology development zones and innovation in knowledge-intensive service firms: evidence from Chinese a-share listed firms. *Int Rev Financ Anal.* (2021) 78:101883. doi: 10.1016/j.irfa.2021.101883

48. Howell A. Heterogeneous impacts of China's economic and development zone program. *J Reg Sci.* (2019) 59:797–818. doi: 10.1111/jors.12465

49. Peng J, Liu Y, Ruan Z. *Study on the Optimal Allocation of Public Service Facilities From the Perspective of Living Circle—A Case Study of Xiangyang High-Tech Zone, China* (2022). doi: 10.21203/rs.3.rs-1825476

50. Chen J, Long X, Lin S. Special economic zone, carbon emissions and the mechanism role of green technology vertical spillover: evidence from Chinese cities. *Int J Environ Res Public Health.* (2022) 19:11535. doi: 10.3390/ijerph191811535

51. Chen S, Liu X. Innovation spillovers in production networks: evidence from the establishment of nal high-tech zones. *China Econ Q Int.* (2022) 2:42-doi: 10.1016/j.ceqi.2022.03.001

52. Guo Y, Tong L, Mei L. Evaluation and influencing factors of industrial pollution in Jilin restricted development zone: a spatial econometric analysis. *Sustainability.* (2021) 13:4194. doi: 10.3390/su13084194

53. Palani G, Arputhalatha A, Kannan K, Lakkaboyana SK, Hanafiah MM, Kumar V, et al. Current trends in the application of nanomaterials for the removal of pollutants from industrial wastewater treatment—a review. *Molecules.* (2021) 26:2799. doi: 10.3390/molecules26092799

54. Dong F, Pan Y, Li Y. How public and government matter in industrial pollution mitigation performance: evidence from China. *J Clean Prod.* (2021) 306:127099. doi: 10.1016/j.jclepro.2021.127099

55. Zhou Z, Liu J, Zhou N, Zhang T, Zeng H. Does the "10-Point Water Plan" reduce the intensity of industrial water pollution? Quasi-experimental evidence from China. *J Environ Manage.* (2021) 295:113048. doi: 10.1016/j.jenvman.2021.113048

56. Jiang W, Cao K, Jin L, Cheng Y. How do China's development zones affect environmental pollution under government domination. *Sustainability.* (2022) 14:3790. doi: 10.3390/su14073790

57. Jin S. The promotion effect of development zone upgrade to local import and export//2021 2nd Asia-Pacific conference on image processing. *Electron Comput.* (2021) 2021:557–61. doi: 10.1145/3452446.3452582

58. Tsaramirsis G, Kantaros A, Al-Darraji I, Piromalis D, Apostolopoulos C, Pavlopoulou A, et al. A modern approach towards an industry 4.0 model: From driving technologies to management. *J. Sensors.* (2022). doi: 10.1155/2022/5023011

59. Tao Y, Li M. *2017 Annual report on the development of special economic zones in China//Annual Report on the Development of China's Special Economic Zones (2019).* Singapore: Springer (2022). p. 13–28.

60. Zhou G, Zhang Z, Fei Y. How to evaluate the green and high-quality development path? An FsQCA approach on the China pilot free trade zone. *Int J Environ Res Public Health.* (2022) 19:547. doi: 10.3390/ijerph19010547

61. Jumaniyazov IT, Hazratov B. Foreign experience in the development of special economic zones in Uzbekistan. *Sci. Educ.* (2022) 3:1628–36. Available online at: https://openscience.uz/index.php/sciedu/article/view/3625

62. Liu K, Qiao Y, Zhou Q. Analysis of china's industrial green development efficiency and driving factors: research based on MGWR. *Int J Environ Res Public Health.* (2021) 18:3960. doi: 10.3390/ijerph18083960

63. Jiang Y, Wang H, Liu Z. The impact of the free trade zone on green total factor productivity—Evidence from the shanghai pilot free trade zone. *Energy Policy.* (2021) 148:112000. doi: 10.1016/j.enpol.2020.112000

64. Cheng D, Xue Q, Hubacek K, Fan J, Shan Y, Zhou Y, et al. Inclusive wealth index measuring sustainable development potentials for Chinese cities. *Global Environ Change.* (2022) 72:102417. doi: 10.1016/j.gloenvcha.2021.102417

65. Wang Y. Development characteristics, influencing mechanism and coping strategies of resource-based cities in developing countries: a case study of urban agglomeration in Northeast China. *Environ Sci Pollut Res.* (2022) 29:25336–48. doi: 10.1007/s11356-021-17820-9

66. Li G, Zhou X, Bao Z. A win–win opportunity: the industrial pollution reduction effect of digitonomy development—a quasi-natural experiment based on the "Broadband China" strategy. *stainability.* (2022) 14:5583. doi: 10.3390/su14095583

67. Yang G, Gong G, Luo Y, Yang Y, Gui Q. Spatiotemporal characteristics and influencing factors of to–urbanization–technology–ecological environment on the Yunnan–Guizhou–Sichuan region: an uncooted coupling perspective. *Int J Environ Res Public Health.* (2022) 19:88 doi: 10.3390/ijerph19148885

68. Li L, Li M, Ma S, Zheng Y, Pan C. Does the construction of innovative cities promote urban greenvation? *J Environ Manage.* (2022) 318:1. doi: 10.1016/j.jenvman.2022.115605

69. Yang Z, Li S, Sun D, Li C. Intensive evaluation and high-quality redevelopment of enterprise land a case study in China. *Land.* (2022) 11:43 doi: 10.3390/land11030432

70. Jiang D. The construction of smart city information system based on the internet of things and cloud computing. *Comput Commun.* (2020) 150:158–66. doi: 10.1016/j.comcom.2019.10.035

71. Wen L, Chatalova L, Gao X. Reduction of carbon emissions through resource-saving and environment-friendly regional economic integration: Evidence from Wuhan metropolitan area, China. *Technol Forecast Soc Change.* (2021) 166:120590. doi: 10.1016/j.techfore.2021.120590

72. Jacobson LS, LaLonde RJ, Sullivan DG. Earnings losses of displaced workers. *Am Econ Rev.* (1993) 1993:685–709. doi: 10.17848/wp92-11

73. Zhang H, Xu T, Feng C. Does public participation promote environmental efficiency? Evidence from si-natural experiment of environmental information disclosure in China. *Energy Econ.* (2022:105871. doi: 10.1016/j.eneco.2022.106244

74. Azam M, Uddin I, Khan S, Tariq M. Are globalization, urbanization, and energy consumption cause carbon emissions in SAARC region? New evidence from CS-ARDL approach. *Environ Sci Pollut Res.* (2022) 2022:1–18. doi: 10.1007/s11356-022-21835-1

75. Martínez YU, Arzoz PP, Arregui IZ. Tax collection efficiency in OECD countries improves via decentralization, simplification, digitalization and education. *J Policy Model.* (2022) 44:298–318. doi: 10.1016/j.jpolmod.2022.03.003

76. Gao S, Sun D, Wang S. Do development zones increase carbon emission performance of China's cities? *Sci Total Environ.* (2023) 863:160784. doi: 10.1016/j.scitotenv.2022.160784

77. Fang L, Tang H, Mou M. *Has the Construction of National Independent Innovation Demonstration Zones Reduced the Urban Carbon Emissions? A Quasi-Natural Experiment in China* (2022). doi: 10.21203/rs.3.rs-1520158

78. Zhang Z, Sun Z, Lu H. Does the e-commerce city pilot reduce environmental pollution? Evidence from ities in China. *Front Environ Sci.* (2022) 2022: doi: 10.3389/fenvs.2022.813347

79. Wang Q, Zhao C. Regional difference and driving factors of industrial carbon emissions perfoe in China. *Alexandria Eng J.* (2021) 60:30 doi: 10.1016/j.aej.2020.08.009

frontiers | Frontiers in Ecology and Evolution

TYPE Original Research
PUBLISHED 20 July 2023
DOI 10.3389/fevo.2023.1156981



OPEN ACCESS

EDITED BY
Chengpeng Lu,
Lanzhou University, China

REVIEWED BY
Baogui Xin,
Shandong University of Science and Technology, China
Haoming Guan,
Northeast Normal University, China
Pengyan Zhang,
Henan University, China

*CORRESPONDENCE
Fei Lu
wfuctlf2022@163.com

RECEIVED 02 February 2023
ACCEPTED 06 July 2023
PUBLISHED 20 July 2023

CITATION
Lu F, Ren H and Zhai X (2023) Regional differences and spatio-temporal convergence of environmental regulation efficiency in the Yellow River Basin, China. *Front. Ecol. Evol.* 11:1156981. doi: 10.3389/fevo.2023.1156981



# Regional differences and spatio-temporal convergence of environmental regulation efficiency in the Yellow River Basin, China

Fei Lu[1]*, Huaiguo Ren[2] and Xinglong Zhai[1]

[1]College of Culture and Tourism, Weifang University, Weifang, China, [2]Editorial Department of Journal, Weifang University, Weifang, China

Environmental regulation efficiency facilitates environmental governance performance assessment, ecological protection, and high-quality development. Herein, based on the panel data of 75 cities in the Yellow River Basin from 2007 to 2020, this paper constructed an evaluation index system and measured the environmental regulation efficiency using a super-EBM hybrid distance model. We analyzed the regional differences and dynamic evolution characteristics of environmental regulation efficiency with the help of Dagum's Gini coefficient decomposition and kernel density estimation methods. Furthermore, a spatial econometric model explored the spatio-temporal convergence of environmental regulation efficiency. The main findings show that the environmental regulation efficiency of the overall Yellow River Basin and the upper, middle, and lower reaches showed an increasing trend with significant within-region spatial differences. The differences between all regions had a narrowing trend. The primary source of spatial differences in environmental regulation efficiency was the intensity of transvariation. The dynamic evolution characteristics of environmental regulation efficiency in different regions were quite different, and the spatial polarization phenomenon was more evident in the upper reaches. Except for the overall Yellow River Basin, all regions existed $\sigma$ convergence. The results of spatial convergence estimation indicated absolute and conditional $\beta$ convergence in all regions. The findings provide a factual reference for policies related to establishing policy systems for environmental regulation efficiency and green coordinated development in similar regions of the world.

KEYWORDS

**environmental regulation efficiency, super-EBM model, regional differences, dynamic evolution, spatio-temporal convergence, the Yellow River Basin**

# 1 Introduction

The Yellow River Basin is a distinct geographical region that spans China's three gradient terrains and economic belts, serving as a significant ecological barrier and a key region to defeat poverty in China (Zeng and Hu, 2021). In recent years, the Chinese government has placed the ecological protection and high-quality development of the Yellow River Basin at a prominent national strategic position. It has continued to strengthen environmental regulations, resulting in significant results in eco-environmental protection in the Yellow River Basin. From 2007 to 2020, the total investment in environmental pollution control in nine provinces and regions along the Yellow River in China rose from 5.086 billion USD to 24.144 billion USD, an average annual growth of 1.466 billion USD. However, the Yellow River Basin still faces problems such as a fragile ecological background, severe environmental pollution, and inefficient resource utilization (Liu and Ma, 2020; Zhang and Zhang, 2020). The needs of people continue to vary on how the ecological environment is being improved. According to the 2020 China Ecological and Environmental Bulletin released by the Ministry of Ecology and Environment, 15 of the 20 cities with relatively poor ambient air quality in China are in the Yellow River Basin, indicating that although environmental quality in the basin has improved, its governance performance is not satisfactory. In this context, it is necessary to explore the current development of environmental regulation efficiency in the Yellow River Basin as a whole and by region. However, due to natural and economic factors vary among regions in the Yellow River Basin, there are certain differences in environmental regulation efficiency between regions. So where do the differences originate? What are the evolution characteristics of regional differences in environmental regulation efficiency? Is there any spatial convergence in environmental regulation efficiency among regions? Addressing the above questions can improve our understanding of the current situation and the fundamental characteristics of environmental regulation efficiency in the Yellow River Basin and help us grasp the evolution of the spatial pattern of environmental regulation efficiency, so as to promote relevant research on environmental regulation efficiency in theory and provide a reference basis for the collaborative construction of an environmental regulation system in the Yellow River Basin in practice.

Environmental regulation improves environmental quality and ensures public interest by intervening in the behavior of pollution emission externalities of economic subjects. Implementing environmental regulation for pollution control should consider the technical and economic feasibility. Therefore, as reflected in environmental regulations, good environmental performance must be achieved by relying on the efficiency of pollution control. Facing the growing contradiction between economic development and environmental protection, the role of government regulation in environmental activities has become increasingly apparent, and the concept of environmental regulation efficiency has been developed. Compared with general input–output efficiency, environmental regulation efficiency is the ratio of environmental benefits obtained by the government in exercising its public management function of environmental protection to environmental management costs and is an effective way to assess the performance of government environmental governance (Xue and Liu, 2010; Cheng et al., 2016; Cao, 2021). Environmental regulation efficiency highlights the magnitude of the environmental benefits derived from a particular cost input and measures the effectiveness of the regulation by its value. In recent years, with the continuous deepening of the world's attention to assessing the performance of environmental governance, relevant research on environmental regulation efficiency has become a hot topic in the academic community. Concerning the research on the theory of environmental regulation efficiency, the academic circle has done much productive work. Many scholars have combined the theory of cost-benefit analysis to provide theoretical explanations for environmental regulation efficiency (Erdogan, 2014; Riccardi et al., 2015). Sunstein argued that the cost–benefit analysis theory could promote significant changes in environmental regulation and the combination of environmental science and economics (Sunstein, 1996). Hamamoto constructed an evaluation index system of environmental regulation efficiency through the cost–benefit analysis theory to provide a reference basis for a scientific, reasonable, and comprehensive evaluation of environmental regulation efficiency (Hamamoto, 2006). As for the evaluation of environmental regulation efficiency, existing studies have mainly used the data envelopment analysis (DEA) method (Tang et al., 2017), the stochastic frontier analysis (SFA) method (Xu et al., 2021), the multi-factor comprehensive evaluation method (Cui et al., 2018), the cost elasticity coefficient method (Liu and Wang, 2009), and the data converting function method (Simões et al., 2010) to measure environmental regulation efficiency in terms of the number of environmental policies, the amount of pollution abatement, and the cost of operating pollution control facilities. DEA is widely used in measuring environmental regulation efficiency because it does not require an explicit functional form relating inputs and outputs. It involves the traditional DEA model (Xu et al., 2014; Cheng et al., 2016), the two-stage DEA model (Wu et al., 2017), the three-stage DEA model (Zeng and Niu, 2019), the Malmquist index approach (Tang et al., 2016), the SBM model (Wang and Ma, 2020; Dong and Han, 2021; Wang and Cheng, 2021; Sun et al., 2022a), and the super-SBM model (Huang and Shi, 2015; Yin et al., 2017; Ren et al., 2019).

Regarding regional differences in environmental regulation efficiency, the driving forces mainly include the level of economic development, industrial structure, market environment, urbanization, technology input, and openness to the outside world (Xu et al., 2014; Cheng et al., 2016; Ren et al., 2019). The research methods used to measure regional differences cover the spatial analysis techniques, the Gini coefficient, the indicator observation, and the kernel density estimation (Dong and Han, 2021; Xu et al., 2021). Jia et al. examined the regional differences in the environmental regulation efficiency of the Lanzhou–Xining urban agglomeration in the Yellow River Basin using spatial analysis techniques. They found that the main differences were regional (Jia et al., 2022). Ren et al. used the Gini coefficient to compare the internal differences in the environmental regulation efficiency in three major urban agglomerations in China and found that the Pearl River Delta showed the most apparent internal regional differences (Ren et al., 2019). Although indicators can be

observed visually and their differences compared, the spatial analysis techniques, traditional Gini coefficient, and indicator observation method cannot explain the sources of these differences. Wang and Cheng investigated the distribution dynamics of marine environmental regulation efficiency in China using kernel density estimation and pointed out that the internal differences were gradually increasing (Wang and Cheng, 2021). Kernel density estimation presents an intuitive explanation of the spatial distribution dynamics of environmental regulation efficiency, but it fails to take into account the distribution of the sub-samples and uses the mean value for the calculation, which leads to an averaging of the sample differences and reduces the accuracy of the results. The convergence of environmental regulation efficiency has gradually become the focus of research in economics and the environment as scholars continue to study it. Many scholars used the $\sigma$ convergence model (Li and Luo, 2016), $\beta$ convergence model (Piao, 2020), and club convergence model (Deng et al., 2021) to investigate the convergence of environmental regulation efficiency. Camarero et al. pointed out that both the most efficient countries for environmental regulation and the worst within the Organization for Economic Co-operation and Development (OECD) tend to form convergence clubs (Camarero et al., 2013). Some scholars have argued that there are spatial spillover effects and convergence in environmental regulation efficiency. Fredriksson and Millimet believed that the environmental regulation efficiency of all states in the United States has spatial spillovers and that the states with more efficient environmental regulations have a "demonstration effect" on their neighbors (Fredriksson and Millimet, 2002). Jia et al. identified both spatial spillover effects of environmental regulation efficiency and spatial $\beta$ convergence in the Lanzhou–Xining urban agglomeration (Jia et al., 2022).

Specific results have been achieved in studying environmental regulation efficiency, but several limitations exist. First, the measurement of environmental regulation efficiency mainly adopts the traditional radial DEA model or the non-radial SBM model. Both models have certain restrictions, which often lead to biased measurements of environmental regulation efficiency, thus affecting the scientificity and accuracy of the conclusion. Second, the study of regional differences mainly applies the traditional Gini coefficient method and cannot reveal the source of regional differences in environmental regulation efficiency. In contrast, the Dagum Gini coefficient method effectively solves this problem. Third, in the aspect of the research object, most of the current environmental regulation efficiency measurements are focused on countries (Tang et al., 2016), provinces (Xu et al., 2014), and urban agglomerations (Ren et al., 2019; Wang and Ma, 2020; Sun et al., 2022b). Less attention has been paid to the environmental regulation efficiency of the Yellow River Basin, which is a significant ecological barrier and a rapidly transmutating economic–environmental system in China. Finally, the spatio-temporal characteristics of environmental regulation efficiency are less widely explored, and spatial econometric models are seldom tested for their spatial spillover effects. Therefore, this paper introduces the super-EBM (epsilon-based measure) model containing the undesirable output to measure the environmental regulation efficiency of 75 prefecture-level cities in the Yellow River Basin from 2007 to 2020. Then, the Dagum Gini coefficient, kernel density estimation method, and spatial convergence model are used to analyze the regional differences, dynamic evolution characteristics, and spatio-temporal convergence of environmental regulation efficiency in detail. This paper also puts forward relevant policy suggestions to promote the environmental management of the Yellow River Basin in China under the strategy of ecological protection and high-quality development of the Yellow River Basin.

# 2 Materials and methods

## 2.1 Methods

### 2.1.1 Super-EBM model

A hybrid EBM model with both radial and non-radial information was proposed by Tone and Tsutsui (2010), which accounts for the influence of non-radial slack variables while retaining the majority of the original proportion information from the front projection value. In addition, it addresses the problem of inconsistent input and output element dimensions, allowing for a more accurate and valuable reflection of the efficiency of decision-making units (DMUs). Considering the ranking problem of undesirable output elements and decision units (Andersen and Petersen, 1993; Tone, 2011; Xie et al., 2018), the super-EBM model based on undesirable outputs is defined as follows (Zou et al., 2019):

$$\gamma^{\star} = \min \frac{\theta - \epsilon_x \sum_{i=1}^{m} \frac{w_i^- s_i^-}{x_{ik}}}{\varphi + \epsilon_y \sum_{r=1}^{s} \frac{w_r^+ s_r^+}{y_{rk}} + \epsilon_u \sum_{p=1}^{q} \frac{w_p^{u-} s_p^{u-}}{u_{pk}}}$$

$$\text{s.t.} \sum_{j=1}^{n} x_{ij}\lambda_j + s_i^- = \theta x_{i0},\ i = 1, 2, \ \ldots\ , m$$

$$\sum_{j=1}^{n} y_{rj}\lambda_j - s_r^+ = \varphi y_{i0},\ r = 1, 2, \ \ldots\ , s \tag{1}$$

$$\sum_{p=1}^{n} u_{pj}\lambda_j + s_p^{u-} = \varphi u_{pk},\ p = 1, 2, \ \ldots\ , q$$

$$\lambda_j \geq 0,\ s_r^+ \geq 0,\ s_i^- \geq 0,\ s_p^{u-} \geq 0$$

where $\gamma^{\star}$ represents the environmental regulation efficiency, $\lambda_j$ refers to the linear combination coefficient of DMU$_j$, $x_{ij}$, $y_{rj}$, and $u_{pj}$ represent the $i$-th input, $r$-th and $p$-th denote desirable output and undesirable output of DMU$_j$, respectively, $s_i^-$, $s_r^+$, and $s_p^{u-}$ represent slack variables, $\theta$ represents the radial planning parameter, $\epsilon_x$, $\epsilon_y$, and $\epsilon_u$ represent the non-radial weight of input, desirable output, and undesirable output, respectively.

### 2.1.2 Dagum Gini coefficient and its decomposition

Dagum decomposed the Gini coefficient into the contribution of within-region difference ($G_w$), between-region difference ($G_{nb}$), and the intensity of transvariation ($G_t$) (Dagum, 1997), which effectively solved problems such as the overlap of sample data.

The formula is as follows:

$$G = \frac{\sum_{j=1}^{k}\sum_{h=1}^{k}\sum_{i=1}^{n_j}\sum_{r=1}^{n_h}\left|y_{ji} - y_{hr}\right|}{2n^2\mu} \tag{2}$$

where $G$ represents the overall Gini coefficient, $y_{ji}$ is the environmental regulation efficiency of the city $i$ in region $j$, and $\mu$ is the average environmental regulation efficiency of all cities. The specific formulas of $G_w$, $G_{nb}$, and $G_t$ are as follows:

$$G_w = \sum_{j=1}^{k} G_{jj} p_j s_j \tag{3}$$

$$G_{jj} = \frac{\sum_{i=1}^{n_j}\sum_{r=1}^{n_j}\left|y_{ji} - y_{jr}\right|}{2n_j^2\overline{y_i}} \tag{4}$$

$$G_{nb} = \sum_{j=2}^{k}\sum_{h=1}^{j-1} G_{jh}(p_j s_h + p_h s_j) D_{jh} \tag{5}$$

$$G_t = \sum_{j=2}^{k}\sum_{h=1}^{j-1} G_{jh}(p_j s_h + p_h s_j)(1 - D_{jh}) \tag{6}$$

$$G_{jh} = \frac{\sum_{i=1}^{n_j}\sum_{r=1}^{n_h}\left|y_{ji} - y_{jr}\right|}{n_j n_h(\overline{y_i} + \overline{y_h})} \tag{7}$$

$$D_{jh} = \frac{(d_{jh} - p_{jh})}{(d_{jh} + p_{jh})} \tag{8}$$

$$d_{jh} = \int_0^{\infty} dF_j(y) \int_0^{y} (y - x) dF_h(x) \tag{9}$$

$$p_{jh} = \int_0^{\infty} dF_h(y) \int_0^{y} (y - x) dF_j(x) \tag{10}$$

where $p_j = n_j/n$, $s_j = n_j \quad \overline{y_j}/n\overline{y}$, $\overline{y_j}(\overline{y_h})$ represents the average environmental regulation efficiency of region $j(h)$, $d_{jh}$ represents the difference in gross environmental regulation efficiency influence between regions $j$ and $h$, and $p_{jh}$ represents the first-order moment of transvariation.

### 2.1.3 Kernel density estimation

Kernel density estimation is a highly representative method for examining the differences in particular geographic phenomena, which describes the distribution patterns of random variables by estimating their probability densities (Zhang et al., 2022). Suppose the density function of the random variable $X$ is $f(x)$, and the probability density at point $x$ is as follows:

$$f(x) = \frac{1}{nh}\sum_{i=1}^{n} K\left(\frac{x_i - \bar{x}}{h}\right) \tag{11}$$

where $K(\cdot)$ is the kernel density function, $n$ is the number of observations, $\bar{x}$ is the mean value of observation, and $h$ represents the bandwidth that determines the accuracy and smoothness of the kernel density curve.

### 2.1.4 $\sigma$ convergence

Sigma ($\sigma$) convergence indicates that the deviation of environmental regulation efficiency tends to decrease over time (Rezitis, 2010; Zhang et al., 2022). The coefficient of variation was used to measure the $\sigma$ convergence of environmental regulation efficiency in the Yellow River basin and different regions. The calculation formula is:

$$\sigma = \frac{\sqrt{\sum_{i}^{n_j}(ERE_{jt} - \overline{ERE_{jt}})^2/n_j}}{\overline{ERE_{jt}}} \tag{12}$$

where $ERE_{jt}$represents the environmental regulation efficiency of time $t$ in region $j$.

### 2.1.5 Spatial $\beta$ convergence

$\beta$ convergence is derived from neoclassical growth theory, including absolute $\beta$ and conditional $\beta$ convergence (Liu and Du, 2017; Bigerna et al., 2021; Ram, 2021; Shi et al., 2022). Absolute $\beta$ convergence refers to a gradual convergence to the same state of environmental regulation efficiency across cities over time, without considering external factors. Conditional $\beta$ convergence means that the environmental regulation efficiency of each region eventually converges to its respective steady state after controlling for other influencing factors. Considering the increasing flow of environmental resource factors between regions, it is necessary to incorporate spatial dependence in the convergence of environmental regulation efficiency in the Yellow River Basin. The absolute $\beta$ convergence of the spatial Durbin model (SDM) was built because it can degenerate into the spatial autoregressive model (SAR) and spatial error model (SEM). The proposed model is as follows:

$$\ln\left(\frac{ERE_{i,t+1}}{ERE_{i,t}}\right) = \alpha + \beta \ln(ERE_{i,t}) + \rho\sum_{j=1}^{n} W_{ij} \ln\left(\frac{ERE_{i,t+1}}{ERE_{i,t}}\right) + \theta\sum_{j=1}^{n} W_{ij} \ln(ERE_{i,t}) + \mu_i + \nu_t + \epsilon_{it} \tag{13}$$

The conditional $\beta$ convergence of SDM was further established. The control variables in this model include the level of economic development (GDP), industrial structure (INS), market environment (MKT), degree of economic openness (OPEN), and technological progress (TP). GDP is reflected by per capita GDP and promotes rapid economic development to the detriment of environmental benefits. INS is the secondary industry's ratio to GDP, increasing industrial pollutant emissions and degrading eco-environmental quality. MKT is expressed by the proportion of private and self-employed employment in total employment, and it can improve the government's decision-making system and reasonably allocate regulatory elements. OPEN is measured *via* foreign direct investment (FDI) to indicate the level of environmental regulation intensity thresholds. TP is characterized by the proportion of public budget expenditure on science and technology, and it stimulates the reduction of regulatory costs and

promotes productivity improvement. The conditional $\beta$ convergence of SDM can be expressed as follows:

$$\ln\left(\frac{ERE_{i,t+1}}{ERE_{i,t}}\right) = \alpha + \beta \ln\left(ERE_{i,t}\right) + \rho\sum_{j=1}^{n} W_{ij} \ln\left(\frac{ERE_{i,t+1}}{ERE_{i,t}}\right) + \theta\sum_{j=1}^{n} W_{ij} \ln\left(ERE_{i,t}\right) + \gamma X_{i,t+1} + \delta\sum_{j=1}^{n} W_{ij} X_{i,t} + \mu_i + \nu_t + \epsilon_{it} \quad (14)$$

where $\beta$ is the convergence coefficient, $\rho$, $\theta$, and $\delta$ are spatial coefficients, $W$ is the spatial weight matrix, $ERE_{it}$ and $ERE_{t+1}$ are the environmental regulation efficiency of region $i$ from $t$ to $t + 1$, $X_{it}$ is the control variable, $\alpha$ is the constant term, $\mu$ is the spatial fixed effect, $\upsilon_t$ is the time effect, and $\epsilon$ is the random error term.

## 2.2 Environmental regulation efficiency indicators system

The evaluation of environmental regulation efficiency refers to measuring and evaluating the government's environmental regulation behavior using scientific evaluation methods to achieve a specific goal. Based on the cost–benefit analysis theory and related principles, this study divided the evaluation indicators into cost indicators (input indicators) and benefits indicators (output indicators). Cost indicators select labor input, capital input, and physical resource input. Benefit indicators include pollution control situations and environmental quality status. According to the general rule of DEA method indicator selection (Golany and Roll, 1989), the number of DMUs should not be less than the product of the input and output indicators. At the same time, it should be at least three times the number of input and output indicators. Drawing on the selection of indicators in the existing literature (Huang and Shi, 2015; Cheng et al., 2016; Tang et al., 2016; Zeng and Niu, 2019; Jia et al., 2022; Sun et al., 2022a; Sun et al., 2022b), 17 fundamental evaluation indicators of environmental regulation efficiency in the Yellow River basin were selected in this study. In terms of pollution control indicators, the industrial "three waste" emissions indicator is used as an indicator of undesirable output. Since there is too much missing data for the industrial wastewater emission compliance rate indicator for each prefecture-level city in the Yellow River basin, this indicator is not considered. The price-related indicators are deflated using 2007 as the base period to eliminate the effect of price fluctuations. The input–output indicators system is shown in Table 1.

## 2.3 Overview of the study area

The Yellow River flows through and borders nine provinces and autonomous regions in Qinghai, Sichuan, Gansu, Inner Mongolia, Ningxia, Shanxi, Shaanxi, Henan, and Shandong, with a total length of 5464 km and a basin area of about 2.17 million km$^2$. It is an essential ecological barrier and economic belt in China, and the ecological protection and high-quality development of the Yellow River Basin were elevated to a major national strategy in 2019. In order to delineate the study area of the Yellow River Basin, 75 prefecture-level cities in the upper, middle, and lower reaches of the Yellow River basin were selected for the study based on the principle of "taking the natural river basin as the basis, considering the

TABLE 1 Indicators system of environmental regulation efficiency.

| Indicator type | Indicators name | Indicator characterization |
|---|---|---|
| Input indicators | Labor | Number of employees in the environmental sector (person) |
| | Capital | Investment in sewerage per unit of output (million yuan RMB) |
| | | Total investment in landscaping (million yuan RMB) |
| | | Total investment in environmental sanitation (million yuan RMB) |
| | Physical resources | Number of wastewater treatment plant (unit) |
| | | Number of harmless treatment plants/grounds (unit) |
| | | The density of water supply pipelines in the built district (km/km$^2$) |
| Desirable output indicators | Pollution control | Industrial $SO_2$ removal rate (%) |
| | | Wastewater treatment rate (%) |
| | | The comprehensive utilization rate of industrial solid waste (%) |
| | | Domestic garbage harmless treatment rate (%) |
| | | Industrial smoke (dust) removal rate (%) |
| | Environmental quality | The green coverage rate of the built district (%) |
| | | Public recreational green space per capita (m$^2$) |
| Undesirable output indicators | Industrial "three waste" emissions | Wastewater emissions per unit of output (million t/billion yuan RMB) |
| | | Industrial smoke (dust) emissions per unit of output (t/million yuan RMB) |
| | | Industrial $SO_2$ emissions per unit of output (t/million yuan RMB) |

integrity of the geographical study unit, and the direct correlation between the regional economy and the Yellow River" (Li et al., 2011) (Table 2). Since Sichuan belongs to the Yangtze River Basin, Hanzhong, Ankang, and Shangluo in Shaanxi, Hulunbeier, Chifeng, and Tongliao in Inner Mongolia are classified as northeast China in a broad sense, and Haidong in Qinghai has more severe missing data, these regions are not included in the Yellow River basin examined in this study. The spatial distribution of the Yellow River Basin is shown in Figure 1.

## 2.4 Data sources

The panel data of 75 prefecture-level cities in the Yellow River Basin from 2007 to 2020 in this study were mainly obtained from the China City Statistical Yearbook, the China Urban Construction Statistical Yearbook, the China Urban-Rural Construction Statistical Yearbook, and the statistical yearbooks and bulletins of various cities. Linear interpolation was used to supplement the missing data. Considering the continuity of the data, the data of Laiwu before 2019 was merged into Jinan. The acquired data were classified into the Yellow River Basin's upper, middle, and lower reaches.

# 3 Results

## 3.1 Results of environmental regulation efficiency measurements

With the help of MaxDEA 9.1 Ultra software, the input and output data of 75 prefecture-level cities in the Yellow River Basin from 2007 to 2020 were substituted into the super-EBM model with undesirable outputs, non-oriented, and variable returns to scale, and the environmental regulation efficiency values of various cities and regions over the years were calculated. The results are shown in Figure 2.

The overall average environmental regulation efficiency in the Yellow River Basin increased from 0.588 in 2000 to 0.776 in 2020, with an average annual increase of 1.861%. Specifically, during the study period, the environmental regulation efficiency of the Yellow River Basin showed a U-shaped trend, which first decreased and then increased, reaching the lowest point in 2011. The possible reason is that in the early stage of economic development, most cities in the Yellow River Basin were dominated by resource-intensive industries such as coal, iron and steel, and chemical industries, which were overly dependent on natural resources, resulting in pollutant emissions that were significantly higher than the national average. At the same time, pollution regulation and control were inadequate, traditional production technology and management modes were relatively backward, and a scientific and complete pollution management system still needed to be established, leading to a gradual decrease in environmental regulation efficiency. Since the 18th National Congress of the Communist Party of China (CPC), the national strategic positioning of the development of the Yellow River Basin has become more prominent, along with the in-depth implementation of ecological civilization construction. Most of the cities in the Yellow River Basin have changed their short-sighted development patterns of the long-term pursuit of economic growth while ignoring resource conservation and eco-environmental protection. They have curbed the development inertia of lagging economic development, local environmental pollution, and significant potential risks. They have also reduced the total amount and intensity of pollutant emissions and the carrying capacity of resources. At the same time, pollution regulation and control were inadequate, traditional production technology and management modes were relatively backward, and a scientific and complete pollution management system still needed to be established, leading to a gradual decrease in environmental regulation efficiency. Thus the environmental regulation efficiency is still fluctuating to a certain degree.

In the sub-regional comparison of environmental regulatory efficiency, the upper reaches had the highest average of 0.801, and the lower reaches was the next highest with 0.748. Both regions have long been higher than the overall average of 0.726 in the Yellow River Basin. The middle reaches ranked lower at 0.641, below the Yellow River Basin average. The time-series trend of the sub-regions shows that the environmental regulatory efficiency of all regions has increased at different rates during the study period, and there is a trend toward further development at higher levels. Further analysis reveals that the environmental regulation efficiency in the middle reaches increased by 0.230 and in the upper reaches by 0.053 during the study period, with the former exceeding the latter by more than four times, indicating that the increase in the regions with low environmental regulation efficiency is higher than that in the regions with high environmental regulation efficiency and that the difference in the average environmental regulation efficiency among regions is significantly reduced, showing some convergence characteristics. However, it was also found that the average

TABLE 2 The division of prefecture-level cities in the upper, middle, and lower reaches of the Yellow River Basin.

| Region | Prefecture-level city |
|---|---|
| Upper reaches | Lanzhou, Baiyin, Wuwei, Jinchang, Pingliang, Zhangye, Jiayuguan, Jiuquan, Qingyang, Dingxi, Longnan, Tianshui, Xining, Yinchuan, Guyuan, Wuzhong, Shizuishan, Zhongwei |
| Middle reaches | Hohhot, Baotou, Wuhai, Ordos, Ulanqab, Bayannur, Taiyuan, Datong, Yangquan, Changzhi, Linfen, Jinzhong, Yuncheng, Jincheng, Xinzhou, Shuozhou, Lvliang, Xi'an, Xianyang, Yulin, Baoji, Tongchuan, Weinan, Yan'an |
| Lower reaches | Zhengzhou, Kaifeng, Luoyang, Pingdingshan, Jiaozuo, Hebi, Xinxiang, Anyang, Puyang, Xuchang, Luohe, Sanmenxia, Nanyang, Shangqiu, Xinyang, Zhoukou, Zhumadian, Jinan, Qingdao, Zibo, Zaozhuang, Dongying, Yantai, Weifang, Jining, Tai'an, Weihai, Rizhao, Binzhou, Dezhou, Liaocheng, Linyi Heze |

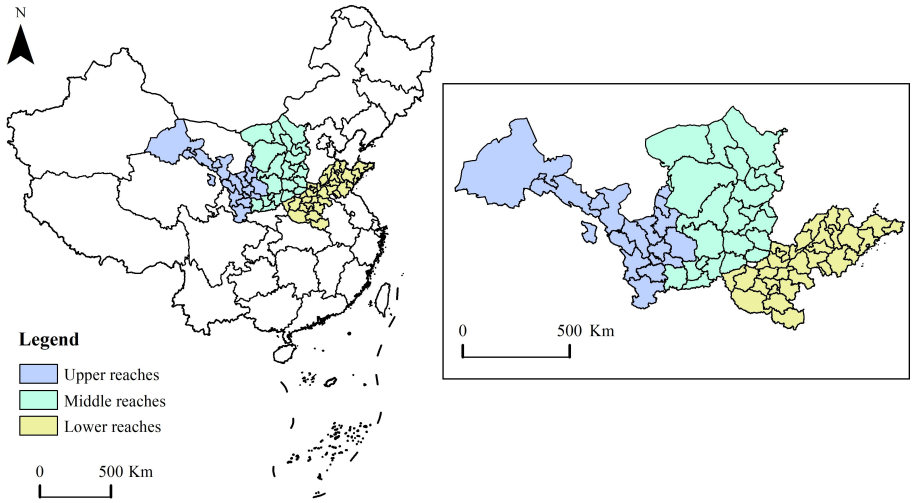


FIGURE 1
Location of the study area in China. The map projection system is World Geodetic System (WGS) 84.

annual increase of environmental regulation efficiency in the upper reaches was 0.460%, much lower than the overall level of the Yellow River Basin. In comparison, the average annual increase in the middle reaches was 2.422%, which shows that the increase in the regions with high environmental regulation efficiency failed to exceed that of the regions with low environmental regulation efficiency. The catching-up effect was noticeable, and then different regions may converge to the same steady state.

## 3.2 Regional differences in environmental regulation efficiency and their sources

The Dagum Gini coefficient and its decomposition method were used to reveal the overall difference in environmental regulation efficiency in the Yellow River Basin, the differences within and among the three regions, and the primary contribution sources. The specific results are shown in Table 3. In particular, the names of the three regions in the table were abbreviated here to provide more result information.

### 3.2.1 Overall and within-region differences

Figure 3 depicts the Gini coefficient and characteristics of change in environmental regulation efficiency for the Yellow River Basin and the three regions considered. During the inspection period, the difference in environmental regulation efficiency in the Yellow River Basin showed an inverted U-shaped fluctuation. The overall Gini coefficient had an average value of 0.253, reaching a maximum value of 0.372 and a minimum value of 0.098 in 2012 and 2018, respectively,

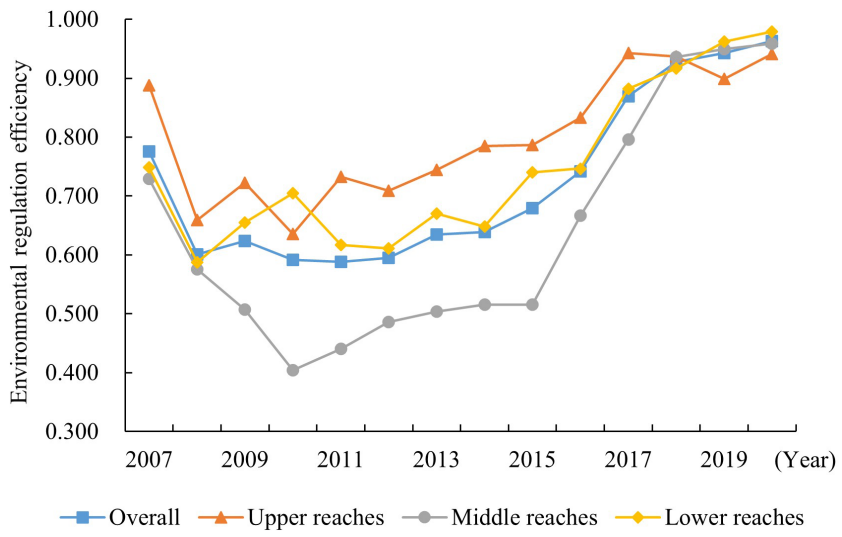


FIGURE 2
Trends of average environmental regulation efficiency by region in the Yellow River Basin.

TABLE 3 The Gini coefficient of environmental regulation efficiency and results of its decomposition.

| Year | Overall | Within-region Gini coefficient | | | Between-region Gini coefficient | | | Contribution (%) | | |
|---|---|---|---|---|---|---|---|---|---|---|
| | | Upper | Middle | Lower | Upper-Middle | Upper-Lower | Middle-Lower | $G_w$ | $G_{nb}$ | $G_t$ |
| 2007 | 0.115 | 0.182 | 0.290 | 0.256 | 0.247 | 0.231 | 0.273 | 34.575 | 15.152 | 50.091 |
| 2008 | 0.331 | 0.262 | 0.304 | 0.371 | 0.289 | 0.336 | 0.351 | 35.279 | 7.881 | 56.840 |
| 2009 | 0.322 | 0.244 | 0.396 | 0.300 | 0.338 | 0.281 | 0.345 | 34.210 | 22.087 | 43.704 |
| 2010 | 0.364 | 0.340 | 0.524 | 0.245 | 0.453 | 0.280 | 0.371 | 31.313 | 31.272 | 37.414 |
| 2011 | 0.365 | 0.247 | 0.483 | 0.329 | 0.392 | 0.303 | 0.398 | 33.264 | 27.720 | 39.016 |
| 2012 | 0.372 | 0.286 | 0.471 | 0.336 | 0.396 | 0.324 | 0.395 | 33.825 | 20.345 | 45.830 |
| 2013 | 0.346 | 0.248 | 0.480 | 0.293 | 0.387 | 0.278 | 0.375 | 33.421 | 22.602 | 43.976 |
| 2014 | 0.333 | 0.244 | 0.415 | 0.298 | 0.357 | 0.288 | 0.350 | 33.138 | 25.360 | 41.502 |
| 2015 | 0.277 | 0.217 | 0.204 | 0.393 | 0.332 | 0.213 | 0.289 | 31.737 | 30.488 | 37.816 |
| 2016 | 0.229 | 0.193 | 0.292 | 0.189 | 0.255 | 0.198 | 0.234 | 33.246 | 19.054 | 47.250 |
| 2017 | 0.151 | 0.103 | 0.175 | 0.147 | 0.154 | 0.135 | 0.160 | 34.148 | 22.625 | 43.200 |
| 2018 | 0.098 | 0.089 | 0.106 | 0.095 | 0.101 | 0.094 | 0.100 | 34.743 | 5.233 | 60.024 |
| 2019 | 0.115 | 0.128 | 0.149 | 0.078 | 0.143 | 0.097 | 0.110 | 32.877 | 11.358 | 55.765 |
| 2020 | 0.117 | 0.130 | 0.136 | 0.090 | 0.135 | 0.105 | 0.111 | 33.309 | 7.406 | 59.285 |
| Average | 0.253 | 0.208 | 0.316 | 0.244 | 0.284 | 0.226 | 0.276 | 33.506 | 19.185 | 47.265 |

indicating that the environmental regulation efficiency in the Yellow River Basin had noticeable differences between cities and that the differences were shrinking.

In terms of within-region differences, the average Gini coefficient values of environmental regulation efficiency in the upper, middle, and lower reaches were 0.208, 0.316, and 0.244, respectively, with the most considerable difference in the middle reaches owing to the convergence of industrial structures in the upper reaches and the relatively balanced input of environmental regulation factors. However, the problem of unbalanced environmental regulation efficiency in the region was prominent in the middle reaches due to its wide coverage area and the heterogeneity of economic level, population characteristics, government regulation, and other factors, the pace of industrial transformation and upgrading and pollution control in core cities was not uniform. In addition, the Gini coefficients of the upper and lower reaches did not exceed the overall Gini coefficient, indicating that the imbalance among

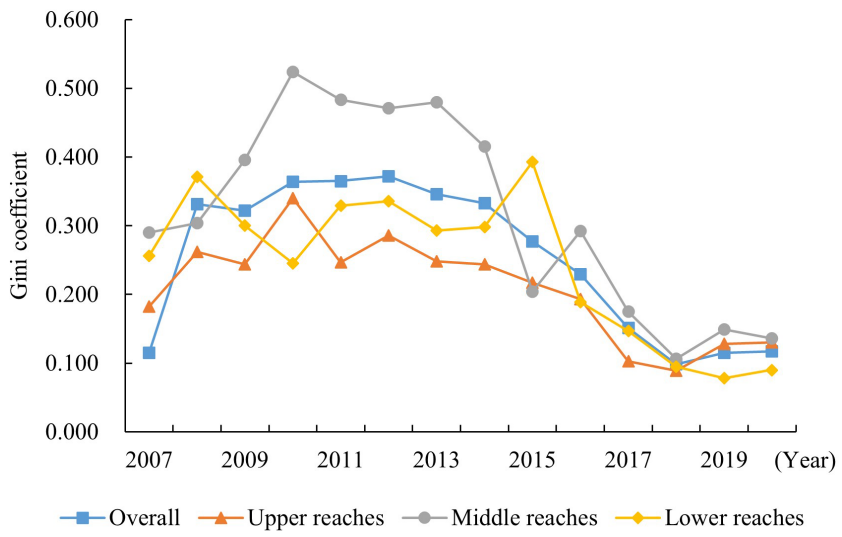


FIGURE 3
Trends in the overall and within-region Gini coefficient of environmental regulation efficiency.

cities within the upper and lower reaches was relatively low. The Gini coefficients of environmental regulation efficiency in the upper, middle, and lower reaches all showed a fluctuating decreasing trend from 0.182, 0.290, and 0.256 in 2007 to 0.130, 0.136, and 0.090 in 2020, with a decrease of 28.571%, 53.103%, and 64.844%, respectively. The difference in the Gini coefficients of the three regions was narrowing, and the regions with a low environmental regulation efficiency were getting closer to the regions with a high environmental regulation efficiency.

### 3.2.2 Between-region differences

As shown in Figure 4, the average Gini coefficient values of environmental regulation efficiency in the upper-middle, upper-lower, and middle-lower reaches were 0.284, 0.226, and 0.276, respectively. Among them, the most considerable differences were found in the upper-middle reaches and the smallest in the upper-lower reaches. From the dynamic evolution trend, the Gini coefficients of environmental regulation efficiency in the upper-middle, upper-lower, and middle-lower reaches exhibited a fluctuating decreasing trend from 0.247, 0.231, and 0.273 in 2007 to 0.135, 0.105, and 0.111 in 2020, with a decrease rate of 45.344%, 54.545%, and 59.341%, respectively, reflecting the evolution of the fluctuating increasing and decreasing trends. This indicates that the differences in the upper-middle, upper-lower, and middle-lower reaches have narrowed significantly from 2007 to 2020. Still, the difference in the upper-middle reaches has narrowed relatively little.

### 3.2.3 Sources and contributions of differences

The contribution rates of the intensity of transvariation ($G_t$), within-region difference ($G_w$), and between-region difference ($G_{nb}$) were measured separately in this paper to reveal the sources of the overall difference in environmental regulation efficiency in the Yellow River Basin. The evolution of these three contribution rates is reflected in Figure 5.

For the magnitude of the contribution rates, the average annual contribution rates of within-region difference, between-region difference, and the intensity of transvariation were 33.506%, 19.185%, and 47.265%, respectively, from 2007 to 2020. The sources of the overall difference in environmental regulation efficiency in the Yellow River Basin were, in order, the contributions of the intensity of transvariation, within-region difference, and between-region difference. Therefore, the most crucial cause of the overall difference in environmental regulation efficiency in the Yellow River Basin is the intensity of transvariation. In other words, reducing the intensity of between-region transvariation should be the focus of future efforts to promote the development of environmental regulation efficiency in the Yellow River Basin. This means the environmental regulation efficiency in the upper, middle, and lower reaches has a particular intersection. In addition, the environmental resource endowment and development levels of certain cities in different regions are similar. As a result, a city with a lower environmental regulation efficiency in the higher-rank region may be lower than a city with a higher value in the lower-rank region. Regarding the dynamic evolution trend, the contribution rate of within-region difference was relatively stable at about 33%. In contrast, the contribution rates of between-region difference and the intensity of transvariation fluctuated more during the observation period. The contributions of within-region difference and the intensity of transvariation have a complementary fluctuating relationship that reinforces each other. The contribution rate of the intensity of transvariation showed a U-shaped trend, and correspondingly, the contribution rate of within-region difference showed an inverted U-shaped trend. The former reached the minimum value of 37.414% in 2010, while the latter reached the maximum value of 31.272% in 2010.

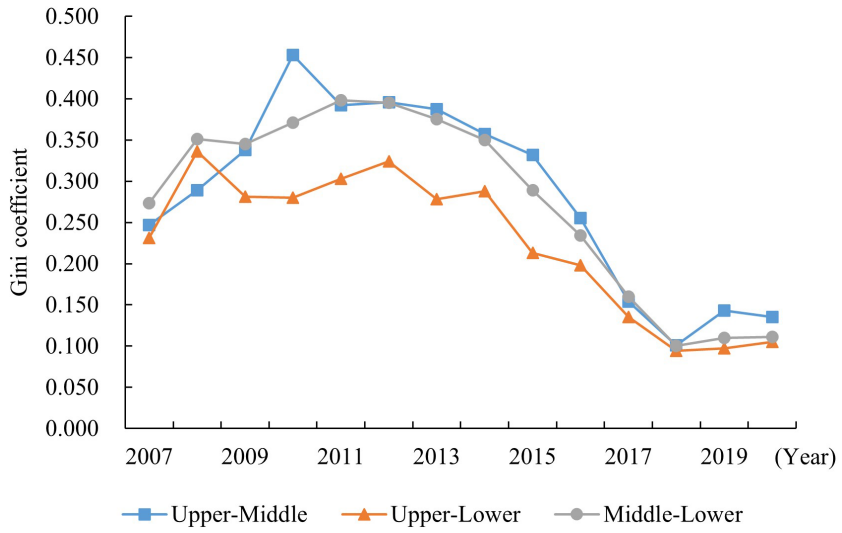


FIGURE 4
Trends in the between-region Gini coefficient of environmental regulation efficiency.

10.3389/fevo.2023.1156981

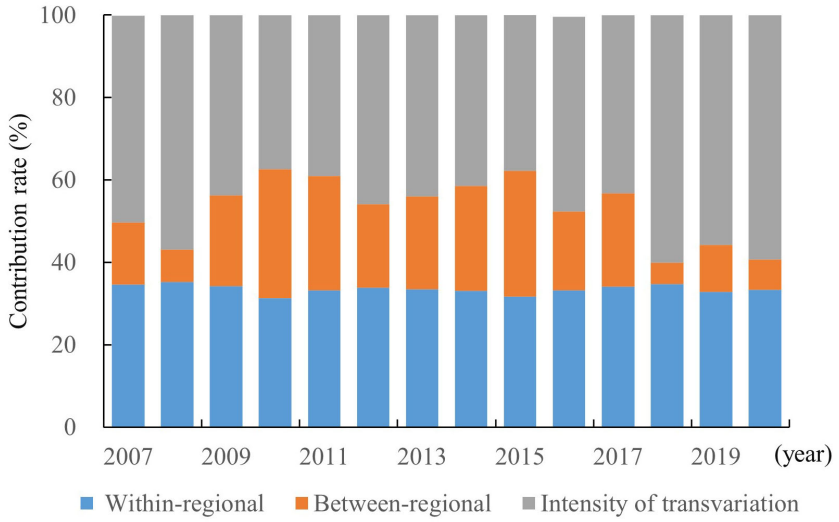


FIGURE 5
Sources of regional difference and their contributions.

## 3.3 Distribution dynamics of environmental regulation efficiency

The Gini coefficients revealed the magnitude and source of environmental regulation efficiency in the Yellow River Basin and represented the relative differences in environmental regulation efficiency but could not describe the dynamic changes in the absolute differences. In this study, we applied the kernel density estimation method to characterize the distribution dynamics of environmental regulation efficiency in the Yellow River Basin and the three regions in terms of location, pattern, extension, and polarization trends. Figure 6 presents a 3D kernel density map of environmental regulation efficiency in the Yellow River Basin from 2017 to 2020.

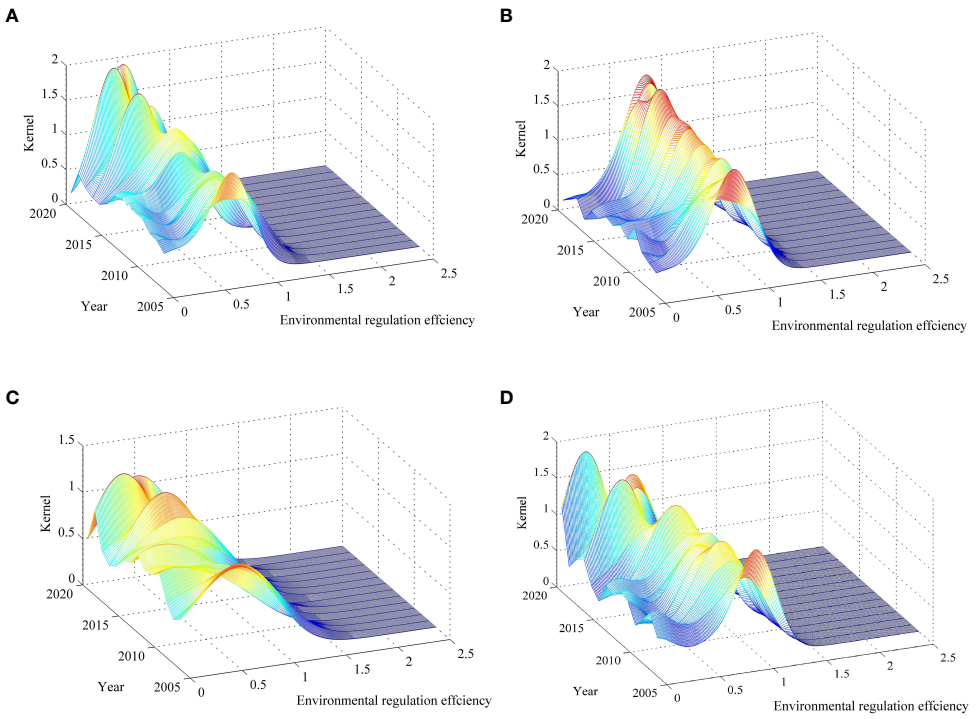


FIGURE 6
Dynamic evolutionary trends of environmental regulation efficiency. **(A)** Overall, **(B)** Upper reaches, **(C)** Middle reaches, and **(D)** Lower reaches.

As illustrated in Figure 6, the distribution curves of the overall Yellow River Basin and the three regions tended to move to the right, indicating that the environmental regulation efficiency of the overall Yellow River Basin and the three regions improved, which is consistent with the trend of environmental regulation efficiency measured in the previous paper. The distribution curves of the upper and lower reaches did not move significantly to the right over time. The efficiency of environmental regulation still needs to be improved, especially with the tightening of resource and environmental constraints and the acceleration of green transformation. Considering the shape of the kernel density curves, the height of the main peak of the distribution curves of the overall Yellow River Basin and the three regions increased. At the same time, the width narrowed, indicating that the absolute difference in the environmental regulation efficiency of the overall Yellow River Basin and the three regions had a particular diminishing trend. The height of the main peak in the middle reaches first decreased as the width widened and then increased as the width narrowed, implying that the dispersion of environmental regulation efficiency tended to increase at the beginning of the inspection period and that the dispersion trends had diminished in recent years. In terms of the extension of the main peak, there was an apparent right-trailing phenomenon in the distribution curves for the overall Yellow River Basin and the three regions, which was mainly due to the existence of cities with high environmental regulation efficiency in each region, such as Qingyang in the upper reaches, Linfen in the middle reaches, and Sanmenxia in the lower reaches. Furthermore, the distribution curves of the overall Yellow River Basin and the three regions had the characteristics of extended convergence, and the gap between the cities with higher environmental regulation efficiency and the cities with average efficiency had been reduced, i.e., the probability of extreme values of environmental regulation efficiency became increasingly unlikely. From the perspective of the polarization characteristics, the distribution curves of the overall Yellow River Basin and the lower reaches had a bimodal peak phenomenon at the beginning of the inspection period. Still, at the end of the period, the distribution curves had a single peak pattern, indicating that the polarization within these regions tended to weaken. The degree of within-regional difference gradually decreased. The distribution curve of the upper reaches consistently showed a bimodal peak, and the difference between the main peak and the side peak was relatively large, indicating a significant spatial polarization phenomenon in the environmental regulation efficiency of this region. On the other hand, the distribution curve of the middle reaches showed a single peak characteristic with a more moderate divergence trend.

## 3.4 Spatio-temporal convergence of environmental regulation efficiency

### 3.4.1 Time series convergence analysis

The $\sigma$ convergence of environmental regulation efficiency in each region of the Yellow River Basin is shown in Figure 7. The coefficient of variation of environmental regulation efficiency in the overall Yellow River Basin showed a repeated rise and declined from 0.195 in 2007 to 0.248 in 2020. In general, there is no $\sigma$ convergence because the variation coefficient at the period's end was higher than at the beginning. The coefficient of variation of the upper reaches had a rising–declining–rising–declining, indicating that there is $\sigma$ convergence in the environmental regulation efficiency of the upper reaches. The coefficient of variation of environmental regulation efficiency in the middle reaches only increased from 2007 to 2010 and showed cyclical ups and downs from 2010 to 2020. Moreover, the coefficient of variation of environmental regulation efficiency in the lower reaches only increased slightly from 2007–2008, 2010–2011, and 2019–2020, and decreased in other years. Therefore, there is $\sigma$ convergence in the middle and lower reaches. The convergence

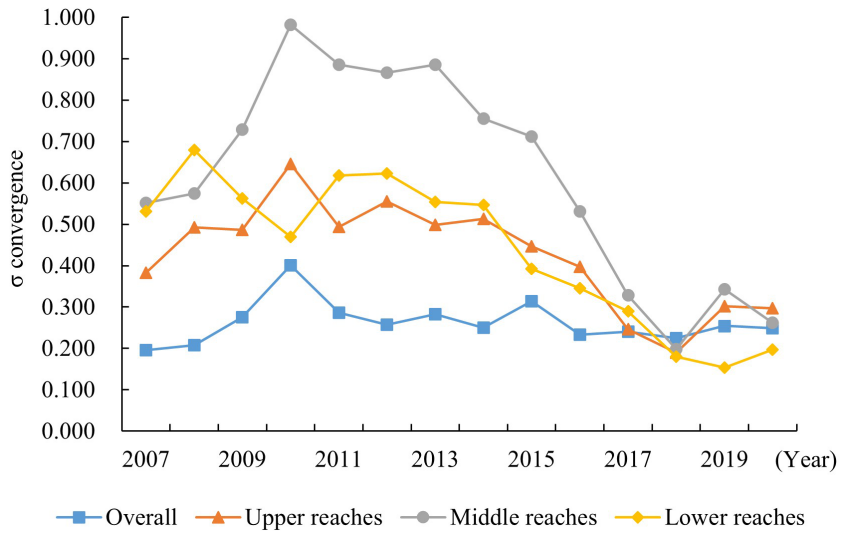


FIGURE 7
Trends of $\sigma$ convergence of environmental regulation efficiency.

speed in the lower reaches was 0.6287, nearing that of the upper and middle reaches, in a "catch-up" situation.

### 3.4.2 Spatial convergence analysis

#### 3.4.2.1 Spatial autocorrelation test

According to Formula (8), the spatial autocorrelation of environmental regulation efficiency in the Yellow River Basin was tested and analyzed using the Rook spatial weight matrix. In order to avoid the "island phenomenon", Xining and Weiwu were set as neighbors. Stata 16.0 software was used to calculate the global Moran's I for the environmental regulation efficiency in the Yellow River Basin from 2017 to 2020 (Table 4). Except for 2007 and 2017, the global Moran's I values were significantly positive during the observation period, indicating that the environmental regulation efficiency in the Yellow River Basin was not randomly distributed. Instead, it showed that the spatial distribution of environmental regulation efficiency tended to exhibit significant spatial correlation and regional clustering. The results of the spatial autocorrelation test indicated that the environmental regulation efficiency in the Yellow River Basin could be analyzed using a spatial econometric model for convergence.

#### 3.4.2.2 Spatial convergence model setting

The spatial convergence model involves spatial lag terms. When solving spatial problems, the traditional least squares regression method presents difficulty acquiring unbiased estimates. Thus, a suitable spatial econometric model was selected using the Wald and Lagrange multiplier (LM) tests. The Hausman test results were for determining whether the model utilized fixed effects or random effects. The Likelihood ratio (LR) test was further judged for the fixed effects model for time-fixed, spatial-fixed, and spatial-time double-fixed. Because of the space limitation, the specific model setting process was not listed in this study. The corresponding author is available upon request.

#### 3.4.2.3 Spatial absolute $\beta$ convergence analysis

The spatial absolute $\beta$ convergence test of environmental regulation efficiency in each region is listed in Table 5. The parameter $s=-\ln(1+\beta)/T$ represents the convergence speed, and $\tau=\ln(2)/s$ represents the half-life cycle (Pan, 2010). It can be seen from Table 4 that, first, the convergence coefficient $\beta$ of the test in the overall Yellow River Basin and the upper, middle, and lower reaches were significantly negative at the 1% level, indicating that there was absolute $\beta$ convergence in environmental regulation efficiency in all of them. Suppose the influence of a series of economic, environmental, and social factors on environmental regulation efficiency is not considered. In that case, the environmental regulation efficiency of the overall Yellow River Basin and the three reaches will converge to their respective steady-state levels in the long run. Combined with the fact that environmental regulation efficiency increases from year to year (see Figure 2), even though the coefficient of variation increases in the short term for each study object (see Figure 7), the trend of increasing and long-term convergence of environmental regulation efficiency is already apparent. Second, there were differences in the convergence speed of environmental regulation efficiency across regions. The convergence speed was 0.0702, 0.0862, 0.0770, and 0.0646 for the overall Yellow River Basin and the upper, middle, and lower reaches. At the same time, the half-life cycle was 9.867, 8.038, 8.971, and 10.737 years, respectively. In other words, the upper reaches had the fastest convergence speed. The cities with lower environmental regulation efficiency in the region had the shortest time to "catch up" with the cities with higher environmental regulation efficiency, followed by the middle reaches and the overall Yellow River Basin. In contrast, the lower reaches had the slowest convergence speed. The environmental regulation efficiency in the upper and middle reaches can maintain a high convergence speed despite the relatively high coefficient of variation, which can be attributed to the interaction within cities through spatial effects. Finally, the Yellow River Basin and the three reaches exhibited different spatial effects. Both independent and dependent variables' spatial lags existed in the Yellow River Basin and lower reaches. The $\rho$ and $\theta$ coefficients of each model were significantly positive at the 5% level, demonstrating that the positive spatial spillover of both environmental regulation efficiency in other cities and the rates of change of environmental regulation efficiency in other cities had an impact on the rate of change of environmental regulation efficiency in this city within the region. The spatial lags of the dependent variable existed in the upper and lower reaches. The $\rho$ coefficients of the models for both regions were significantly positive at the 5% level, indicating that the rate of change of environmental regulation efficiency in this city within the region was affected by positive spatial spillovers from the rates of change in other cities. It should be noted that the absolute $\beta$ convergence of

TABLE 4 The results of Moran's I of environmental regulation efficiency in the Yellow River Basin from 2005 to 2020.

| Year | Moran's I | Zscores | P-value | Year | Moran's I | Zscores | P-value |
|---|---|---|---|---|---|---|---|
| 2007 | 0.087 | 1.279 | 0.101 | 2014 | 0.137 | 1.902 | 0.029 |
| 2008 | 0.104 | 1.809 | 0.046 | 2015 | 0.083 | 2.625 | 0.004 |
| 2009 | 0.102 | 1.459 | 0.072 | 2016 | 0.147 | 1.829 | 0.034 |
| 2010 | 0.113 | 1.595 | 0.055 | 2017 | 0.078 | 0.833 | 0.203 |
| 2011 | 0.250 | 3.335 | 0.000 | 2018 | 0.175 | 2.399 | 0.008 |
| 2012 | 0.091 | 1.325 | 0.093 | 2019 | 0.137 | 2.053 | 0.020 |
| 2013 | 0.143 | 2.132 | 0.019 | 2020 | 0.099 | 1.484 | 0.069 |

TABLE 5 Absolute $\beta$ convergence test results of the environmental regulation efficiency in the Yellow River Basin.

| Model | Overall | Upper | Middle | Lower |
|---|---|---|---|---|
| | Spatial-time double-fixed effects SDM | Spatial-time double-fixed effects SAR | Spatial-time double-fixed effects SAR | Spatial-time double-fixed effects SDM |
| $\beta$ | −0.626*** | −0.701*** | −0.661*** | −0.595*** |
| $\rho/\lambda$ | 0.125*** | 0.021** | 0.065** | 0.093** |
| $\theta$ | 0.141** | | | 0.261*** |
| Hausman | 84.03*** | 58.29*** | 114.75*** | 73.21*** |
| Wald-lag | 5.94** | 0.03 | 2.97* | 23.88*** |
| Wald-error | 8.72*** | 0.10 | 0.46 | 13.39*** |
| LM-lag | | 10.238*** | 7.464*** | |
| Robst-LM-lag | | 22.156*** | 19.350*** | |
| LM-error | | 2.386 | 1.585 | |
| Robst-LM-error | | 14.304*** | 13.471*** | |
| Spatial effects | 73.52*** | 27.09*** | 66.57*** | 34.84*** |
| Time effects | 159.49*** | 54.51*** | 53.91*** | 50.80*** |
| Log-likelihood | 427.9634 | 114.6240 | 113.6536 | 224.3129 |
| sigma$^2$ | 0.024*** | 0.022*** | 0.028*** | 0.021*** |
| s | 0.070 | 0.086 | 0.077 | 0.065 |
| $\tau$ | 9.867 | 8.038 | 8.971 | 10.737 |
| N | 975 | 234 | 312 | 429 |
| $R^2$ | 0.186 | 0.190 | 0.227 | 0.217 |

*, **, and *** represent significance at the 10%, 5%, and 1% levels, respectively.

environmental regulation efficiency across the regions was conducted under the assumption that the level of economic development, industrial structure, market environment, degree of economic openness, and technological progress were similar across regions, which is not the case, so further analysis on conditional $\beta$ convergence is needed.

#### 3.4.2.4 Spatial conditional $\beta$ convergence analysis

Table 6 presents the results of the conditional $\beta$ convergence test for the environmental regulation efficiency of 75 cities and regions in the Yellow River Basin. The selection process for the different spatial econometric models is the same as for the absolute $\beta$ convergence analysis. The results show that taking into account the different economic, environmental, and social characteristics of the overall Yellow River Basin and the three regions, the $\beta$ coefficients of the overall Yellow River Basin and the upper, middle, and lower reaches were all still significantly negative at the 5% level, indicating that the environmental regulation efficiency of all of them showed significant conditional $\beta$ convergence, with the convergence speed of 0.071, 0.092, 0.080, and 0.066, while the half-life cycle was 9.760, 7.571, 8.618, and 10.504 years, respectively. With the inclusion of control variables, the convergence speed of all regions was accelerated to varying degrees. At the same time, the half-life cycle was shortened, indicating that the control variables can effectively promote the $\beta$ convergence of environmental regulation efficiency in the overall Yellow River Basin and the three regions so that the cities with lower environmental regulation efficiency needed less time to "catch up" with the cities with higher environmental regulation efficiency. The overall Yellow River Basin and the three regions also exhibited different spatial effects. In contrast, the spatial effects in individual regions differed from those in the absolute $\beta$ convergence analysis. In particular, the type of spatial effect in the overall Yellow River Basin changed from SDM to SAR, indicating that the spatial spillover of environmental regulation efficiency in other cities disappeared. Otherwise, the type of spatial effect in the upper reaches changed from SAR to SDM. Apart from these, it did not differ from the absolute $\beta$ convergence analysis.

### 3.4.3 Robustness tests

The Pyatt Gini coefficient was used to measure the regional differences in environmental regulation efficiency and the primary sources of contribution in the Yellow River Basin to examine the findings of the previous study based on the Dagum Gini coefficient

TABLE 6 Conditional $\beta$ convergence test results of the environmental regulation efficiency in the Yellow River Basin.

| Variables | Overall | Upper | Middle | Lower |
|---|---|---|---|---|
| | Spatial-time double-fixed effects SAR | Time-fixed effects SDM | Spatial-time double-fixed effects SAR | Spatial-time double-fixed effects SDM |
| $\beta$ | −0.629*** | −0.705*** | −0.673*** | −0.603*** |
| $\rho/\lambda$ | 0.073** | 0.044** | 0.056*** | 0.079** |
| $\theta$ | | 0.083** | | 0.219*** |
| Hausman | 106.81*** | 147.20*** | 158.12*** | 64.55*** |
| Wald-lag | 10.55 | 16.66** | 11.76* | 23.20*** |
| Wald-error | 6.30 | 16.80** | 9.88 | 18.86*** |
| LM-lag | 8.849*** | | 7.756*** | |
| R-LM-lag | 43.838*** | | 24.315*** | |
| LM-error | 0.267 | | 1.160 | |
| R-LM-error | 35.256*** | | 17.719*** | |
| Spatial effects | 36.32*** | 9.62 | 34.26*** | 18.87** |
| Time effects | 155.49*** | 41.79*** | 45.75*** | 51.71*** |
| Log-likelihood | 427.1545 | 125.1941 | 92.8780 | 228.6742 |
| sigma$^2$ | 0.024*** | 0.020*** | 0.032*** | 0.020*** |
| s | 0.071 | 0.092 | 0.080 | 0.066 |
| $\tau$ | 9.760 | 7.517 | 8.681 | 10.504 |
| N | 975 | 234 | 312 | 429 |
| $R^2$ | 0.164 | 0.100 | 0.159 | 0.199 |

*, **, and *** represent significance at the 10%, 5%, and 1% levels, respectively.

(Pyatt, 1976). It can be easily seen that the Pyatt Gini coefficient and decomposition were generally consistent with the Dagum Gini coefficient, which indicates that the conclusions drawn from the Dagum Gini coefficient were robust and reliable. Due to space constraints, the composition of the Pyatt Gini coefficient needed to be more detailed here, and specific Gini coefficient data needed to be reported. The corresponding author is available upon request.

The spatial conditional $\beta$ convergence analysis was conducted using the geographic distance weight matrix and the economic geography nested weight matrix to examine the robustness of spatial convergence, and the results are shown in Table 7. The $\beta$ coefficients of the overall Yellow River Basin and the upper, middle, and lower reaches were all significantly negative at the 5% level under both types of weight matrices, implying that the spatial convergence conclusion of this paper was robust.

## 4 Discussion

Environmental regulation efficiency facilitates environmental governance performance assessment, ecological protection, and high-quality development. Based on the input–output indicators system, this study identified the differences and convergence of environmental regulation efficiency in the Yellow River Basin.

First, the average value of environmental regulation efficiency in the Yellow River Basin from 2007 to 2020 was 0.726, which is lower than the results of the Yangtze River Economic Belt and coastal urban agglomerations in China (Ren et al., 2019; Wang and Ma, 2020). The results are lower because our study considered the impact of undesirable output indicators such as industrial "three waste" emissions on environmental regulation, which makes our calculation more scientific. Second, the environmental regulation efficiency in the Yellow River Basin has great within-region differences, and the differences within the middle reaches are the largest. The average contribution to the intensity of transvariation was 47.265%, indicating that the intensity of transvariation is the main source of spatial differences in environmental regulation efficiency. Compared with traditional empirical analysis, the difference and contribution analysis in this study can more scientifically show the characteristics of environmental regulation efficiency in the Yellow River Basin. Finally, the environmental regulation efficiency in the Yellow River Basin has obvious characteristics of spatial absolute and conditional $\beta$ convergence, and the environmental regulation efficiency of each city tends to a

TABLE 7 Spatial convergence robustness test results.

| | Weight type | $\beta$ | $\rho/\lambda$ | $R^2$ |
|---|---|---|---|---|
| **Overall** | Geographic distance weight matrix | −0.710*** | 0.123*** | 0.160 |
| | Economic geography nested weight matrix | −0.585*** | 0.266*** | 0.193 |
| **Upper** | Geographic distance weight matrix | −0.591*** | 0.685*** | 0.162 |
| | Economic geography nested weight matrix | −0.513*** | 0.128* | 0.127 |
| **Middle** | Geographic distance weight matrix | −0.510*** | 0.018*** | 0.090 |
| | Economic geography nested weight matrix | −0.669*** | 0.211*** | 0.178 |
| **Lower** | Geographic distance weight matrix | −0.731*** | 0.119* | 0.168 |
| | Economic geography nested weight matrix | −0.425*** | 0.165** | 0.173 |

*, **, and *** represent significance at the 10%, 5%, and 1% levels, respectively.

common steady state. Among them, the upper reaches has the fastest convergence speed, and the lower reaches has the slowest convergence speed. Under the influence of the level of economic development, industrial structure, market environment, degree of economic openness, and technological progress, the convergence speed of all regions is accelerated to varying degrees, which indicates that the control variables can promote the steady-state convergence of environmental regulation efficiency in the overall Yellow River Basin and the three regions. The analysis based on spatial convergence significantly shows the characteristics of the spatial evolution of environmental regulation efficiency in the Yellow River Basin, which can compensate for the lack of research on the dynamic evolution trend of environmental regulatory efficiency (Cheng et al., 2016; Jia et al., 2022).

Our contribution includes three aspects. First, the super-EBM model was used to measure the environmental regulation efficiency in the Yellow River Basin from multiple dimensions of cities, regions, and overall, solving the problem of non-radial slack, radial ratio information, and the pros and cons of various effective decision-making units (DMUs), which helped to enrich the measurement method to some extent. Second, we analyzed the regional differences in environmental regulation efficiency in the Yellow River Basin from the perspectives of composition and source. We also revealed the dynamic evolution characteristics of regional differences, which can provide empirical support for policies based on regional circumstances. Finally, the spatial absolute and conditional $\beta$ convergence across regions in the Yellow River Basin were verified in light of the spatial effects, which provided guidance and reference for establishing environmental regulation efficiency policy systems and green coordinated development. Our findings and research methodology can provide references for similar regions to select appropriate environmental regulation tools based on local conditions and explore a new way of economic development and eco-environmental protection.

## 5 Conclusions and policy implications

In this paper, we calculated the environmental regulation efficiency of 75 cities in the Yellow River Basin from 2007 to 2020 using the super-EBM model containing the undesirable output. Further, we analyzed the regional differences, dynamic evolution, and spatio-temporal convergence of environmental regulation efficiency among regions using the Dagum Gini coefficient, kernel density estimation method, and spatial econometric model. The main findings are as follows: First, the average environmental regulation efficiency of the overall Yellow River Basin and the upper, middle, and lower reaches had an increasing trend. The average environmental regulation efficiency in the upper and lower reaches was higher than the overall average, while that in the middle reaches was lower than average but increased fastest. Second, the overall Yellow River Basin and the three regions had obvious within-region differences, and the differences within the middle reaches were the largest. The differences between all regions had a narrowing trend. The regional differences between the upper and middle reaches and the middle and lower reaches were higher than those between the upper and lower reaches. The intensity of transvariation was the main source of spatial differences in environmental regulation efficiency, and the within-regional difference was the second source, with the lowest contribution to the between-regional difference. Third, the gap between the cities with higher environmental regulation efficiency and those with average efficiency had been reduced in the Yellow River Basin. The upper reaches had a significant spatial polarization phenomenon and maintained a certain level. The dynamic evolutionary characteristics of the overall Yellow River Basin and the lower reaches were relatively similar, the within-region polarization tended to weaken, and the differences gradually decreased. Finally, the coefficient of $\sigma$ convergence of environmental regulation efficiency in the overall Yellow River Basin was increasing to some extent, so there is no $\sigma$ convergence. Meanwhile, the coefficients of $\sigma$ convergence for environmental regulation efficiency in the upper, middle, and lower reaches showed a fluctuating decreasing trend, which indicates $\sigma$ convergence, and the convergence speed in the lower reaches was fast. Overall, the upper, middle, and lower reaches all had significant spatial absolute and conditional $\beta$ convergence, and they will converge to their respective steady-state levels over time. Their conditional $\beta$ convergences were faster than absolute $\beta$ convergences with shorter half-life cycles, indicating that

economic, environmental, and social factors such as the level of economic development, industrial structure, market environment, degree of economic openness, and technological progress accelerated the convergence of regional differences.

To further improve the environmental regulation efficiency in the Yellow River Basin, the following policy implications are derived based on the results: First, it is necessary to increase environmental investment and support in the middle reaches of the Yellow River to continuously narrow the gap in environmental regulation efficiency between the middle and lower reaches. As one of the regions with the most significant and fastest-growing pressures on resources and the environment, the middle reaches should optimize the combination of environmental regulation tools, strictly control the scale of highly polluting and energy-consuming industries, and curb the transfer of polluting industries to it, and taking the development of a circular, low-carbon, and green economy as an opportunity to promote the transformation of the economic growth mode to a low consumption and pollution economic development mode. Second, through administrative means such as breaking regional boundaries, improving the property rights trading system for resources and the environment, and optimizing the supply of services, we will facilitate the cross-regional flow of urban input factors, environmental information sharing, and policy coordination, especially by creating conditions and preferential policies for environmental governance exchange and cooperation between cities with lower environmental regulation efficiency and higher cities. Innovative explorations can be considered in constructing resource-sharing platforms, eco-environmental restoration, policy co-benefits, and other win-win benefits. Third, we should be wary of the dangers of over-polarization and the widening disparity in environmental regulation efficiency in the upper reaches of the Yellow River Basin and instead concentrate on improving the diffusion and radiation effects of cities at the growth poles of environmental regulation efficiency to neighboring cities. By establishing a collaborative governance mechanism, breaking the "siphon effect" and reasonably weakening the polarization effect, we can achieve a balanced development of environmental regulation efficiency in the upper reaches. The two core cities of Lanzhou and Xining, in particular, play the role of radiation diffusion of industrial structure transformation and upgrading with the implementation of the western development strategy and accelerate the neighboring cities to improve the proportion of strategic new industries to continuously promote the synergistic improvement of environmental regulation efficiency with the environmental construction of the Lanzhou–Xining urban agglomeration. Finally, the rate of change in environmental regulation efficiency is influenced by various factors. We should fully implement the new development concept, strengthen the development potential according to our own environmental resources endowment and comparative advantages, accelerate the convergence speed of environmental regulation efficiency by transforming and upgrading industrial structures, enhancing independent innovation capability, improving the market economy system and harmonizing fiscal and environmental policies, and then promote the economic development and ecological protection of the Yellow River Basin.

There are still limitations to the study of differences and convergence in environmental regulation efficiency in the Yellow River Basin. Due to the difficulty of data acquisition, this study selected research samples from 75 prefecture-level cities in the Yellow River Basin, but the research on regional differences and convergence in environmental regulation efficiency at the county level based on micro-perspectives will be the focus of our future research. In addition, the club convergence of environmental regulation efficiency at the county level should also be further analyzed on the basis of their initial values. Meanwhile, the number of control variables can also restrict the spatial conditional $\beta$ convergence conclusions. In future research, we intend to increase the number of control variables and continuously improve the research results.

## Data availability statement

The raw data supporting the conclusions of this article will be made available by the authors, without undue reservation.

## Author contributions

FL: conceptualization, software, data curation, and writing—original draft preparation. HR: methodology and writing—reviewing. XZ: editing and visualization. All authors contributed to the article and approved the submitted version.

## Funding

This research was funded by the Humanities and Social Sciences Project of Shandong Province (Grant NO. 2021-YYGL-33), and the Art and Science Key Project of Shandong Province (L2022Z06170458).

## Conflict of interest

The authors declare that the research was conducted in the absence of any commercial or financial relationships that could be construed as a potential conflict of interest.

## Publisher's note

# References


Andersen, P., and Petersen, N. C. (1993). A procedure for ranking efficient units in data envelopment analysis. *Manage. Sci.* 39 (10), 1261–1294. doi: 10.1287/mnsc.39.10.1261

Bigerna, S., Bollino, C. A., and Polinori, P. (2021). Convergence in renewable energy sources diffusion worldwide. *J. Environ. Manage.* 292, 112784. doi: 10.1016/j.jenvman.2021.112784

Camarero, M., Castillo, J., Picazo-Tadeo, A. J., and Tamarit, C. (2013). Eco-efficiency and convergence in OECD countries. *Environ. Resour. Econ.* 55 (1), 87–106. doi: 10.1007/s10640-012-9616-9

Cao, C. (2021). The legal and regulatory structure of public participation in government environmental management. *J. Anhui. Univ. (Philos. Soc. Sci).* 1), 100–106. doi: 10.13796/j.cnki.1001-5019.2021.01.013

Cheng, Y., Ren, J., Chen, Y., and Xu, C. (2016). Spatial evolution and driving mechanism of China's environmental regulation efficiency. *Geogr. Res.* 35 (1), 123–136. doi: 10.11821/dlyj201601011

Cui, X., Fang, C., and Zhang, Q. (2018). Coordination between environmental regulation intensity and urbanization quality: case study of Beijing-Tianjin-Hebei Urban Agglomeration. *J. Nat. Resour.* 33 (4), 563–575. doi: 10.11849/zrzyxb.20170208

Dagum, C. (1997). A new approach to the decomposition of the Gini income inequality ratio. *Empir. Econ.* 22 (4), 515–531. doi: 10.1007/BF01205777

Deng, Y., Yang, X., Ma, Q., and Wang, K. (2021). Regional disparity and convergence of China's ecological welfare performance level. *China Pop. Resour. Environ.* 31 (4), 132–143.

Dong, H., and Han, Y. (2021). Spatial-temporal evolution and influencing factors of environmental regulation efficiency of urban agglomerations in the Yangtze River Economic belt. *Resour. Environ. Yangtze. Basin.* 30 (9), 2049–2060.

Erdogan, A. M. (2014). Foreign direct investment and environmental regulations: a survey. *J. Econ. Surv.* 28 (5), 943–955. doi: 10.1111/joes.12047

Fredriksson, P. G., and Millimet, D. L. (2002). Strategic interaction and the determination of environmental policy across U.S. States. *J. Urban. Econ.* 51 (1), 101–122. doi: 10.1006/juec.2001.2239

Golany, B., and Roll, Y. (1989). An application procedure for DEA. *Omega-int. J. Manage. S.* 17 (3), 237–250. doi: 10.1016/0305-0483(89)90029-7

Hamamoto, M. (2006). Environmental regulation and the productivity of Japanese manufacturing industries. *Resour. Energy Econ.* 28 (4), 299–312. doi: 10.1016/j.reseneeco.2005.11.001

Huang, Y., and Shi, Q. (2015). Research on environmental efficiency and environmental total factor productivity in China's regional economies. *China Pop. Resour. Environ.* 25 (12), 25–34.

Jia, Z., Zhao, J., Yang, Y., and Chen, X. (2022). Spatial pattern and spatial convergence of environmental regulation efficiency of Lanzhou-Xining urban agglomeration in the Yellow River Basin. *Sci. Geogr. Sin.* 42 (4), 568–578. doi: 10.13249/j.cnki.sgs.2022.04.002

Li, M., Cai, S., and Qin, C. (2011). An analysis of situation of economic spatial dissimilarity in the Yellow River Valley. *Geogr. Res.* 31, 3, 379–383+419. doi: 10.15957/j.cnki.jjdl.2011.03.005

Li, J., and Luo, N. (2016). Analysis of convergence, spatial spillover effects and causes of chinese regional environmental efficiency. *Soft. Sci.* 30 (8), 1–5. doi: 10.13956/j.ss.1001-8409.2016.08.01

Liu, H., and Du, G. (2017). Regional inequality and stochastic convergence in China. *J. Quant. Tech. Econ.* 34 (10), 43–59. doi: 10.13653/j.cnki.jqte.2017.10.003

Liu, C., and Ma, Q. (2020). Spatial association network and driving factors of high quality development in the Yellow River Basin. *Econ. Geogr.* 40 (10), 91–99. doi: 10.15957/j.cnki.jjdl.2020.10.011

Liu, Y., and Wang, H. (2009). Research on the efficiency evolution trend and countermeasures of environmental regulation. *Ecol. Econ.* 11), 172–175.

Pan, W. (2010). The economic disparity between different regions of China and its reduction - an analysis from the geographical perspective. *Soc. Sci. China* 1), 72–84 +222-223.

Piao, S. (2020). Analysis of convergence of provincial environmental efficiency of China and dynamic processes. *Manage. Rev.* 32 (8), 52–62+105. doi: 10.14120/j.cnki.cn11-5057/f.2020.08.005

Pyatt, G. (1976). On the interpretation and disaggregation of GINI coefficients. *Econ. J.* 86 (342), 1–17. doi: 10.2307/2230745

Ram, R. (2021). Income convergence across the U.S. states: further evidence from new recent data. *J. Econ. Financ.* 45 (2), 372–380. doi: 10.1007/s12197-020-09520-w

Ren, M., Wang, X., Liu, L., Sun, F., and Zhang, W. (2019). Spatio-temporal change and influencing factors of environmental regulation in China's coastal urban agglomerations. *Sci. Geogr. Sin.* 39 (7), 1119–1128. doi: 10.13249/j.cnki.sgs.2019.07.010

Rezitis, A. N. (2010). Agricultural productivity and convergence: Europe and the United States. *Appl. Econ.* 42 (8), 1029–1044. doi: 10.1080/00036840701721026

Riccardi, R., Bonenti, F., Allevi, E., Avanzi, C., and Gnudi, A. (2015). The steel industry: a mathematical model under environmental regulations. *Eur. J. Oper. Res.* 242 (3), 1017–1027. doi: 10.1016/j.ejor.2014.10.057

Shi, R., Irfan, M., Liu, G., Yang, X., and Su, X. (2022). Analysis of the impact of livestock structure on carbon emissions of animal husbandry: A sustainable way to improving public health and green environment. *Front. Public Health* 10. doi: 10.3389/fpubh.2022.835210

Simões, P., De Witte, K., and Marques, R. C. (2010). Regulatory structures and operational environment in the Portuguese waste sector. *Waste. Manage.* 30 (6), 1130–1137. doi: 10.1016/j.wasman.2009.12.015

Sun, Y., Miao, S., Cui, Y., and Jia, Y. (2022a). Analysis of ecological environment regulation efficiency measurement and driving factors in Beijing, Tianjin and Hebei. *Stat. Decis.* 16), 66–71. doi: 10.13546/j.cnki.tjyjc.2022.16.013

Sun, Y., Miao, S., Cui, Y., and Li, X. (2022b). Study on the spatial correlation network of ecological and environmental regulation efficiency in Beijing-Tianjin-Hebei urban agglomeration. *City* 11), 3–18.

Sunstein, C. R. (1996). Congress, constitutional moments, and the cost-benefit state. *Stanford. Law Rev.* 48 (2), 247–309. doi: 10.2307/1229364

Tang, D., Tang, J., and Ma, T. (2016). Environmental regulation efficiency and TFP in China - econometric explanation based on SBM-undesirable and DEA-Malmquist. *J. Arid. Land. Resour. Environ.* 30 (11), 7–12. doi: 10.13448/j.cnki.jalre.2016.342

Tang, D., Tang, J., Xiao, Z., Ma, T., and Bethel, B. J. (2017). Environmental regulation efficiency and total factor productivity - Effect analysis based on Chinese data from 2003 to 2013. *Ecol. Indic.* 73, 312–318. doi: 10.1016/j.ecolind.2016.08.040

Tone, K. (2011). A slacks-based measure of efficiency in data envelopment analysis. *Eur. J. Oper. Res.* 130 (3), 498–509.

Tone, K., and Tsutsui, M. (2010). An epsilon-based measure of efficiency in DEA - A third pole of technical efficiency. *Eur. J. Oper. Res.* 207 (3), 1554–1563. doi: 10.1016/j.ejor.2010.07.014

Wang, Z., and Cheng, F. (2021). Spatio-temporal differentiation and influencing factors of China's marine environmental regulation efficiency. *Geogr. Res.* 40 (10), 2885–2896. doi: 10.11821/dlyj020201124

Wang, J., and Ma, Y. (2020). Research on the time series and spatial differentiation of industrial environmental regulatory efficiency in the Yangtze River Economic Belt. *J. Ind. Tech. Econ.* 1, 113–121. doi: 10.3969/j.issn.1004-910X.2020.01.013

Wu, J., Xiong, B., An, Q., Sun, J., and Wu, H. (2017). Total-factor energy efficiency evaluation of Chinese industry by using two-stage DEA model with shared inputs. *Ann. Oper. Res.* 255 (1), 257–276. doi: 10.1007/s10479-015-1938-x

Xie, H., Zhang, Y., and Choi, Y. (2018). Measuring the cultivated land use efficiency of the main grain-producing Areas in China under the constraints of carbon emissions and agricultural nonpoint source pollution. *Sustainability* 10 (6), 1932. doi: 10.3390/su10061932

Xu, C., Ren, J., and Cheng, Y. (2014). Influence factors and temporal-spatial evolution of environmental regulation efficiency in Shandong province. *Econ. Geogr.* 34 (12), 35–40. doi: 10.15957/j.cnki.jjdl.2014.12.006

Xu, W., Xu, Z., and Liu, C. (2021). Heterogeneity analysis of environmental regulation efficiency based on SFA. *Sci. Geogr. Sin.* 41 (11), 1959–1968. doi: 10.13249/j.cnki.sgs.2021.11.009

Xue, W., and Liu, J. (2010). Environmental regulation and its evaluation in China. *China Pop. Resour. Environ.* 20 (9), 70–77.

Yin, C., Zhu, F., and Deng, L. (2017). Analysis of environmental efficiency and its determinants in the development of the western regions in China during the past fifteen years. *China Pop. Resour. Environ.* 27 (3), 82–89.

Zeng, G., and Hu, S. (2021). Impact of technological innovation on urban green development in the Yellow River Basin. *Sci. Geogr. Sin.* 41 (8), 1314–1323. doi: 10.13249/j.cnki.sgs.2021.08.002

Zeng, X., and Niu, M. (2019). Evaluation of urban environmental efficiency in China under high quality development conditions. *Chin. Environ. Sci.* 39 (6), 2667–2677. doi: 10.19674/j.cnki.issn1000-6923.2019.0316

Zhang, X., Yang, L., Zhang, X., and Xu, J. (2022). Research on the development trend, evolution, and spatial local characteristics of the intelligent smart medical industry in the Yangtze River Economic Belt. *Front. Public Health* 10. doi: 10.3389/fpubh.2022.1022547

Zhang, K., and Zhang, Y. (2020). The evolution of regional economic disparity in the Yellow River Basin at different spatial scales. *Econ. Geogr.* 40 (7), 1–10. doi: 10.15957/j.cnki.jjdl.2020.07.001

Zou, X., Wang, Y., Wu, T., Yin, Y., Tu, X., and Xu, G. (2019). Threshold effect of agricultural population transfer on cultivated land use efficiency in Jiangxi Province. *Resour. Sci.* 41 (8), 1576–1588. doi: 10.18402/resci.2019.08.16

# Frontiers in Public Health

**Explores and addresses today's fast-moving healthcare challenges**

One of the most cited journals in its field, which promotes discussion around inter-sectoral public health challenges spanning health promotion to climate change, transportation, environmental change and even species diversity.

---

## Discover the latest Research Topics

See more →

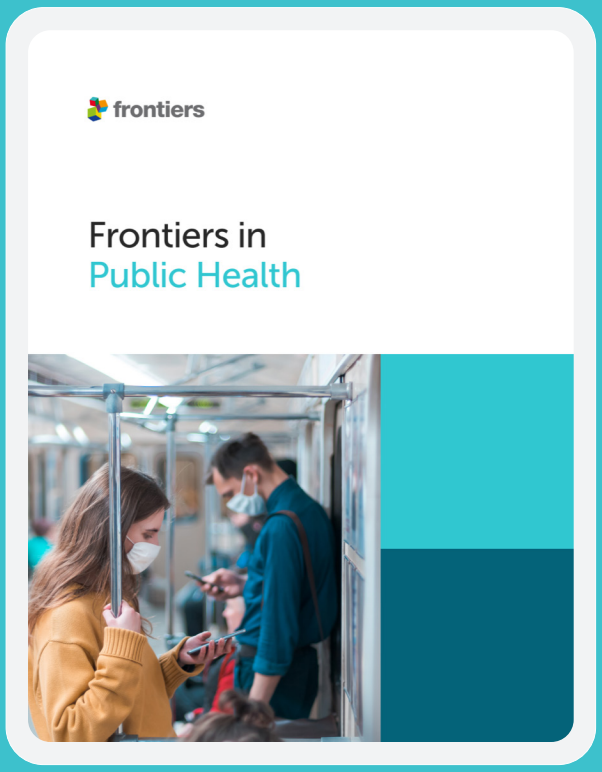


**Frontiers**

Avenue du Tribunal-Fédéral 34
1005 Lausanne, Switzerland
frontiersin.org

**Contact us**

+41 (0)21 510 17 00
frontiersin.org/about/contact